Seismic Performance of Prefabricated Steel Frame Structures with Buckling-Restrained Braces

Seismic Performance of Prefabricated Steel Frame Structures with Buckling-Restrained Braces

Yuan Xu

BEng, MEng

Griffith School of Engineering and Built Environment

Griffith University

Submitted in fulfilment of the requirement of the degree of

Doctor of Philosophy

February 2019

Synopsis

The concept of "prefabrication" has been increasingly applied in the civil construction industry. While satisfying the requirements for the rapid development of advanced modular constructions, prefabrication may not be an appropriate choice in earthquake regions due to its poor seismic performance. On the other hand, as one of the most favoured options in seismic design, steel structures also face many challenges. Most of the steel frames used in strong seismic areas have field-welded moment-resisting connections. This is despite the fact that on-field welding of beam-column connections lacks construction quality assurance and is prone to industrial accidents. The brittle fractures in welded steel beam-column connections caused by earthquakes can also lead to structural collapse. Further, the costs of repairing or replacing the earthquake-damaged structures can be exorbitant.

To satisfy both seismic and prefabrication requirements, this PhD dissertation recommends a prefabricated steel-frame system with bolt-connected beams and columns incorporating buckling restrained braces (BRBs). In this system, the welded rigid connections are replaced by bolted connections which only require on-site assembly by bolting. The potential damage to the main structural members caused by earthquake ground motions can be effectively reduced. This is because the BRBs are introduced to resist most of the lateral seismic loads whereas the bolt-connected beams and columns are designed to carry gravity loads only and hence they remain elastic.

The focus of this dissertation is on the seismic performance of the proposed bolted-frame system with BRBs. To this end, a methodology for the numerical modelling of the structural behaviour of the system using OpenSees is developed. Its effectiveness is validated against existing experimental results in published literature. An experimental study including the tests of three 2-storey frames has also been undertaken to investigate

their dynamic responses under cyclic loadings. The experiment results are discussed and compared with numerical predictions in terms of hysteretic behaviour, energy-dissipating capacity, and stiffness degradation. In addition, a parametric study is carried out on two groups of models namely the R- and P-Groups each of which comprises 9-storey and 5-storey frames. The frames in the R-Group are with moment-resisting beam-column-brace connections; those in the P-Group are with non-moment-resisting ones. The emphasis of the parametric study is on the impact of the beam-column-brace connection rigidity and the BRB area distributions on the seismic resistance capacity of the system. Furthermore, a fragility analysis is conducted to fully understand the structural demand caused by various levels of ground shaking. For this purpose, 12 prototype frames with three different storey heights and various numbers of non-moment resisting bays have been designed and analysed.

This analytical and experimental PhD research has led to the conclusion that the proposed bolted-frame system with BRBs is able to provide a reliable performance under seismic actions. In general, the system performs well in energy dissipation under severe earthquakes, especially if the BRBFs are constructed with moment-resisting beam-column-brace connections. In terms of the stiffness ratio (S_r), the ideal value is found to be between 3 and 5 regardless of the building height. For the design distribution of BRB areas along the storey height, the most uniform patterns of the inter-storey drift ratios are produced when the said areas are distributed proportionally to the storey shear force. Further, in terms of fragility, with the same building height, the probabilities of exceeding a given performance level are always higher with more numbers of NMRBs, and with the same numbers of NMRBs, the taller buildings have less likelihood to collapse. Finally, in regard to collapse prevention, the proposed system is only recommended to use with no more than 3 NMRBs.

Acknowledgements

First and foremost, I would like to express my utmost and sincere gratitude to my principal supervisor Professor Hong Guan who has not only provided boundless guidance throughout the period of this PhD research with her rigorous scholarship, but also looked after me in life with her considerate personality. I also wish to extend my appreciation to my principal supervisor as well as my spiritual mentor, Professor Emeritus Yew-Chaye Loo AM, who has provided constant and positive advice and has inspired me to complete this research. My gratitude also extends to my co-supervisor, Dr Hassan Karampour, for his invaluable guidance and support in completing this thesis.

My deepest gratitude goes to my external supervisor, Professor Xuejun Zhou, at Shandong Jianzhu University, Jinan, China who was also my supervisor for my Master's degree. Over the past seven years, Professor Zhou has offered me constant academic guidance and moral support. He and his family always treat me as part of their family. This project would not have been accomplished without his generous help.

I would also like to acknowledge the funding provided by the Housing and Urban-Rural Department of Shandong Province, China (Project name: "Research of Key Technology for Fully Prefabricated Steel Structural System Based on Building Components"), and the financial support from Chinses Scholarship Council, the 12-month Engineering top-up scholarship and tutorship offered by Griffith School of Engineering and Built Environment, which were essential to my PhD study.

I am grateful to my friends in Gold Coast and Brisbane, especially my partner Jie Sun and my friend Yanyang Gu, for their love, friendship and patience to get me through my hardest time. Finally yet importantly, I would like to dedicate this thesis to my beloved parents for their understanding, unconditional love, selfless support and constant encouragement throughout this worthy journey.

Statement of Originality

This work has not previously been submitted for a degree or diploma in any university. To the best of my knowledge and belief, the thesis contains no material previously published or written by another person except where due reference is made in the thesis itself.

Yuan Xu

February 2019

Table of Contents

List of Abbreviations

AISC	American Institute of Steel Construction
BRB	Buckling Restrained Brace
BRBCF	Buckling Restrained Braced Composite Frame
BRBF	Buckling Restrained Braced Frame
BRBF-EF	BRBF and an Adjoining Non-Moment Resisting Frame with End-Plate Beam-Column Connections
BRBF-FF	BRBF and an Adjoining Non-Moment Resisting Frame with Fin Plate Beam-Column Connections
CBE	Consequence-Based Engineering
CDF	Cumulative Distribution Function
CF	Composite Frame
CFT	Concrete-Filled Tube
CPD	Cumulative Plastic Ductility Ratios
CSBRB	Core-Separated Buckling Restrained Brace
CSM	Capacity Spectrum Method
DI	Dial Indicators
DL	Design Dead Load
DL	Ground Beam
DM	Displacement Meters
EDC	Energy Dissipation Capacity
EDP	Engineering Demand Parameter
FEA	Finite Element Analysis
FEM	Finite Element Method
IDA	Incremental Dynamic Analysis
IM	Intensity Measure
KL	Frame Beam
KZ	Frame Column

LL	Design Live Load
LS	Limit State
MRF	Moment-Resisting Frames
MSA	Multiple Stripe Analysis
Mw	Magnitude of Earthquake
NMRB	Non-Moment-Resisting Bay
PCBRB	Perforated Core Buckling Restrained Brace
PDT	Pseudo-Dynamic Test
PGA	Peak Ground Acceleration
RC	Reinforced Concrete
R-Group, P-Group	Frames With Moment-Resisting Beam-Column-Brace Connections; Frames With Non-Moment-Resisting Beam-Column-Brace Connections
RSN	Record Sequence Number
SCBF	Special Concentrically-Braced Frame
SC-BRB	Self-Centring Buckling Restrained Brace
SMA	Shape Memory Alloy
SMRFs	Special Moment-Resisting Frames
THA	Time History Analysis
URM	Unreinforced Masonry

List of Notations

a_0, b_0	Thickness and width of material sample
A_c	Area of the cross section
b	Strain-hardening ratio
C_{jl} *(LS)*	Limit state capacity for the j^{th} component of the l^{th} mechanism
d	Diameter of bolt rod
d_e	Effective diameter of bolt rod
D_{jl}	Demand evaluated for the j^{th} structural component of the l^{th} mechanism
DCR_{LS}	Critical demand to capacity ratio for a desired LS
E	Elastic modulus
E_b	Elastic modulus of BRB
E_0	Initial elastic tangent
f_u	Ultimate strength
f_y	Yield strength
f_v^b	Design values of the shear strengths of bolts
f_t^b	Design values of the tensile strengths of bolts
g	Gravity acceleration
H	Total height of the cross section of beam and column
k_b'	Lateral stiffness of the BRB
k_s	Stiffness of main frame without BRB
K	Rotational stiffness
K_i	Secant stiffness coefficient in loop i
L_0, L_c, L_t	Gauge length, parallel length, total length of material sample
L_b	Length of BRB

M	Actual connection moment
M_p	Plastic moment capacity of the beam
M_{fin}	The maximum moment transferring capacity of the fin-plate connection
M-θ	Moment-rotation
n_v	Number of bolts on the cross section
N	The number of record ground motions
N_{mech}	Number of considered potential failure mechanisms
N_l	Number of components taking part in the l^{th} mechanism
N_v^b	Shear capacity of bolt
N_t^b	Axial capacity of bolt
P	Horizontal force
$P_{LS\|IM}$	Probability of EDPs exceeding LS given IMs
P_{max}	Maximum compressive strength of BRB
P_y	Yield load of frame
R	Parameter to control the transition from elastic to plastic branches
R_y	Material overstrength factor
s	Horizontal displacement
S_a	Small-amplitude first-mode spectral acceleration
S_r	Stiffness ratio of BRBF
T_f	Flange thickness
T_w	Web thickness
u_y	Yield displacement of brace
$u_{p_i}^{max}$	Maximum plastic axial deformations during loop i
$u_{p_i}^{min}$	Minimum plastic axial deformations during loop i
W	Flange width
Δ_f	Deformation quantity used to control loading of the test frame
Δ_{fe}	Maximum elastic deformation of the test frame

Δ_y	Yield displacement of frame
Δ_{max}	Maximum displacement of frame
β	Compression strength adjustment factor
$\beta_{EDP\|IM}$	Standard deviation of distribution of non-collapse EDPs given IMs
δ	Elongation percentage
θ_p	Rotational capacity
θ_r	Actual connection rotation
σ_y	Yield stress
σ_u	Ultimate tensile stress
$\sigma_{ln\,\beta_{DCR_{LS}\|S_a}}$	Logarithmic standard deviation for DCR_{LS} given S_a
ω_y	Stain hardening factor
$\eta_{DCR_{LS}\|S_a}$	Median for DCR_{LS} given S_a
η_{IM}	Median of utilised IMs
η_{EDP}	Median of estimated EDPs
$\eta_{EDP\|IM}$	Median of distribution of non-collapse EDPs given IMs

List of Figures

List of Tables

List of Publications

Refereed Conference Publications:

Xu, Y., Guan, H., Zhou, X.J. and Loo, Y.C. (2015) Preliminary seismic analysis of fabricated steel frame systems with pin beam-column connections and buckling restrained braces. International Conference on Performance-based and Life-cycle Structural Engineering. Brisbane, Australia, 09-11 December, 2015: 768-775.

Xu, Y., Guan, H., Karampour, H., Loo, Y.C. and Zhou, X.J. (2016). Earthquake-resistant performance of a steel frame model with inverse-chevron buckling restrained braces. 24th Australian Conference on the Mechanics of Structures and Materials. Perth, Australia, 6-9 December, 2016: 692-697.

Xu, Y., Guan, H., Karampour, H., Loo, Y.C. and Zhou, X.J. (2018). Seismic performance of prefabricated BRBF with moment-resisting and non-moment-resisting beam-column-brace connection. 3rd Australasian Conference on Computational Mechanics. Geelong, Australia, 12-14 February, 2018.

Submitted journal paper:

Xu, Y., Guan, H., Karampour, H., Loo, Y.C. and Zhou, X.J. Seismic performance of prefabricated BRBF with moment-resisting and non-moment-resisting beam-column-brace connections. Asian Journal of Civil Engineering, 2018, under review.

CHAPTER 1

INTRODUCTION

1.1 Background

Earthquake is one of the most devastating occurrences of nature. A high-intensity earthquake can cause serious destruction to infrastructure of all kinds. In 1995's Kobe earthquake, a great number of buildings were destroyed and elevated highways toppled (Scawthorn and Yanev, 1995). On March 12, 2008, a magnitude (M_W) 7.9 earthquake struck Sichuan Province in China, and led to the destruction of tens-of-thousands of buildings, accompanied by innumerous causalities. These seismic events demonstrate the severe consequences of constructing weak structures in active seismic hazard zones. Compared to the world's seismically active regions, Australia has relatively low chances of suffering from intensive earthquakes. However, it has been reported that earthquakes with M_W greater than 6.0 have indeed occurred in recent times (Gaull et al., 1990). According to a 2015 investigation (McCue, 2015), earthquakes with magnitudes of 5+ have occurred in Australia over the past few years. All this has attracted many researchers' attention to this, the seismicity of the intraplate environment.

In the past century, our knowledge of seismicity and earthquake resistant structures has significantly improved. Scientists and engineers have come up with various methods

for resisting seismic loads on structures. These include ductile moment resisting frames, base isolation systems, and seismic bracing systems. Among these, the steel moment frame is one of the most widely used methods for resisting seismic loading (Naeim and Kelly, 1999).

In 1994, after the Northridge earthquake (Mahin, 1998), various observations of the damaged buildings were made to determine the reasons for building collapses, in order to discover the design weakness and to improve the design guidelines for steel framed structures. It was found that the said earthquake damaged approximately 100,000 different types of buildings, including the rigid masonry and concrete structures which are expected to show relatively poor performance under earthquake (Holguin, 1998). However, it was also noted that multi-level steel frame buildings with welded connections did not satisfy the seismic-resistance expectation either. Widespread brittle fractures in welded steel beam-column connections were also detected as being caused by the earthquake. These unanticipated failures in the connections led to the loss of moment resistance capability of the steel frames which led to their collapses.

The unexpected poor performance of the weld-connected steel frames raised the alarm bells in the structural engineering field. As a result, concerned government authorities started reviewing the performance of buildings, and developing reliable and cost-effective methods for inspecting, evaluating, repairing, and rehabilitating of steel frame buildings. In addition, new seismic design criteria were also introduced for high-intensity earthquake regions (Mahin, 1998).

1.2 Research Motivation

According to the observed behaviour of structures during earthquakes, the capability of maintaining strength as well as energy dissipation capacity has been recognised as the most desirable mechanical characteristics in providing seismic resistance (Black, 2002). However, the most commonly used welded beam-column connections which are

supposed to provide certain stiffness for the frames did not show expected performance during previous earthquakes. Field surveys after major disastrous earthquakes have shown that the quasi-brittle fractures in welded beam-column connections of steel moment resisting frame buildings, were the leading cause of human fatalities and economic losses (Uriz and Mahin, 2008). Over the past decades, many ideas for improving the capability of absorbing large portions of seismic energy have been developed by various researchers. The use of yielding metallic components as the energy dissipation devices within the skeleton of a building has become the most popular one (Kelly et al., 1972; Whittaker et al., 1991; Tsai et al., 1993).

In addition to the problems associated with welded connections, the huge costs of repairing or replacing damaged structural members after a severe earthquake are another main challenge to designers. As the conventional seismic design of steel frame structures relies on inelastic deformation of structural members or the yielding of the connections for dissipating input earthquake energy, the individual structural members designed by this principle are prone to damage after being shaken by a design-level earthquake. As a result, significant expense would again be required to repair or replace the damaged structural components.

Added to all these woes, the building and construction industry has been facing ever-increasing public demands in safeguarding civil infrastructure against such natural hazards as earthquakes. It is obvious that conventional structural design approaches can no longer satisfy the needs for the rapid development of advanced modular constructions. Besides, there are recognised drawbacks in terms of high-volume workload in construction site, such as lacking construction quality assurance and high likelihood of industrial accidents (Faella et al., 1999). Consequently, the concept of "prefabrication" has been increasingly applied to civil construction works.

Prefabrication entails the assembling of structural components that are manufactured under factory conditions, and then transported to construction sites for incorporation

into the designed building or other civil engineering works. Prefabricated construction methods involve a variety of technologies, which basically all aim to increase efficiency and productivity, as well as reduce time and economic costs.

In populous countries with high seismic activities such as China, Japan, and the USA, sustainable construction through the adoption of prefabrication in commercial and residential buildings has become a trend in modern construction industry. This is due to limited availability of land, intensive construction demand, and most importantly, the construction speed, safety, and cost effectiveness that prefabrication can offer. Besides, as the components of steel structures can be initially processed off-site, construction of a fully prefabricated steel structure will require bolted only assembly instead of on-site welding. To foster sustainability, the Chinese government for instance has been vigorously promoting the concept of the Industrialised Buildings System as an alternative solution for the current construction market. Indeed, published studies have acknowledged the benefits of quality prefabricated constructions, in terms of low cost, high productivity and minimal environmental impact (Yee and Eng, 2001; Pheng and Chuan, 2001; Chan and Hu, 2002; Eastman et al., 2003; Pasquire et al., 2005; Blismas et al., 2006; Jaillon and Poon, 2008).

However, there is a general concern among designers regarding prefabrication in terms of seismic resistance. Poor performance of prefabricated frame systems has been observed in Eastern European and Central Asian countries where these framework systems have been widely adopted. The deficiency is due mainly to connection failure, insufficient stiffness and strength of columns. It appears thus that conventional prefabrication is not necessary an appropriate choice for countries in earthquake-disaster prone areas (Baghchesaraei et al., 2016). In view of all this, the lateral resisting structural components with buckling restrained braces (BRBs), as described hereunder, may be utilised for improving the stiffness and strength of prefabricated structures.

As the most popular lateral resisting structural component, the traditional structural

bracing has been facing its own challenges. Although it greatly improves the stiffness of a frame under minor lateral loads, the buckling of individual braces under compression, in an earthquake, has a dramatic effect on the strength and stiffness of the braced frame. Once it occurs, the strength is reduced, and the frame loses further stiffness in every successive load cycle. This problem has been rectified by using the novel BRBs which have become popular in building constructions over the past decade (Xie, 2005).

Figure 1.1 shows the application of BRBs in a steel frame. It has been demonstrated (Sabelli et al., 2003; Kiggins and Uang, 2006) that the BRBs have similar strength and ductility behaviour in both compression and tension, thereby being able to absorb significant amount of energy under cyclic loading. As such, the BRBs can be a superior replacement for conventional braces in an earthquake-resistant steel framed structure. As energy dissipation in steel braced frames mainly relies on the inelastic deformation of the diagonal members, the application of BRBs can significantly increase the energy dissipation capacity of the overall structural system. Consequently, demands for inelastic deformation of other structural members are dramatically reduced. In recent decades, buckling restrained braced frames (BRBFs) have become more and more common in seismic prone regions because of their proven and relatively stable hysteretic behaviour, as well as their significant ductility and large energy dissipation capacity (Black et al., 2004; Xie, 2005). Therefore, utilising the BRBFs in prefabricated construction could satisfy the twin demands of structural performance and sustainability. Potentially, this construction system also has a satisfactory seismic behaviour under earthquake actions.

Figure 1.1 Application of buckling restrained braces (BRBs)

For an earthquake-resistant building which satisfies both seismic and prefabrication requirements, a prefabricated steel frame system with all bolt-connected beams and columns incorporating BRBs is proposed in this PhD dissertation. This system adopts solely bolted connections for both the buckling-restrained braced bay as well as the non-braced bays (i.e. non-moment-resisting bays). All the structural components of the proposed system can be prefabricated and then assembled on site. In the proposed system, the lateral earthquake forces are resisted by the BRBs. For this reason, the potential damage to the building as a whole due to earthquake ground motions can be prevented because the main structural members, namely the bolt-connected beams and columns, remain elastic. In the system, it is also able to separate the gravity-resistant members from the lateral motion-resistant members, as illustrated in Figure 1.2. As may be seen in Figure 1.2(2) the non-moment-resisting bays only withstand gravity loads due to its much lower rigidity. On the other hand, the BRBF (Figure 1.2 (1)) is responsible for resisting the lateral loads.

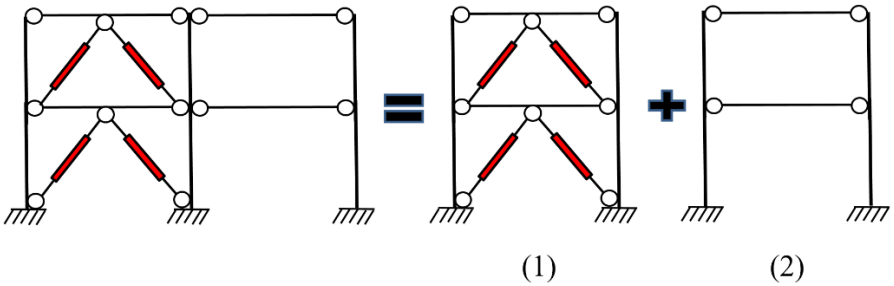

Figure 1.2 Prefabricated steel frame with BRBF (Note: (1) represents the BRBF; (2) represents the non-moment-resisting bay)

In addition to these enhanced structural characteristics, with all connections being bolted, the on-site assembling speed can be significantly improved since no welding work is necessary. Further, following an earthquake, any and all potentially damaged lateral load-resisting (BRB) members can be rapidly replaced at a fraction of the cost required for a major rehabilitation (as would be in the case of an earthquake-damaged conventional building).

1.3 Objectives and Scope

In view of the considerable structural and economic benefits of the proposed seismic-resisting prefabricated steel frame system with buckling-restrained braces, this dissertation is devoted to a numerical and experimental study of the said structural system. The specific objectives of this PhD project are to:

- study the force-transferring mechanisms of the proposed structural system;
- uncover the influence of rotational stiffness of beam-column connections on the force-transferring mechanisms of the proposed system;
- investigate the seismic resistance capacity of the structural system by evaluating the hysteretic behaviour, energy dissipation capacity and stiffness degradation of the test specimens through the experimental study;
- assess the comprehensive seismic performance of the structural system, including the influence of number of storeys, number of non-moment-resisting bays and BRB area distributions through the numerical study;

- analyse the probabilities of failure of the structural system under uncertain quantities, i.e., earthquake intensities through the fragility analysis;
- put forward reasonable suggestions for improved design theory and methodology.

1.4 Thesis Outline

In all, this thesis is organised into eight chapters including this, Chapter 1 Introduction. The contents of Chapters 2 to 8 are enumerated below:

Chapter 2 presents a literature review of the three major components of the proposed system: prefabricated buildings, bolted beam-column connections and the BRBs/BRBFs (buckling restrained braces/buckling restrained braced frames). The background, latest advancements and current application of the three components are discussed. This chapter also helps establish the research direction and formulate the proposed development work.

Chapter 3 focuses on the main methodologies adopted in this research. The basics of modelling connections in ABAQUS are presented to examine the rotational capacity responses of bolted connections employed in the proposed prefabricated system. Subsequently, the numerical modelling techniques using OpenSees for investigating the proposed system are developed and validated via an existing experimental study.

Chapter 4 first provides a review of the existing experimental study on BRBFs. Then it discusses in detail the experimental program undertaken on three half-scale 2-storey models:

- two double-bay frames consisting of a BRBF and an adjoining non-moment resisting frame;
- one single-bay BRBF (without a non-moment resisting frame).

The discussion is conducted in terms of the planning, design, and laboratory test procedure of the frame specimens, as well as the design and fabrication of the test rig used for the present tests.

Chapter 5 records the experimental observations of three cyclic loading tests and one pushover test on the models described in Chapter 4, and discusses the experimental results in regard to the hysteretic behaviour, energy-dissipating capacity, and stiffness degradation of the test specimens. Then the test results are compared with the numerical predictions.

Chapter 6 details a series of parametric studies on the proposed system. The chosen parameters includes beam-column-brace rigidity, building height, and BRB area distributions. Factors affecting the seismic performance are examined by evaluating the inter-storey drifts based on the results obtained from the OpenSees finite element models.

Chapter 7 describes the basic concepts of fragility assessment, and performs a fragility analysis to evaluate the probabilities of failure of the structural system under uncertain quantities, i.e., earthquake intensities. Cloud method is chosen for the seismic evaluation in which 12 designed models with three different building heights and four different numbers of non-moment-resisting bays are analysed. For the purpose of making design recommendations, the obtained fragility curves of all the models are then discussed in detail.

Finally, Chapter 8 presents a summary of the research outcomes. The conclusions and the needs for future research are also outlined therein.

CHAPTER 2

LITERATURE REVIEW

2.1 General Remarks

The proposed prefabricated structural system assembles buckling restrained braced (BRB) frames (BRBF) and non-moment-resisting frames with bolted beam-column connections. Therefore, the prefabrication buildings, the bolted beam-column connections and the BRBFs are the three major components in such a system. Over the past decades, the structural performance and challenging issues of both beam-column connections and BRBFs have been studied from different aspects which have been well addressed in the existing literatures. To identify the research gap and set a clear research direction for this study, this chapter presents a detailed review of literature relevant to the abovementioned two subjects, covering not only the bolted connections and BRBFs, but also the significant role BRBs play in BRBFs.

First of all, a brief overview of the prefabricated buildings is carried out. The development of prefabrication in construction industry, as well as its benefits and limitations are introduced. Secondly, the classifications of bolted beam-column connections are introduced, and a review of existing analysis methods for connections is presented. Furthermore, related research on the main types of bolted connections by using these existing methods is also discussed. For BRBs and BRBFs, the history of

development is presented, followed by the detailed review of different BRB types, experimental and numerical studies of BRBs/BRBFs, as well as general design methods for BRBFs.

2.2 Overview of Prefabrication

Prefabrication is an act of collecting components of a structure which are manufactured off-site and transporting these components to the construction site for installation. Prefabrication application has seen an increasing trend in the modern construction industry, as it aims to increase the speed of construction and to reduce costs.

As stated in Kim (2009), the earliest prefabricated houses were built in 1624 in England and was sent to Massachusetts. In 1790, simple timber-framed shelters were shipped from England to Australian settlements in New South Wales as hospitals, storehouses and cottages. Although these structures were not completely prefabricated, these early applications with reduced labour and construction cost has become a forerunner of today's prefabrication. As a result of World War II, residential buildings in Europe were significantly damaged. To cope with the increasing demand for housing, a huge number of prefabricated construction has been undertaken (Zhang and Skitmore, 2012).

During 1960s when the demand of housing is at its peak, various precast concrete building systems were created (Pan et al. 2007). In 1996, it was reported that the levels of precast construction were as high as 43% in Denmark, 40% in the Netherlands, 31% in Sweden and Germany (Jaillon and Poon, 2009).

In the early 1970s, prefabricated system became popular in the US. Unlike the large-scale prefabricated approach used in Europe due to the high post-war demand, a more individualised prefabrication style has become a focus for residential buildings (Fan, 2010).

Since mid-1980s, prefabricated construction in terms of industrialised housing (IH) has been developed in Japan, and it has grown into a great industry sector today (Barlow et al. 2003).

In Singapore, prefabricated system was introduced in the early 1980s and several of the prefabrication systems were developed by local and overseas contractors (Wong and Yeh, 1985). In Malaysia, industrialised building systems (IBSs) have been established since the 1990s. The IBSs provide a much needed solution to the considerable emphasis on building construction activities in the Malaysia Seventh Five-Year Plan with very rapid growth in numbers (Badir et al., 2002).

In China, the first prefabricated housing was attempted in the early 1970s, and it mainly adopted the former Soviet Union's large boardroom building technique (Wang, 2006). During the end of 1980s, the concept of "industrialised housing" was brought up to meet the increased housing demand (Chu, 2009). At the end of 1990s, guidelines and technology standards for housing industrialisation were developed with policy support from the Chinese government, including "Coding Standards for Architectures", "Technical Assessment for Residential Projects", "Standards for Architectural Design" and "Standard for Modular Coordination of Dwelling Houses" (Zhang and Skitmore, 2012). Since mid-2000s, the use of architectural precast concrete has been increasing due to the growing labour costs and increasing demand for energy saving and environmental protection (Zhang et al., 2014). As reported in Yang et al. (2012), the project "prefabricated shear wall structure system" was completed in 2005 by Vanke Corporation. In 2009, the Nantong Construction Engineering General Contracting Enterprise has successfully implemented the "whole prefabricated shear wall structure system". In 2015, Changsha BROAD group built a 57 story, 800 apartment skyscraper (Mini Sky City) in 19 working days by assembling the prefabricated modules (Boafo et al. 2016).

Over decades of research study and industry applications, many benefits have been

recognised for prefabricated buildings. Badir et al. (2002) confirmed that one major benefit is the savings in labour and material costs. Mokhtar and Mahmood (2008) considered the use of prefabrication to be one of the most effective waste minimisation methods possible in the construction industry. Jaillon and Poon (2009) noted several significant advantages of prefabrication compared with traditional construction, such as improved quality control, reduction of construction time, construction waste, dust and noise on-site, and labour requirements on-site. On the other hand, some limitations have also been identified from several studies (Tam et al., 2007; Tam et al., 2005; Chiang et al., 2006), such as high overall cost, lack of standard components, lack of skilled labour and lack of hoist equipment capacity in implementing prefabrication practice.

Although prefabrication construction can offer many benefits, its applications have been more focused on low-rise concrete buildings. Relevant studies and applications in steel building structures are still limited. Therefore, this thesis seeks to bridge some of the research gaps in the prefabricated steel structures.

2.3 Bolted Connections

The strength and ductility of steel frames greatly depend on the performance of the beam-to-column connections (Chen et al., 1996). Conventional designs of beam-column connections in a steel frame are always based on idealised assumptions: the behaviour of the connections is either fully rigid, which means no relative rotation occurs at the connection and the moment can be transferred from the beam to the column, or purely pinned, which implies that the beam end can freely rotate and the end moment of the beam is always zero. However, it has been commonly recognised that either bolted or welded beam-column connections provide certain level of rigidity in reality (Chen and Kishi, 1989). Due to the complexity and non-linearity of the connection properties (i.e., material and geometry), there are commonly observed uncertainties in connection behaviours. Note that this PhD project focuses on the

prefabricated steel frames which are assembled with solely bolted connections. Thus, bolted connections are reviewed below in terms of the analysis methods, classifications, as well as their structural behaviours.

2.3.1 Classifications of bolted connections

Wilson and Moore (1917) performed the first study of the rotational stiffness of beam-column connections. A large amount of experimental studies have subsequently been conducted to testify the rotational behaviours of bolted beam-column connections. Their experimental results led to the classification of the connections into four major types: web-angle connection, fin-plate connection, top- and seat-angle connection and end-plate connection, as shown in Figure 2.1.

Between 1950 and 1983, Goverdhan (1983) collected the results of 230 tests including all the connection types mentioned above. Nethercot (1985a, 1985b) investigated more than 700 tests. In addition to all the types examined by Goverdhan (1983), T-stub connections with or without web angles were also included. From 1936 to 1986, Chen and Kishi (1989) expanded the data bank collected by Goverdhan (1983) by examining 303 experimental tests conducted from all over the world. In 1995, Abdalla and Chen (1995) updated the data bank with 46 additional tests, including all the main connection types as well.

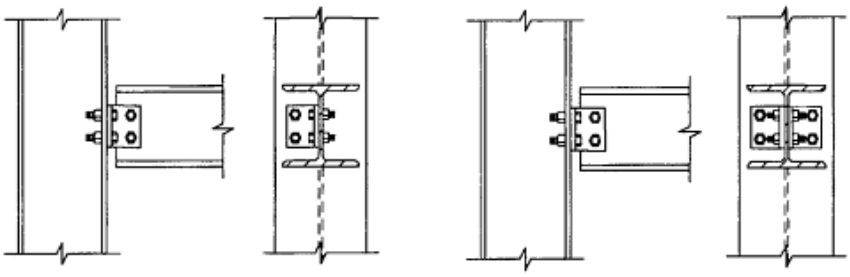

(a) Web-angle connection (left: Single; right: Double)

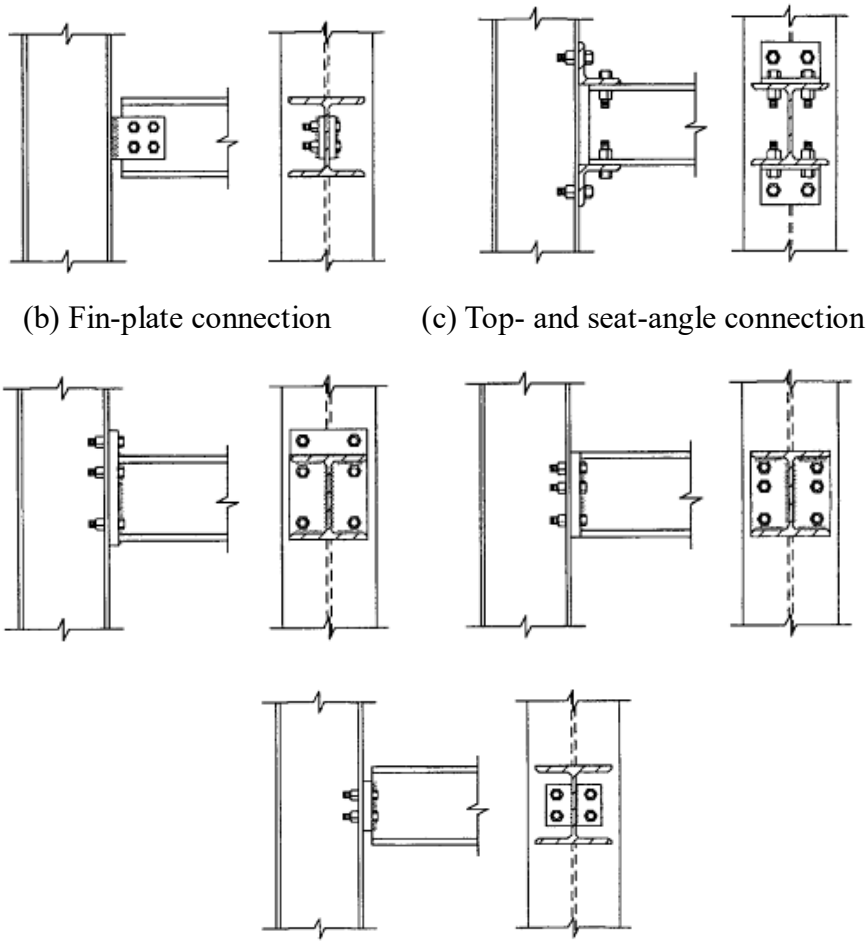

(b) Fin-plate connection (c) Top- and seat-angle connection

(d) End-plate connection (top left: Extended; top right: Flush; bottom: Header)

Figure 2.1 Different types of beam-column connections (EN 1998-3)

2.3.2 Commonly used methods for predicting rotational behaviour of bolted connections

Previous studies have shown that the rotational behaviour of beam-column connections must be considered when carrying out structural analysis of any frame (Diaz et al., 2011; Jaspart and Maquoi 1990; Bayo et al., 2006). When incorporated into the global analysis of a structure, the true behaviour of a beam-column connection can be represented by using the moment-rotation curve (M-θ curve), shown in Figure. 2.2. In this figure, the mechanical properties of the connection are represented in terms of the rotational stiffness K *(N·m/rad)*, plastic moment capacity M_p ($N{\cdot}m$), and rotational capacity θ_p (*rad*).

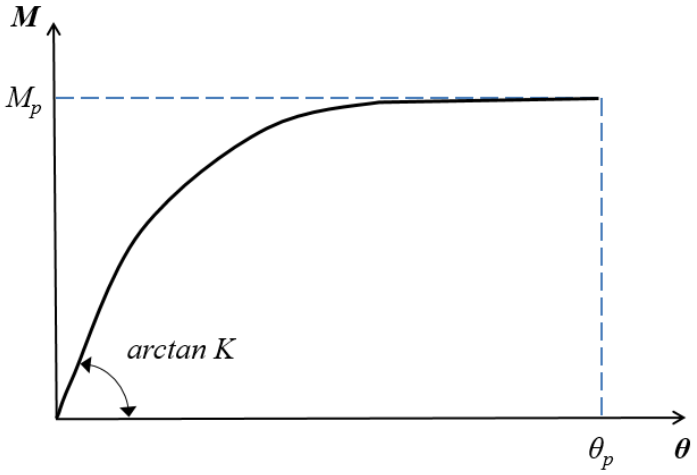

Figure 2.2 Typical moment-rotation curve of beam-column connections

There are several methods for modelling the rotational behaviour of beam-column connections. These methods can be grouped into: experimental, numerical, analytical, mechanical, and empirical (Diaz et al., 2011).

Experimental testing is the most accurate way to provide reliable results for connection behaviours. Over the past century, an extensive number of experiments on steel beam-column connections have been carried out, which enabled the generation of the existing data banks coving a variety of connections to be used as a reference in design practice (Goverdhan, 1984; Nethercot, 1985; Kishi and Chen 1994; Weynand et al., 1998). However, laboratory experiments require substantial fund investment, technical support and manpower resources, making the experimental methods primarily for research purpose only.

The development of numerical simulation techniques is rapidly increasing as the experimental studies for examining connection behaviours are not always practical for individual building design. The finite element analysis (FEA) based method is a relatively ideal alternative to obtain almost precise simulation results. In addition, local effects which are difficult to be measured in the experimental tests can also be examined through numerical studies. Therefore FEA is becoming an effective and cost-saving

way to simulate complicated connection behaviours. Numerous numerical simulations have been conducted since the first finite element study in 1972 (Bose et al., 1972), and the methods used have been gradually improved over the last 40 years or so. As a result, most of the researchers and designers choose to use finite element simulations for predicting a reasonably precise connection behaviour in structural engineering practice.

In the analytical models, rotational stiffness and moment capacity of a connection on the basis of its geometrical and mechanical properties can be achieved by using basic mechanics concepts (Kishi et al., 1993): equilibrium, compatibility and material constitutive relations. The most well-known analytical models include the one created by Chen et al. (1989) and Yee and Melchers (1986). It should be noted that in determining the connection behaviours, certain assumptions are always required depending on the mechanism of connection components. However, various geometric variables usually affect the outcomes of parametric studies and inherent uncertainties of the connection may also influence the connection behaviour, making the analytical methods relatively inaccurate (Kim et al., 2006).

Mechanical models (Faella et al., 2000; Faella and Rizzano, 1994; Liew et al., 1993; Jaspart, 1991), also known as the spring models, are also popular in simulating the connection behaviours. In such a model, all connection components can be considered as springs with different stiffnesses, so that the components can be examined individually by replacing them with springs or rigid links, subsequently the overall connection behaviour can be obtained by assembling all the components together. Moreover, inelastic law is generally considered to take into account nonlinearities of constitutive relationships of components in this method. Although the mechanical models offer a practical approach for simulating the complex behaviour of connections without the very intensive and time-consuming computational finite element analyses, the prediction of the complicated hysteretic response has remained challenging (Kim et al., 2010).

Empirical models (Frye and Morris, 1975; Krishnamurthy, 1978; Kulkreti et al., 1987; Attiogbe and Morris, 1991; Faella and Rizzano, 1994) were developed from empirical formulations based on the existing data banks generated from other prediction methods. This method is to fit a mathematical representation to the moment-rotation curves of connections, which combines the geometrical and mechanical properties of the connections from the data banks. However, due to the limitation of insufficient data bank, the empirical models can only provide approximate results but cannot be used for all types of connections (Moncarz and Gerstle, 1981).

2.3.3 Existing research on major types of bolted connections

In this section, existing work on four types of bolted connections, web-angle connection, fin-plate connection, top- and seat-angle connection and end-plate connection (shown in Figure 2.1), are reviewed. Note that the detailings and assembly methods of these types of connections are different. The suitability of a given connection in constructions practice largely depends on the functioning purpose of the structural applications. Literature indicates that the latter two connections have been more popularly used than the former two connections, hence more research studies have been devoted to the latter two connection types (EN 1998-3).

2.3.3.1 Web-angle connection

Web-angle connections are classified into single web-angle and double web-angle connections (Figure 2.1 (a)).

Single web-angle connections consist of an angle bolted to beam web and column flange (Figure 2.1(a)). Generally, the moment rigidity for designing the single web-angle connections is about half of the double web-angle connections (Pirmoz et al., 2008).

A double web-angle connection includes two web angles which symmetrically connect

beam web and column flange, as shown in Figure 2.1 (b).

In 1936, the pioneering tests on double web-angle connections were implemented by Rathbun (1936) using rivets as fasteners. About two decades later, in the 1950s, high strength bolts have been widely used to take place of rivets in most specifications for the design of steel structures. To understand the connection behaviour of high strength bolts in conjunction with rivets, Bell et al. (1958) carried out experiments on riveted and bolted beam-to-column connections. A study with the same connection was conducted by Lewitt et al. (1966), which supplemented the connection data banks established from the previously published research.

To date, with the accumulation of experimental data and practical examples, double web-angle connections with high strength bolts have been used prevalently. This is attributable to the rigidity of this types of connections which is stiffer than that of the single web-angle and single plate connections (Pirmoz et al., 2008).

2.3.3.2 Fin-plate connections

Fin-plate connections (Figure 2.1(c)), also known as single plate connections, are similar to single web-angle connections. A fin-plate connection consists of a length of plate welded in the workshop to the supporting column, to which the supported beam web is bolted on site. Fin-plate connection is one of the most popular beam-column connections used in countries like the UK (where the bolted connections are the most in use), as it can be the quickest connections to erect (Steel Construction.info, 2018).

As no small parts are necessary except bolts, a big advantage of fin-plate connections is, in general, the lower fragmented structure compared with most other pinned connection types. The main problem of fin-plate connections during the assembly is that it is not possible to specifically compensate the manufacturing tolerances, e.g. overlength or short length of the beam (Dlubal, 2018).

The calculation and design of fin-plate connections are relatively simple, as given in Eurocode 3 (EN 1993-1-8). In recent decades, the scientific investigations of fin-plate connections are mainly focused on the behaviour of such connections in fire, most tests show that the resistances of fin-plate connections are significantly reduced in high temperature (Wald et al., 2006; Sarraj et al., 2007; Yu et al., 2009). This problem is not unlike the other types of connections which has also been studied extensively (Al-Jabri et al., 2006; Yu et al., 2008; Dai et al., 2010).

2.3.3.3 Top- and seat-angle connections

A typical top- and seat-angle connection is shown in Figure 2.1(d). The characteristics of the top- and seat-angle connection have been written in the former American Institute of Steel Construction (AISC) specification (1978): (1) The seat-angle is influenced to transfer only vertical reaction and should not give significant restraining moment on the end of the beam; and (2) the top-angle is merely for laterally stability and is not considered to carry any gravity loads.

Ricles et al. (2001) proposed posttensioned top- and seat-angle moment connections for steel moment-resisting frames (MRF). A numerical model was developed for inelastic static analyses of interior connection sub assemblages as well as dynamic time history analyses of a six-storey steel MRF. A self-cantering capability and adequate stiffness, strength, and ductility were observed from these analyses. Time history analysis results showed that the seismic performance of a posttensioned steel MRF subject to the earthquake records studied exceeds the performance of an MRF with typical welded connections subject to the same earthquake records.

Subsequently, nine large-scale subassembly tests (Ricles et al., 2002) were conducted to investigate the behaviour of this type of post-tensioned wide flange beam-to-column connection for steel MRFs subjected to seismic loading conditions. The parameters investigated in the study included the angle thickness, angle gage length, beam flange reinforcing plates, connection shim plates, and posttensioning force. The test results

demonstrated that posttensioned connections were able to provide excellent elastic stiffness, strength, and ductility under cyclic loading, with energy dissipation occurring primarily in the angles. The initial elastic stiffness of the connection was comparable to that of a fully restrained welded connection. In addition, the connection had essentially no residual deformation following several cycles of inelastic storey drift.

Citipitioglu et al. (2002) proposed different 3D finite element models of bolted connections with top- and seat-angles. In the models, contact between all components was modelled, including the effect of friction. The modelling results showed that the effect of friction on the initial stiffness of the joint can be neglected. The effect of bolt pretension was similar to that of friction, although it could increase the ultimate moment of the joint by up to 25%. This study also demonstrated the effects of clamping through the bolts and contact between the components on the overall non-linear moment-rotation response.

The behaviour of bolted top- and seat-angle connections with web angles subjected to combined shear force and moment was evaluated by Pirmoz et al. (2009). In their study, geometric and mechanical properties were used as parameters in their 3D parametric finite element models. All of the connection parts, including the beam, column, angles and bolts were modelled using solid elements. The contacts between surfaces were modelled by surface-to-surface contact elements. The comparison between these results with experimental results gained a satisfactory agreement. This study further investigated the influence of the axial tensile load on the initial connection stiffness and moment capacity, and the results indicated that the increase of the axial load can cause a significant reduction of moment capacity. And it was demonstrated that the finite element model has the potential to estimate connection moment-rotation behaviour under combined axial tension and moment loading.

2.3.3.4 End-plate connections

End-plate connections have been used extensively since the late 1960s and they are the

most popular beam-column connection types currently in use worldwide (Kaushik et al., 2013). Therefore, studies focused on end-plate connections are much more than those of other connection types. As the connection behaviour is studied mainly through numerical simulation in this PhD project, most of the numerical investigations of end-plate connections are thus reviewed herein.

In general, end-plate is welded to the beam end along the web, or along both web and flange in factories and bolted to the column on field. End-plate connections can be classified into three types as extended end-plate connections, flush end-plate connections or header connections, depending on the depth of the plate (Figures 2.1(d)). It is commonly recognised that end-plate connections are always carrying a relatively high rotational stiffness, and some of them can be considered as fully restrained connections rather than partially restrained connection (Davison et al., 1987). Since the moment at the beam end can be mostly transferred to the column, this connection type is preferred in resisting earthquake loads (Chen et al., 1996).

In 1970s, Krishnamurthy and Graddy (1976) innovatively modelled three-dimensional (3D) end-plate connections. In their study, eight-node brick elements were employed to model the end-plate connection for analysing the contact between different components and preloaded bolts. Comparing with the less expense 2D results, their 3D analyses have demonstrated an increased accuracy. Kukreti et al. (1987) proposed a methodology based on the similar finite element modelling techniques used in Krishnamurthy and Graddy (1976)'s study to analytically develop the moment-rotation relationship for a bolted steel end-plate connection. The methodology was then verified against the experimental results of their selected test specimens and applied to a parametric study to determine the effect of various geometric and applied forces (i.e., moment) on the prediction of the failure level of end-plate connections.

In the early 1990s, large and unstiffened extended end-plate connections with eight bolts at the tension flange were studied by Chasten et al. (1992). In their research, shell

elements for the end-plate and beam flanges and plane stress elements for the beam web was utilised in the finite element analysis models for acquiring the prying force of contact between the end-plate and column flange. The analytically predicted bolt forces (end-plate moment) were compared with the experimentally measured forces and reasonable agreement was found. Further, simple design rules for unstiffened extended end-plate connections were presented.

In 1994, Sherbourne and Bahaari (1994) developed a finite element model to determine the moment-rotation relationships of steel bolted end-plate connections. The end-plate, beam and column flanges, webs, and column stiffeners were considered as plate (shell) elements while each bolt shank was modelled using six spar elements in ANSYS (Moaveni, 2011). Three-dimensional interface elements were used to simulate the interface between the column flange and the adjoining end-plate that may become out of contact.

Isolated extended end-plate connections of finite elements were summarised in a series reports from Bursi and Jaspart during 1997 to 1998 (Bursi and Jaspart, 1997a, 1997b, 1998) to study the modelling techniques using FEA to investigate the structural behaviour of these types of connections. Their models were made up of 3D brick elements and contact elements. The effect of element type, preloading, different constitutive relationships, and friction coefficient were considered in these models.

Troup et al. (1998) developed a 3D numerical model of an extended end-plate connection. Simplified bilinear stress-strain curves for the steel sections and bolt shank were generated through the finite element analysis. Material nonlinearity was taken into account for steel members and connecting components in the 3D connection model. Additionally, geometric nonlinearity was also considered due to the changing area of contact between the connection interfaces. The numerical model was then calibrated against the experimental results obtained from a full-scale static testing of bolted end-plate connections, in terms of the moment-rotation relationship.

In 2000, Bahaari and Sherbourne (2000) developed a detailed 3D finite element model to study 8-bolt unstiffened extended end-plate connections using primarily shell elements. Increasing thicknesses of end-plate and column flange thicknesses around the bolt hole were considered, whereas the dimensions of the bolt head or nut remained consistent in the model. Truss elements were utilised on bolt shanks connecting corresponding nodes between the end-plate and column flange while 3D interface elements were used to establish the contact between the column flange and back of the end-plate. The FE model was then applied for case studies, the study results highlighted the significance of end-plate and column flange interaction and bolt positioning.

Sumner et al. (2000) also used FEM to build 4- and 8-bolt extended unstiffened moment end-plate connections. Their model included: solid eight-node brick elements for the beam section and column flange, which included plasticity effects; solid twenty-node elements for the bolts and end-plate; and contact elements between the end-plate and the rigid column flange. The numerical models were verified against experimental tests and proved to be reasonably accurate. It was also suggested that the extended moment end-plate connections can be designed to provide a great deal of ductility in seismic force resisting moment frames and that the finite element method can be used to predict the structural behaviour of end-plate connections.

Maggi et al. (2005) performed parametric analyses on the behaviour of bolted extended end-plate connections using 3D finite element models calibrated using the experimental results. Material nonlinearities, geometrical discontinuities, large displacements and contact to account for geometric discontinuities have been taken into consideration in the model. A good agreement has been found in the comparisons between the numerical and experimental data in terms of the moment-rotation curves, displacements of the end-plate, and reaction forces on bolts.

Abolmaali et al. (2005) established a 3D finite element model for flush end-plate

connections using 8-noded solid isoparametric elements for the beam, column, end-plate and bolts. Geometric and material nonlinearities, contact and pretension in the bolts were considered in the model. The model was verified against Kukreti et al. (1987)'s test results conducted and reported for flush end-plate connections. Moreover, regression equations were developed for the ultimate moment capacity, initial stiffness and rigidity parameter of the model equations as functions of geometric variables of the flush end-plate connections.

In recent decade, Mohamadi-shooreh and Mofid (2008) revealed the results of several parametric analyses on the initial rotational stiffness of bolted flush end-plate beam splice connections using FEM. Twenty-node brick elements, material behaviour, geometrical discontinuities and large displacements were considered in the finite element analyses. The model was well confirmed by comparing with existing experimental results in terms of the moment-rotation relationship (Urbonas and Dainiunas, 2006).

Lemonis and Gantes (2009) proposed a methodology based on the component method to estimate the moment-rotation curve of structural beam-to-column joints. In their study, cases including bolted connections with end-plates and with angles were examined. Consistent results including stiffness, strength and rotational capacity were found between the experimental tests and proposed FE modelling.

Díaz et al. (2011) conducted a detailed study of the behaviour of beam-column extended end-plate connections by 3D FE analysis. Eight-node brick elements with full integration and incompatible modes were used for modelling the beam, column, and extended end-plate, bolts (head, nut and shank) while contact elements were used for all contact surfaces of the connection. The results have shown a good agreement with the real behaviour of connections in published experiments (Janss et al., 1987). The model was also used to develop a meta-model for use in the design and optimization of semi-rigid connections.

In summary, bolted connections are one of the most common elements used in the construction of steel structures. The mechanisms and modelling techniques of different types of bolted connections have been widely studied over the past decades. Critical review of the existing studies of bolted connections is expected to provide a guidance on the design of the beam-column connections of the proposed structural system.

2.4 Review of Buckling Restrained Braces (BRBs) and Buckling Restrained Braced Frames (BRBFs)

2.4.1 Brief history of buckling-restrained braces (BRBs)

Steel braces have long been used for building the system of resisting lateral loadings. They are frequently used by designers due to their feasibility and cost efficiency in design and construction (Taranath, 2011). The functional characteristics of the lateral system comprised of steel braces are to resist lateral loadings from earthquake forces and wind actions. They can effectively reduce lateral drift when rationally arranged in structures, especially in steel frames (Della Corte et al., 2011). However, an underlying problem of this system is that conventional steel braces subjected to compressive loading always incur unexpected buckling before the yield compressive stress is reached.

To further illustrate this problem, a buckled conventional brace and its typical unsymmetrical hysteretic behaviour are sketched in Figure 2.3 (a) and (c), respectively. The potential risk of these buckling braces in buildings has bothered engineers for long, since the steel braces may lose efficacy unexpectedly under cyclic loadings such as an earthquake event. For example, Sabelli's study (2001) has indicated that in some well-designed braced-steel buildings, several structural members were subjected to damages over a design level earthquake, which were attributed to the buckling of braces.

To solve this problem, the prototype of a new steel brace – buckling-restrained braces (BRBs) was invented in Japan in 1971 and was tested by Watanabe et al. (1988). They introduced new design details and investigated size effects on the buckling restrained performance of these new braces. The results have shown that most specimens did not experience buckling failure before yield strengths were reached, and high energy absorption was recorded after eight times load cycles. The deformed shape of a typical BRB being subjected to cyclic loadings is shown in Figure 2.3 (b), and the typical symmetrical hysteretic behaviour loop of BRBs is displayed in Figure 2.3 (d).

The major distinguishing behaviours between BRBs and conventional braces are the symmetricity of the hysteretic loops of BRBs. The symmetrical loop (Figure 2.3 (d)) indicates that these braces perform equally in terms of compression and tension. Thus, they exhibit not only the buckling restrained properties, but also better energy dissipation capacities and earthquake resistance. The unsymmetrical loop (Figure 2.3 (c)) of the conventional brace reveals a poor performance in an earthquake.

After decades of development, BRBs have been employed in many modern buildings. Since the 1980s in Asia, 2000 in the United States, and 2005 in Europe – BRBs have played an important role in earthquake-resistant designs. They have been used in reconstruction of existing buildings and design of braced structures (Clark et al., 2000; Black et al., 2002; Antonucci et al., 2006). Based on the available reviews of the development of BRBs (Sabelli, 2001; Xie, 2005; Wijanto, 2012), a timeline of the major events in the history of BRB development is summarised in Figure 2.4.

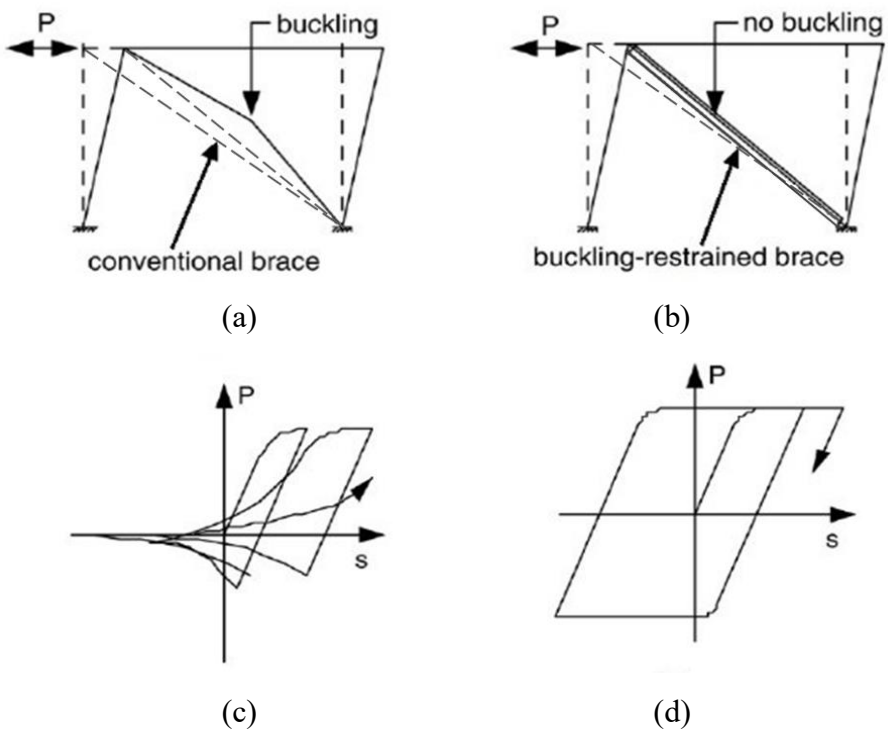

Figure 2.3 The typical behaviour of a conventional brace and a BRB (Xie, 2005) (Note: P denotes the horizontal force (*kN*); s denotes the horizontal displacement (*mm*) of the frame)

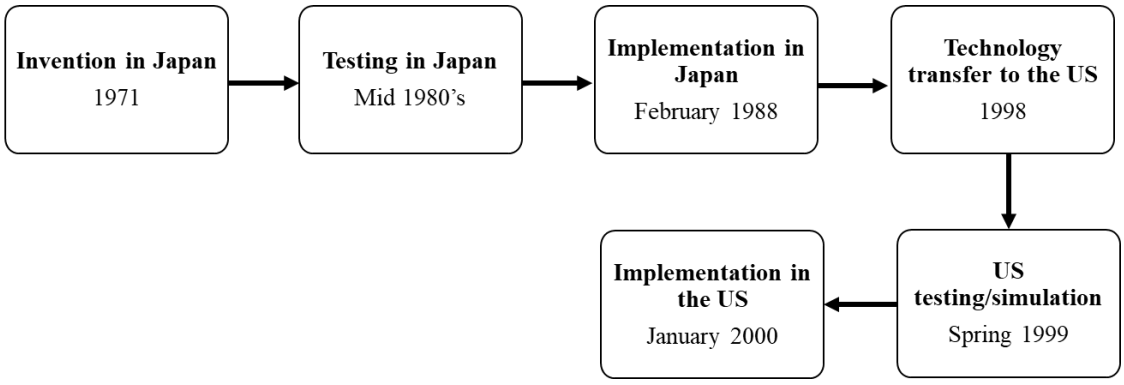

Figure 2.4 Timeline of BRB developments

2.4.2 Types of BRBs

The development of the structural form of a BRB has experienced three stages.

Figure 2.5 (Sabelli, 2001) shows the constitution of a typical BRB in the early stage, which consists of a conventional brace, a casing, and filler materials. The conventional brace (core plate) in a BRB is usually composed of three segments, namely, a restrained

yielding segment, the transition segment, and the projection segment (Figure 2.5 (b)). The casing, typically a steel or concrete tube, encloses the yielding segment with so-called de-bonding materials such as concrete mortar to absorb shock and resist buckling. A gap between the filler material and the core plate, called a bond-preventing layer, is shown on the cross-sectional view (Figure 2.5 (d) and (e)). The gap has to be set to enable the core plate to freely expand with tension and shrink with compression within the de-bonding layer (Xie, 2005). However, the accuracy of the location is difficult to be controlled due to the complexities involved with the pouring and curing of concrete (Guo et al., 2017), and the concrete-filling process were found to cause high expense.

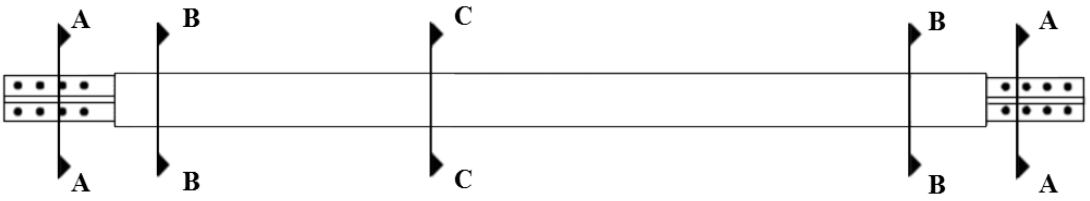

(a) Plan of a BRB

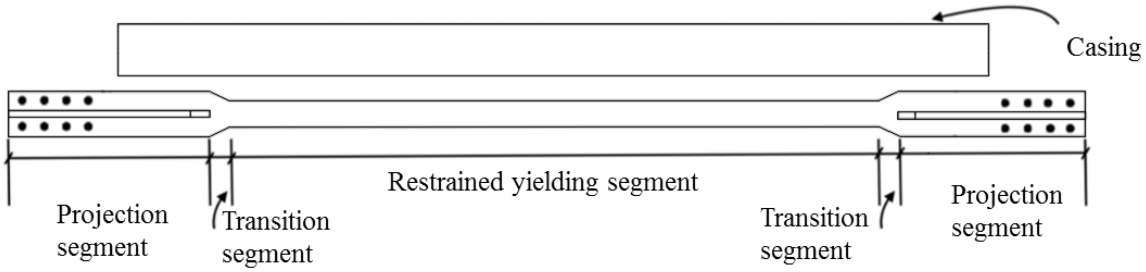

(b) Plan of core plate and the casing

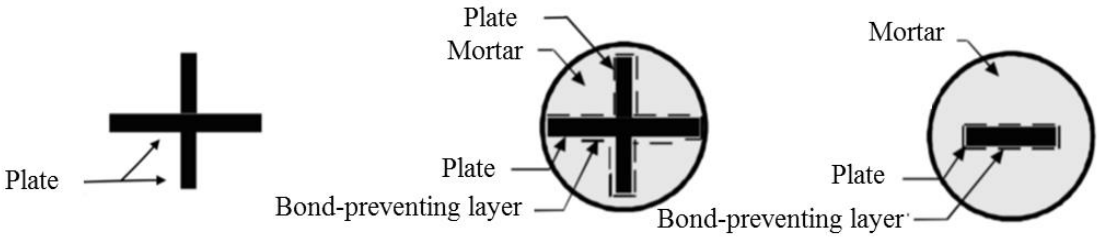

(c) Section A-A (d) Section B-B (e) Section C-C

Figure 2.5 Typical components of a BRB (Sabelli 2001)

More recently, the light-weight all-steel assembled BRBs were developed as an alternative of the concrete-filled BRB (Iwata et al., 2000; Tsai et al., 2004; Mazzolani

et al., 2009; Chou and Chen 2010; Genna and Gelfi, 2011). Apart from the much lighter weight, the all-steel BRBs have several other advantages: (a) easy and convenient on-site assembling, (b) both the inner core and the external restraining system can be directly inspected or replaced after an earthquake.

In most recent studies, new types of BRBs are still being developed to improve the BRB behaviours in different aspects. Wang et al. (2013) adopted aluminium alloys to manufacture BRBs with the aim of improving the durability of BRBs in corrosive environments. Guo et al. (2015) proposed a light-weight BRB called the core-separated buckling restrained brace (CSBRB). The CSBRB consists of two or more chord members, where each chord member is a common single-core BRB. These chord members are connected together by continuous web plates or several steel battens longitudinally. It showed that the CSBRB had increased sectional second moment of area and overall flexural stiffness, hence exhibited significantly increased load-carrying efficiency. Piedrafita et al. (2015) proposed a perforated core buckling restrained brace (PCBRB). The core of the PCBRB consists of a perforated steel yielding plate, which is guided and partially stabilized by the restraining casing.

BRBs are commonly arranged in spans of building frames in various shapes and configurations. These braced building frames are called buckling-restrained braced frames (BRBFs). From left to right, Figure 2.6 shows spans with simplified BRB configuration shapes: the chevron shape, the inverted-chevron shape, the multi-storey X-shape and the diagonal shape. Note that the K-shape and the single-storey X-shape, which are popular brace arrangement types in conventional braced frames, are not suitable for the BRB arrangement (Taranath, 2011), hence these types of brace arrangements are not shown in Fig 2.6. Additionally, in Figure 2.7, the detailed configuration of two BRBs is sketched to show the connections and the real scale of BRBs in steel frames.

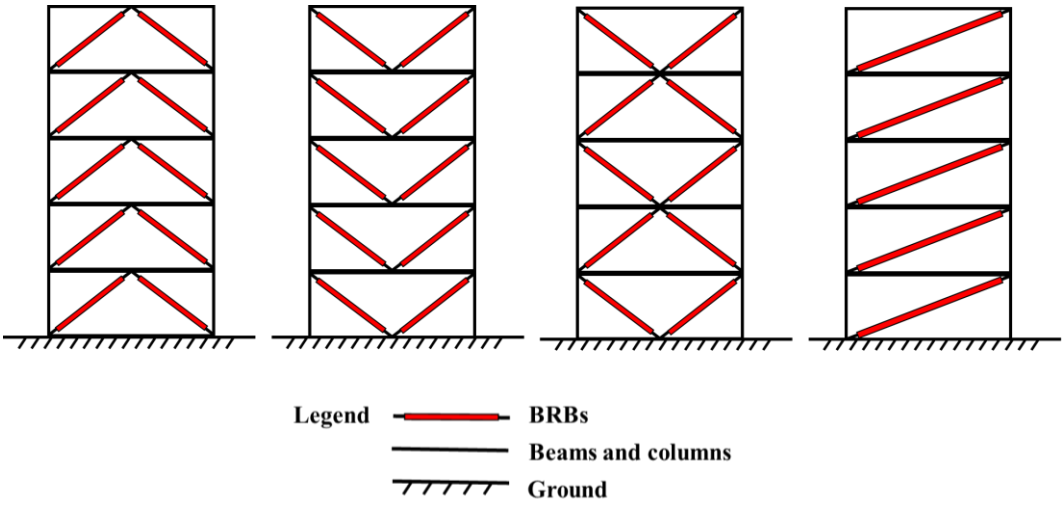

Figure 2.6 BRB arrangement (Sabelli, 2001; Taranath, 2011)

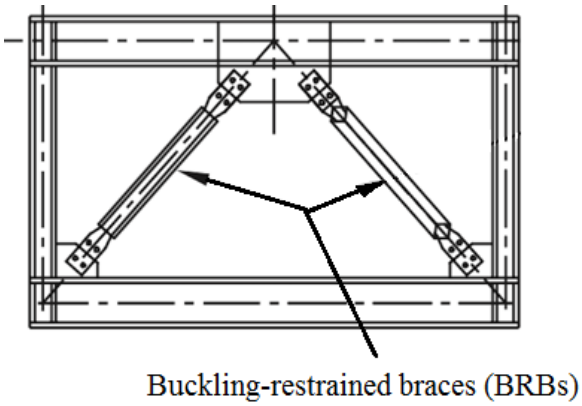

Figure 2.7 Local details of BRB configuration in a frame (Taranath, 2011)

2.4.3 Existing experimental studies of BRBs and BRBFs

During the period from 1970s to 1990s, many experiments were conducted under a collaborative effort between the Tokyo Institute of Technology and the Nippon Steel Corporation in Japan (Hussain, 2006). Although most of their reports are in Japanese and/or have not been published in scientific journals, relevant test set-up and results can be found from citations of other researchers (Black et al., 2002; Xie 2005; Hussain et al., 2006; Della Corte et al., 2011).

Specifically in 1973, pioneering studies conducted by Wakabayashi et al. (as cited in Xie, 2005) tested BRB specimens with various de-bonding materials through pull-out

experiments. In later tests they adopted epoxy resin as the de-bonding material.

In order to determine the buckling-proof behaviour, fourteen specimens were tested on the shaking table (Figure 2.8 (a)). The recorded hysteretic loops of a BRB specimen is displayed in Figure 2.8 (b), which can be referred to the typical curve introduced in Figure 2.3 (d). This spindle shape established by Wakabayashi et al. (as cited in Xie, 2005) indicates similar responses of the BRB specimen when subjected to compressive and tensile loadings.

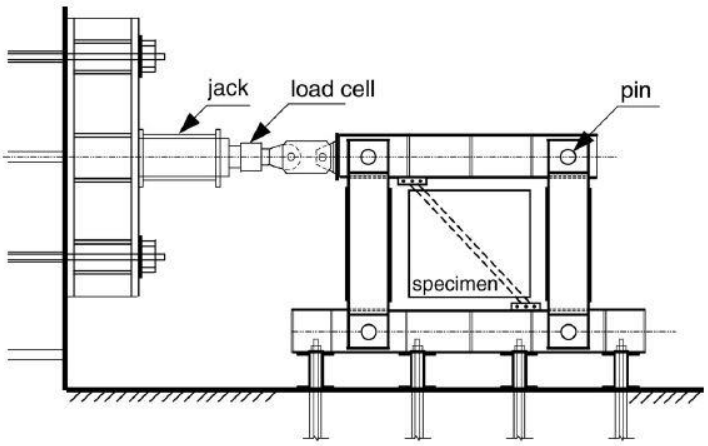

(a) Shaking table test

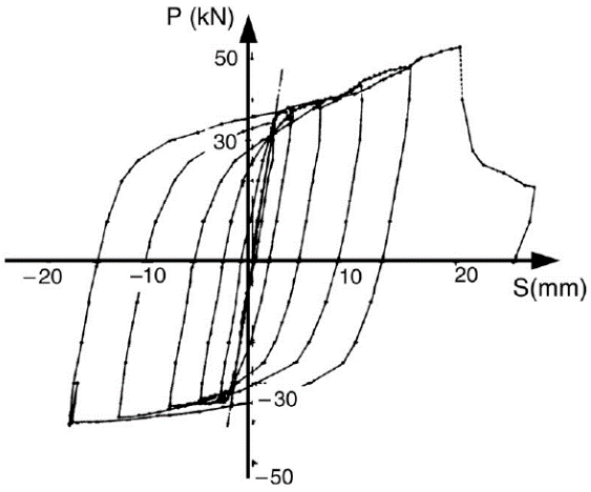

(b) BRB behaviour

Figure 2.8 1/5-scale BRB specimens tests and the hysteresis behaviour (as cited in Xie, 2005)

For the sake of verifying the behaviour of BRBs in the real case, two half-scale BRBFs were tested (Figure 2.9 (a)) (as cited in Xie, 2005). BRBs in the two-storey two-span experimental frame have shown a similar behaviour to the previously tested fourteen BRB specimens. As a typical result shown in Figure 2.9 (b), all BRBs have exhibited hysteretic curves of spindle shape and high energy dissipation ability.

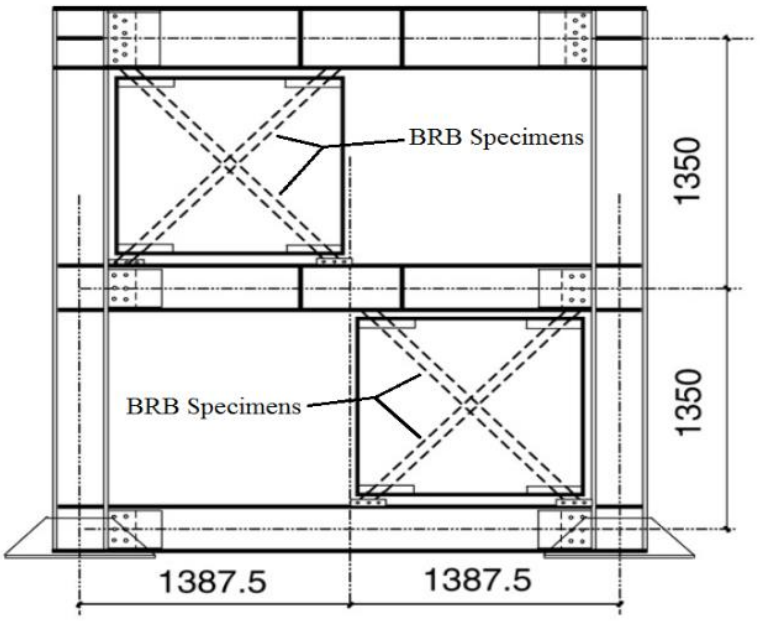

(a) BRBF test (units: *mm*)

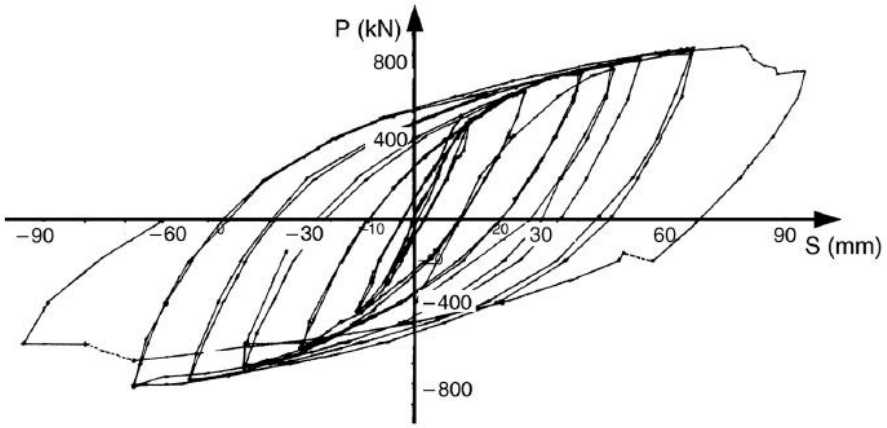

(b) BRB behaviour

Figure 2.9 Tests of half-scale BRBFs and the hysteresis behaviour (as cited in Xie, 2005)

Subsequently, Watanabe et al. (Watanabe et al., 1988) tested five BRB specimens to investigate the influences of diversified casing size of BRBs with same core plate size. Testing results indicated that buckling still occurred in specimens when the buckling Euler yield load P_E of the infilled concrete is lower than the actual yield load P_Y of the core steel plate. To provide adequate stiffness, these researchers recommended a P_E/ P_Y ratio greater than 1.5 in the BRB design.

Hasegawa et al. (as cited in Black et al., 2002) conducted tests on BRB specimens. The load inputs adopted by the experiments were different from previous studies, i.e., real ground motion records rather than artificial cyclic loadings. The ground motions were recorded by Kobe Marine Observatory in 1995 Kobe and 1940 El earthquake. The researchers reported that stable symmetrical hysteresis behaviour of BRBs was recorded throughout the tests.

Konomi et al. (as cited in Black et al., 2002) reported numerous tests on both BRBs and BRBFs. Their studies was motivated by the observed brittle fracture of some moment connections after the 1995 Kobe earthquake. The event authenticated that the design capacity of welded connections cannot always be achieved through inelastic deformation, and the energy dissipation amount may not be adequate. Their study investigated the effect of adding BRBs to moment-resisting frames which were specifically included to dissipate energy through plastic deformation. The tests indicated that the BRBs were able to absorb almost all earthquake energy, and the performance of the frame with BRBs was much greater than those with conventional braces.

Black et al. (2002) reported the BRB specimen tests conducted for the first BRB implementation in the US. Cumulative Plastic Ductility ratios (CPD, the cumulative plastic axial deformation over the yield deformation) were defined in the report to evaluate the deformation capacity of BRBs (Eq. (2-1)).

$$CPD = \sum_i \frac{\left|u_{p_i}^{max} - u_{p_i}^{min}\right|}{u_y} \quad (2\text{-}1)$$

where $u_{p_i}^{max}$ and $u_{p_i}^{min}$ are the maximum and minimum plastic axial deformations during each loop *i* into the inelastic range and u_y is the yield displacement of the brace. In the tests, the maximum CPD of the specimen was found to be very large and reached an average value of around 1000 (Black et al., 2002; Merritt et al., 2003). This demonstrated that BRBs can provide buildings with seismic resistance to more than one frequent earthquake.

In 2010, a series of cyclic loading tests on a BRBF was carried out at the Taiwan National Centre for Research on Earthquake Engineering (NCREE) (Lin et al., 2012). The tested full-scale BRBF was a three-storey single-bay frame with six BRBs equipped, as shown in Figure 2.10. In this BRBF, apart from the bolted beam-column connections in the first floor, all the other BRB-column and beam-column connections were welded. For each BRB, the cross-sectional area was 1110 mm^2 (15×74 mm) and the yield strength of the core plate was 383 kN. The test results showed that the inter-storey drift demands were relatively small, and the frame responses from the tests were satisfactorily predicted by numerical models using OpenSees. It was found that the bulging resistance of the steel casing can be computed from an equivalent beam model which is constructed based on the geometric configurations of the BRB. This research also concluded with recommendations on the seismic design of thin BRB steel casings against local bulging failure. Details of the test set up and the relevant test results will be given in Chapter 3, Section 3.3.4 when validating the numerical methodology proposed in this study.

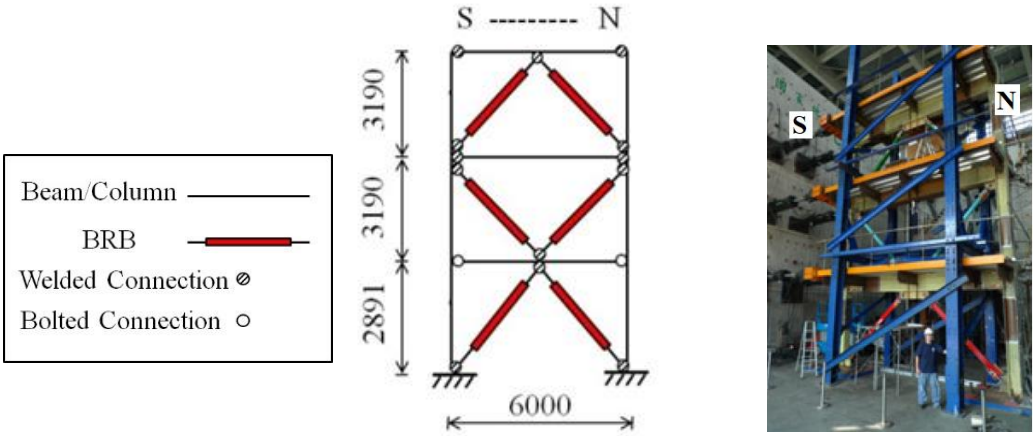

(a) Frame model (b) Test set up

Figure 2.10 Experiments at NCREE (Lin et al., 2012) (Unit: mm)

Sabelli et al. (2003) discussed the mechanical benefits of BRBs and BRBFs, and assessed the performance of several three- and six-storey concentrically braced buildings which utilize BRBs. The models were analysed by using the time-history method, adopting a set of ground motion records. A case of six-storey model was reported in detail. The results showed that the behaviour of the studied frames with BRBs is satisfactorily predicted in terms of structural responses, and the application of BRBs is proven to be capable of preventing buckling failure which is often encountered in conventional concentric braced frames.

Based on Sabelli et al. (2003)'s study, Kiggins and Uang (2006) brought up a dual system of BRBF which consists of BRBFs and moment-resisting bays, to reduce the permanent drift caused by significant earthquake shaking. In order to improve the BRBF system discussed in Sabelli et al. (2003)'s research (Figure 2.11), the moment-resisting frames were designed as a backup system, shown in Figure 2.12. Nonlinear time-history analysis was conducted to assess the performance of the dual system. It was revealed that the system had a 10% -12% reduction of the storey drift ratio. Although the ductility is only slightly reduced, the reduction of the residual drift is significant.

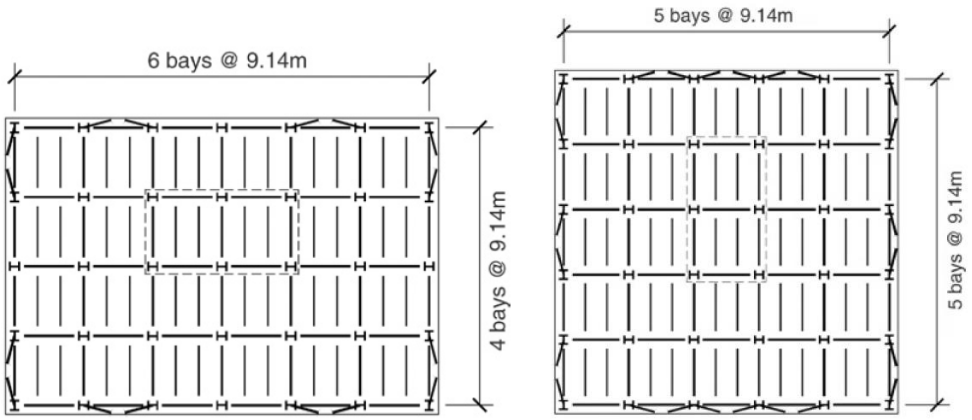

(a) 3-storey building (b) 6-storey building

Figure 2.11 The frame system discussed in Sabelli et al. (2003)

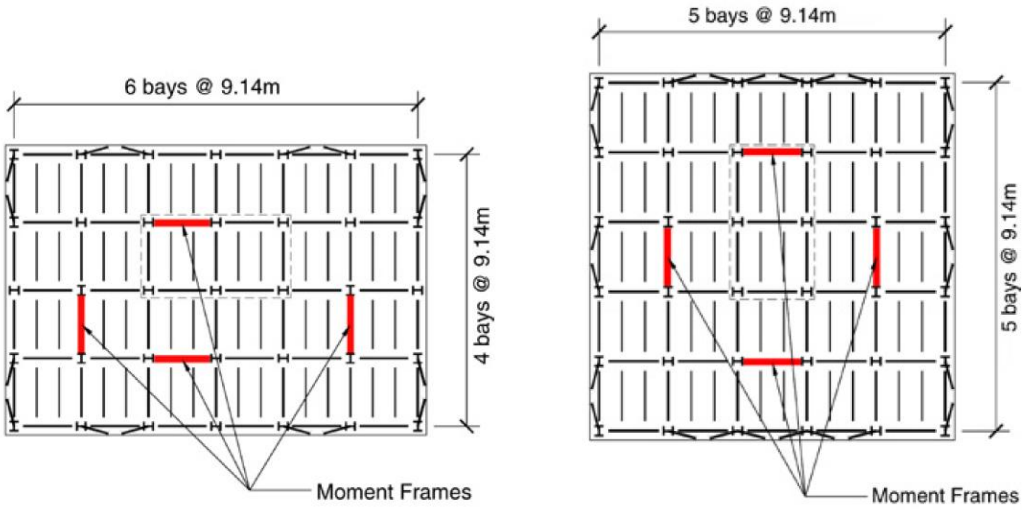

(a) 3-storey building (b) 6-storey building

Figure 2.12 The dual system proposed in Kiggins and Uang (2006)'s research

Fahnestock et al. (2007) reviewed the previously conducted large-scale BRBF tests, and concluded that those tests have exhibited poor performance in storey drifts of between 0.02 and 0.025 rad. Their study also indicated that large stiffness of the typical beam-column-brace connection leads to large flexural demands causing undesirable failure modes. Therefore, an improved BRBF was properly designed, by modifying the beam-column-brace connection details, to achieve more desirable structural behaviours of BRBFs. The improved BRBF was tested by using a hybrid pseudo dynamic testing method. According to the test results, the storey drift was found to be significantly

reduced and the BRBs exhibited excellent performance without producing any stiffness or strength degradation.

Palmer et al. (2012) presented experimental tests on a 3-demensional (3D) special concentrically-braced frame (SCBF) and a BRBF, both are 2-story, 1 bay by 1 bay frames, under bi-directional loading. The results showed that when comparing to the SCBF, the BRBF had much severe damage in the beams and columns because of its large structural deformations. The research also indicated that the impact of bi-directional loading on the structural response was minimal. Later in 2014, the same researchers summarised the said 3D test on BRBF and planar (2D) tests on six single-story, 1-bay BRBFs (Palmer et al., 2014; Christopulos, 2005), and concluded that although the hysteretic behaviour of the BRBFs was good, the severe damage and instability may occur at large storey drifts.

Jia et al. (2014) tested a 1/3 scaled 2-storey 1 bay buckling restrained braced composite frame (BRBCF) system. The tested frame consists of concrete-filled steel columns with circular hollow section, steel beams and BRBs. For comparison, a simple bare composite frame (CF) without BRBs was also tested. The BRBCF exhibited no strength or stiffness degradation under the large drift imposed by the cyclic test, which indicated a good ductility and energy dissipation capacity. The tests also showed damage in the beam-column-BRB connection region, an issue which was recommended to be considered in the design of BRBCF. It was also suggested that the maximum frame drift of the tested frame before failure was governed by the rotational capacity of the beam-column-BRB connections, not the axial deformation of the BRB.

Ozcelik et al. (2017) tested 10 BRBs including conventional BRBs and BRBs with new end restraints (steel hollow section and steel plates used as an additional restraint mechanism at both ends). According to the test results, the stiffness of the BRBs were consequently improved and the new restraints allow the BRBs to demonstrate a stable hysteretic behaviour, therefore the out-of-plane buckling at both ends could be effectively resisted.

2.4.4 Existing numerical studies of BRBs and BRBFs

Over the past decades, research on the seismic performance of BRBFs have been carried out through finite element method based numerical approaches. Software packages OpenSees (Mazzoni et al., 2006) and DRAIN-2DX (Prakash et al., 1993) are the most in use and trustworthy tools for simulating the overall behaviour of BRBFs under seismic conditions. In general, with the abovementioned simulation platforms, fibre elements are often used to model the columns and wide flange beams, and the inelastic truss element are commonly adopted to model the BRBs in the numerical model, unless otherwise specified.

In early studies (Clark et al., 1999; Sabelli et al., 2003), a few shortcomings of BRBFs were pointed out. Specifically, due to the low post-yield stiffness of BRBs, BRBFs were found to likely have large residual drifts and a concentration of plastic deformation demand at one story. To solve these problems, Kiggins and Uang (2006) proposed a dual system which contains both BRBFs and special moment-resisting frames (SMRFs), to provide more post-yield stiffness therefore reducing the residual drifts. In their numerical models, the axial compressive strengths of the braces were set to be 110% of their tensile counterparts, and the post-yield stiffnesses were conservatively set to be zero. Nonlinear time-history analysis was carried out using the computer program DRAIN-2DX (Prakash et al., 1993) on 3- and 6-story models to investigate the seismic performance of the dual system proposed by Kiggins and Uang (2006). The numerical results demonstrated that the maximum storey drift ratio was reduced by about 10% to 12% when the dual system was used. Moreover, the addition of the moment-resisting frames significantly reduced the permanent storey drifts of the BRBF. Ariyaratana and Fahnestock (2011) also investigated the performance of the dual systems mentioned above. Non-linear time history analysis was adopted using OpenSees to evaluate the seismic responses of four 7-storey BRBFs and dual BRBF-SMRFs. The results further proved that using MRFs assembled in parallel with BRBFs is an effective way of reducing residual drifts.

The maximum expected ductility demand for braces is another issue questioned by researchers. Fahnestock et al. (2003) studied the responses of a four-storey BRBF using DRAIN-2DX. In their numerical model, rigid offsets were used at the ends of the beams and columns to account for the rigidity of their panel zones. Moreover, the isotropic hardening was considered in the modelling of BRBs. The time-history analysis results showed that BRB maximum ductility demands can be as high as 20 to 25, which exceed the maximum value of 7.5 anticipated by the recommended provisions of BRBFs. The cumulative brace ductility demand, according to the same researchers, reached up to 99 under the design earthquake intensity and 171 under the maximum expected earthquake intensity. These values are much less than the cumulative ductility capacity of 400 obtained from the existing experimental results. The demand/capacity ratio 171/400=0.43 suggests that seismic design of BRBs is not governed by low-cycle fatigue phenomena.

Korzekwa and Tremblay (2009) conducted a 3D finite element analysis to reproduce the cyclic inelastic behaviour of an all-steel buckling restrained brace test specimen using ABAQUS (Hibbett et al., 1998). In their numerical models, the ductile core and the buckling restraining mechanism were modelled using 20-node C3D20 quadratic brick elements and the bolts connecting the guide plates were modelled using infinitely stiff springs, thus the global and local stiffness of the brace can be both represented realistically. The contact forces between the brace core and the casing were found to be resisted in flexure by the casing, and were the cause of longitudinal frictional forces that induced axial compressive forces in the casing when imposing the displacement cycles in compression.

López-Almansa et al. (2012) proposed a series of mechanics-based numerical models of the cyclic behaviour of BRBs which composed of a steel core embedded in a mortar or steel casing. To reproduce the accurate BRB behaviours, three models were proposed in software package ABAQUS (Hibbett et al., 1998). The first model considering the

multiaxial plasticity and isotropic damage with a large displacement formulation was created to describe the steel core. The second and the third models, i.e. an isotropic damage model and a contact penalty model, were developed respectively to simulate the behaviour of the mortar and interface sliding. The results of a number of simulations verified the ability of the proposed models, and the accuracy of the modelling approach was further proved by the comparison with their two sets of experimental results.

Eatherton et al. (2014) conducted a numerical study to investigate how the self-centring BRB (SC-BRB) performs in real construction. The SC-BRB was implemented by using concentric tubes held flush with pretensioned shape memory alloy (SMA) rods, in conjunction with a BRB that dissipates seismic energy. A nonlinear model was developed using the OpenSees (Mazzoni et al., 2006) to simulate the cyclic behaviour of the SC-BRB. Specifically, a hysteretic material model considering the residual strain was developed for SMA. The SC-BRB with large self-centring ratios (as large as 4) was found to dissipate sufficient earthquake energy when computationally subjected to a suite of ground motions. Furthermore, it was shown that the self-centring ratio for the most efficient SC-BRBF design should be in a low range between 0.5 and 1.5.

Hoveidae et al. (2015) numerically investigated BRBFs assembled with short core BRBs which are expected to be easily fabricated, inspected and replaced after a severe earthquake. It was proposed that the reduced core length in a BRB might reduce the frictional forces acting at the core and buckling restraining mechanism interface, therefore reduce the compression strength adjustment factor in the brace. Nonlinear time history analyses were conducted using ETABS (Habibullah, 1989) on 4- and 10-storey buildings equipped with short core BRBs, as well as full core (conventional) BRBs for comparison. The minimum core length of the BRB was determined by considering the low cycle fatigue life of the core plate and the maximum anticipated strain demand under standard loading protocol. The numerical results demonstrated that the short core BRB system was able to partially reduce the storey and residual storey drifts in the braced frames.

2.4.5 Design methods and standards

In this section, the available design methods including code methods and other recommended design procedures are introduced as follows.

AISC 2010 ((AISC 2010), also known as the 2010 edition of "Seismic Provisions for Structural Steel Buildings" published by the American Institute of Steel Construction (AISC), gives design rules for BRBFs. However, it specifies testing of BRBs as a method of quality control. The testing is to ensure conformance of requirements in both strength and deformation for the BRBs selected for a project. It should be noted that various factors affecting the seismic performance of BRBs in BRBFs within different structural systems are not well understood, therefore the requirement for testing is intended to provide assurance that the BRBs will function as expected.

In the design procedure of a BRBF, the balance between the design yield force of the BRB and the expected increase in plastic deformation of the brace should be considered (Della Corte et al., 2011). The design yield force is typically calculated by dividing the elastic seismic demand with a specific factor, which should be carefully considered based on the deformation capacity of the BRB. Eurocode 8 (EN 1998-1, 2004) uses the behaviour factor q, while AISC 2010 Seismic Provisions (AISC 341-10) uses the response modification factor R for this purpose.

In addition to an appropriate BRB design, experimental and numerical studies (Fahnestock et al., 2007) carried out in recent years suggested that the prevention of inelastic deformation of other frame element is important to improve the global mechanism of BRBF. The elements that are expected to remain elastic are required to have sufficient high capacity, which has formed the basis of BRBF design in AISC 2010 (Della Corte et al., 2011).

Several European studies (Bosco and Marino, 2013, Bosco et al., 2015) have been

focused on developing a design procedure and recommended behaviour factors for European application of BRBFs. However, Zsarnóczay and Vigh (2017) mentioned that these studies are lacking breadth as the seismic evaluation should cover various environment. Vigh et al. (2017) proposed a design procedure for BRBF and provided the seismic design parameters and capacity design rules by enhancing Eurocode 8 specifications on steel concentrically braced frames. Rules for static and dynamic analyses, calculation of material and structural overstrength, unbalanced loads, braced frame column sections and a BRBF-specific behaviour factor were the major concerns in Vigh et al. (2017)'s study.

Apart from the classical code-specified design procedures, the performance-based design methods also serve as alternatives for the BRBF design. Choi and Kim (2006) proposed an energy-based design procedure for BRBF using hysteretic spectra and accumulated ductility spectra. The advantage of using this method is that the inter-storey drifts are uniform over the structure height, which results in uniform damage distribution.

A displacement-based design method for braced steel structures and dual systems incorporating moment-resisting frames and BRBFs was developed (Della Corte et al., 2010; Maley et al., 2010) to provide an alternative design method. This methodology has been proven to offer the possibility of having direct and better control of the level of seismic damage.

2.5 Concluding Remarks

In this chapter, a review of the literature was presented focusing on the three main components of the prefabricated system: prefabricated buildings, the bolted beam-column connections and BRBs/BRBFs. An overview of prefabricated buildings was first carried out. Then the classification of bolted beam-column connections were introduced, followed by the review of existing analysis methods for connections and

relative research of the main types of bolted connections by using these methods. Subsequently, the development of BRBs and BRBFs were discussed in the following aspects: (1) different types of BRBs; (2) experimental and numerical studies of BRBs/BRBFs; (3) general design methods for BRBFs.

Surveying the literature shows that the studies and application of prefabrication in steel building structures are still limited, this emphasizes the necessity of the present study. Moreover, end-plate connections, fin-plate connections and top- and seated-connections are widely used in practice, which can be employed in the proposed prefabricated system. It should be noted that web-angle connections are not chosen in this study due to their similarity to the fin-plate connections. The studies on BRBFs demonstrate their good energy dissipation capability in seismic regions, however, research on prefabricated BRBF with non-moment-resisting frame system is limited. Therefore, in-depth study is expected to assess the seismic performance and vulnerability of the proposed prefabricated system.

In summary, although the existing experimental and numerical studies are not typically focussed on prefabricated BRBF and non-moment-resisting frame systems, the research outputs being reviewed are considered a valuable source which will provide a useful guidance to the proposed experimental tests and numerical investigations introduced in Chapters 4 and 6. Note that the relevant published literature in fragility analysis will be reviewed and discussed in Chapter 7 with detailed methodology and analysis procedure, to better support the fragility assessment of the proposed structural system.

CHAPTER 3

ANALYTICAL APPROACH

3.1 General Remarks

This project mainly consists of analytical study and experimental study. Specifically, finite element method (FEM) is used for the analytical study. FEM, as a widely used numerical simulation technique to determine boundary value problem solutions, disperses a continuous object with infinite degrees of freedom into problem of finite degrees of freedom. The obtained results by using FEM always provide engineers approximate solution. Thus, in this study the FEM results will be verified against existing experimental results.

Software packages ABAQUS (Hibbett et al., 1998) and OpenSees (McKenna et al., 2006) are adopted for the numerical investigation of the rotational stiffness of beam-column connections and structural seismic behaviour of the proposed system, respectively. In this Chapter, the basics of modelling connections in ABAQUS are discussed. Rotational capacity responses of three different type of bolted connections employed in the proposed system using ABAQUS is presented. Subsequently, the numerical modelling technics by using OpenSees for investigating the proposed system are developed and validated against an existing experimental study.

3.2 Finite Element Analysis of the Connections in ABAQUS

In this section, analysis of the rotational capacity of the connections employed in the proposed system is discussed. FEM software ABAQUS is used for the simulation. The modelling procedure is introduced, followed by the modelling details: mesh, boundary and loading conditions, interactions and material properties etc. Subsequently, the non-linear material and geometric analysis is applied to obtain the rotational stiffness of (1) the designed bolted end plate connection, (2) the fin plate connection and (3) the top- and seat- angle connection.

3.2.1 Basic concepts

To establish a finite element model in ABAQUS, (1) parts need to be created separately in the part module, (2) different material properties may need to be defined in the property module, (3) the model is assembled in the assembly module by combining different parts, (4) in the interaction module the parts are connected to each other using constraints by defining the degrees of freedom to be connected with another part. In this module, interactions such as friction behaviour can be defined; (5) the loads acting on the model are defined in the load module, as well as boundary conditions. (6) The model is then meshed in the mesh module depending on the element type and the geometry of the model.

The FEM procedure in ABAQUS consists of (a) pre-processing which is to establish finite element models, (b) computational analysis of the established models, (c) post-processing of the modelling results, as depicted in the flow-chart of Figure 3.1.

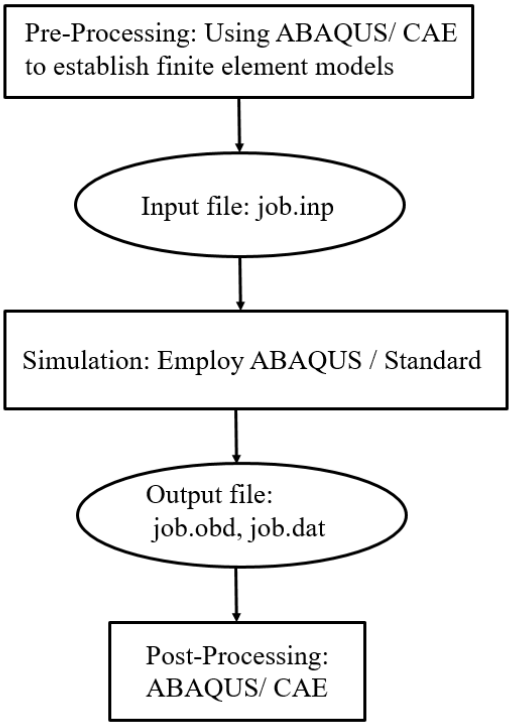

Figure 3.1 ABAQUS analysis process flow chart

In the present study, ABAQUS is used to obtain the moment-rotation behaviour of the connections, and is later used to model the connections in the BRB frames using OpenSees.

3.2.2 Geometric dimensions

Three different types of bolted connections: (1) fin-plate connection, (2) end-plate connection and (3) top- and seat-angle connections are designed following EC3 (CEN 2005), as the pinned connections are not expected to have moment transfer capacity, the design criteria of the connections is just to satisfy the structural requirements. As shown in Figure 3.2 (a), the fin-plate connection consists of a rectangular fin-plate welded to the column, and bolted to the web of the beam by six bolts. The end plate connection (Figure 3.2(b)) is made up of a rectangular plate welded to the beam web initially, and bolted to the column flange. The top- and seat-angle connection (Figure 3.2(c)) has two angles connecting the top and bottom beam flanges to the column flange by bolts. The beams and columns used in all connections are H-shape steel, and for the

ease of comparison, the dimensions are the same in all the simulated connections. The class for all bolts analysed in this study are Grade 5.6 and the diameter of each bolt is 20*mm*. The lengths of the column and the beam are set as 1000*mm* and 500*mm*, respectively. Detailed dimensions of the model are listed in Table 3.1.

Table 3.1 Detailed dimensions of the models

Element	Parameters	Values (mm)
Beam	Depth	400
	Web depth	374
	Flange width	200
	Flange thickness	13
	Web thickness	8
Column	Depth	500
	Web depth	460
	Flange width	500
	Flange thickness	20
	Web thickness	16
Fin-plate	Depth	310
	Width	220
	Thickness	10
End-plate	Depth	310
	Width	220
	Thickness	10
Top and seat angle	Width	160
	Thickness	10
	Length	220

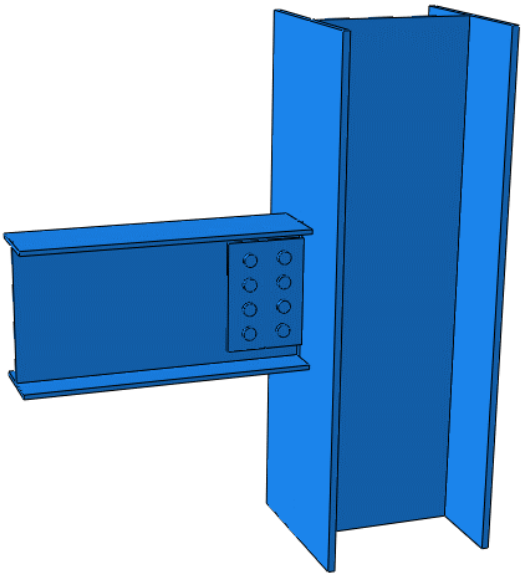

(a) Fin-plate connection

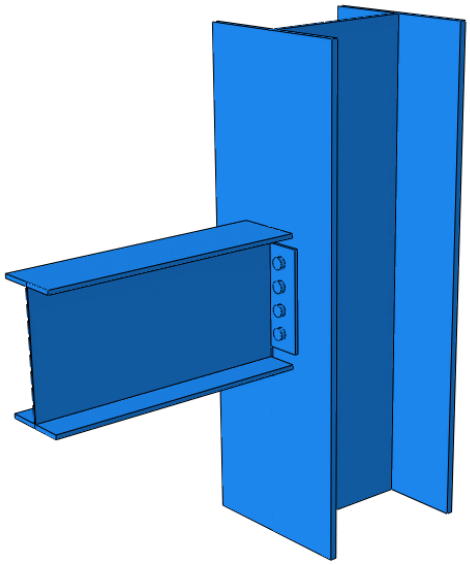

(b) End-plate connection

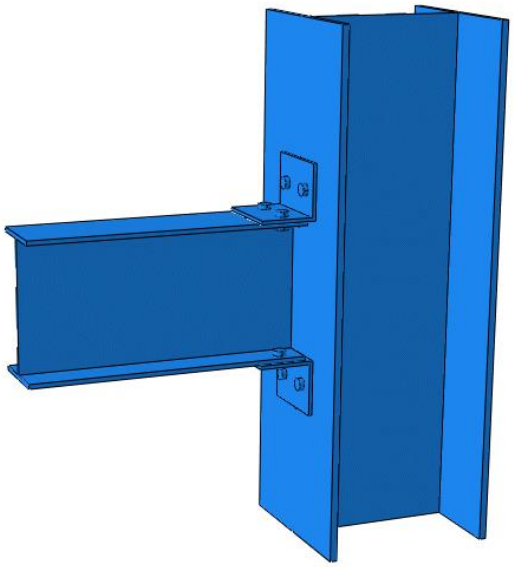

(c) Top- and seat-angle connection

Figure 3.2 Configuration of the designed fin-plate connection/*mm*

3.2.3 Modelling techniques

The modelling procedures used in this study adopt Citipitioglu et al. (2002)'s approach for 3D FEM analysis of bolted steel beam-column connections, which had been validated with existing experimental study (Azizinamini et al. 1985). The detailed techniques are describes as follows:

Non-linear 3D continuum elements are used for all parts of the connections. Specifically, shell element (S8R5W) is employed for the specimens to capture the bending-donated issues more effectively. Six-node wedge elements (C3D6) are also used to model the core of the bolts. In a developed model, the accuracy of the simulation largely depends on the mesh size. A finer mesh usually increases the accuracy of the model. In this study, the mesh size for the end plate, fin plate and angles is taken as w/20, where w is the width of the plates (for the angles, w is the width of an angle on one side).

The surface to surface contact is also applied to the models. The contact areas are the bolt shank-to-bolt holes and bolt head-to-components. The bolts clamp the components

together in order to resist the applied rotation. The formulation used for the surface-to-surface contact involves a "master-slave" type algorithm (Hibbitt et al., 1993), the selection of master and slave surfaces is essential as it is directly related to the simulation accuracy and convergence. In general, it is best to choose the bigger, stiffer, and coarser-meshed body as the master surface. The coefficient of friction for the contact surface between the fin-plate and beam web is taken as 0.44 (AISC, 1995). The initially welding points are simulated using tie contact to ensure the same value of displacement at the contacting surfaces.

Figure 3.3 shows the schematic diagram of the connections, the boundary condition, and the loading conditions. A pin support is assumed to restrain the top and bottom of the column, while the beam is restrained by a vertical roller. A 15*mm* downward prescribed displacement is applied to the restrained boundary of the beam, in order to generate a bending moment to the connection. Note that the boundary and loading conditions of the fin-plate connection shown in Figure 3.3 (a) are identical with the end-plate connection and top- and seat-angle connection.

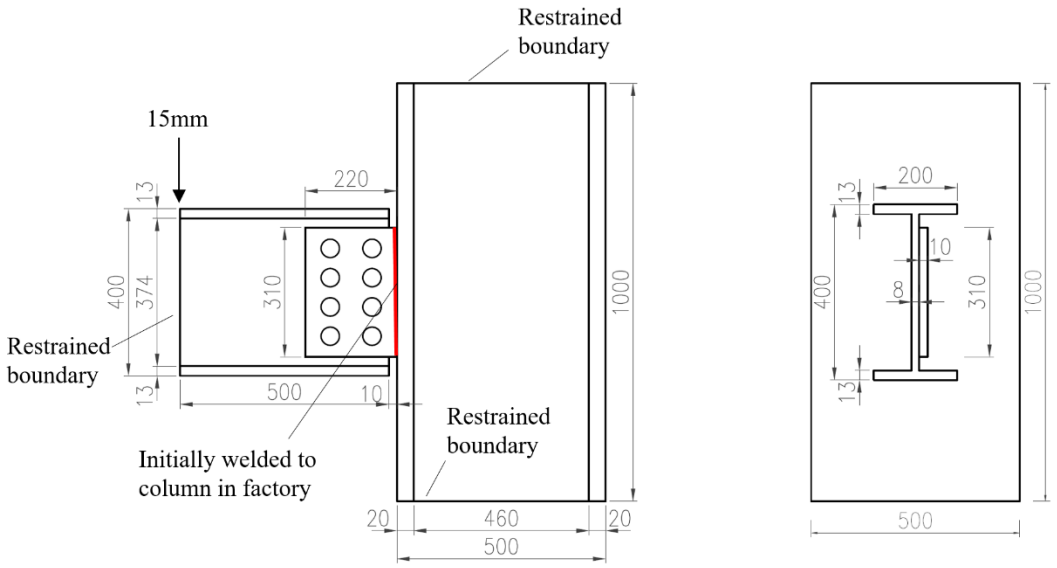

(a) fin-plate connection

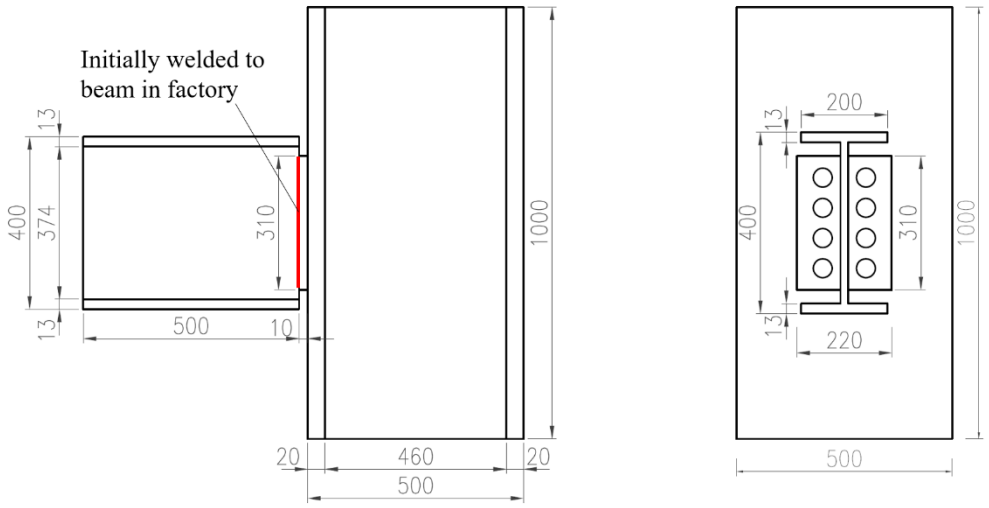

(b) end-plate connection

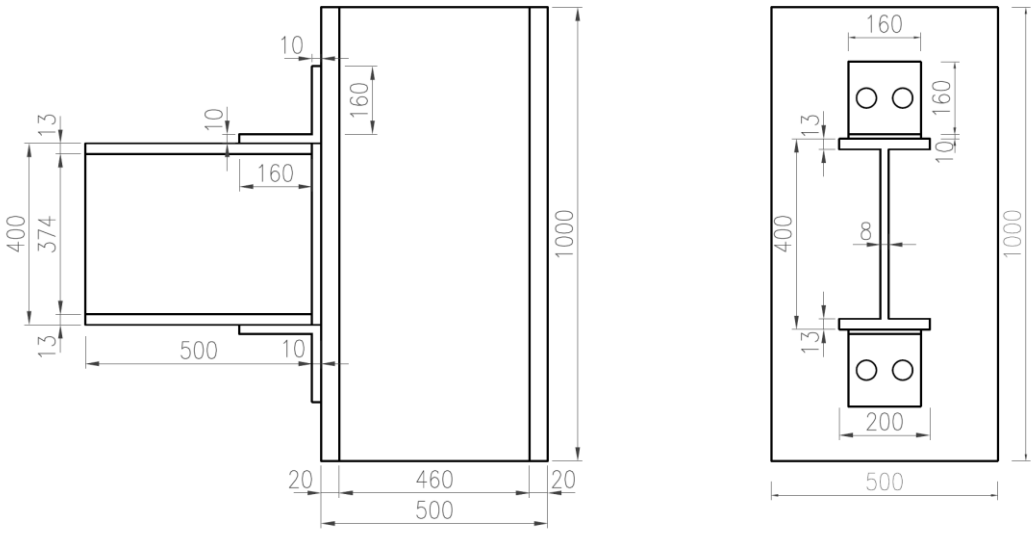

(c) top- and seat-angle connection

Figure 3.3 Configuration of the designed connections/*mm*

3.2.4 Material properties

Steel is a relatively ideal homogeneous material, its mechanical properties of compression and tension are basically the same. To describe its constitutive relationship accurately, von Mises yield criterion and associated flow rule are usually adopted in numerical analysis. The commonly used steel constitutive models in ABAQUS include ideal elastic model, bilinear model, trilinear model and full-curve model. In this study,

classic bilinear model is adopted (Citipitioglu et al., 2012), the steel constitutive model is shown in Figure 3.4, and parameters of the model are listed in Table 3.2. Note that the initial elastic tangent E_0 is taken as 206 *GPa*, and the strain-hardening ratio, b (ratio between post-yield tangent and initial elastic tangent) is taken as 0.001 (Krauss, 1999).

Table 3.2 Properties of materials

Material	Yield strength (f_y/*MPa*)	Ultimate strength (f_u/*MPa*)
Steel members	235	375
Bolts	300	500

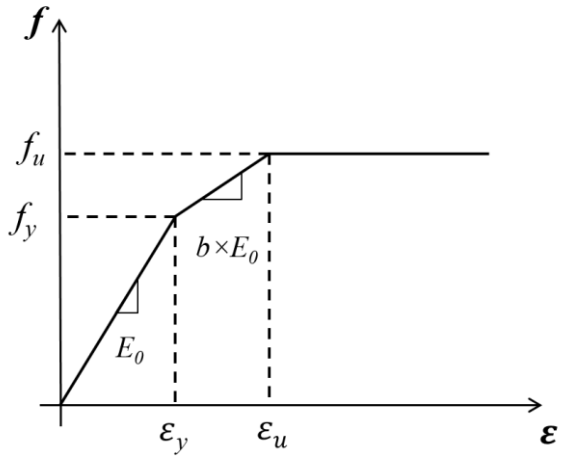

Figure 3.4 Stress-strain curve of steel

3.2.5 Modelling results and discussion

Figure 3.5 shows the von-Mises stress distribution and the deformed shape of the connection under the action of the prescribed displacement for the three connections respectively. For each connection, the stresses within the connection are generally low except at very few points, which indicates a relatively weak moment-transfer capability of the connection. Specifically, the highest stress of the fin-plate connection distributes at the pin plate around the bolts position. For end-plate connection, it happens at the junction between the beam web and end plate. For the top- and seat- connection, the stress reaches the highest values at the corner position of the angles.

The rotational stiffness comparison of the connections are plotted in Figure 3.6. It can be observed from the figures that the actual connection moments for each connection are 34*kNm*, 29*kNm*, 22*kNm* respectively. The fin plate connection shows the best moment transfer capacity while the top- and seat- angle connection behaves the weakest moment-rotation relationship. As mentioned in Chapter 2, *Eurocode3 Part1.8 (EC3)* (CEN 2005) classified joints as rigid, nominally pinned or semi-rigid by their stiffness and strength. The classification boundaries in terms of the initial rotational stiffness and strength are shown in Figure 3.7. As can be seen from the figure, a joint is classified as pin connection when the actual connection moment is lower than ¼ of the plastic moment capacity of the beam. In this study, the plastic moment capacity of the beam is 269.8*kNm*, therefore the ¼ of the plastic moment capacity 67.45*kNm* is greater than the maximum actual connection moment of all the connections (34*kNm*). The low connection moments demonstrate the flexibility of the analysed bolted connection as expected. Therefore, the beam-column connections can be assumed as purely pinned when substitute to the entire frame for further study on structural behaviours.

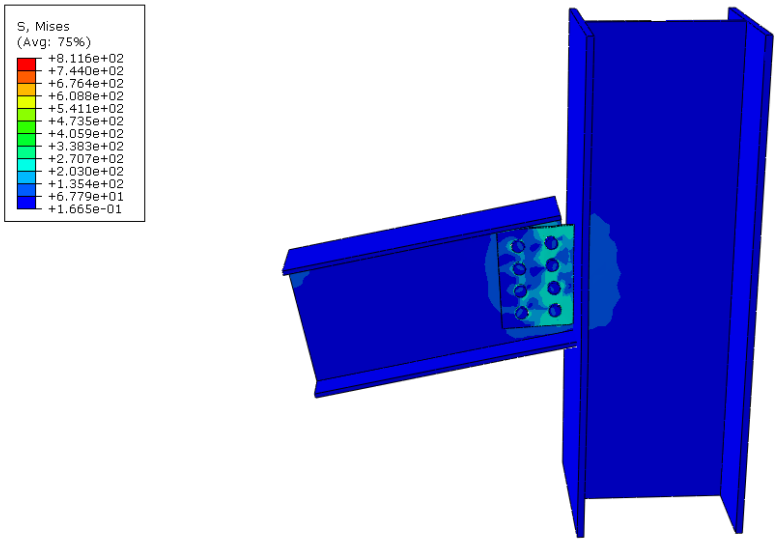

(a) Fin-plate connection

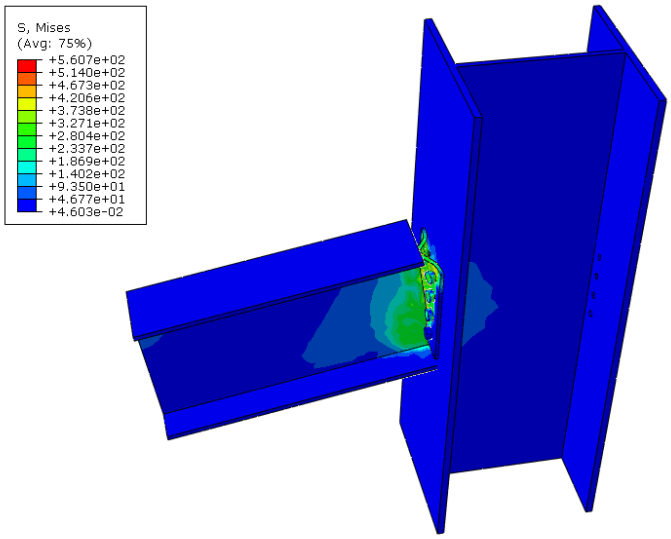

(b) End-plate connection

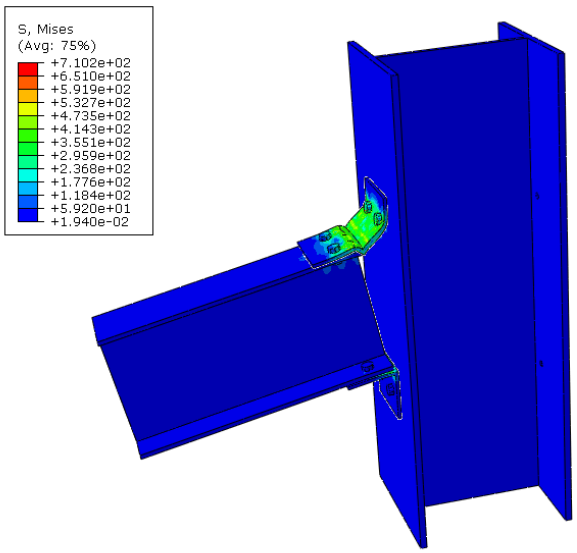

(c) Top- and seat-angle connection

Figure 3.5 von-Mises stress distribution (Unit: *MPa*)

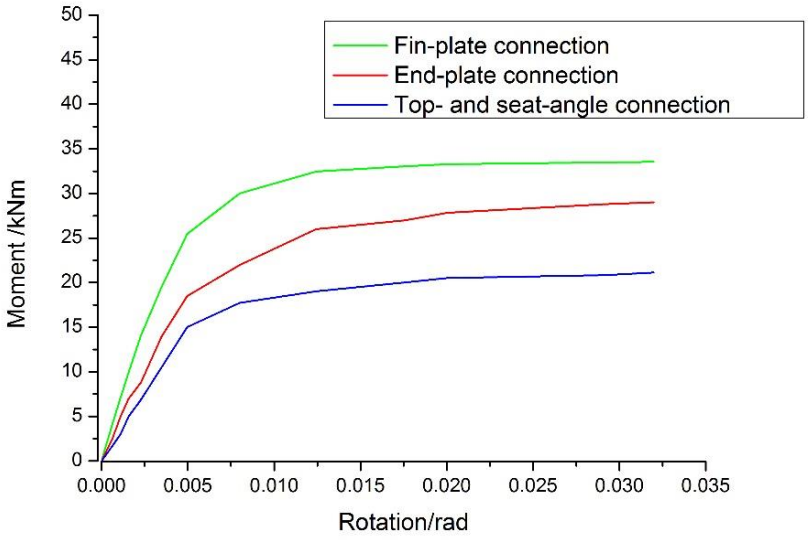

Figure 3.6 Rotational stiffness comparison of modelled connections

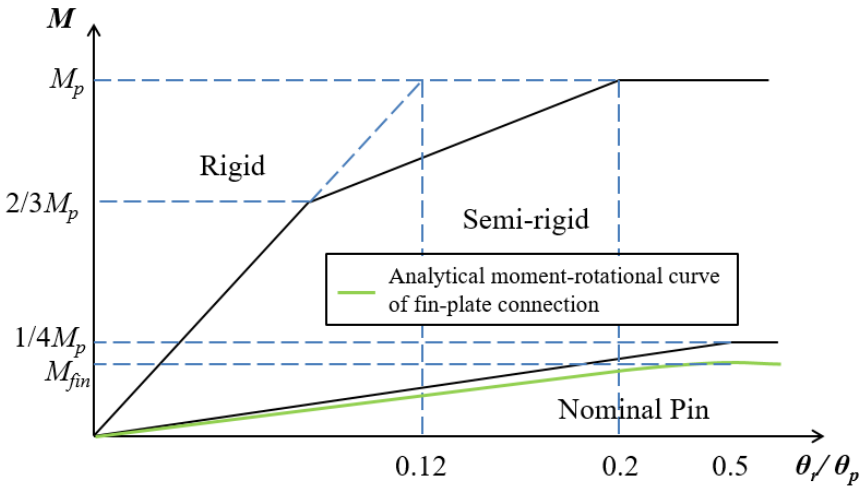

Figure 3.7 *EC3* classification system

Note: M=actual connection moment; M_p=plastic moment capacity of the beam; M_{fin}=the maximum moment transferring capacity of the fin-plate connection; θ_r=actual connection rotation; θ_p=plastic rotation

3.3 Finite Element Analysis of the Proposed System Using OpenSees

This section will initially present a brief overview of the open-source, computational framework Open System for Earthquake Engineering Simulation (OpenSees) (McKenna, 1997; http://opensees.berkeley.edu), then introduces the techniques of modelling procedure for the proposed system. The numerical approach will subsequently be validated by an existing experimental study. Additionally, the experimental models will be designed and examined by the verified methodology.

3.3.1 Basic concepts

OpenSees is an open system that is composed of a series of earthquake engineering simulation application module components. This system is mainly used in the analysis of seismic response of structural and geotechnical systems under seismic action and it has increasingly become one of the most influential open platforms for earthquake engineering research (Lu et al., 2015). The unique feature of OpenSees is that it broke through the traditional research protocols and establishes a novel approach through the developing of the open-source.

3.3.2 Element and material selection

3.3.2.1 Element and section

As a powerful finite element analysis simulation platform, OpenSees provides the user with a variety of elements to choose from. Plane linkage elements as the most widely used elements in OpenSees, mainly consist of zero-length elements, truss elements, beam-column elements, joint elements and so on.

In the present study, 2D models are considered to capture the seismic performance of the proposed system. Force-based beam column elements are used to simulate the main structural components. This element is a nonlinear element based on the iterative force-

based formulation. In this case, it is preferred over the displacement-based beam column element for an improved accuracy of the solution, as well as a faster local and global quantities convergence.

For the beams in the braced bay and all the columns in which the flexure deformations may occur, their sections are divided into discrete fibres for the distribution of plasticity. The main idea of fibre sections is to separate the analysed section into a number of discrete fibre section while neglecting shear deformation. The member section can be assumed to accord with the plane cross-section assumption (that plane cross-sections remain plane and perpendicular to the longitudinal axis after bending), while assuming that the strain of each fibre distributed uniformly in a uniaxial stress-strain state (Mazzoni et al., 2006). Therefore, the force-displacement relationship of the section can be calculated according to the uniaxial stress-strain relationship of fibre material (for this case is the Steel01 material shown in Figure 3.10). For instance, a fibre division of cross section is shown in Figure 3.8.

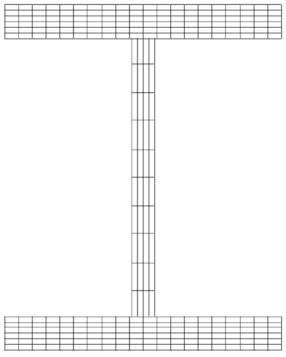

Figure 3.8 Section fibre division

For the beams in the non-braced bays, as they are connected to the columns through pin beam-column connections, the plasticity will hardly occur at the beam ends during loading. Therefore, elastic section (in which the fibre sections are not involved) is considered for a more rapidly computation.

For the pin connections exhibiting zero rotational stiffness, pairs of slave and master nodes are defined at the corresponding beam-column connections and are connected using zero-length spring elements (Figure 3.9). In the spring element, the master and slave nodes share the same translational degrees of freedom to ensure identical kinetic behaviour. Truss elements are used to model BRBs as they are supposed to be hinge connected to the column in reality.

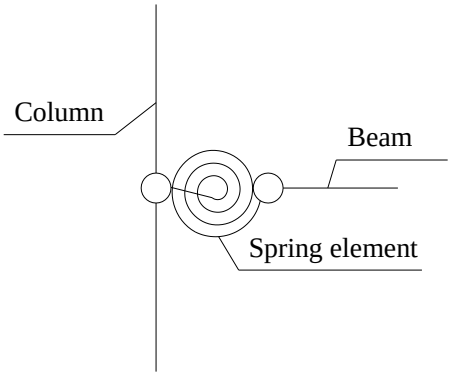

Figure 3.9 Zero-length element model

3.3.2.2 Material

To take into account material nonlinearity, "steel 01" material is applied to simulate beam and column behaviour. Steel01 is a uniaxial bilinear material with kinematic hardening and optional isotropic hardening described by a non-linear evolution equation. As the illustrated constitutive law shown in Figure 3.10, steel 01 model was characterised by parameters consist of initial elastic tangent, E_0; yield stress, f_y ; strain-hardening ratio, b (Heo and Kunnath, 2009).

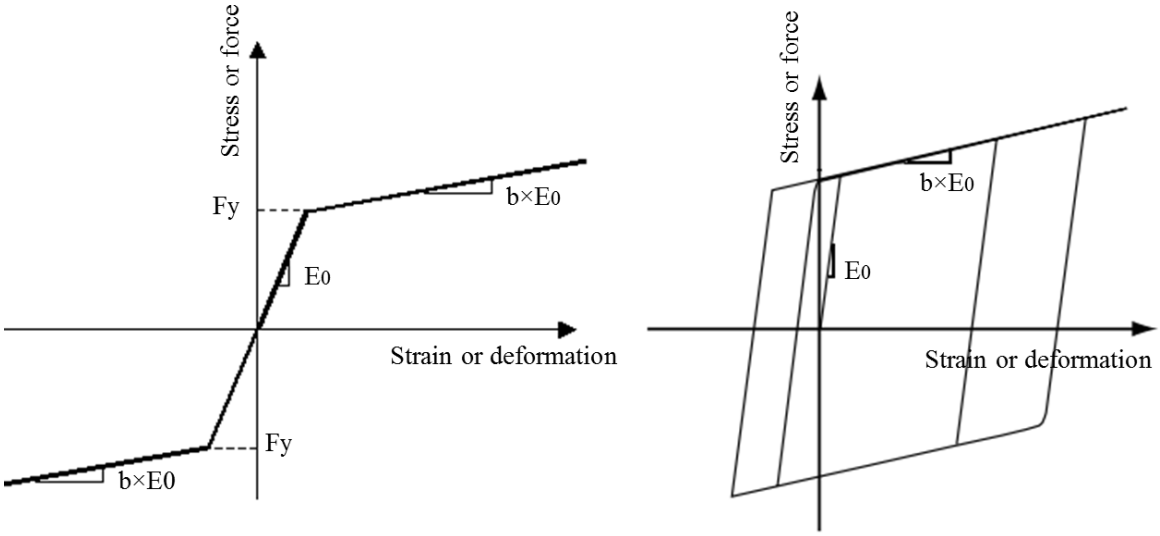

(a) Stress-stain curve (b) Hysteretic response loop

Figure 3.10 Constitutive model of steel 01

In Korzekwa and Tremblay's previous study (2009), it has been proved that BRBs in numerical modelling can be represented by a simple, one-dimensional, pin-ended truss element that has the appropriate effective uniaxial force-displacement properties. Clark et al. (1999) found quite good agreement between experimental and numerical results for a large-scale BRB which in the numerical analysis was represented by a standard Menegotto-Pinto (1973) model.

Therefore, "steel 02" material with hysteretic behaviour in both tension and compression (Uriz and Mahin, 2008) is employed to simulate the BRBs. This OpenSees material was developed following Menegotto-Pinto steel cyclic formulation (1973) with isotropic strain hardening included. The constitutive law of steel 02 (Figure 3.11) is close to bilinear steel 01, but the transition from initial stage to post yielding stage is smoother than steel 01. Moreover, fatigue material is combined with "steel 02" to account for the effects of low cycle fatigue.

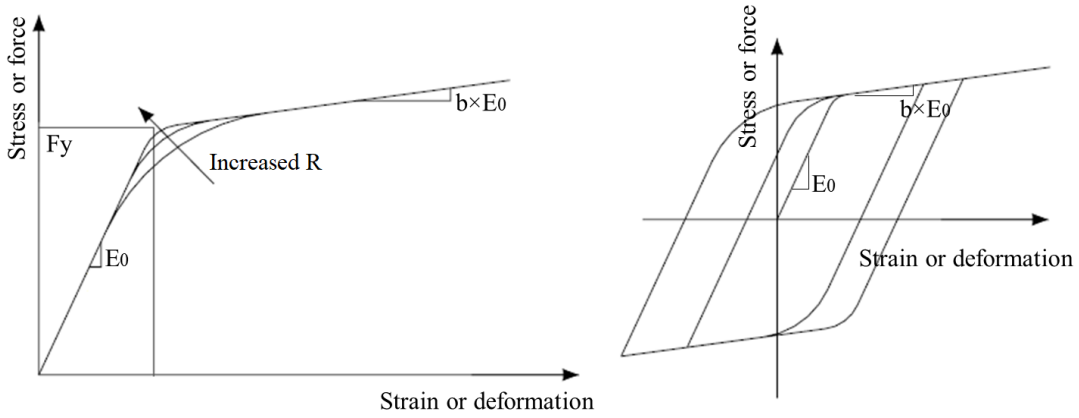

(a) Stress-strain curve (b) Hysteretic response loop

Figure 3.11 Constitutive model of steel 02 (b: strain-hardening ratio (ratio between post-yield tangent and initial elastic tangent), R: parameters to control the transition from elastic to plastic branches.)

3.3.2.3 Coordinate transformation

To capture the P-δ effects (also known as geometric non-linearity) in the columns and BRBs, coordinate transformation is performed to transform the beam element stiffness and the internal forces from the principal coordinate to the global coordinate system.

3.3.3 Nonlinear dynamic analysis method

In this study, the main dynamic analysis method used to examine the structural seismic behaviour is time-history method, which is able to provide nonlinear evaluation of dynamic structural response due to an applied load that varies with time.

3.3.3.1 Time history analysis

Time-history analysis as a nonlinear dynamic analysis, combines the ground motion records with a detailed structural model, applying data over increment steps as a function of acceleration, force, moment or displacement. The structural response at any time can be obtained by integrating equilibrium equations because the eigenvalues generated are based on the time history responses. The closer the spacing of time steps, the more accurate the solution will be. Therefore, this analysis method is recognised to

be a time domain analysis and is capable of producing structural responses with relatively high accuracy.

However, in order to obtain a reliable prediction of probabilistic distribution of structural response, multiple analyses are needed using various ground motion records, for the reason that the calculated response have a very high sensitivity to the characteristics of every single ground motion used as seismic input.

Since the properties of the seismic response are decided by the intensity, or severity, of the seismic shaking, a completed evaluation needs numbers of nonlinear dynamic analyses at different levels of intensity to fulfil the different possibilities of earthquake scenarios (Katsanos et al., 2010).

3.3.3.2 Ground motion record selection and scaling

Since the seismic wave is non-stationary and random, it is affected by its occurrence of the fault location, fracture mode of fault, epicentral distance, geological conditions and many other uncertain factors during wave propagation. Several earthquakes from the same seismic source and spread to the same site are generally different. Even on the same site, with the same seismic intensity, the earthquake acceleration records (peak acceleration, waveform, duration and spectrum) may vary considerably (Naeim et al., 2004).

Different seismic waves can significantly influence the deviation of time-history analysis outputs. The input seismic waves have direct and decisive impact to nonlinear dynamic response analysis. Therefore, to ensure the reliability of nonlinear dynamic analysis, it is essential to select correct seismic waves. It is investigated by existing research that the peak acceleration, spectrum and duration should be the primary conditions for selecting ground motion records (Neaim et al. 2004; Hancock et al. 2006). Generally it also requires to adjust the seismic record by scaling the peak acceleration to reach the target spectrum acceleration. However, most of the seismic actions are

complex. The above three conditions are inadequate to be seismic wave selection standard and cannot satisfy seismic analysis requirements in many cases, especially when the number of selected ground motion records is limited and there are large differences among the records in terms of seismic acceleration, the discreteness of structural responses is even more apparent.

It is explicitly stipulated in Chinese seismic design code (GB50011, 2010) that when the time-history method is adopted in the analysis, at least 2 sets of strong earthquake records and 1 set of artificial earthquake wave should be selected based on the intensity, the design seismic group and site-class. Their average seismic influence coefficient curve should be in conformity with the seismic influence coefficient curve when adopting the response spectrum method; the maximum value for its acceleration time-history may be adopted according to Table 3.3. When adopting elastic time-history analysing method, the structure base shear force obtained from each time-history curve should not be less than 65% of that from the response spectrum method, and the average value from several time-history curves should not be less than 80% of that from the response spectrum method.

Table 3.3 Maximum values for the seismic acceleration of ground motion used in time-history analysis

Seismic action	Intensity 6	Intensity 7	Intensity 8	Intensity 9
Frequently earthquake	18	35 (55)	70 (110)	140
Rarely earthquake	---	220 (310)	400 (510)	620

Note: Values in brackets are related to the design basic acceleration of ground motion of 0.15g and 0.30g, respectively, for Intensities 7 and 8.

3.3.4 Numerical validation against an existing study

3.3.4.1 Validation against a 5-bay 3-storey BRBF

To verify the modelling approach, the finite element (FE) models are validated against a published experimental test conducted by Lin et al.'s (2012). In Lin's pseudo-dynamic experiments, the prototype frame was based on a three-storey office building in the city of Los Angeles. A single-bay of this building (shown in Figure 3.12) with BRBs in chevron and inverse-chevron configurations was tested. In this BRBF, apart from the bolted beam-column connections in the first floor, all the other BRB-column and beam-column connections were welded. The time-history method was used to study the seismic resistance of this BRBF. Comparisons with one of Lin's tests are undertaken herein.

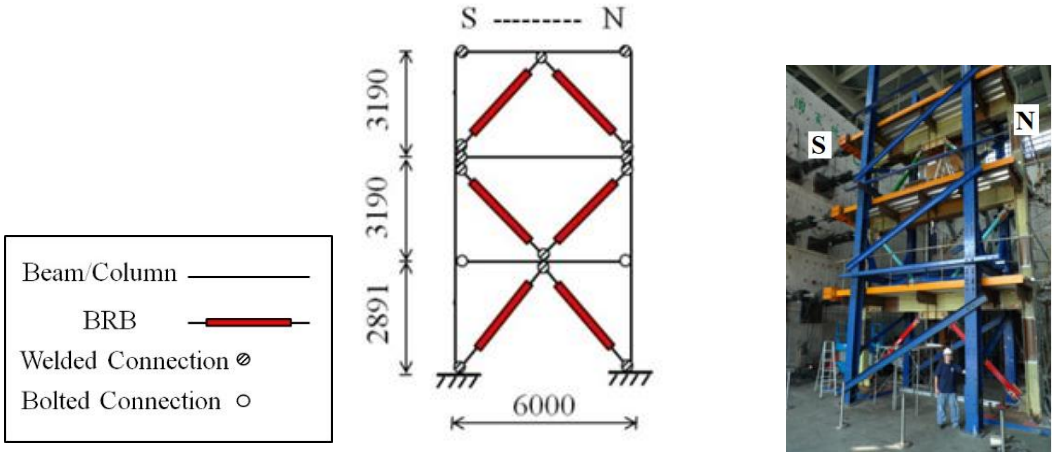

(a) Frame model (b) Test set up

Figure 3.12 Lin et al.'s (2012) test (all dimensions are in *mm*)

The input earthquake for the test frame (Lin et al 2012) was adopted from LA03 ground accelerations with a peak ground acceleration (PGA) of 530 gal. The ground accelerations and the elastic response spectrum of the LA03 are shown in Figure 3.13. A damping ratio of 5% was considered when scaling the ground accelerations. All the parameters including the structural member sizes and seismic conditions incorporated in the OpenSees model used for validation, are identical to those of the test frame. Given

the rotational stiffnesses of both the welded and bolted connections are relatively small, approximately zero rotational stiffness is assumed for both connections in the frame model.

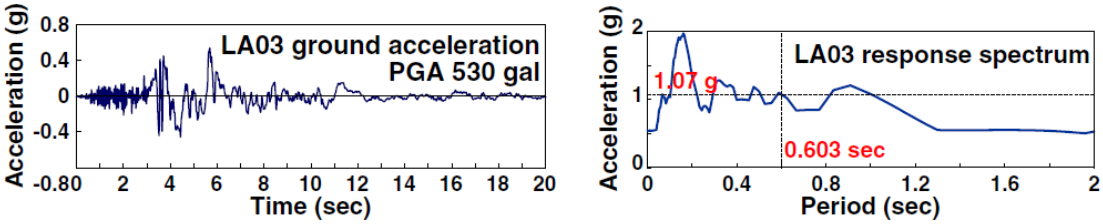

(a) (b)

Figure 3.13 (a) LA03 ground acceleration and (b) 5% damped elastic response spectrum (Lin et al., 2012)

3.3.4.2 Comparison between OpenSees and experimental results

The inter-storey drift ratios obtained from Lin et al.'s (2012) experiment and those from the current OpenSees simulation are compared in Figure 3.14. Note that the inter-storey drift ratio of the third storey is smaller than those in the other two storeys. This is because the stiffness of the third storey is larger than the other two storeys in Lin's model. The comparison shows some minor discrepancies between the numerical and experimental results. A possible reason for this could be due to the idealised pin behaviour assumed for the beam-column connections in the numerical model, whereas in the experiment the connections might exhibit a certain level of rotational stiffness.

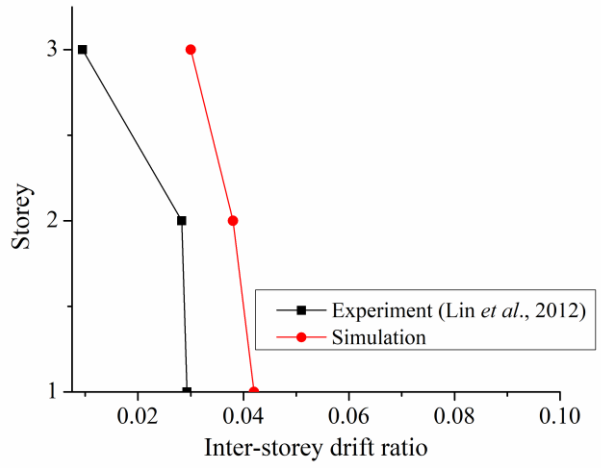

Figure 3.14 Comparison between experimental and numerical inter-storey drift results

From Figure 3.15, it can be observed that the experimental axial forces of the BRBs in all three stories are reasonably well predicted by the numerical simulation. The only exception is observed in the measured axial force of 1BRB_S (Figure 3.14(c)), which was due to the unexpected bulging in that particular BRB during Lin's test.

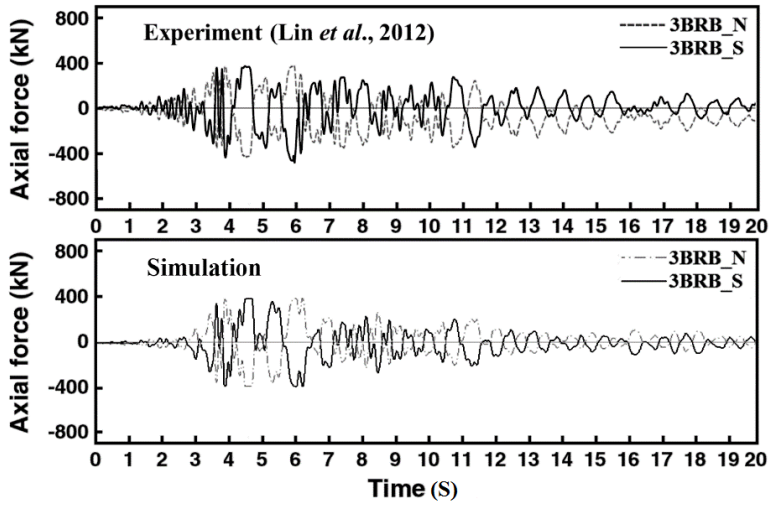

(a) 3rd storey BRBs

(Note: 3BRB_N/S represents the BRB in 3rd storey, the same for all other figures)

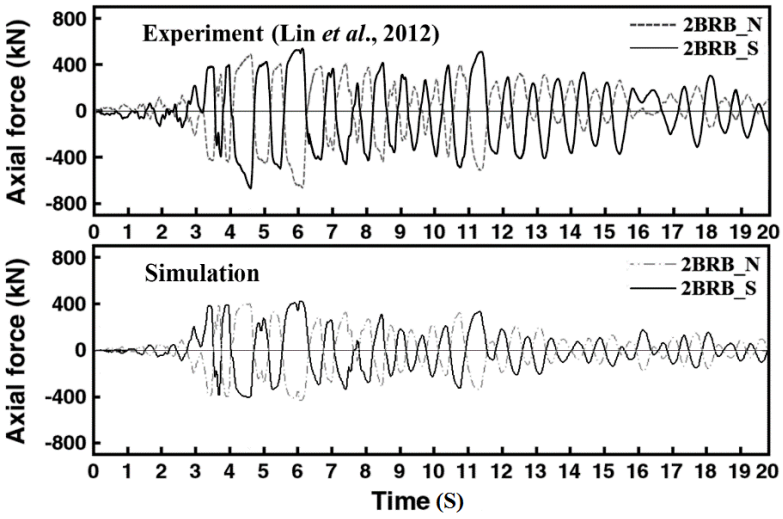

(b) 2nd storey BRBs

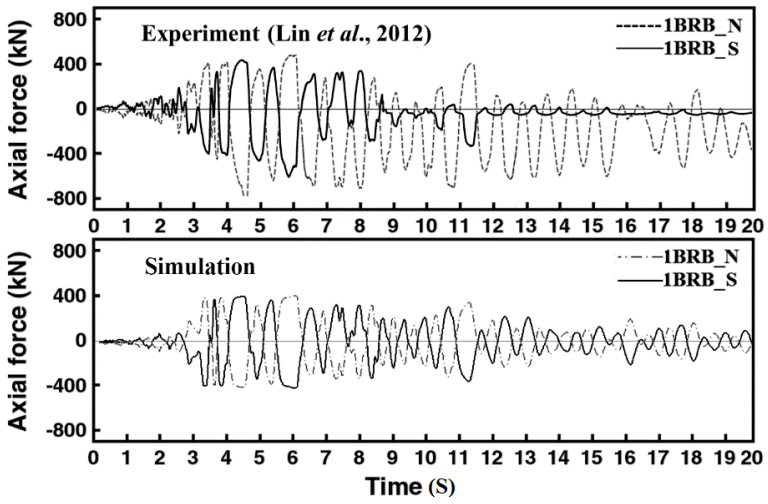

(c) 1st storey BRBs

Figure 3.15 Comparison between experimental and numerical time history results of the axial forces in respective BRBs

The hysteretic loops for the north BRBs (BRB_N) and south BRBs (BRB_S) are shown in Figures 3.16 and 3.17, respectively, where the axial forces are plotted versus the core plate strains for individual BRBs. Note that the core plate in a BRB refers to the bearing component designed to resist the full axial force developed in the bracing. Figures 3.16 and 3.17 indicate that, except for the damaged BRB in the 1st storey (1BRB-S in Figure 3.17), the simulation results agree reasonably well with the experimental records. The minor discrepancies in the comparison might be caused by the additional frictional resistance existing in the core plate which is not considered in the simulation. Notwithstanding, the comparison confirms the accuracy of the numerical modelling approach.

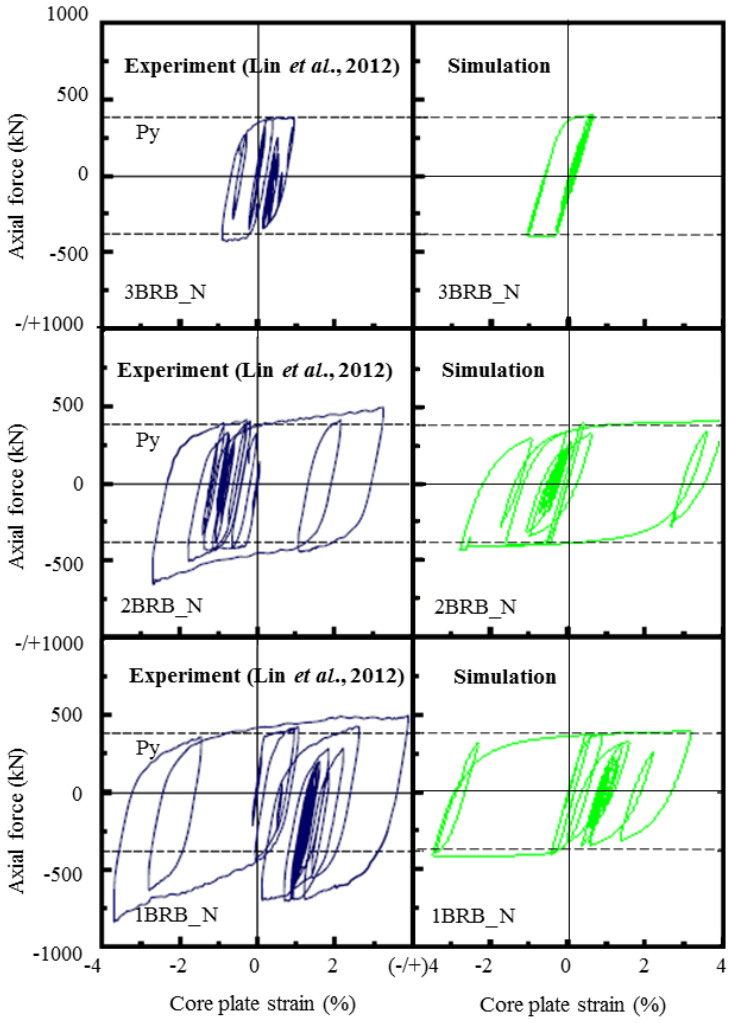

Figure 3.16 Comparison between the experimental and numerical results of the hysteretic loops of the north BRBs

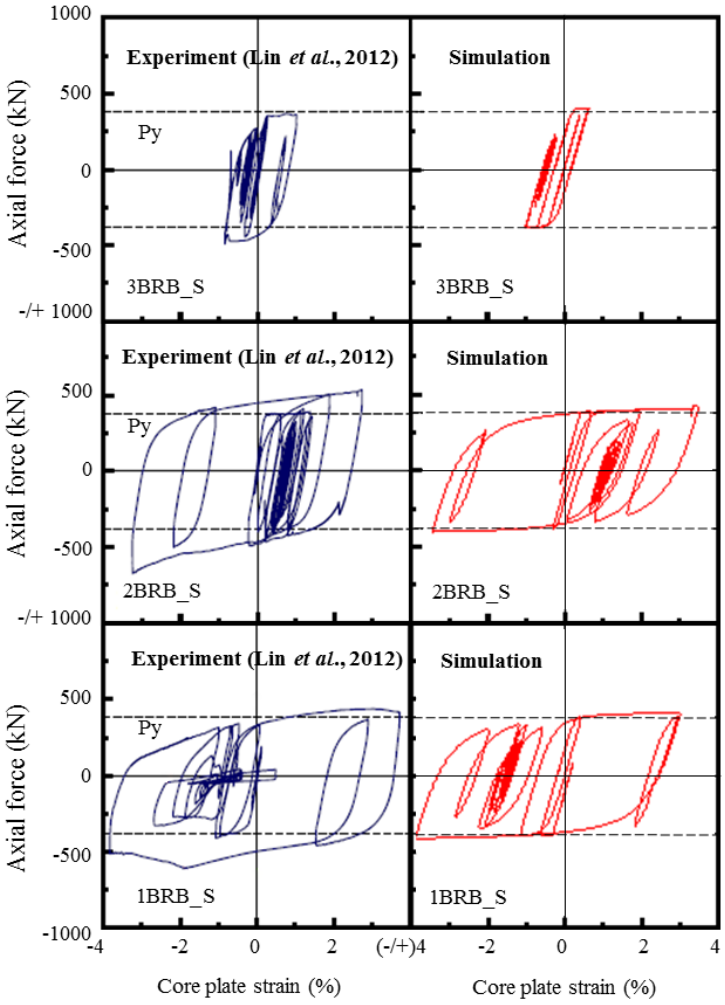

Figure 3.17 Comparison between the experimental and numerical results of the hysteretic loops of the south BRBs

The lateral storey displacement time histories predicted by the present simulation are compared in Figure 3.18 with Lin et al.'s (2012) experimental measurements with a good agreement. Despite the presence of some minor differences in the comparison, the overall accuracy of the numerical modelling approach can be validated.

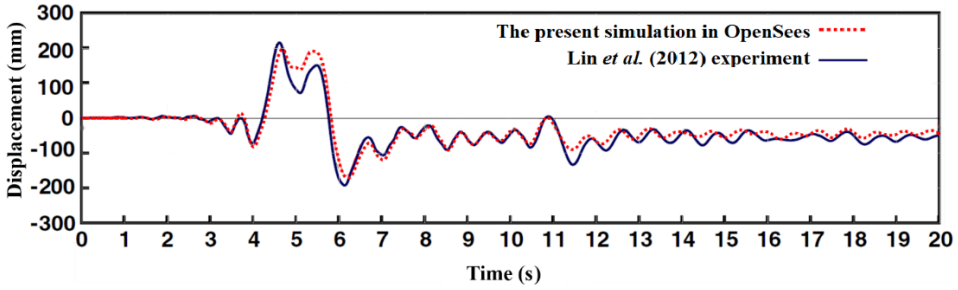

(a) 3rd storey

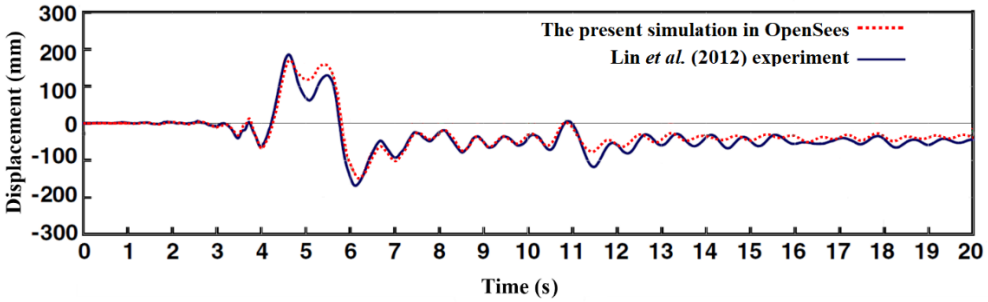

(b) 2nd storey

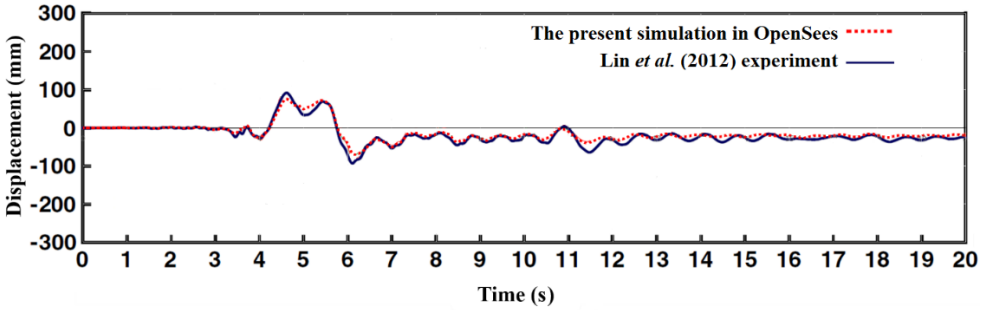

(c) 1st storey

Figure 3.18 Comparison between the experimental and numerical results of the lateral storey displacement time histories

3.4 Concluding Remarks

This chapter introduced the numerical approach of modelling three-dimensional beam-column connections and two-dimensional entire system by using ABAQUS and OpenSees.

For the three-dimensional beam-column connections modelling, numerical techniques were first presented, then applied to three different bolted connections (End plate

connection, fin plate connection and top- and seat- angle connection) to investigate the rotational capacity. The results obtained from the modelling showed that although the fin plate connection shows the best moment transfer capacity while the top- and seat-angle connection behaves the weakest moment-rotation relationship, all three types of connections should be classified as pin connection as their actual connection moments are lower than ¼ of the plastic moment capacity of the beam. Therefore, in the future study, the beam-column connections can be assumed to be purely pin connections in the proposed system.

In this chapter, the finite element models were developed and validated against existing experimental results available in the literature. The numerical predictions obtained from the numerical simulation were presented in terms of the inter-storey drift ratio, the axial force time-history of BRBs, the hysteretic loops of the BRBs, and the storey displacement time history. The simulated results agreed well with the existing experimental measurements with minor discrepancies. The purpose of this comparison is to validate the modelling approach to be used for simulating the structural behaviour of the proposed BRB structural system.

CHAPTER 4

EXPERIMENTAL PROGRAM

4.1 General Remarks

This chapter presents the details of the experimental program undertaken on three half scaled 2-storey models: two double-bay frames consisting of a buckling retrained braced frame (BRBF) and an adjoining non-moment resisting frame, and one single-bay BRBF (without a non-moment resisting frame). Note that the beams and columns in the non-moment resisting frames are all connected by bolts, therefore the moments in such a frame are expected to be minimal. In this chapter, a review of the existing experimental study on BRBFs is presented first, followed by the descriptions of the planning, design, testing procedure of the frame specimens, as well as the design and fabrication of the test rig used for the present testing. The test specimens were designed by software package SAP2000 (2006), and were subsequently assembled and tested under cyclic loads. The corresponding numerical models were analysed by the finite element analysis package OpenSees (McKenna et al., 2006) which will be compared with the experimental results.

The experimental program of this study aimed at investigating the seismic performance of the proposed structural system; the rotational capability of the bolted beam-column

connections; and the contribution of the bolted non-moment-resisting frame to the whole structural system under seismic actions.

4.2 Existing Experimental Work on BRBFs

This section briefly reviews published and representative experimental work on BRBFs. In particular, the regular design criteria for the BRBFs and the design and fabrication of test rigs are investigated. Although the test set-up varies in different studies, some common features found in the existing experimental work can still be adopted in the current experimental program.

4.2.1 Fahnestock et al. (2006)

Fahnestock et al. (2006) conducted a series of pseudo-static tests on a 3/5 scaled 4-storey frame. It was the first large-scale multi-storey BRBF testing program and was intended to better understand the performance of the BRBF system. The prototype building was designed based on the AISC Seismic Provisions for Structural Steel Buildings (AISC, 2005a), Minimum Design Loads for Buildings and Other Structures: SEI/ASCE 7-05 (Structural Engineering Institute, 2005), and the equivalent-lateral-force procedure in the International Building Code 2000 (International Code Council, 2000).

The test frame was a planar structure with eight in-plane attachments, namely, four load points and four reaction points, as shown in Figure 4.1. The load was applied through imposed lateral displacement histories at all levels by actuators that were attached to the reaction wall, which were recorded from the numerical nonlinear time history analysis results obtained before the tests. The two column bases were anchored to the strong floor, and two link devices were connected to the ground-level. It should be noted that the beam-column-brace connection used in this test was a pinned connection as shown in Figure 4.2. A bolted beam splice using double structural tees was introduced

between the beam and the beam stub to transfer axial force but provide minimal flexural resistance.

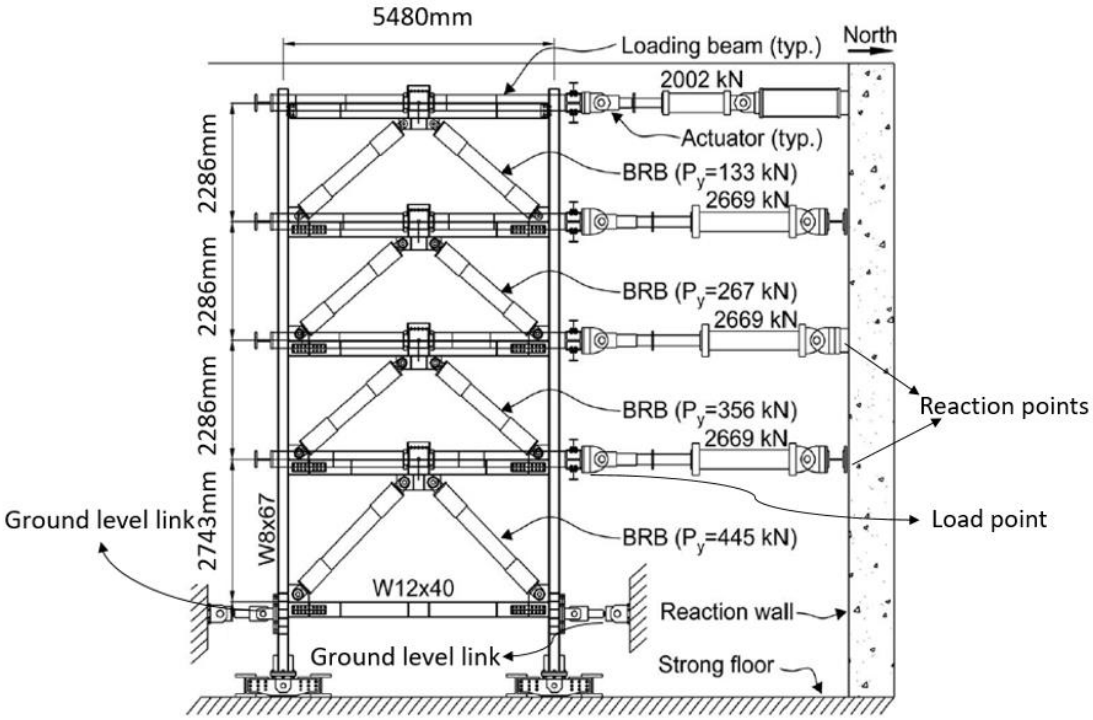

Figure 4.1 Test set up used by Fahnestock et al. (2006)

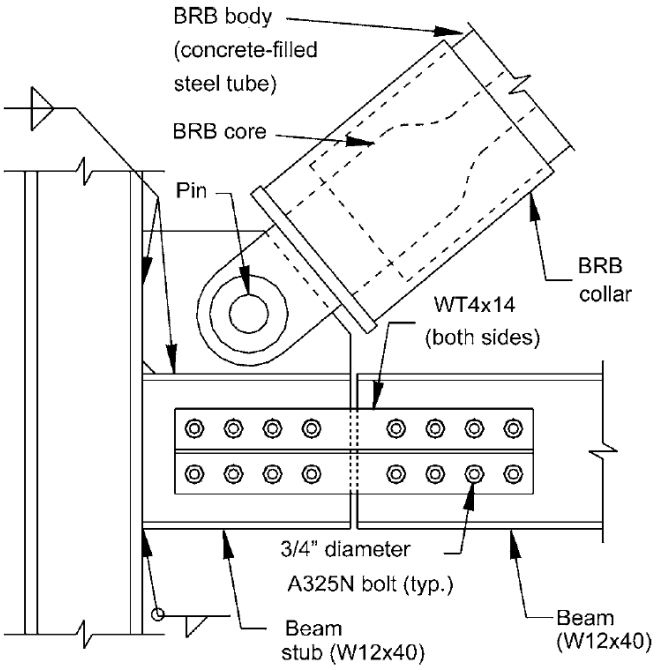

Figure 4.2 Beam-column-brace connection used by Fahnestock et al. (2006)

4.2.2 Tsai et al. (2008)

Tsai et al. (2008) conducted a series of pseudo-dynamic tests (PDTs) of a planar full-scale 3-storey 3-bay BRBF using concrete-filled tube (CFT) columns (Figure 4.3) at Taiwan National Centre for Research on Earthquake Engineering, using networked PDT techniques. Their project adopted the displacement-based seismic design procedures (Loeding et al., 1998; Medhekar and Kennedy, 2000) for the design of the frame specimen. The Taiwan seismic building draft code (2002, denoted as "Taiwan code 2002") was used for the seismic design and all steel beams and CFT columns were designed using AISC-LRFD. The tests adopted pseudo-dynamic ground motions as input which were scaled to represent 50%, 10%, and 2% probabilities of exceedance in 50 years' seismic hazard levels.

As illustrated in Figure 4.3, the testing frame consists of one braced bay at the centre and two non-braced bays on both sides. Only the exterior beam-to-column connections in each floor were moment connections; all the other beams and columns were connected through beam web and were assumed not to transfer any bending moments. In addition, 4, 3 and 3 actuators, each having $\pm 980kN$ force and $\pm 50cm$ stroke capacities, were applied at the 1st, 2nd and 3rd floor, respectively. Each footing was anchored down using four $69mm$ diameter post-tension bars to the strong floor.

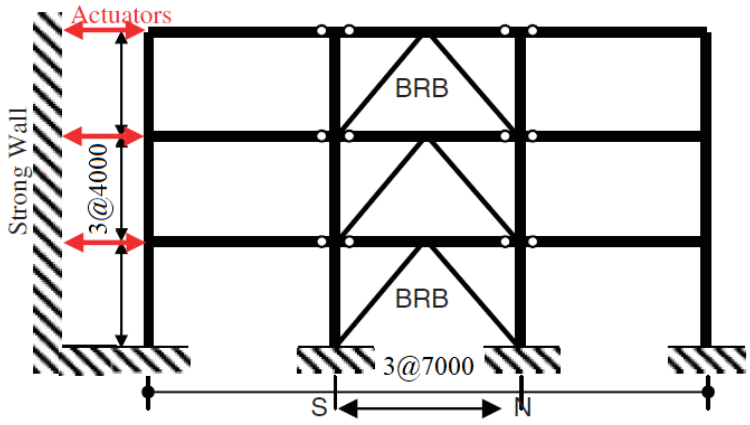

Figure 4.3 Schematic plan of BRBF tested by Tsai et al. (2008) (unit: *mm*)

4.2.3 Berman and Bruneau (2009)

Berman and Bruneau (2009) proposed a novel beam-column-brace connection for BRBF where the gusset is only connected to the beam and is offset from the column face by $d_b/2$, as shown in Figure 4.4. Their proposed connection was expected to avoid the out-of-plane gusset buckling and any unexpected moment transferred to the BRBs. This connection was then tested in a three-storey frame under quasi-static loading. The design of the BRBF was based on a structural fuse concept (structural fuse can be taken as disposable or easy to repair elements after damage, while the main structure remains in functioning) formulated by Vargas and Bruneau (2009a) following the 2005 AISC Seismic Provisions for Steel Buildings (AISC 2005a). The compressive buckling strength of the gusset can be checked using Section of J4.4 of the AISC Specifications for Structural Steel Buildings (AISC 2005b) and free-edge buckling can be checked as per Astaneh-Asl (1998). As shown in Figure 4.5, in the test the lateral support to the specimen was supplied by the reactive mass frame which provides negligible resistance in the plane of the specimen, via the use of three-dimensional rockers at the top and bottom of each column at each story, while implementing out-of-plane resistance through double-angle braces between the columns in that direction.

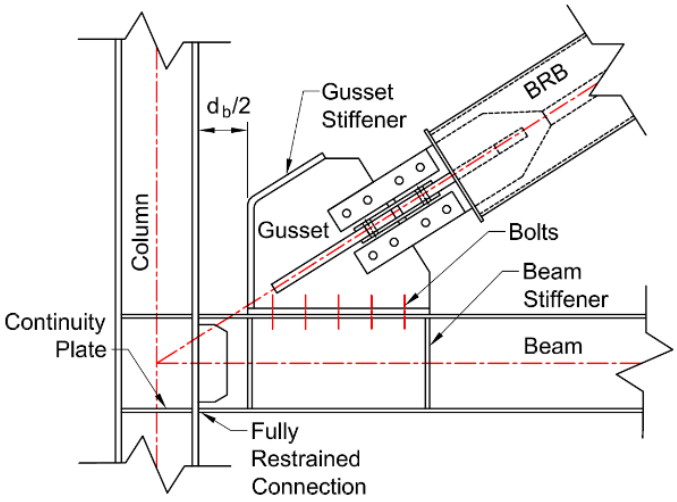

Figure 4.4 Proposed gusset connection by Berman and Bruneau (2009)

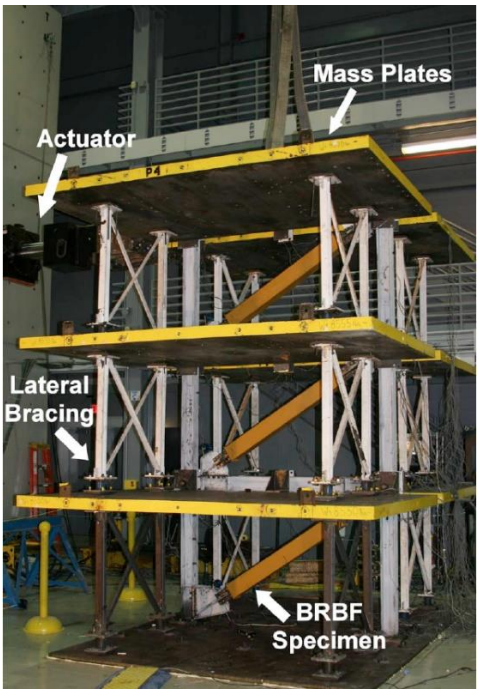

Figure 4.5 Test setup by Berman and Bruneau (2009)

4.2.4 Lin et al. (2012)

A series of hybrid and cyclic loading tests were carried out on a three-storey single-bay full-scale BRBF at the Taiwan National Center for Research on Earthquake Engineering in 2010 (Lin et al., 2012). The design of the BRBF followed the procedures prescribed in the seismic steel building provisions from the American Institute of Steel Construction (AISC). Specifically, the design of the BRBs' steel casing and the end connections incorporates the maximum compressive strength $P_{\max}$ (N) described in the abovementioned provision:

$$P_{max} = \beta \times R_y \times \omega_y \times f_y \times A_c \tag{4-1}$$

where β is the compression strength adjustment factor, R_y is the material overstrength factor, ω_y is the stain hardening factor, f_y (MPa) is the yield strength and A_c (mm^2) is the area of the cross section.

In the testing frame, all BRB connections were welded end connections. The elevation of the BRBF and the specimen setup in Lin's tests are shown in Figure 4.6.

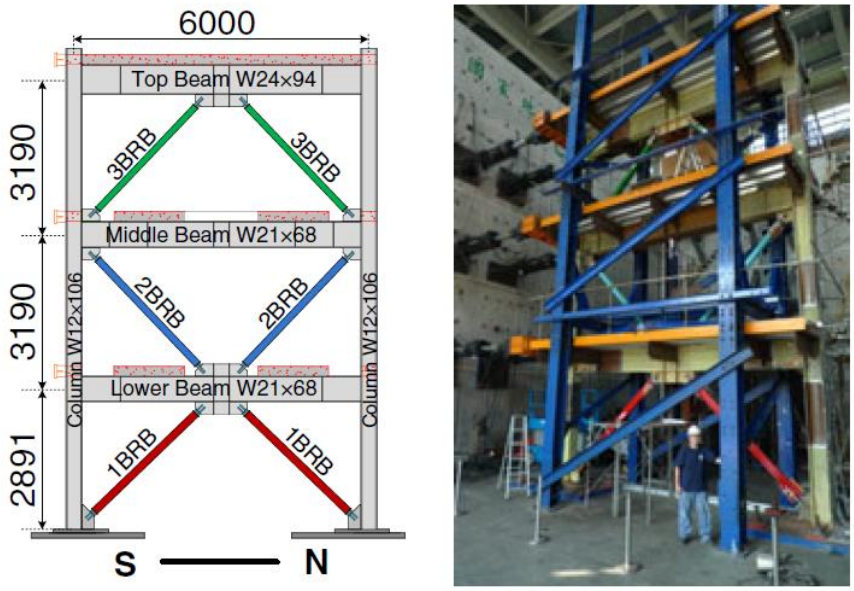

Figure 4.6 Hybrid and cyclic loading tests by Lin et al. (2012) (unit: *mm*)

4.2.5 Chou et al. (2012)

Chou et al. (2012) conducted cyclic tests on a one-story, one-bay BRBF subassembly based on a prototype three-storey BRBF with a single-diagonal sandwiched BRB and corner gusset. To enhance the out-of-plane stability of the connection, a dual-gusset-plate configuration similar in size to the single gusset-plate configuration was also adopted in the study. The schematic elevation of the prototype frame and the testing frame are shown in Figure 4.7. The design of the BRBF was performed following the International Building Code (IBC) 2000, and the design procedure for the gusset plates was adopted based on the AISC specification.

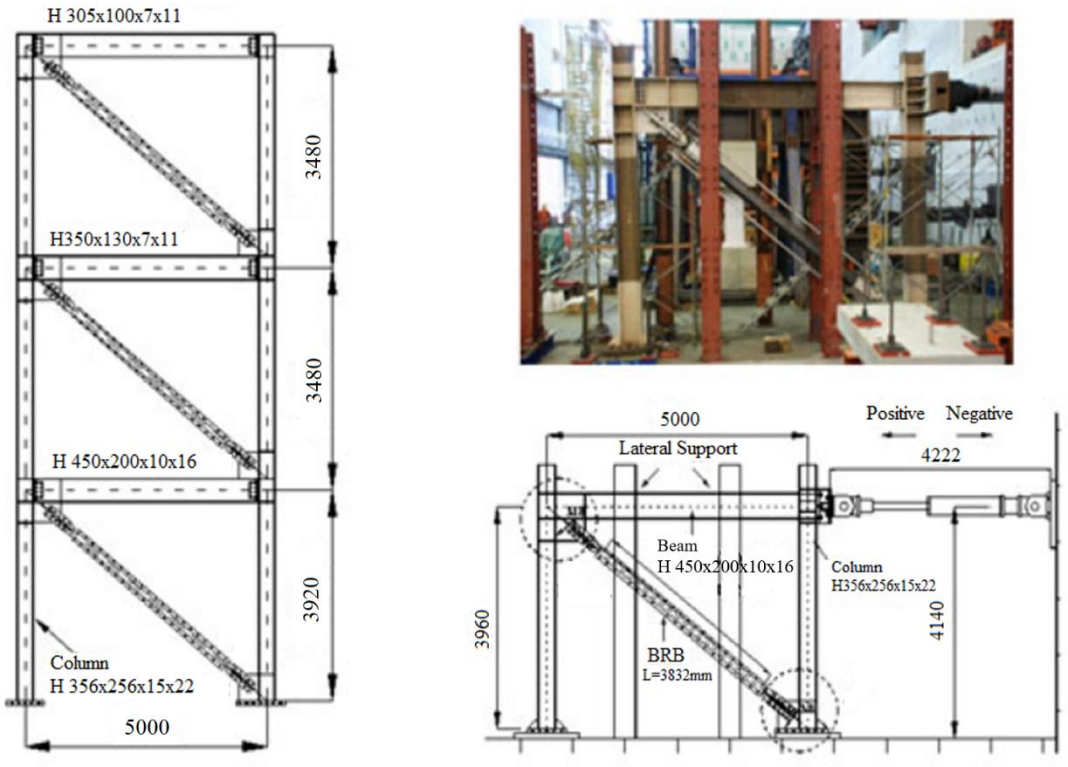

(a) Prototype Elevation (b) Subassembly Frame used by Chou et al. (2012)

Figure 4.7 Cyclic tests by Chou et al. (2012) (unit: *mm*)

4.3 Current Experimental Design

In this study, the testing frames include three different specimens. The first two are standard frames consisting of a BRB frame (BRBF) and an adjoining non-moment-resisting frame. The difference between the two is the assembly of the frames, i.e. fin plate beam-column connections (BRBF-FF) and end-plate beam-column connections (BRBF-EF). The third frame is a single BRBF.

For all three frames, each span is 3m long with a typical height of 1.5m for each story. H-shaped steel is used for both the beams and columns, while low strength steel is employed for the BRBs. The schematic diagram and notation of all the members of a standard frame and a single BRBF, as well as the setup of the test are shown in Figures 4.8 to 4.9. Note that the beams are denoted by KL1 to KL4, the columns are designated by KZ1 to KZ3, and the ground beams are nominated by GB1 to GB3 in the BRBF.

Given that the actuator is connected to the top of KZ1 on the left side of the frame, the BRBs are designed in the form of chevron configurations in the second storey to resist the horizontal loads together with the second storey beam, and inverse-chevron configurations are designed in the first story.

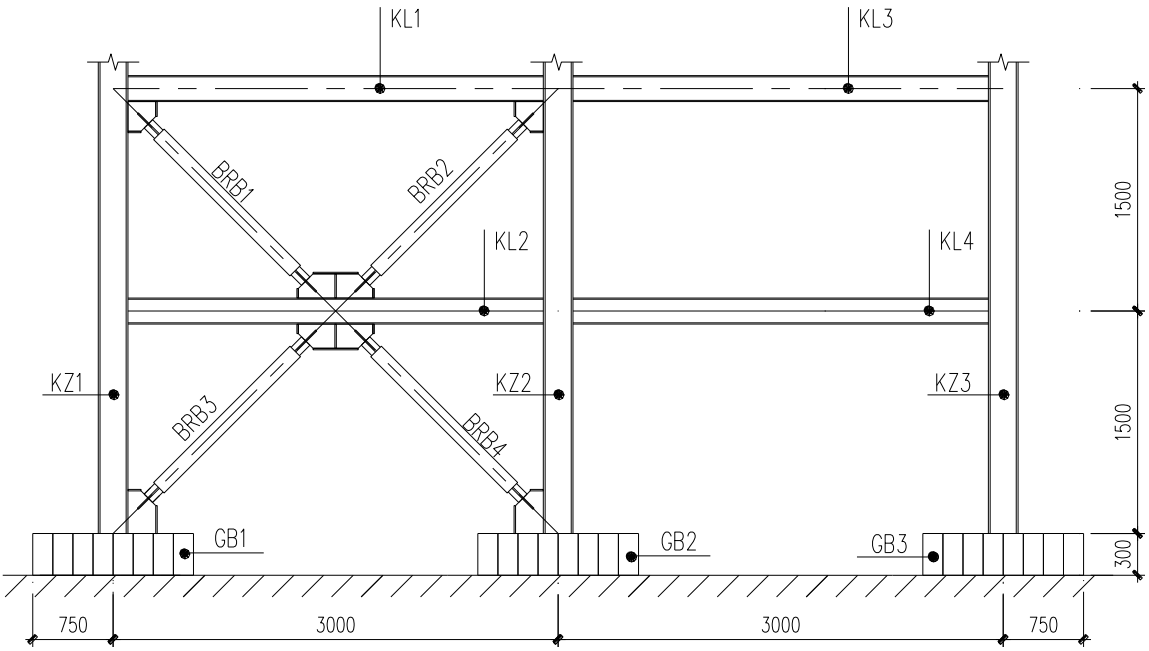

(a) Elevation

(b) Experiment setup

Figure 4.8 Standard BRBF with non-moment resisting frame (unit: *mm*)

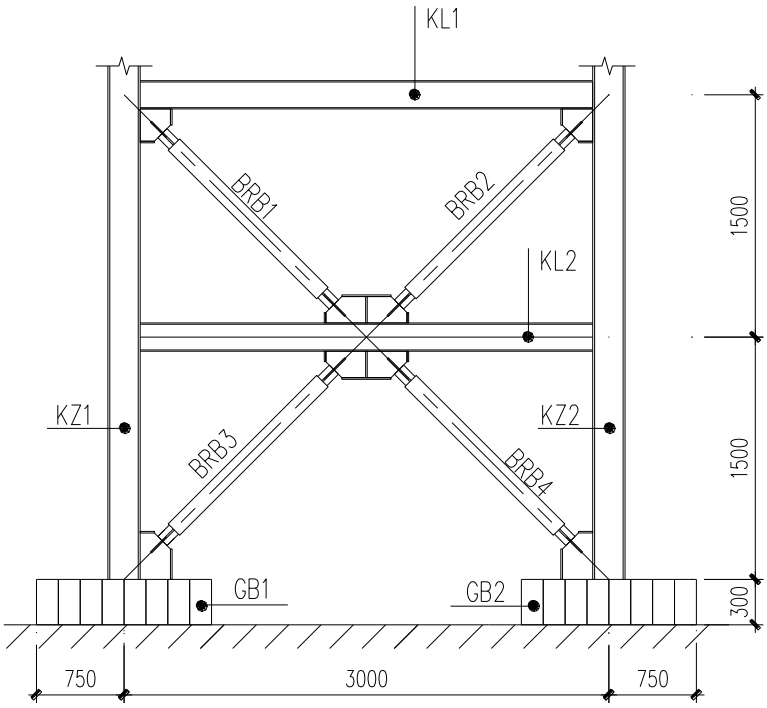

(a) Elevation

(b) Experimental setup

Figure 4.9 Single BRBF (unit: *mm*)

The design of the specimens in the testing frames consists of three stages. In the first stage, the beams and columns are designed by considering gravity loads only. In the second stage, a displacement-based seismic design procedure is applied to the BRB design. Last but not the least, the beam-column connections are designed in the third

stage by using the equivalent bending moment method. It should be noted that the difference between the elastic and inelastic deformation modes is much less dramatic than for a conventional concentrically braced frame (where members intersect at a node, the centroid of each member passes through the same point). Because of this, an inelastic dynamic analysis is not typically required for the BRBF design (Fahnestock et al., 2003). Therefore, a static analysis is conducted in SAP2000 to model the BRBF design.

4.3.1 Design of beams and columns

The test was planned to be conducted at the Structural Engineering Lab of Shandong Jianzhu University, China, where the external supervisor of this thesis Professor Xuejun Zhou is employed. Considering the space limitation of the laboratory and specific objectives of the experiment, only half scaled models were tested. The original dimension of the frame was determined by applying the empirical values and then scaled down to half of the original dimension. Subsequently, the size of beams and columns are designed by considering the vertical loads only. The frame was designed in accordance with the current Chinese seismic design provision (GB50011 2010). The design dead load (DL) of the floor is $3.68kN/m^2$ and that of the roof is $2.94kN/m^2$. The design live load (LL) is $2kN/m^2$ for each floor. The design load combinations considered 1.2DL+1.6LL. Note that the selection of the beams and columns where also constrained by the profile steel supplied by the manufacturer. Therefore, the availability of the steel sections was also considered for the design. According to the above considerations, the size and material properties of all members of the frame specimen are summarised in Tables 4.1 and 4.2.

Note in the test that, the equivalent point load of the design load combination applied to each column is relatively small, making the axial compressive ratio of the columns to be conservatively safe which will result in a better ductility of the entire frame.

Considering the worst case scenario, the maximum allowable axial compressive ratio of 0.3 (according to the Chinese Steel Structure Code (GB50017 2003)) for each column was adopted in the test, resulting in a vertical load of 250kN, to examine the performance of the system under the ultimate condition.

Table 4.1 Member sizes of specimen（unit: *mm*)

Member	Notation	Section profile	Size
Column	KZ	H	HW200×200×8×12
Beam	KL	H	HN175×90×5×8
Ground beam	DL	H	HW300×300×10×15

Table 4.2 Material properties of beams and columns

Elastic Modulus (*MPa*)	Yield Strength (*MPa*)	Ultimate Strength (*MPa*)
2.16E+05	330	455

4.3.2 Design of BRBs

This section presents the results of applying the displacement-based seismic design procedures (Powell, 2008) to the design of BRBs. The design also follows the Chinese seismic provision (GB50011, 2010) and the BRB manufacturer's recommendation. Note that it is assumed in this study that the earthquake responses of the BRBF are essentially governed by the first vibration mode.

Two seismic hazard levels were considered in the tests, frequent earthquake and severe earthquake, for which the probabilities of exceedance in 50 years are 10% and 2% respectively (GB50011, 2010). The seismic fortification intensity is 8°, and the design basis earthquake acceleration value is 0.3g (g represents the gravity acceleration). The design earthquake group is 2 and the construction field belongs to Site-class II. The

structural safety was specified as the second class, and the design working life is 50 years. As no specific performance criteria are prescribed by the Chinese code for the proposed system yet, the performance criteria were chosen according to the upper bound limit of the storey drift specified in the current seismic design code (GB50011, 2010). For the 10/50 and 2/50 events, the inter-storey drift ratio limits were set at 1/250 and 1/50 radians, respectively. It is assumed that the profile of the structural first modal design displacement can be simplified as an inverted triangle. Once a target drift level is selected, each storey displacement can be determined. For example, under the 10/50 event, the storey drift ratio limit is 1/250, thus the target storey drift ratio is 1/250, and the target storey drift is 6*mm* as per the storey height of 1500*mm*; for the 2/50 event and the corresponding target drift ratio of 1/50, the target storey drift is 30*mm*. Moreover, in the BRB design, it is recommended that the axial force of the BRBs should just reach its yield force under frequent earthquakes, starts to yield under medium earthquakes, and completely enters the plastic stage under severe earthquakes. According to the abovementioned assumptions and principles, the design of the BRBs should follow an iterative process, which is described as follows:

4.3.2.1 Selection of the BRB material

It is known that to enhance energy dissipation, BRB's yield strength is usually made intentionally low by employing low-yield steels. Considering the usually long procurement process of the low-yield steel, Q100LY steel (yield stress=100*MPa*) which was readily to be purchased was used in the design.

4.3.2.2 Calculation of the BRB forces under the target storey drift

As shown in Figure 4.10, a 250*kN* vertical dead load was applied to the top of each column as described in Section 4.3.1.This is to ensure the ductility of the columns, because ductility capacity of columns can be deprived by high axial compression, as it can prompt buckling. To simulate the two different seismic conditions, two sets of

horizontal loads F, being 200*kN* and 350*kN* which, represent the frequent earthquake and severe earthquake, respectively, were applied at the top of the frame. The procedure for derivation of these lateral forces is described below.

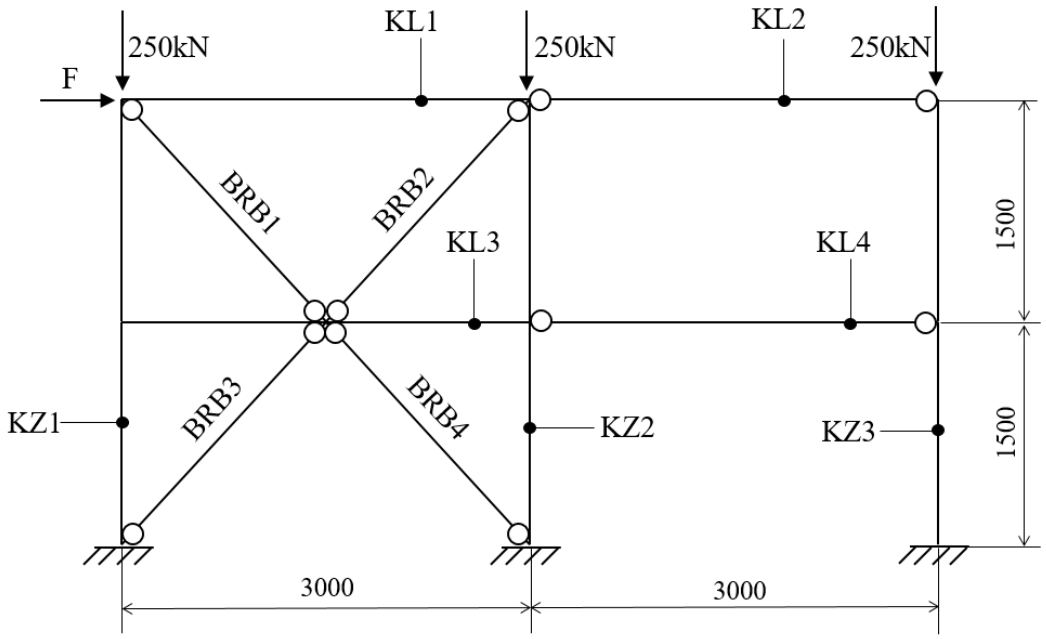

Figure 4.10 Schematic of the model (unit: *mm*)

The equivalent horizontal force F imposed on the frame that represent the earthquake intensities can be obtained based on the displacement control method. Under frequent earthquakes, the target storey drift ratio was set as 1/250 as discussed above to represent the seismic intensity. As can be seen in Table 4.3, when the inter-storey drift ratio equals 1/250 at KZ1 where the maximum inter-storey drift ratio occurs, the base shear force of the frame is calculated as 200*kN*. Applying this force as the equivalent horizontal force at the top of the frame, the axial force in the BRBs can be calculated and summarised in Table 4.4.

Table 4.3 Lateral displacement and storey drift ratio of the analytical model when F=200*kN*

	Elevation (*m*)	Lateral displacement (*mm*)	Story drift (*mm*)	Story height (*mm*)	Inter-storey drift ratio
KZ1	3.000	9.4	6	1500	1/250
	1.500	3.4	3.4	1500	1/441
KZ2	3.000	8.6	5.4	1500	1/278
	1.500	3.2	3.2	1500	1/469
KZ3	3.000	8.5	5.4	1500	1/278
	1.500	3.1	3.1	1500	1/484

Table 4.4 Axial force in BRBs when F=200*kN*

	BRB1	BRB2	BRB3	BRB4	Average of the absolute values
Axial force (*kN*)	-111.07	104.86	94.15	-103.97	103.5

Note: Tensile force is positive and compressive force is negative

Similarly to the case of frequent earthquakes, the equivalent horizontal force of the severe earthquakes was obtained in the same manner. Although the ultimate upper bound of storey drift ratio under severe earthquakes suggested by the Chinese Seismic code is 1/50, the target inter-storey drift ratio should be lower for the safety concern. Therefore, a maximum inter-storey drift ratio 1/82 which occurs at KZ1 was set as the target inter-storey drift ratio. The inter-storey drift ratios at all other columns are summerised in Table 4.5, and the base shear force which equals the equivalent horizontal force was calculated as 350*kN*. Applying F=350*kN* at the top of the frame, the axial force in the BRBs can be calculated and are summarised in Table 4.6.

Table 4.5 Lateral displacement and storey drift ratio of the analytical model when F=350*kN*

	Elevation (*m*)	Lateral displacement (*mm*)	Inter-storey drift (*mm*)	Story height (*mm*)	Inter-storey drift ratio
KZ1	3.000	28.4	18.4	1500	1/82
	1.500	10	10	1500	1/150
KZ2	3.000	27.2	17.3	1500	1/87
	1.500	9.9	9.9	1500	1/152
KZ3	3.000	27.1	17.4	1500	1/86
	1.500	9.7	9.7	1500	1/155

Table 4.6 Axial force in BRBs when F=350*kN*

	BRB1	BRB2	BRB3	BRB4
Axial force (*kN*)	-140.859	135.555	117.432	-121.974

Note: Tensile force is positive and compressive force is negative

4.3.2.3 Calculation of the BRB areas

As the BRBs are expected to yield when the inter-storey drift ratio is 1/250, and completely enter into plastic stage when the inter-storey drift reaches up to 1/50, the yield strength of the BRBs should be under the average value summarised in Table 4.4, which is 103.5*kN*. Therefore, it can be assumed that the initial yield strength of the BRBs is 103.5*kN*. Given the overstrength ratio of the BRB material is 1.1 (GB50011 2010), and the yield strength of the steel is 100*MPa*, the initial area of BRBs can be calculated to be 940mm^2. This area is eventually optimised to be 900mm^2 due to the manufacturing limits. As a result, the design yield force of BRB was calculated to be 99*kN*. Therefore, as can be seen from Table 4.4, BRB1, BRB2, BRB4 all yield and

BRB3 approaches to yield when the maximum storey drift ratio is 1/250.

4.3.2.4 Serviceability Check

The elongation of BRB1 was found to be 4.56*mm* when F=200*kN*. Given the maximum elongation rate of BRBs is 1/100 as suggested by the Chinese seismic code GB50011 (2010), and the effective length of BRB (the full length of BRB minus the length of the unrestrained non-yielding segment at BRB ends) is 1500*mm*, the maximum elongation of BRB is 15*mm*, which is much larger than 4.56*mm*. Besides, the BRB manufacturer advised that the maximum elongation rate can be up to 1/80, which means that the BRB can elongate up to 18.75*mm* without rupture.

When F=350*kN*, BRB1, BRB2, BRB3 and BRB4 yielded to different extent. At the point of yielding, the elongation of BRB was 13.08*mm*. This was still less than the maximum elongation of 15*mm* as specified by the seismic provision. Therefore, the above calculated BRB areas can meet the requirements of this test. The mechanical properties of the BRBs are summarised in Table 4.7.

Table 4.7 Mechanical properties of BRB

Elastic modulus (*MPa*)	Yield strength (*MPa*)	Overstrength ratio	Core area (mm^2)	EA/L (*kN/mm*)	Yield force (*kN*)	Yield stiffness Ratio
2.06E+05	100	1.1	900	87.41	99	0.04

4.3.3 Design of bolted beam-column connections

In the proposed BRBF system, bolted beam-column connections are employed at the non-braced bay to facilitate easy fabrication with maximum efficiency. As the rigid beam-column connection increases the earthquake force by adding up the BRBF stiffness, the bolted beam-column connection with relatively low rotational stiffness is

expected to bring higher overall flexibility to the BRBF system, therefore resulting in higher seismic performance of the system. To illustrate the rotational stiffness of the beam-column connections, a numerical modelling study using ABAQUS was performed in Chapter 3. It showed that the flexible end-plate connection and the fin-plate connection (Figure 4.11) had very limited ability to transfer bending moment, which can be regarded as pinned connections. Therefore, both types of connections were adopted in the design.

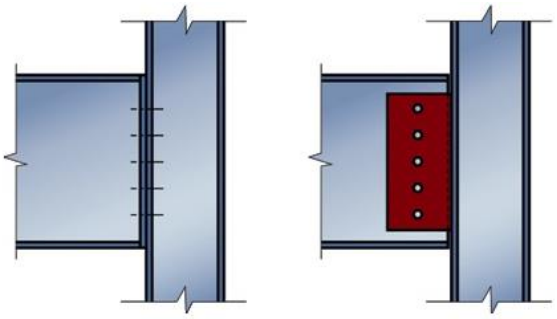

(a) Flexible end plate connection (b) Fin plate connection

Figure 4.11 Two types of primed beam-column connections

The aim of the design was to prevent premature fracture of the bolts and the failure of the end-plate or the fin-plate. Because the connections are not expected to resist any bending moment, only the axial force in the beam was considered in the design. Considering the size of the connecting end-plate and fin-plate for the half-scaled testing frame, the smallest M16 high-strength bolts were chosen. According to the Chinese Steel Structure Code (GB50017, 2003), the shear capacity N_v^b and the axial capacity N_t^b shall respectively satisfy:

$$N_v^b = n_v \frac{\pi d^2}{4} f_v^b \tag{4-2}$$

$$N_t^b = \frac{\pi d_e^2}{4} f_t^b \tag{4-3}$$

where n_v is the number of bolts on the cross section; d is the diameter of the bolt rod;

d_e is the effective diameter of the bolt rod; f_v^b and f_t^b are the design values of the shear and tensile strengths of bolts, respectively. Note that the effective diameter of a bolt (thread) is defined as the diameter of the imaginary co-axial cylinder which intersects the surface of the thread in such a manner that the intercept on a generator of the cylinder, between the points where it meets the opposite flanks of a thread groove, is equal to half the nominal pitch of the thread.

Detailed dimensions of the fin-plate and end-plate beam-column connections adopting the abovementioned formulas are shown in Figure 4.12.

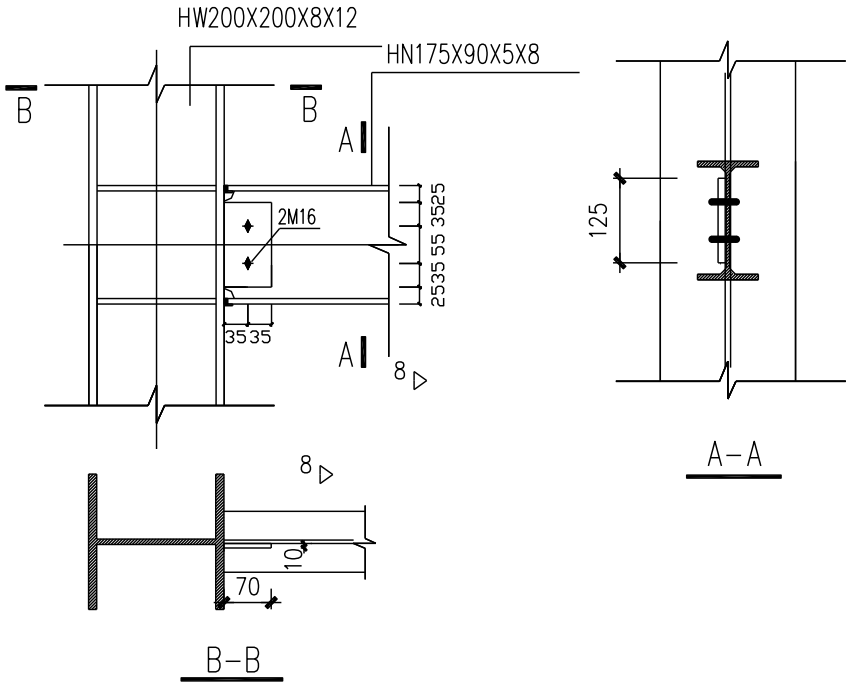

(a) Fin plate beam-column connection

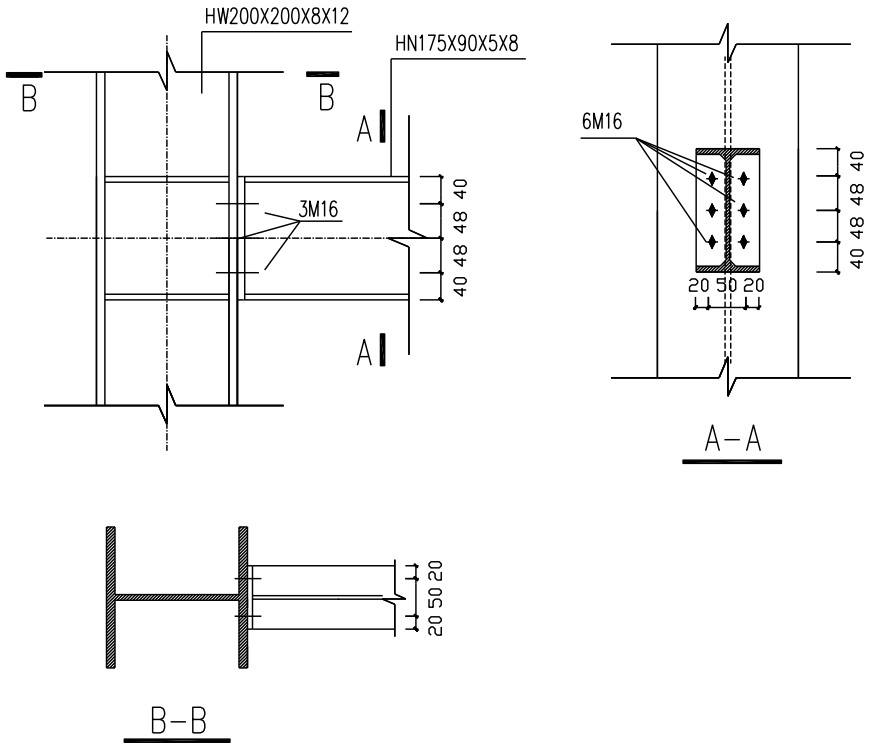

(b) End plate beam-column connection

Figure 4.12 Details of beam-column connections (unit: *mm*)

4.3.4 Design of support structure

In the test, the columns are welded to the designed ground beams which are denoted as DL, to achieve the support rigidity. Each ground beam can be fixed to the ground through four M80 bolts. The details of the ground beams and their connections to the column feet are shown in Figure 4.13. Note that to reinforce the connection between the column feet and the ground beams, stiffeners were added to the bottom of the columns and welded to the ground beams, as can be seen in Figure 4.13 (a).

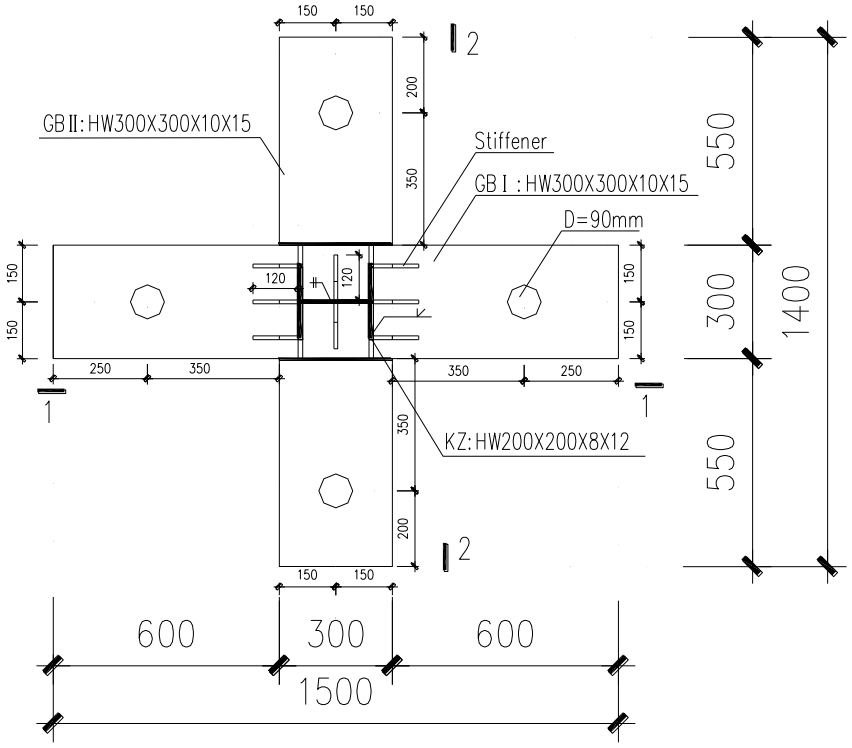

(a) Column feet and ground beam plan view

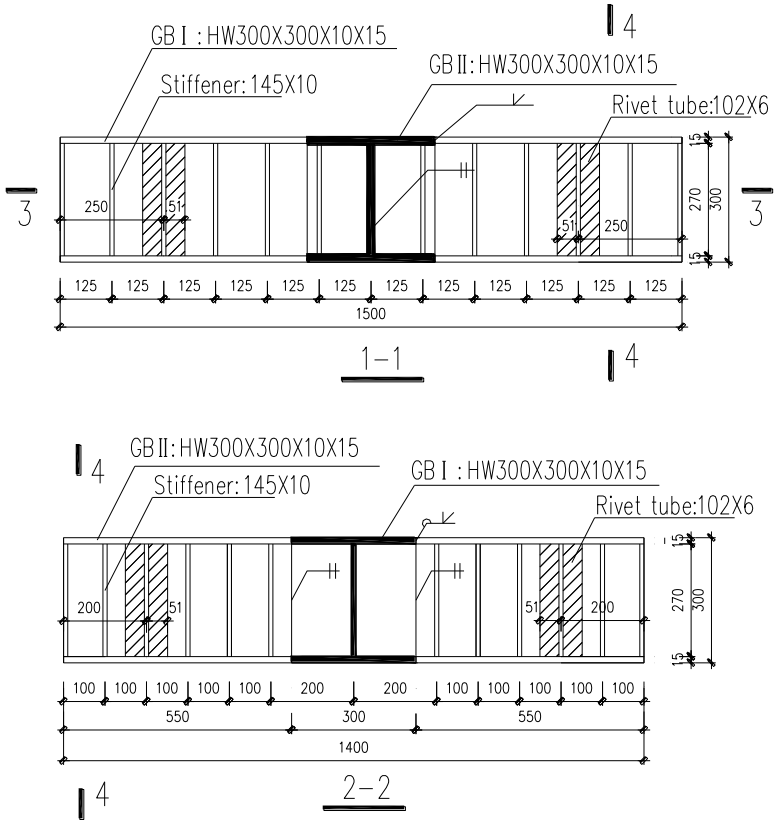

(b) Sections 1-1 and 2-2

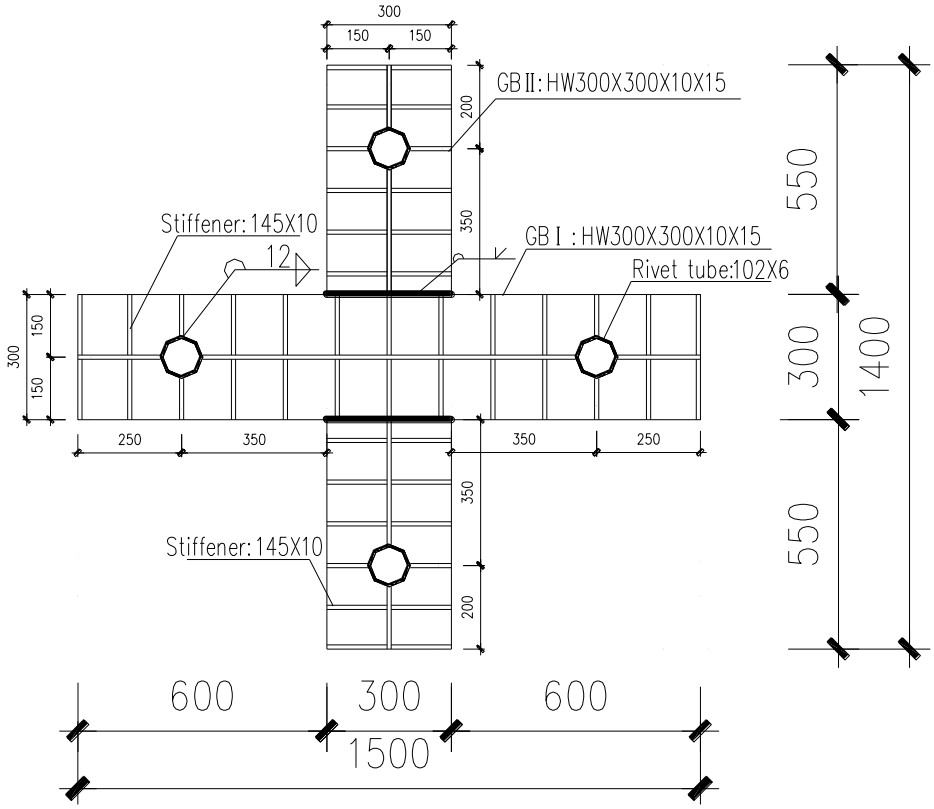

(c) Section 3-3

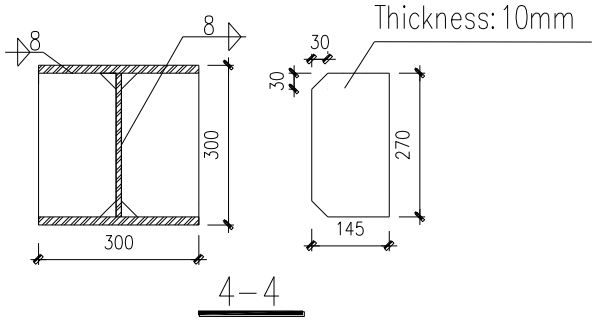

(d) Section 4-4

Figure 4.13 Details of column feet and ground beams (unit: *mm*)

4.4 Material Characteristic Test (Tensile Test)

The purpose of the material characteristic test was to testify the elastic modulus E, yield stress σ_y, ultimate tensile stress σ_u, and elongation percentage δ. The design of the tested sample for H-shaped steel followed the Chinese national standard: Steel and Steel Products - Location and Preparation of Test Pieces for Mechanical Testing (GB/T2975, 1998). Figures 4.14, 4.15 and Table 4.8 show the sampling point and detailed sample

sizes for this test. The manufactured test samples and the test picture are shown in Figures 4.16 and 4.17, respectively. A total of three samples, viz, S1-1, S1-2 and S1-3 were tested.

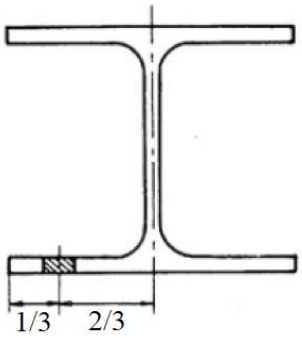

Figure 4.14 Sampling point

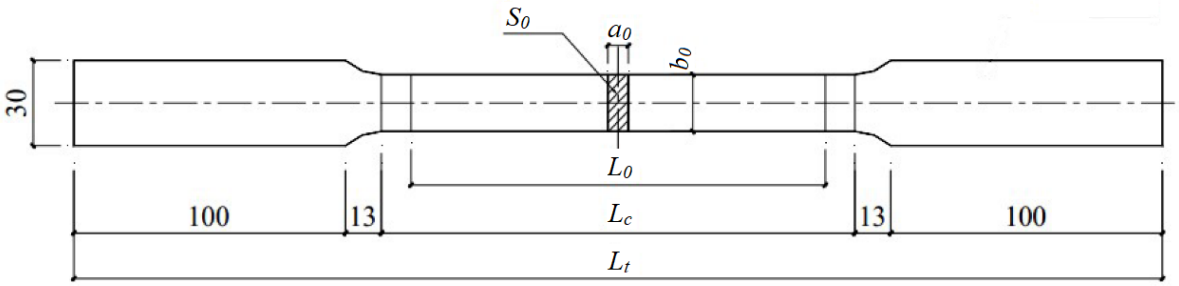

Figure 4.15 Sample size (unit: *mm*)

(Note: a_0-thickness, b_0-width, L_0-gauge length, L_c-parallel length, L_t-total length)

Table 4.8 Sizes of the material characteristic test sample

Number of samples	Thickness $a_0\,(mm)$	Width $b_0\,(mm)$	Gauge length $L_0\,(mm)$	Parallel length $L_c\,(mm)$	Total length $L_t\,(mm)$
3	10	20	90	115	350

Figure 4.16 Samples for the tensile test

Figure 4.17 Tensile test equipment

The tensile test results are summarised in Table 4.9 and Figure 4.18. In the numerical verification of the experimental work which will be discussed in Chapter 5, material properties of beams and columns obtained from the tensile test will be adopted in the numerical models.

Table 4.9 Tensile test results

Samples	Thickness a_0 (mm)		Yield strength f_y (MPa)	Ultimate tensile strength f_u (MPa)	Elastic modulus E $\times 10^5$ (MPa)
	Nominated	Measured			
S1-1	10	9.4	325	455	2.09
S1-2	10	9.4	315	455	2.07
S1-3	10	9.3	330	465	2.04
Average	10	9.37	323.3	458.3	2.07

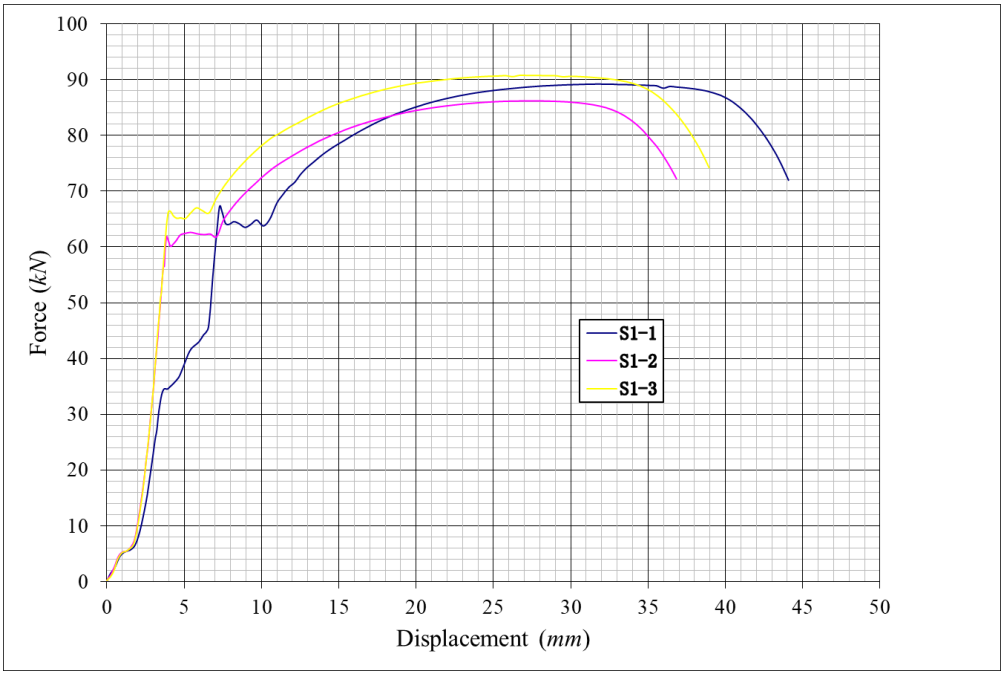

Figure 4.18 Force-displacement relationship from the tensile test

4.5 Test Rig Setup

In order to ensure the testing frames to undergo in-plane deformation only under loading, a side support system was set up to connect with the reaction frame. The support system consists of two lateral beams which were bolted on the reaction frame, and parallel to the testing frame; two connecting tubes which provide out-of-plane stability to the lateral beams; and four sliding circular steel tubes which were fixed to the lateral beams on one side, and seated on pulleys on the other side right next to the web of the second-floor beam, as shown in Figure 4.19.

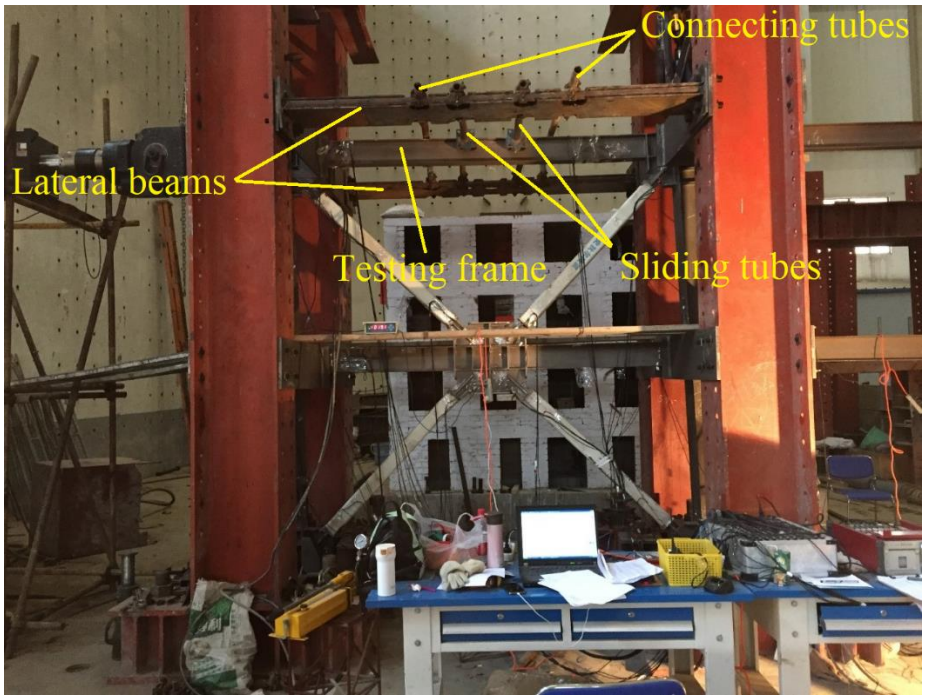

Figure 4.19 Out-of-plane supporting system

This experiment employed the low cyclic loading method. The lateral cyclic load was provided by MTS electro-hydraulic servo actuator which was fixed to the reaction wall on one side and bolted to the top left of the frame on the other side. The travel distance of the actuator is $\pm 150mm$. The static vertical loads exerted at the columns were applied through three hydraulic jacks. To ensure consistent vertical loads during the horizontal motion of the frame, roller sliding blocks were placed between the column top and the hydraulic jack. To achieve the fixed end constraint for the boundary condition, the columns were welded to the ground beams. The schematic of the experimental set up is presented in Figure 4.20.

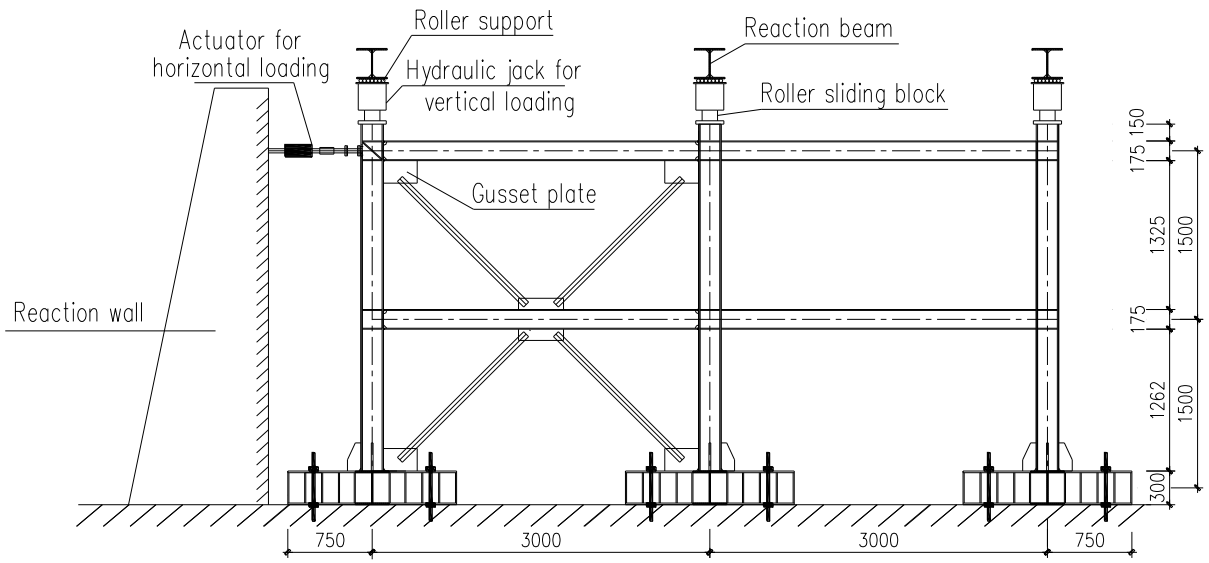

Figure 4.20 Experimental set up (unit: *mm*)

4.6 Measurement System

The measurement system consists of an electric sensor, an automatic static data acquisition unit and a computer. The main measurements include horizontal displacements at the end of the beams, and strains of the structural components. Figure 4.21 shows the arrangement plan of displacement meters (DM) and dial indicators (DI). DMs and DIs were set up at the right side of the column top and the column base, respectively, to measure the storey drift and the slippage of the frame. Additionally, to obtain the rotation of the pin beam-column connection in the non-moment resisting frame, two extra displacement meters were placed on the column, above and below the beam end (i.e. DM2 and DM3 were placed at the right end of KL3).

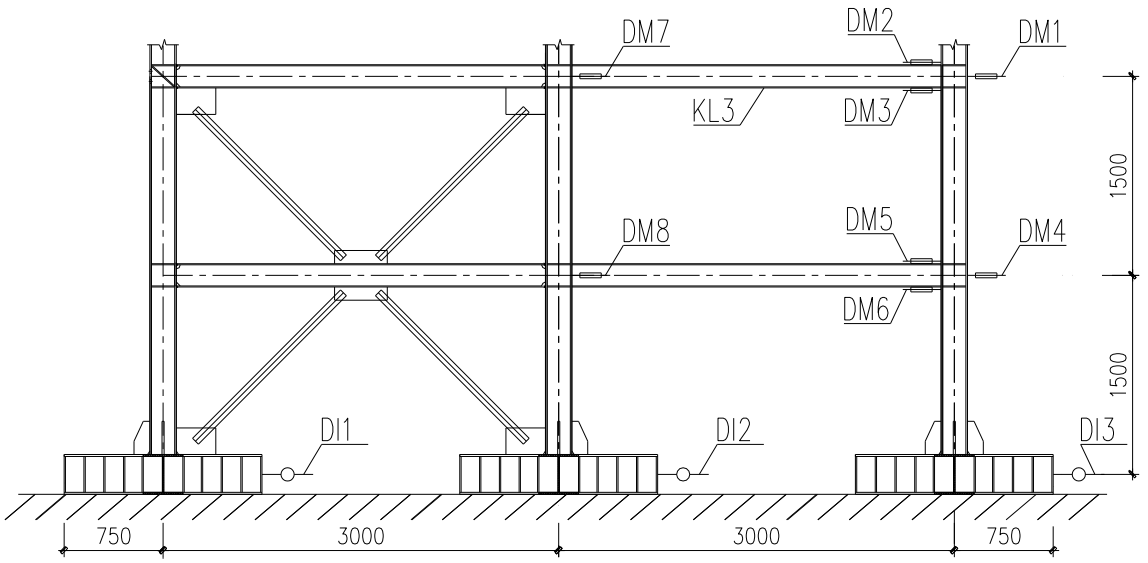

Figure 4.21 Arrangement plan of displacement meters (DM) and dial indicators (DI) (unit: *mm*)

Figure 4.22 indicates the arrangement plan of strain gauges and strain rosettes. The strain gauges were distributed along the longitudinal axis at the webs of the ends of the columns and beams, beam-column connection panel zones, the gusset plates and the steel plate of BRBs.

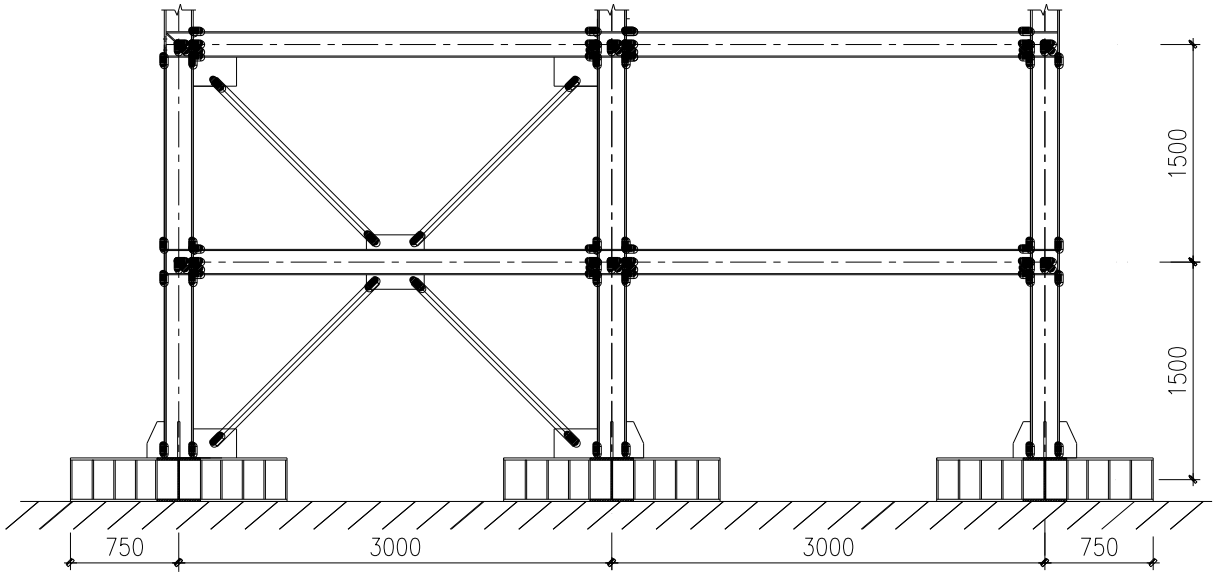

Figure 4.22 Arrangement plan of strain gauges (unit: *mm*)

4.7 Loading Protocol

4.7.1 Cyclic test loading scheme

Quasi-static simulations were conducted using the displacement control method. The loading protocol follows the loading protocol provisions outlined in the Chinese seismic provision (GB50011, 2010). Brief definitions used in the calculation of target displacements for cyclic loading are provided in Table 4.10.

Table 4.10 Loading protocol definitions

Symbol	Definition
Δ_f	Deformation quantity used to control loading of the test frame
Δ_{fe}	Maximum elastic deformation of the test frame

In the test, 250kN vertical loads were first exerted on all the columns through hydraulic jacks. After the pressure was stabilised, a small lateral load was applied to the top left of KZ1 through the actuator, collinear with the centre line of KL1 (See Fig.4.10). Then a small step size of Δ_f was applied in the initial phase until the test frame reached its maximum elastic displacement Δ_{fe}. Subsequently, the multiple of Δ_{fe} (2 Δ_{fe}, 3 Δ_{fe}, 4 Δ_{fe}, 5 Δ_{fe}, 6 Δ_{fe} ……) step size were acted. Every full cyclic loading stage included three identical cycles, and every loading cycle consisted of four steps: (1) applied the target displacement at the testing frame and held the load for three minutes; (2) unload until the frame went back to the initial position; (3) applied the same target displacement in the opposite direction and held the load for three minutes; (4) unload until the frame went back to the initial position. Note that the displacement controlled rate is 0.5 mm/s. The loading protocol for the two BRBFs with different beam-column connections was identical as the rotational capacity of both of the connections were very limited.

4.7.2 Pushover test loading scheme

The pushover test loading scheme followed a similar method to the cyclic loading test. Quasi-static simulation based on the displacement control method was adopted. Instead of applying the displacement in two opposite directions, one way (push or pull) displacement was imposed on the frame. The step size was relatively steady or being constant, compared to the cyclic loading test.

4.8 Concluding Remarks

This chapter presents the experimental program on three half scaled 2-storey models: two buckling retrained braced frame (BRBF) with non-moment resisting frames which were assembled with two different bolted only beam-column connections; and one single 2-storey BRBF (without non-moment resisting frame). Published experiments are reviewed in terms of the test frame design, set up, and connection details. Subsequently the experimental techniques used in the present experiment are given in some details. Specifically, the experimental specimen design, test rig setup, measurement method and loading scheme are described.

CHAPTER 5

EXPERIMENTAL RESULTS AND NUMERICAL COMPARISON

5.1 General Remarks

This chapter presents the experimental results of three half scaled 2-storey specimens: two double-bay frames consisting of a buckling retrained braced frame (BRBF) and an adjoining non-moment resisting frame (BRBF-EF and BRBF-FF), and one single-bay BRBF (without a non-moment resisting frame). The results will be used to (1) improve understanding of the inelastic cyclic behaviour of the proposed structural system; (2) assess the relation between the mechanical behaviours of BRBFs with bolted unbraced bay and those of a single BRBF; (3) evaluate the capability of the numerical models developed in Chapters 3; and (4) provide recommendations for further analysis and modelling of the proposed structural system. The numerical models developed are subsequently used in Chapter 6 for parametric study to assess the response and performance of a variety of steel braced frame systems.

The experimental observations of three cyclic loading tests and one pushover test are presented in details in Section 5.2. Subsequently, the experiment results are discussed with respect to the hysteretic behaviour, energy-dissipating capacity, and stiffness degradation. Finally, the numerical results are compared to the experimental ones for validation.

5.2 Experimental Observations

Before the commencement of the tests, the specimens were calibrated to be in the upright position. This is to avoid the initial out-of-plane deformation and the influence of *P-delta* effect. The bolts connecting the ground beams and the floor were then tightened up once the vertical alignment was done. Subsequently, the support system was set up to ensure the out-of-plane stability.

The structural responses of the three experimental models are similar under the cyclic loadings. Specifically, detailed experimental observations are described below.

5.2.1 Cyclic loading test for BRBF-EF

A pre-loading procedure was first applied to the testing frame to ensure the proper performance of the measuring devices, including displacement meters (DM), dial indicators (DI), and the digital strain meter. After the experimenting system was tested to be stable, the loading of the cyclic test commenced. The setup of the experimenting has been shown in Figure 4.8.

The loading protocol followed the method introduced in Section 4.7. An initial horizontal displacement Δ_f (as defined in Section 4.7.1)=1.2mm was applied to the frame until the test frame reached its maximum elastic displacement Δ_{fe}=4.8mm, which was obtained from the numerical analysis detailed in Section 5.4, then the multiple of Δ_{fe} step size were acted. In the initial stage of the loading process, there was no obvious phenomenon observed in the testing frame. At Δ_f=28.8mm, "popping" noises were heard from the BRBs which could be from the internal concrete crushing. Meanwhile, the steel core of BRBs began to display visible axial extension from the bond preventing material, as shown in Figure 5.1. From then, during the "push-pull" actions, the extension and compression of BRB cores were constantly observed, which implies adequate axial deformation capability of BRBs. Not surprisingly, no noticeable yielding was observed in the beam, columns or gusset plates during the entire loading process.

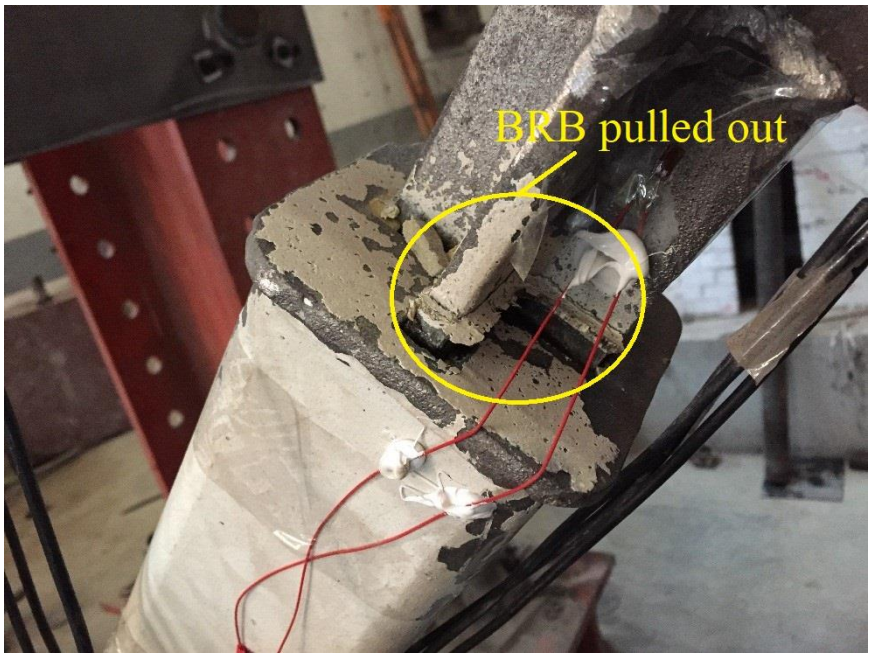

Figure 5.1 Axial extension of BRB core in BRBF-EF specimen

At Δ_f= 38.4*mm*, KL1 connecting to the actuator started to show the tendency of out-of-plane deformation. Figure 5.2 shows the rotation of the actuator due to the deformation of KL1. This is because the cross sectional area of the beams are relatively small, although the out-of-plane support system reduced the effective length of the beam, the compression capability of KL1 was still quite limited. Therefore, in case when KL1 buckled, the test was terminated at Δ_f= 38.4*mm*. After unloading, no visible plastic deformation was observed in the test frame, implying sufficient ductility and energy-dissipation capacity of the structural system.

Figure 5.2 Rotation of the actuator on BRBF-EF specimen

5.2.2 Cyclic loading test for BRBF-FF

The observations of the second test for the BRBF with fin-plate connections in the non-braced bay (BRBF-FF) are very similar to those for BRBF-EF. Δ_{fe} is identical to the first test, and is equal to 4.8mm from the numerical results (details are given in Section 5.4.2). AT Δ_f= 24mm, visible axial extension of BRB1 (Figure 4.8 (a)) was observed as the core steel was pulled out from the bond preventing material. With increased Δ_f during the loading, and the extension and compression of BRBs can be observed accordingly, and the extension of BRB is shown in Figure 5.3.

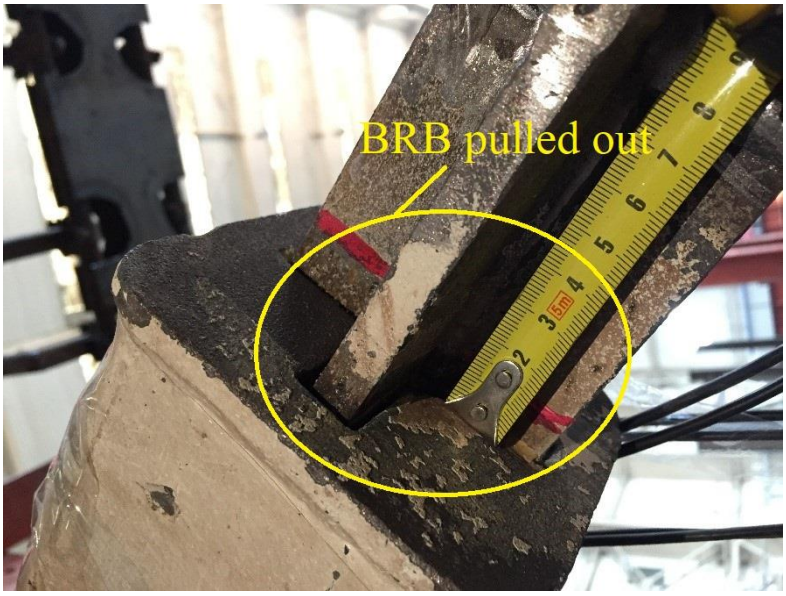

Figure 5.3 Axial extension of BRB core in BRBF-FF specimen

At Δ_f = 33.6*mm*, small, yet noticeable out-of-plane rotation was found at the actuator, due to the tendency of buckling at KL1. Then, the test was ended and the pushover test was performed instead as described in Section 5.2.3.

5.2.3 Pushover test for BRBF-FF

In order to prevent the frame from deforming out-of-plane, a pulling action instead of pushing was horizontally applied to the frame. Displacement control was also adopted in the pushover test. The initial displacement of the frame before the commencement of the pushover test was 25.2*mm* (the remained horizontal displacement after unloading of the cyclic test). The displacement was applied in the opposite direction with the initial increment of 5*mm*. After five increments, the horizontal displacement Δ_f returned to zero. When the "pull-over" test commenced, the increment of displacement remained at 5*mm* in the same direction until Δ_f = -25*mm*, the increment was then reduced to 2*mm* in order to observe the possible yielding in the test specimen. However, no strength reduction was observed during the loading process. The horizontal force measured from the actuator constantly increased until the test ended at Δ_f =-133*mm*. After the "pull-over" test finished, visible structural deformation was found as the residual displacement shown in Figure 5.4. Nevertheless, no yielding was observed in the

structural beams or columns, which indicates excellent ductility and energy dissipation capacity of the structural system.

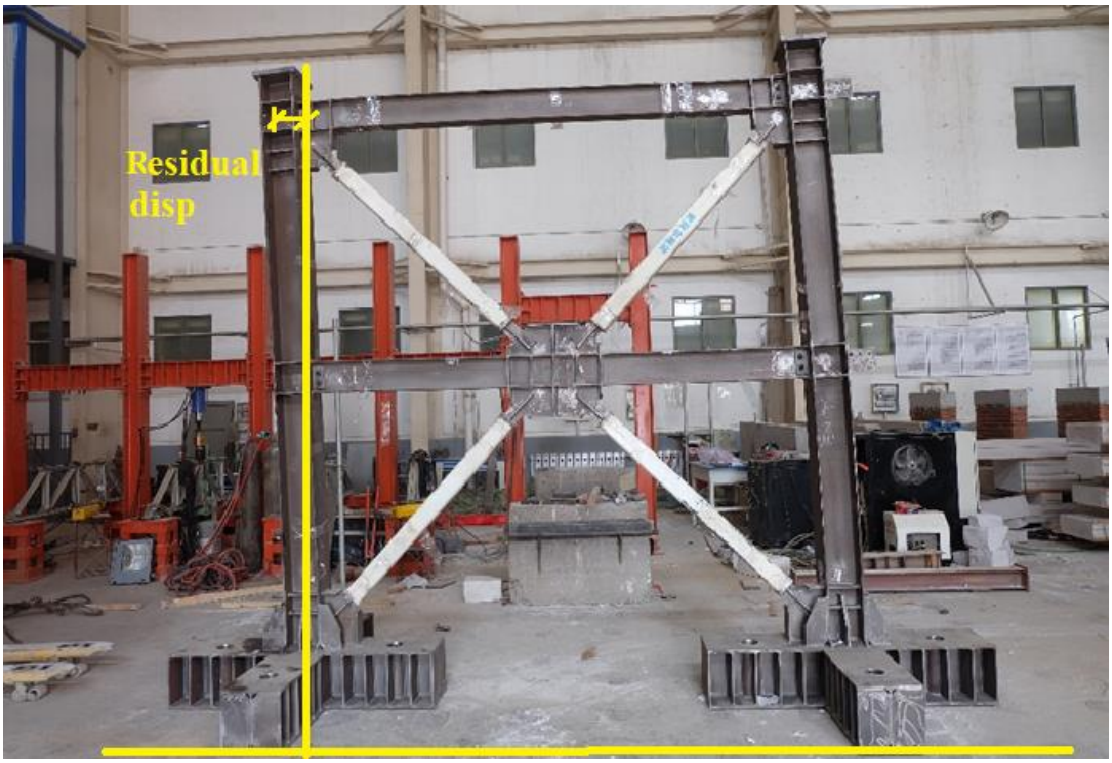

Figure 5.4 Disassembled BRBF-FF specimen after test

5.2.4 Cyclic loading test for single BRBF

The third test was a cyclic loading test for the single BRBF. This test also adopted 4.8*mm* as the maximum elastic displacement for the loading. Similar to the first two cyclic loading tests, crushing sound from BRB4 (Figure 4.8 (a)) was heard when the horizontal displacement Δ_f reached 28.8*mm*. It should be noted that the BRBs in the single BRBF yielded at the same displacement with those in specimens BRBF-EF and BRBF-FF. This is because the non-moment-resisting bays in BRBF-EF and BRBF-FF provide very limited stiffness to the BRBF, therefore results in a similarity of the structural behaviours of the three specimens. Subsequently, as the BRB steel core was observed to be pulled out from the steel tube, the BRBs yielded successively. The test ended when the displacement went up to 52.8*mm*. The frame integrity remained without any clearly visible plastic deformation, as can be seen in Figure 5.5.

Figure 5.5 Single BRBF after test

5.3 Experimental Data Analysis

Lateral stiffness, strength, deformability and energy-dissipating capacity are the main factors in evaluating the seismic performance of the proposed system. Therefore, the hysteresis curve, skeleton curve, energy dissipation capacity and stiffness degradation coefficient were generated from the experimental output.

5.3.1 Hysteresis curve

The hysteresis curve represents an important force-displacement relationship which indicates material nonlinearity of a system subjected to cyclic loading. It is useful for characterising the dynamic response of the system, as well as indicating the states of strength and stiffness degradation.

Figure 5.6 shows the hysteresis curves of the three tests. The figures plot the actuator force versus the 2nd storey drift (i.e., the maximum displacement of the frame). It can be observed from these figures that the tensile force is always greater than the compressive force in a cyclic circulation. This is possibly due to the slight loosening of

the bolts connecting the actuator and the tested specimen during the loading process. When the bolts were tightened up again, the specimen might not have been placed back at the exact original position, therefore led to the slight difference in tension and compression.

As illustrated in Figures 5.6 (a) and (b), the hysteresis behaviours of BRBF-EF and BRBF-FF are very close to the ideal behaviour which displays stable and non-degenerating loops. The amount of area enclosed by the hysteresis loops is large and the loops follow approximately the same path for each of the higher loading cycles. Nevertheless, in the cyclic test for BRBF-EF, the supporting system was not reinforced properly, which resulted in a slight out-of-plane rotation of the 2nd storey beam during pushing action. As can be seen in Figure 5.6 (a), the hysteresis loop in the first quadrant increases almost linearly when the displacement is greater than 9.6*mm*, this is because the 2nd storey beam started to slightly lean onto the supporting system when being pushed at a relatively large force-displacement level. This problem was corrected in the following tests. In Figure 5.6 (b), the sudden change in the first quadrant for BRBF-FF is due to the unexpected rotation of the actuator, and when this happened, the test was terminated.

While BRBF-EF and BRBF-FF displayed almost ideal hysteresis behaviour, the single BRBF demonstrates slightly pinched hysteresis loops. Typically, pinched hysteresis loops reflect the behaviour of a structure that have members buckled when subjected to compressive loads. However, in the case of the single BRBF, the pinched loops are not due to the buckling of members but are the result of the change in stiffness due to the deformation of the BRBs after yielding.

Figure 5.7 illustrates the base shear force versus the roof drift of BRBF-FF under the pushover test. The force-displacement relationship follows a linear pattern initially, then the increase of the base shear force slows down as the frame entered into the plastic stage. Although the profile of the curve is not quite smooth due to the rotation of the

actuator during the multiple loading with small increment, the base shear force did not decrease during the entire loading process. This indicates a considerable plastic deformation capacity of the frame specimen BRBF-FF.

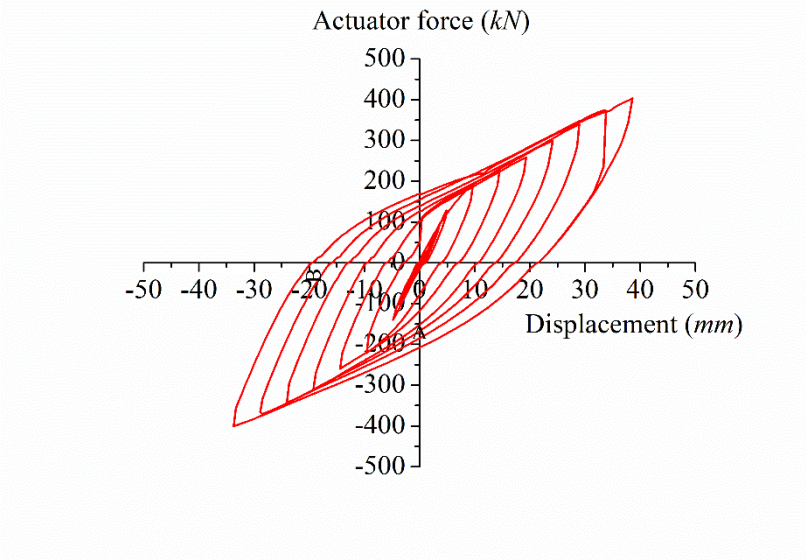

(a) BRBF-EF

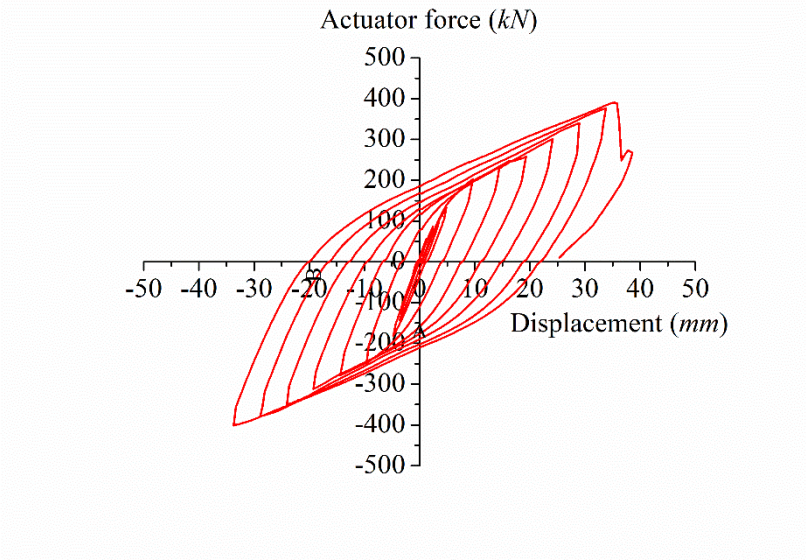

(b) BRBF-FF

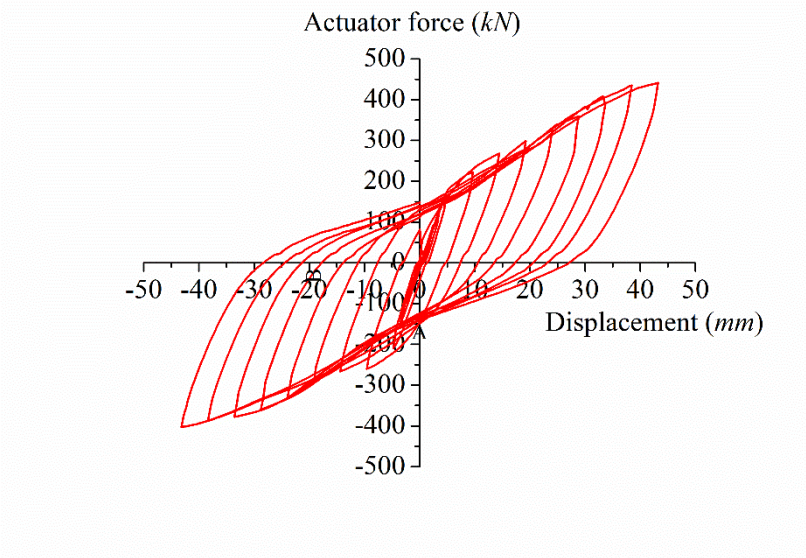

(c) Single BRBF

Figure 5.6 Hysteresis curves of three test specimens

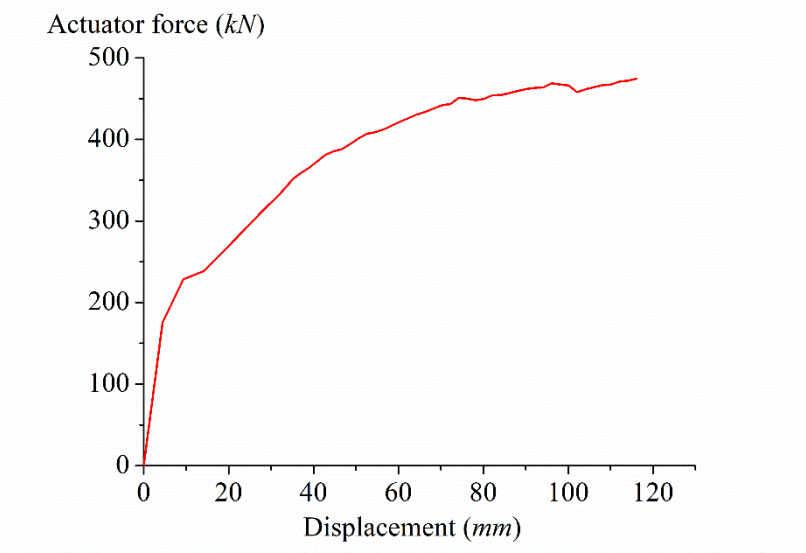

Figure 5.7 Base shear-roof drift relationship of BRBF-FF under pushover test

5.3.2 Skeleton curve (backbone curve)

A skeleton curve, also known as the backbone curve, is the profile of peak values forming the cyclic envelope of a hysteresis curve. Skeleton curves can show the accurate characterisation of strength and stiffness relationships as a structure progresses through hysteretic behaviour.

Figure 5.8 shows a standard skeleton curve which can be used to obtain the yield load and yield displacement. The "Specification for seismic test of buildings JGJ/T 101" (2015) specifies three typical characteristic points on this figure. Point A represents the yield point, from which the structure enters into plastic stage. At point A, the y-coordinate P_y is the yield load and the x-coordinate Δ_y is the yield displacement. Point B marks the maximum load (P_{max}) and corresponding displacement (Δ_{max}) of the frame when the lateral load attained P_{max}. After point B, the strength and stiffness of the structure begin to decrease. Point C is the failure point where the lateral load falls to 85% of P_{max}, and Δ_u is the corresponding ultimate displacement at 0.85 P_{max}.

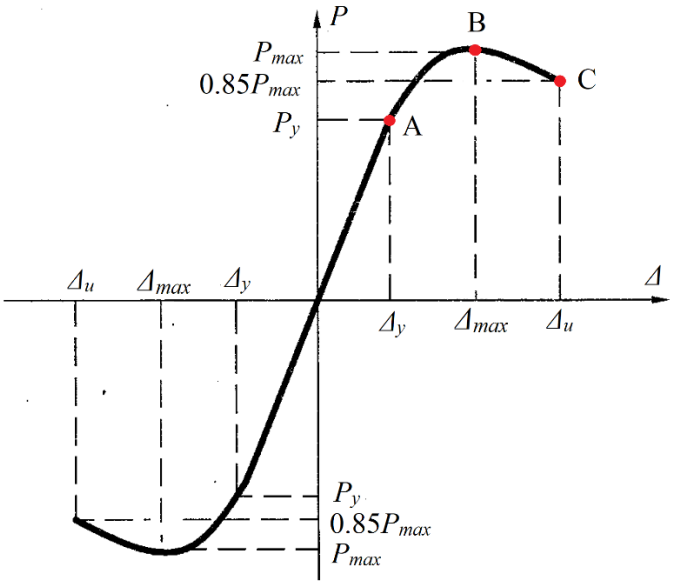

Figure 5.8 Schematic diagram of a standard skeleton curve (JGJ/T 101, 2015)

Figure 5.9 demonstrates the skeleton curves obtained from the tests of the three specimens. As shown in the figure, except that the actuator rotated at the end of the test for BRBF-FF, there is no decrease found in the curves. This implies that there was no strength degradation in tension or compression for the specimens throughout the tests. Note that all three tests reached point A where the elastic deformation is 4.8*mm*. However, none of the tests reached point B due to the limitations in the measurement device.

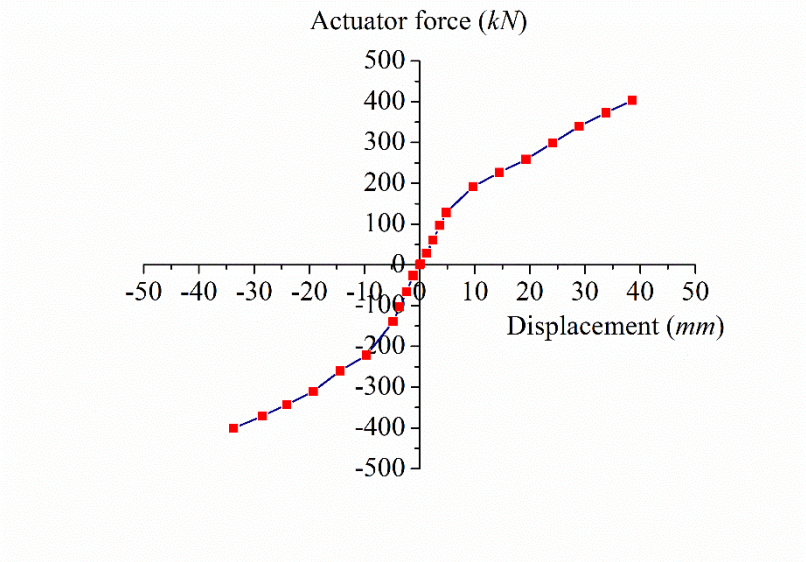

(a) BRBF-EF

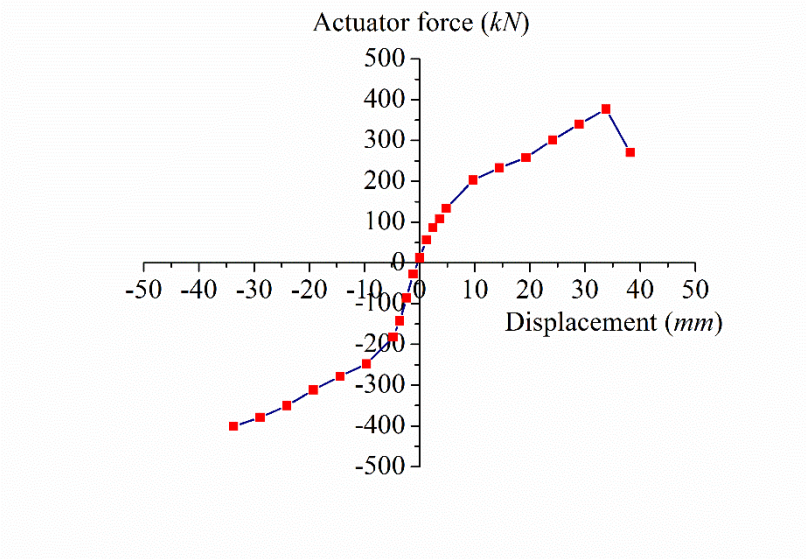

(b) BRBF-FF

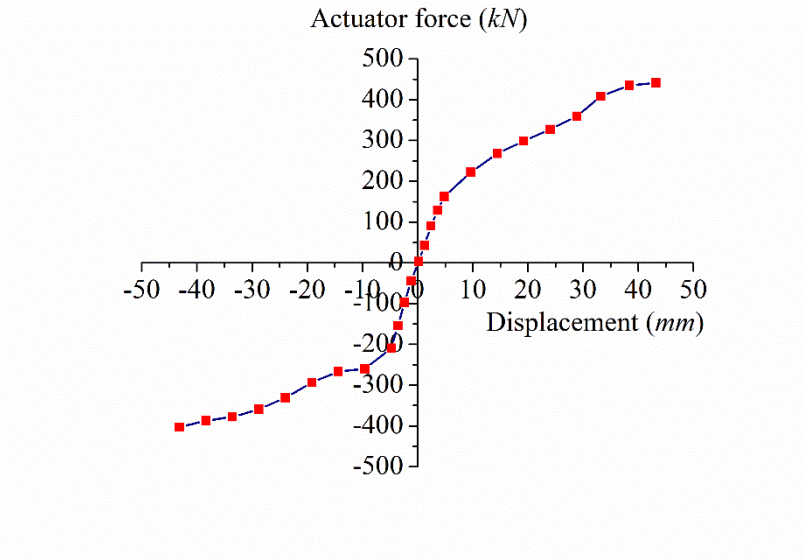

(c) Single-BRBF

Figure 5.9 Skeleton curves of three test specimens

5.3.3 Energy dissipation capacity

Energy dissipation capacity (*EDC*) is one of the indicators of structural seismic performance. Under cyclic loads, the area covered by the hysteresis loop represents the energy dissipation capacity of a structure. For a given hysteresis loop of a structure (Figure 5.10), the energy dissipation capacity *EDC* of the structure can be calculated as follows:

$$EDC = \frac{S_{(ABC+CDA)}}{S_{(OBE+ODF)}} \tag{5-1}$$

where $S_{(ABC+CDA)}$ represents the area enclosed by the hysteresis loop; $S_{(OBE+ODF)}$ represents the corresponding triangular area. Obviously, a greater value of *EDC* demonstrates a better energy dissipation capacity of the structure.

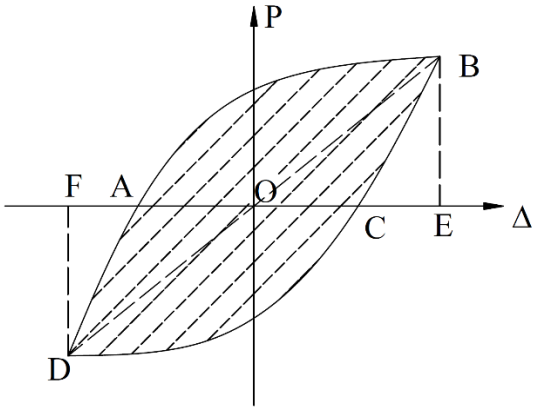

Figure 5.10 Schematic diagram of energy dissipation capacity calculation (JGJ/T 101, 2015)

The values of *EDC* of the three tested specimens are summarised in Tables 5.1 to 5.3 and Figure 5.11 for all three specimens. Tables 5.1 to 5.3 list the applied displacements with the corresponding loop numbers. Also included in the tables are the hysteresis loop area $S_{(ABC+CDA)}$, the corresponding triangular area $S_{(OBE+ODF)}$ and the calculated *EDC* value for each loop in the tests. As can be observed in Figure 5.11, for all the three specimens, there was barely any energy dissipation before the 4th loop. This is because the structures still remained elastic before the said loop, at which the horizontal displacement is 4.8*mm*. Between the 4th and the 6th loops, the *EDC*s of the frames increase significantly. This is because the BRBs during this stage yielded successively, therefore the earthquake energy was dissipated through the axial deformation of the BRBs. It should be noted that the EDC of the single BRBF during the 4th to 6th loops is slightly higher than those of BRBF-EF and BRBF-FF, possibly due to its better deformation capacity. After the 6th loop, the *EDC*s of BRBF-EF and BRBF-FF are still slowly increasing, while that of the single BRBF is tending to be flattened after a slight drop. This implies that the assemblies of the non-moment-resisting frames (BRBF-EF and BRBF-FF) are able to enhance the ductility of the BRBFs, which result in a higher EDC under earthquake activities.

Table 5.1 Energy dissipation capacity for BRBF-EF

Applied displacement (*mm*)	Loop number	$S_{(ABC+CDA)}$ (*kN·mm*)	$S_{(OBE+ODF)}$ (*kN·mm*)	*EDC*
±1.2	1	9.74	65.37	0.15
±2.4	2	33.55	303.52	0.11
±3.6	3	81.03	720.23	0.11
±4.8	4	187.8	1290.83	0.15
±9.6	5	1820.72	3982.09	0.46
±14.4	6	4497.71	7034.75	0.64
±19.2	7	7539.74	10963.27	0.69
±24.0	8	10947.97	15469.70	0.71
±28.8	9	14845.59	20390.99	0.73
±33.6	10	20171.17	26088.82	0.77

Table 5.2 Energy dissipation capacity for BRBF-FF

Applied displacement (*mm*)	Loop number	$S_{(ABC+CDA)}$ (*kN·mm*)	$S_{(OBE+ODF)}$ (*kN·mm*)	*EDC*
±1.2	1	9.32	101.82	0.09
±2.4	2	44.52	413.25	0.11
±3.6	3	115.08	903.10	0.13
±4.8	4	305.23	1517.10	0.20
±9.6	5	2227.67	4342.39	0.51
±14.4	6	5244.24	7386.29	0.71
±19.2	7	8271.4	10980.89	0.75
±24.0	8	11855.04	15697.64	0.76
±28.8	9	16436.65	20798.07	0.79
±33.6	10	20895.41	26251.09	0.80

Table 5.3 Energy dissipation capacity for single BRBF

Applied displacement (*mm*)	Loop number	$S_{(ABC+CDA)}$ (*kN·mm*)	$S_{(OBE+ODF)}$ (*kN·mm*)	*EDC*
±1.2	1	11.58	103.96	0.11
±2.4	2	49.71	450.86	0.11
±3.6	3	133.43	1018.36	0.13
±4.8	4	429.21	1782.68	0.24
±9.6	5	2802.61	4626.92	0.61
±14.4	6	5377.5	7702.46	0.69
±19.2	7	7550.87	11369.19	0.66
±24.0	8	9572.71	15798.72	0.61
±28.8	9	13574.37	20690.85	0.66
±33.6	10	17204.11	26273.32	0.65
±38.4	11	20412.51	31563.23	0.65
±43.2	12	25009.26	36467.77	0.69

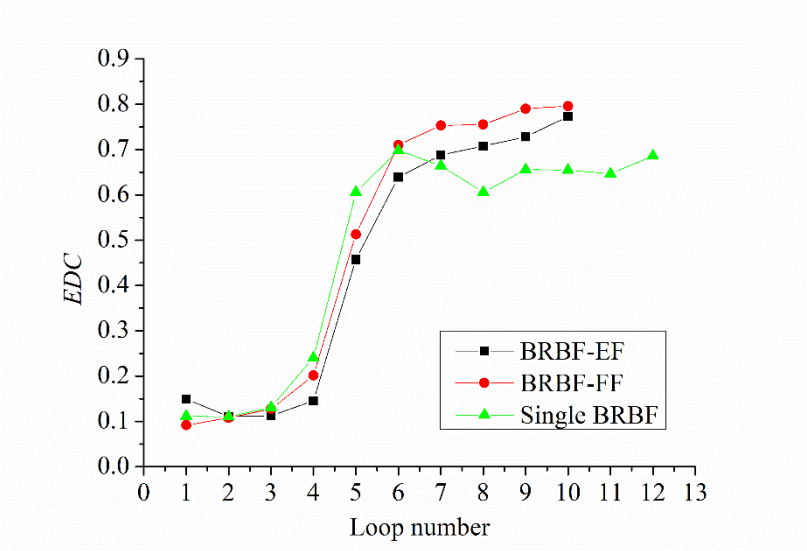

Figure 5.11 Energy dissipation capacity *EDC* of three specimens

5.3.4 Stiffness degradation

Structural components and systems often exhibit certain level of stiffness degradation when subjected to reverse cyclic loading. Stiffness degradation can be evaluated by the *secant stiffness coefficient* K_i (JGJ/T 101, 2015).

$$K_i = \frac{|+F_i|+|-F_i|}{|+X_i|+|-X_i|} \tag{5-2}$$

where $\pm F_i$ are the maximum base shear forces (actuator forces) in loop i, $\pm X_i$ are the maximum displacements in loop i.

The K_i values are calculated for each loop of the tests and numerical analyses for all three specimens, and are summarised in Table 5.4. It can be observed that the numerically predicted horizontal secant stiffnesses for BRBF-EF and BRBF-FF systems are slightly larger than that of the single BRBF as expected. However the test results show smaller stiffnesses especially for BRBF-EF, which could be due to the pin connections in the non-moment resisting bay not being fully tightened, thereby causing frictions at the pin joints. Such a phenomenon was less obvious in the later loading cycles because the increased applied load became more dominant.

To further observe the stiffness degradation of the tested frames, Figure 5.12 plots the K_i/K_1 versus the structural displacement (roof drift) throughout the tests. In the early stage of loading, all the values of K_i/K_1 for the three frames exceed 1.0 which represents an elastic behaviour. Note that the small increase of the structural stiffness in the elastic stage is due to the actuator not having been in perfect contact with the frame during the initial loading cycles. From the 4th loop for BRBF-FF, and the 5th loop for BRBF-EF and the single BRBF, the stiffness degradation started to occur in the frames as the values of K_i/K_1 decrease to lower than 1.0. The stiffness ratios K_i/K_1 at $\pm 33.6mm$ for the specimens are 0.5 for BRBF-EF, 0.33 for BRBF-FF, and 0.33 for the single BRBF.

Table 5.4 Secant stiffness coefficient K_i for three test specimens

Applied displacement (*mm*)	Loop number	$K_{i\text{-}BRBF\text{-}EF}$		$K_{i\text{-}BRBF\text{-}FF}$		$K_{i\text{-}single\ BRBF}$	
		Test	Numerical	Test	Numerical	Test	Numerical
±1.2	1	22.73	45.3	35.07	45.3	36.12	44.1
±2.4	2	26.42	45.3	35.95	45.3	39.32	44
±3.6	3	27.72	42.1	34.79	42.1	39.16	41.2
±4.8	4	27.83	34.6	32.73	34.6	38.72	33.8
±9.6	5	21.44	20.9	23.39	20.9	25.11	19.9
±14.4	6	16.84	15.9	17.68	15.9	18.57	14.9
±19.2	7	14.76	13.7	14.78	13.7	15.42	12.7
±24.0	8	13.33	12.4	13.52	12.4	13.71	11.3
±28.8	9	12.37	11.4	12.44	11.4	12.47	10.4
±33.6	10	11.46	10.5	11.53	10.5	11.78	9.5
±38.4	11	-	-	-	-	10.70	8.8
±43.2	12	-	-	-	-	9.77	8.2

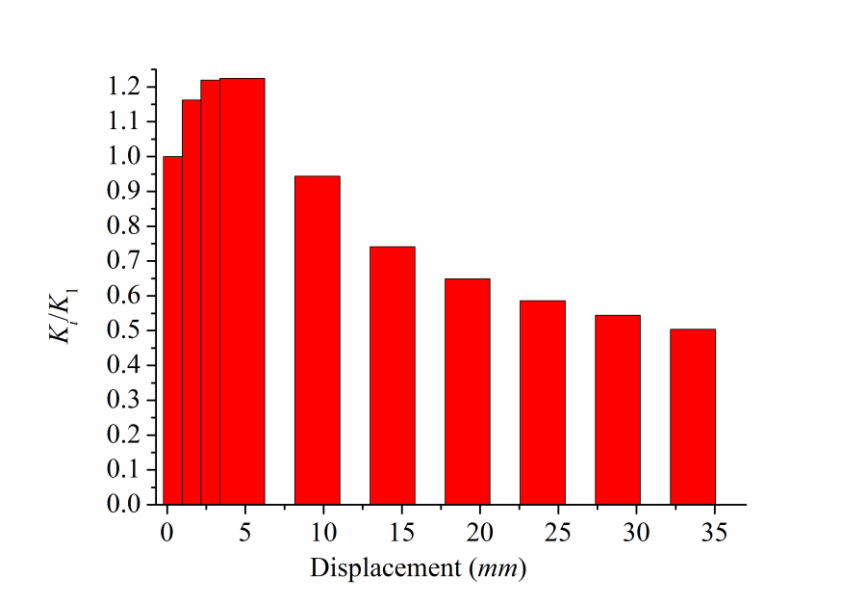

(a) BRBF-EF

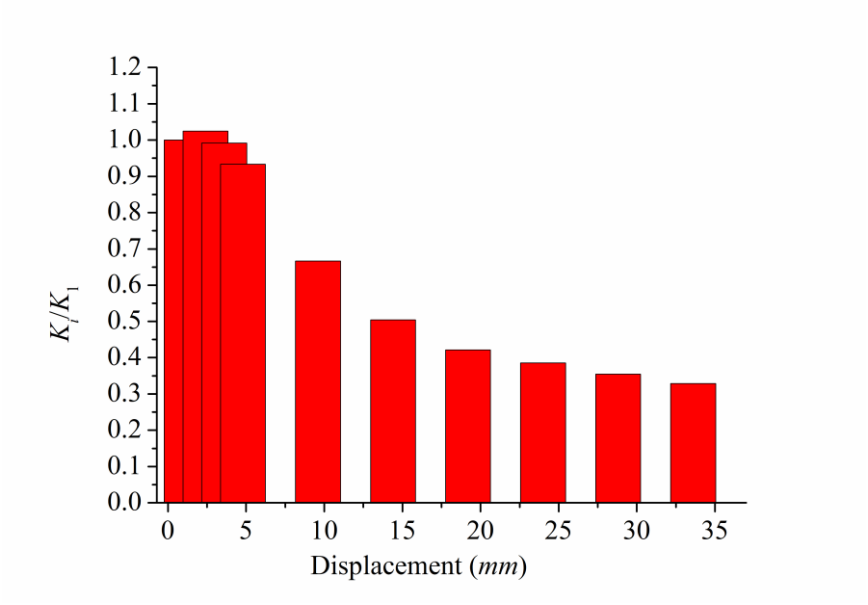

(b) BRBF-FF

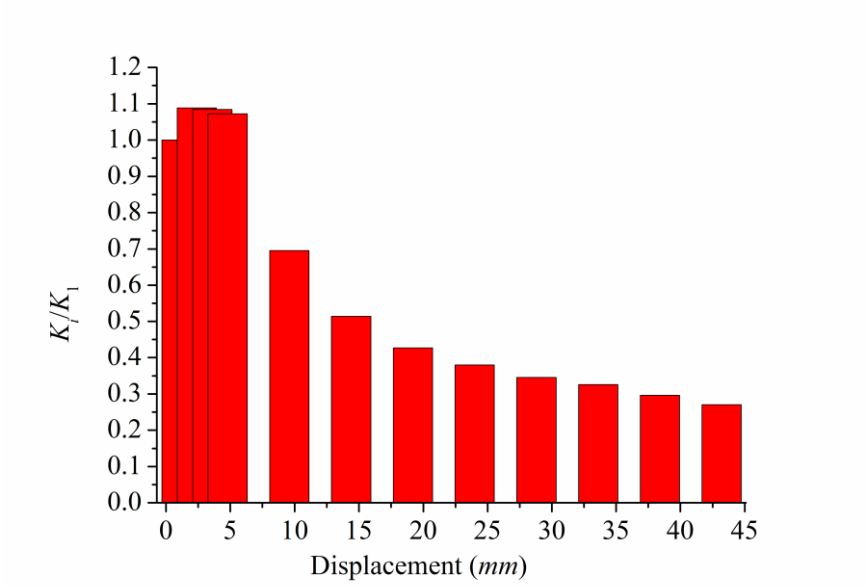

(c) Single BRBF

Figure 5.12 Stiffness degradation of three tests specimens

5.4 Experimental and Numerical Result Comparisons

5.4.1 Numerical techniques

The finite element analysis software OpenSees (McKenna et al., 2006) was used to predict the structural behaviour of the three test specimens, i.e. BRBF-EF, BRBF-FF, and single BRBF. The numerical approach including the element types, the material

behaviour and geometric nonlinearity follow the methodology introduced in Chapter 3, Section 3.3. Note that for the numerical models of all three specimens, the columns were assumed to be fully fixed to the ground. Furthermore, the numerical models for BRBF-EF and BRBF-FF were identical as the beam-column connections (end-plate connections for BRBF-EF and fin-plate connections for BRBF-FF) in the non-moment-resisting bays were all assumed to be purely pinned, therefore the non-moment-resisting bays provide no stiffness to the BRBF in the numerical models. This also explains the reason why the numerically and statically predicted elastic horizontal deformations Δ_{fe}=4.8mm for BRBF-EF, BRBF-FF and the single BRBF are identical. The value Δ_{fe}=4.8mm has been adopted to the tests as the maximum elastic displacement, after which, the experimental displacement was increased at 4.8mm increment.

5.4.2 Result comparison

To numerically replicate the cyclic behaviour of the test specimens, a displacement-controlled, quasi-static algorithm was applied in OpenSees to the numerical models described above. In the numerical analysis, the incremental horizontal displacement identical to the experimental displacement history, was applied to the top left nodal point of the model which corresponds to the application point of the actuator force in the tests.

Figures 5.13 to 5.15 show the comparisons between the numerical values and the experimental ones in the form of the overall hysteresis behaviour and skeleton curve. Note that the energy dissipation and stiffness degradation capabilities can be directly calculated from these curves. In these figures, the experimental base shear force takes the value of the actuator force. All the skeleton curves (Figures 5.13 (b), 5.14 (b) and 5.15 (b)) demonstrate a clear bilinear behaviour differentiating the elastic and plastic stages by Δ_{fe} =4.8mm. The actual base shear forces for Specimens BRBF-EF, BRBF-FF and single BRBF when BRB started yielding (the structural behaviour entered the plastic stage) are 135kN, 140kN and 155kN, respectively, which are very close to the numerical prediction. According to the experimental measurements from the strain

gauges on the columns, when the sectional bending moment reached yield moment, the base shear forces for the columns in all three specimens were approximately 400*kN*. This can also be reflected from the numerical pushover analysis results shown in Figure 5.14 (c), when the base shear force is slightly over 400*kN*, this force is found not to grow much while the displacement is still increasing. Also in Figures 5.13, 5.14 and 5.15, the numerical model predicts slightly larger displacements than those observed in the tests, this is due to the assumed infinitely rigid boundary conditions in the numerical model. In addition, the minor discrepancies in the result comparisons may be associated with the actual shearing deformations in the beam-column connections which were not considered in this analysis. For the analysis results presented, only flexural and axial deformations are considered. The imperfections of the experimental setup is also believed to contribute to the discrepancies to a certain extent. Furthermore, as the instantaneous horizontal actuator forces obtained from the tests are only approximate, especially for the later cycles, the correlation of the numerical and experimental results is considered to be satisfactory.

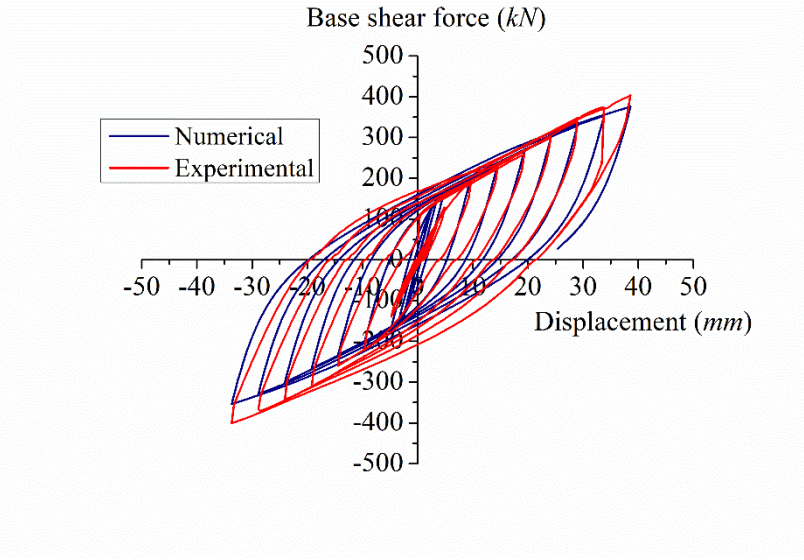

(a) Hysteresis curve

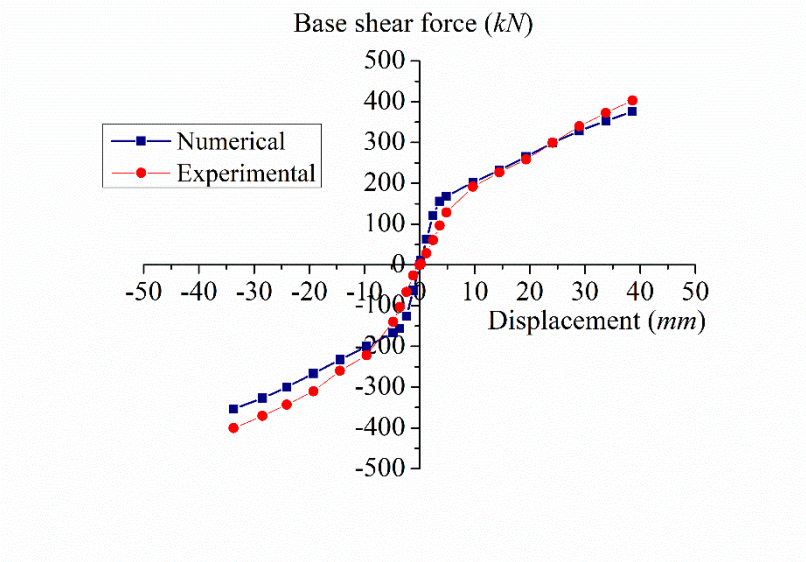

(b) Skeleton curve

Figure 5.13 Comparison between experimental and numerical results for BRBF-EF

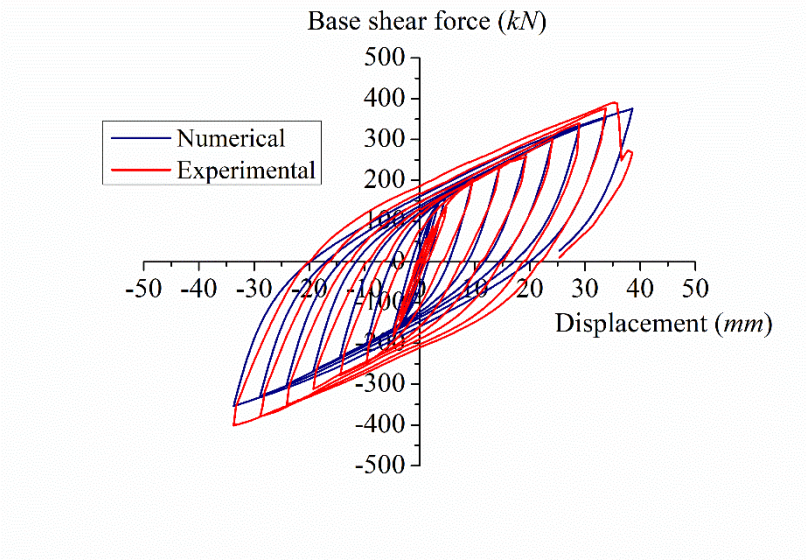

(a) Hysteresis curve

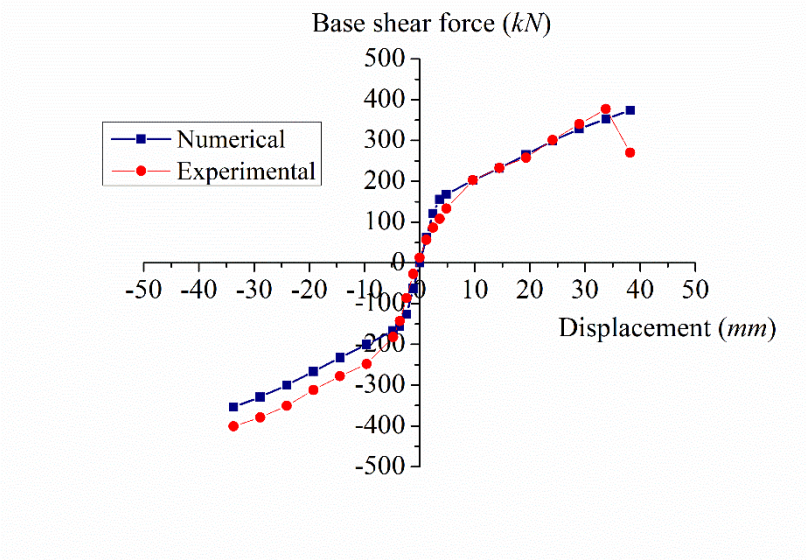

(b) Skeleton curve

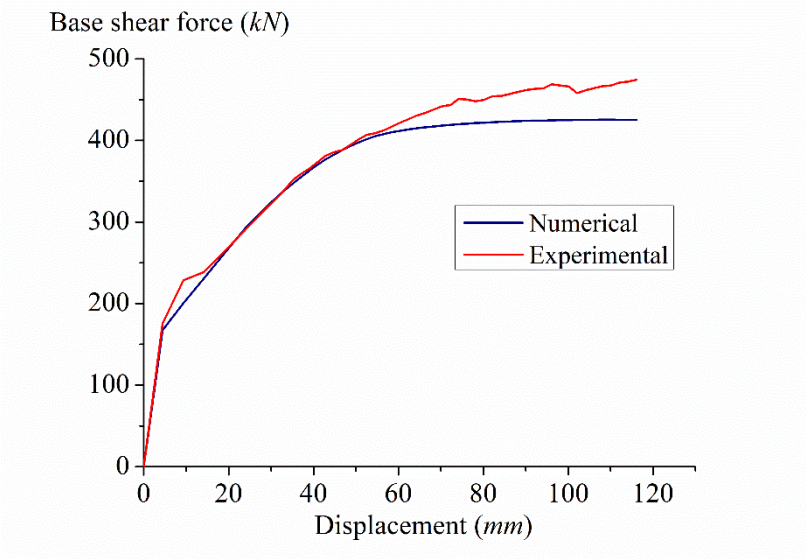

(c) Pushover result

Figure 5.14 Comparison between experimental and numerical results for BRBF-FF

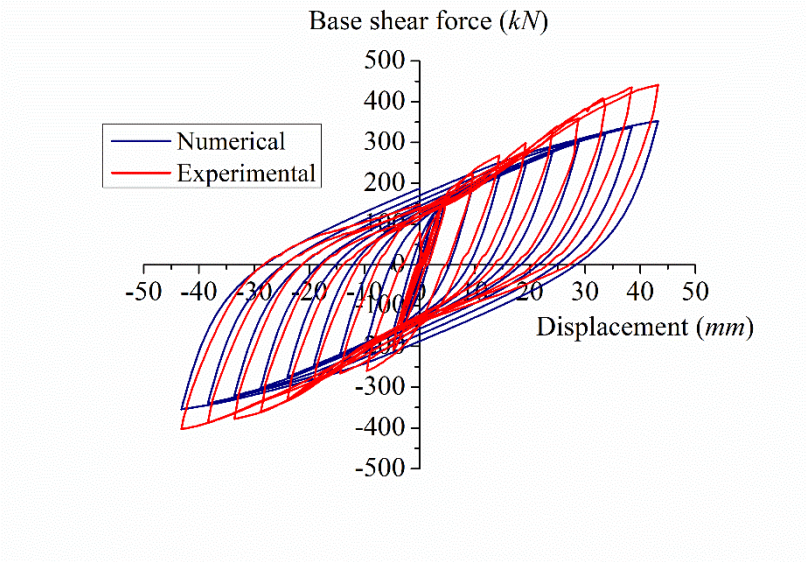

(a) Hysteresis curve

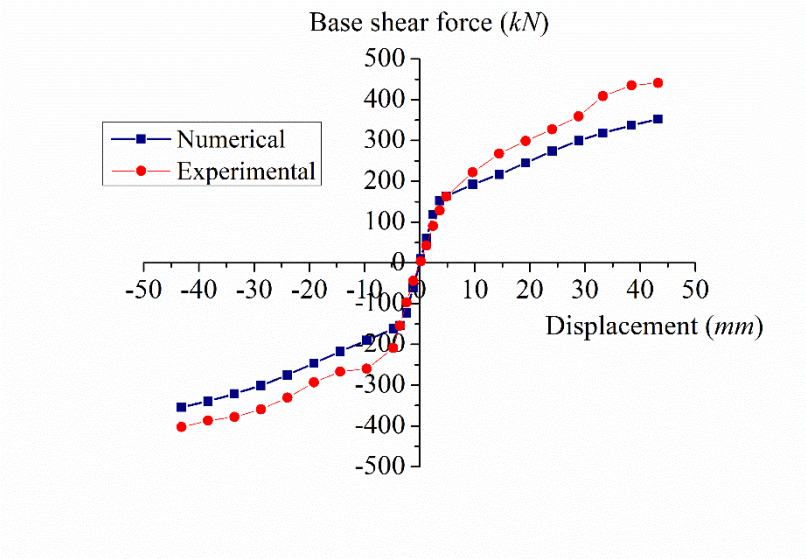

(b) Skeleton curve

Figure 5.15 Comparison between experimental and numerical results for the single BRBF

5.5 Concluding Remarks

This chapter presents the detailed experimental observations of three half scaled 2-storey frame specimens introduced in Chapter 4. The experiment results are discussed with regard to the hysteretic behaviour, the skeleton curve, the energy dissipating capacity, and the stiffness degradation.

The OpenSees models used in this chapter utilised simple rigid boundary conditions and purely pinned beam-column connections in the non-moment resisting bays. These assumptions imply that the rotational stiffness of the beam-column connections has a negligible contribution to the global behaviour. This is the main reason for the slight discrepancies between the numerical predictions and the experimental results. Nevertheless, the OpenSees models have proven to provide a reasonable approximation of the observed behaviour of the tested specimens.

As the experimental study only covers frames with limited number of storeys and non-moment-resisting bays demonstrating certain seismic dynamic responses, a parametric study is therefore presented in Chapter 6 to further investigate the impact of the beam-column-brace connection rigidity and the BRB area distributions on the seismic resistance capacity of the proposed BRBF system. Further, a fragility analysis on 12 prototype frames with three different storey heights and four numbers of non-moment resisting bays is conducted in Chapter 7 to fully understand the structural demand caused by various levels of ground shaking.

CHAPTER 6

PARAMETRIC STUDY

6.1 General Remarks

To fully understand the structural seismic performance and comprehensively evaluate the proposed BRBF system, a series of parametric studies of the proposed system has been performed using the verified numerical modelling approach introduced in Chapter 3. The modelling details and outcomes of the parametric studies are summarised in this Chapter. Specifically, the impact of the beam-column-brace connection rigidities and the BRB area distributions on the seismic resistance capacity of the system is studied. Two groups of models, namely the R- and P-Groups, each of which comprises 9-storey and 5-storey frames, are investigated. The frames in the R-Group are with moment-resisting beam-column-brace connections; those in the P-Group are with non-moment-resisting ones. Further, the design approach for BRB areas is evaluated in terms of the structural seismic performance. The findings could be beneficial for design purposes for such BRBF structures.

6.2 Beam-column-brace Connection Rigidity

As introduced in Chapter 3, the bolted beam-column connections in the proposed BRBF system can be assumed as purely pin. However, when the beam-column connections are assembled with the BRBs, the rigidities of the beam-column-brace connections may

be changed. Therefore, both moment-resisting and non-moment-resisting behaviours of the beam-column-brace connections merit further investigations in this chapter. For conventional beam-column connections, bolt connections (shown in Figure 6.1 (a)), bringing a certain level of flexibility, exhibit a relatively pin-type behaviour. However, when braces are connected to the beam-column connections, the gusset plates which are the most commonly used connection units between the braces and the main frame can provide a certain degree of rigidity to the beam-column connections (Figure 6.1 (b)). As a result, the beam-column connections in the braced bay tend to perform more rigidly, thus providing moment-resisting capability. Another popular beam-column connection type, as shown in Figure 6.2 (a), consists of a short section beam stub factory welded onto the column flanges. The stub sections are prepared for bolting usually at a location where the bending moment is reduced. When the braces are connected to a gusset plate, the rigidity of the beam-column connection is not increased as the bolted connection between the beam and the column is away from the gusset plate (Figure 6.2 (b)), and the beam-column connection still demonstrates a pin behaviour.

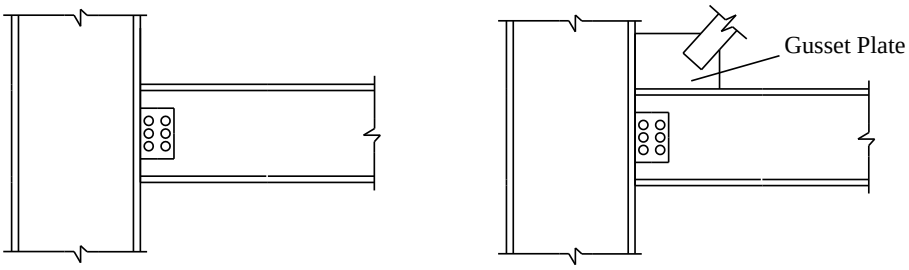

(a) Without BRB (b) With BRB

Figure 6.1 Conventional beam-column-gusset plate connection (rigid behaviour)

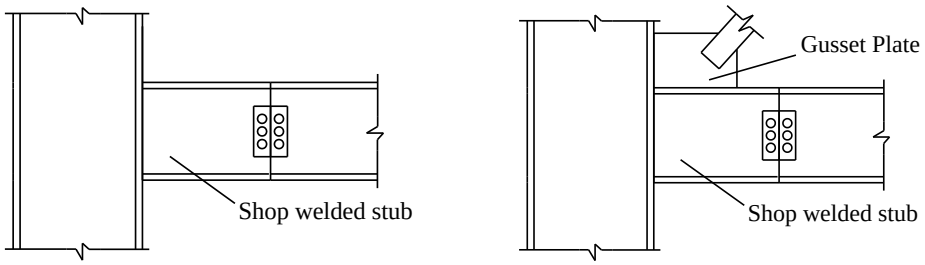

(a) Without BRB (b) With BRB

Figure 6.2 Beam-column-gusset plate connection with a stub (pin behaviour)

In this study, dynamic time-history analyses will be conducted to further validate the practicability of the proposed BRBF system. Furthermore, to investigate the influence of the stiffness of beam-column connections on the seismic response of the proposed system, both pin and rigid connections will be considered for the braced bay. In the numerical analyses, the conventional beam-column-gusset plate connections (Figure 6.1 (b)) are modelled as rigid connections, while those with stub (Figure 6.2 (b)) are modelled as pin connections.

6.3 Numerical Analysis of 5-Storey and 9-Storey BRBFs

6.3.1 The BRBF design procedure

To offer a better understanding of the analysis and design aspects of prefabricated steel frame structures with BRBs, a flowchart is presented in Figure 6.3 demonstrating the basic analysis and design procedure for this system. This procedure will be followed for the 5-storey and 9-storey BRBFs studied in the following sections.

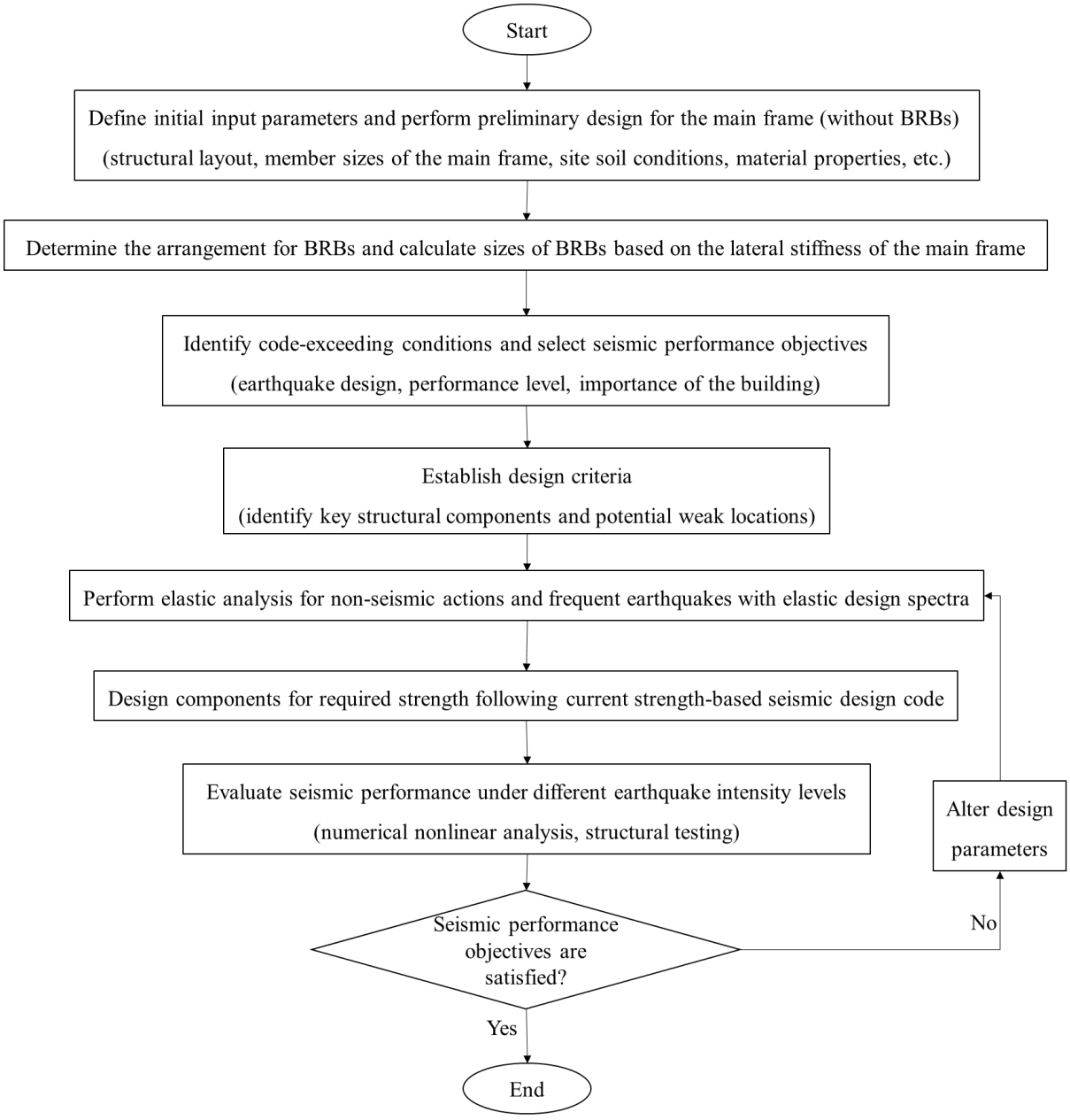

Figure 6.3 Flowchart of analysis and design procedure for prefabricated steel frames with BRBs

6.3.2 The BRBF models

Four 3-bay frame models of the proposed BRBF system are studied using the OpenSees software (McKenna et al., 2006). The middle bay is braced with BRBs and the side bays are made of non-moment-resisting bolted connections. Two distinctive mid-bay configurations, namely, the P-group and the R-group, are both considered in 5-storey and 9-storey frames of 3*m* storey height. P-group is the prototype structure with non-

moment-resisting beam-column-brace connections (Figure 6.2 (b)) within the middle bay, i.e., they are assumed as pinned in the modelling. R-group is with moment-resisting beam-column-brace connections (as shown in Figure 6.1 (b)) which are considered as rigid during the analysis. All other connections at the non-moment-resisting side bays are assumed as pinned as they have very limited rotational stiffness when applying prefabrication to all beam-column connections in the non-moment-resisting bays (Xu et al., 2015). The modelling techniques including the element types, the material behaviour and geometric nonlinearity follow the methodology introduced in Chapter 3, Section 3.3.

In accordance with the current Chinese seismic design provision (GB50011, 2010), the frame models are designed for a high seismic zone where the probabilities of exceedance in 50 years' seismic hazard levels are 2-3%, with the seismic fortification intensity of 8°, and the design basis earthquake acceleration value of 0.3g (g represents the gravity acceleration). The design earthquake group is 2 and the construction field belongs to Site-class II. The structural safety is specified as second class, and the design working life is 50 years. The plan and elevation of the models are shown in Figure 6.4. The plan dimension is 21.6m×21.6m comprising 3 bays in each direction. All columns are assumed to be fixed to the ground. As the structure is symmetrical about all axes, a 2D model is created to represent the structure. Beams and columns adopt I-shaped steel sections with the yield stress of 235MPa. The design dead and live loads of the floor are 3.6kPa and 2kPa respectively. Detailed parameters of the models are listed in Table 6.1.

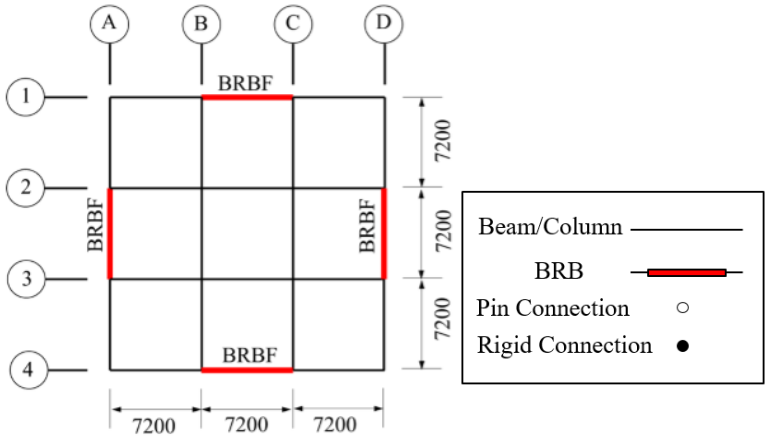

(a) Plan view of the model

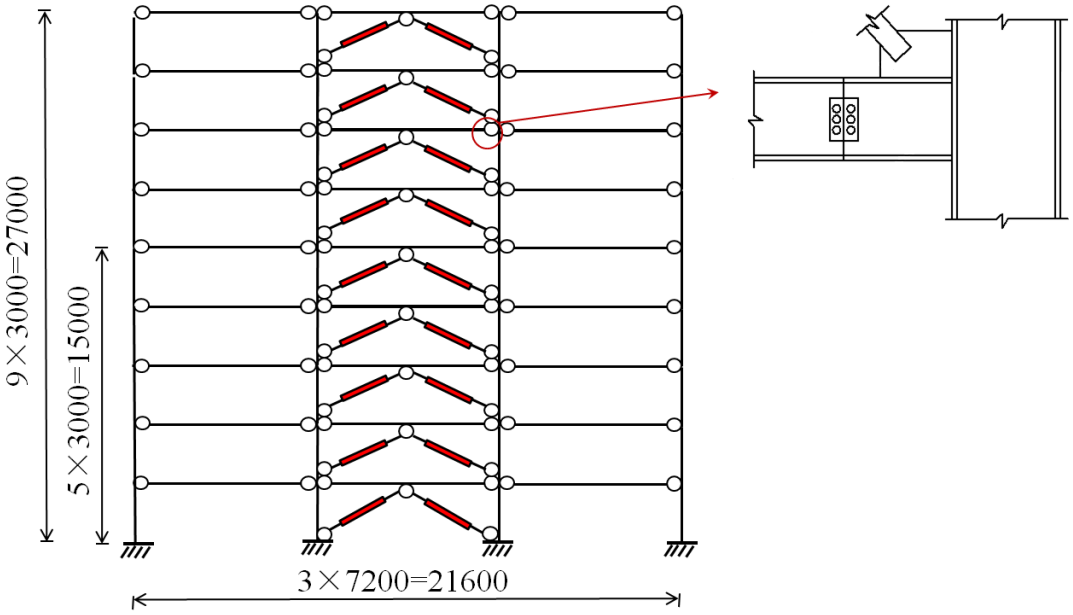

(b) Elevation of the P-group models (5- and 9-storeys)

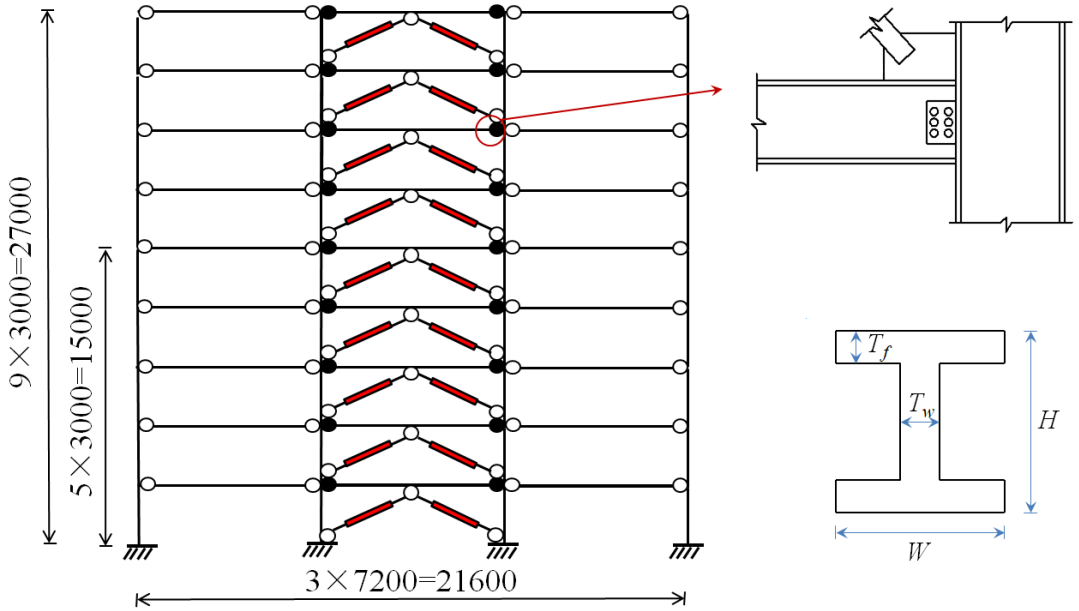

(c) Elevation of the R-group models (5- and 9-storeys)

Figure 6.4 BRBF models showing connection details and beam/column cross sections (all dimensions are in *mm*)

Table 6.1 Detailed parameters of the models

	5-storey	9-storey
Model height (*m*)	15	27
Dimension of beam (*mm*) ($H \times W \times T_w \times T_f$)	250×150×6.5×9	300×200×10×16
Dimension of column (*mm*) ($H \times W \times T_w \times T_f$)	300×300×10×12	400×400×16×25
Yield stress of BRB (*MPa*)	160	160

(Note: H represents the total height of the cross section of beam and column, W represents the flange width, T_w is the web thickness, T_f is the flange thickness, as shown in Figure 6.4 (c).)

To determine the required cross-sectional area of the BRB at the bottom floor of the 5-storey or the 9-storey BRBFs, the following procedure based on Kim and Choi (2004)'s study is undertaken:

(a) The lateral stiffness of each BRB (the arrangement of BRBs on each floor is inverted chevron), k_b', is calculated as:

$$k_b' = \frac{1}{2} \times S_r \times k_s \tag{6-1}$$

where k_s is the lateral stiffness of the main frame without BRB which is determined through a pushover analysis performed in SAP2000. Note that for the sake of comparison, only the moment-resisting beam-column connections for the middle bay is considered in the pushover analysis. In Equation (6-1), S_r is the stiffness ratio of the BRBF which is an assumed constant based on the study of Kim and Choi (2004).

(b) The axial stiffness of the BRB, k_b , is calculated from the following equation:

$$k_b = \frac{k_b'}{\cos^2 \theta} \tag{6-2}$$

where θ is the angle between the BRB and the beam.

(c) The required area of the BRB at the bottom floor, A_b, is then calculated as:

$$A_b = \frac{k_b L_b}{E_b} \tag{6-3}$$

where E_b and L_b are the elastic modulus and the length of the BRB, respectively.

In the following analyses, S_r is taken as integers from 1 to 8 (Kim and Choi, 2004) and thus 8 sets of the BRB areas are considered for both the 9-storey and the 5-storey models. The storey-wise distributions of the BRB areas are assumed to be proportional to the storey shear force ratios which are obtained through pushover analyses performed in SAP2000. Note that the member sizes, material properties, loading and boundary conditions of the SAP2000 models are identical to the corresponding OpenSees models. The normalised storey shear force and the corresponding BRB areas at each floor are presented in Tables 6.2 and 6.3, for 9- and 5-storey models, respectively. Note that the normalised storey shear force for the 1st storey is set to 1 for both models.

Table 6.2 Details of normalised storey shear forces and the corresponding BRB areas for 9-storey models

Storey	Normalised storey shear force	BRB Area (mm^2)							
		S_r=1	S_r=2	S_r=3	S_r =4	S_r =5	S_r =6	S_r =7	S_r =8
9	0.20	106	211	317	423	530	634	740	845
8	0.38	200	399	599	798	1002	1198	1397	1597
7	0.53	282	564	845	1127	1414	1691	1972	2254
6	0.67	352	704	1057	1409	1768	2113	2465	2818
5	0.78	411	822	1233	1644	2062	2465	2876	3287
4	0.87	458	916	1374	1832	2298	2747	3205	3663
3	0.93	493	986	1479	1972	2475	2959	3452	3945
2	0.98	517	1033	1550	2066	2593	3099	3616	4133
1	1.00	528	1057	1585	2113	2652	3170	3698	4227

Table 6.3 Details of normalised storey shear forces and the corresponding BRB areas for 5-storey models

Storey	Normalised storey shear force	BRB Area (mm^2)							
		S_r =1	S_r =2	S_r =3	S_r =4	S_r =5	S_r =6	S_r =7	S_r =8
5	0.33	53	106	160	213	266	319	372	425
4	0.60	96	191	287	383	479	574	670	766
3	0.80	128	255	383	511	638	766	893	1021
2	0.93	149	298	447	596	745	893	1042	1191
1	1.00	160	319	479	638	798	957	1117	1276

6.3.3 Input earthquakes

Four recorded earthquake ground motions from PEER (Pacific Earthquake Engineering

Research Center) database, namely, RSN-9, RSN-21, RSN-28 and RSN-59 are selected as the input for the modelling by matching a site-specific target response spectrum based on intensity, design seismic group and site class. Figure 6.5 indicates that the response spectra of the selected ground motions match the target response spectrum reasonably well. Horizontal ground motions with peak ground acceleration (PGA) of 510gal (1gal=1cm/s^2) which is representative of a severe earthquake, are imposed on the models. A damping ratio of 2% which is commonly adopted in steel frame buildings is used for the non-linear dynamic time-history analysis.

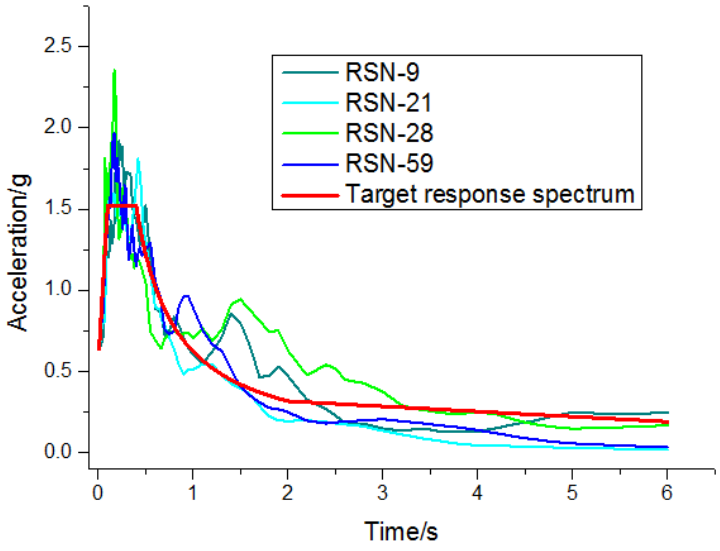

Figure 6.5 Response spectrum of input earthquake records

6.3.4 Results and discussion

The fundamental period of vibration for 5-storey and 9-storey models can be found in Tables 6.4 and 6.5. Figures 6.6 and 6.7 show the envelope of the inter-storey drift ratios of all the studied cases (9-and 5-storey, P-Group and R-Group, S_r = 1 to 8) under the action of the abovementioned four different seismic ground motions. Note that the inter-storey drift ratio is calculated by dividing the maximum lateral storey drift by the height of the corresponding storey.

In general, even though the seismic responses from different earthquake input vary due to the randomness of the earthquake waves, it can be seen that the overall inter-storey

drift ratios in the P-group are evidently larger than those of the R-group counterparts in both 9- and 5-storey models. It is observed from Figures 6.6 (9-storey models) and 6.7 (5-storey models) that the differences between the P-group and R-group inter-storey drift ratios are quite distinct especially for the BRBF stiffness ratios from S_r 1 (i.e. S_r=1 and similar thereafter) to S_r 4. Specifically for the 9-storey models, under most ground motions (except for RSN59), the inter-storey drift ratios in the P-group are mostly found to increase along the structural height, with the maximum ratio occurring at the roof level. This is however not the case for the R-group where the maximum ratios are typically observed around the mid height of the structures and they tend to converge at the roof level.

As the S_r values increase from 5 to 8, both groups show more uniform inter-storey drift ratios along the height and the differences between the two groups become less obvious. This indicates that when S_r increases, the influence of the stiffness of the beam-column-brace connections (P- and R-groups) on the overall structural behaviour becomes less significant accordingly.

Additionally, the predicted inter-storey drifts of all models in the P-group except P9-S_r 1 are lower than the upper bound value of severe earthquakes (i.e., 0.02 shown in Figures 6.6 and 6.7), as specified by the Chinese code (GB50011, 2010). All models in the R-group meet the upper bound requirement of the inter-storey drift. Through comparison of the results of the P- and R-groups shown in Figure 6.6 for the 9-storey BRBFs, it can be deduced that the R-group exhibits smaller inter-storey drift ratios and demonstrates more effective seismic capability when subjected to earthquakes.

Table 6.4 Fundamental period of vibration for 5-storey models

	S_r=1	S_r=2	S_r=3	S_r =4	S_r =5	S_r =6	S_r =7	S_r =8
P-5	1.58	1.17	0.98	0.86	0.79	0.73	0.69	0.65
R-5	1.46	1.12	0.95	0.84	0.77	0.72	0.68	0.64

Table 6.5 Fundamental period of vibration for 9-storey models

	S_r=1	S_r=2	S_r=3	S_r =4	S_r =5	S_r =6	S_r =7	S_r =8
P-9	1.60	1.21	1.06	0.97	0.90	0.85	0.82	0.79
R-9	1.54	1.20	1.05	0.95	0.89	0.84	0.81	0.78

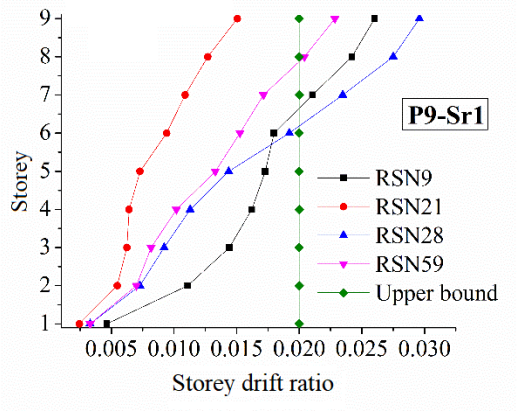

(a)

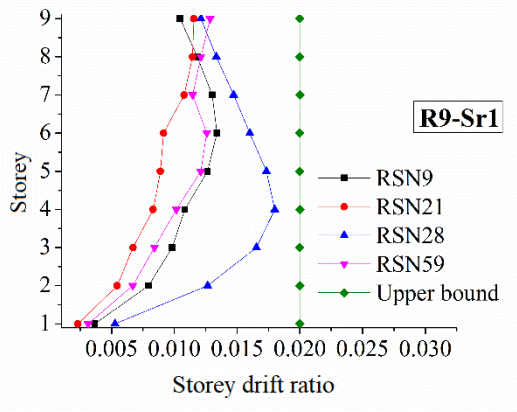

(b)

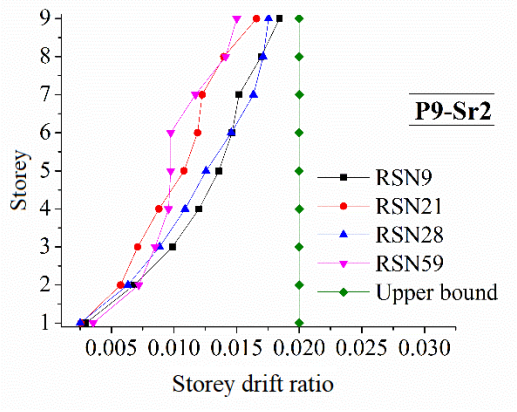

(c)

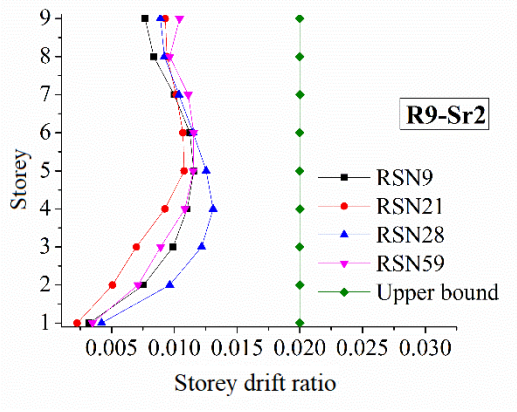

(d)

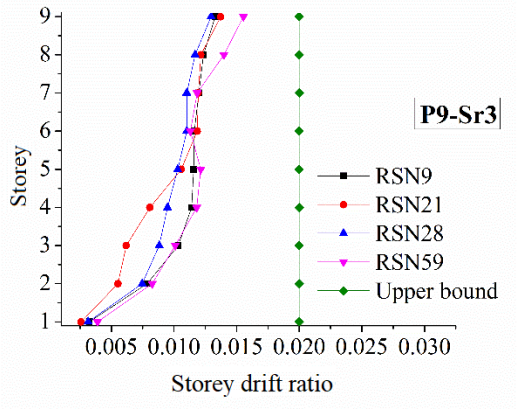

(e)

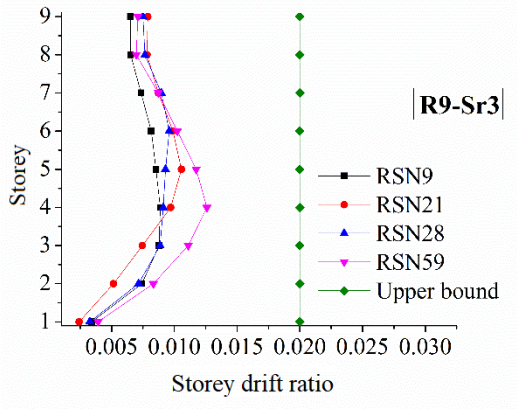

(f)

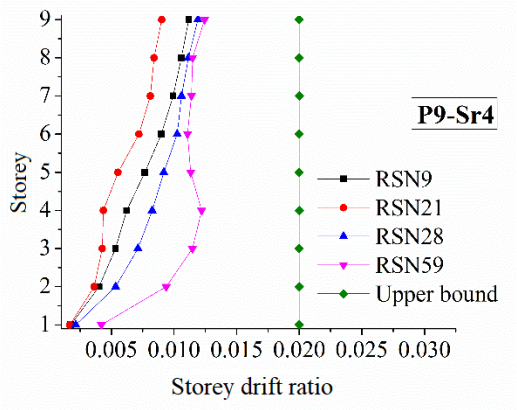
P9-Sr4
RSN9
RSN21
RSN28
RSN59
Upper bound
Storey
Storey drift ratio
0.005 0.010 0.015 0.020 0.025 0.030

(g)

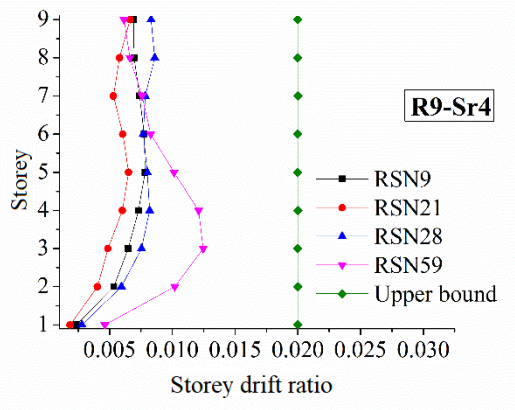
R9-Sr4
RSN9
RSN21
RSN28
RSN59
Upper bound
Storey
Storey drift ratio
0.005 0.010 0.015 0.020 0.025 0.030

(h)

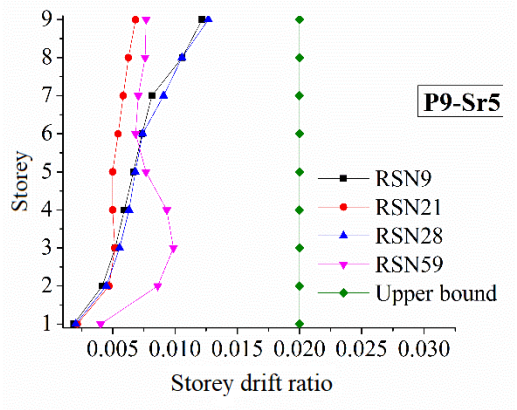
P9-Sr5
RSN9
RSN21
RSN28
RSN59
Upper bound
Storey
Storey drift ratio
0.005 0.010 0.015 0.020 0.025 0.030

(i)

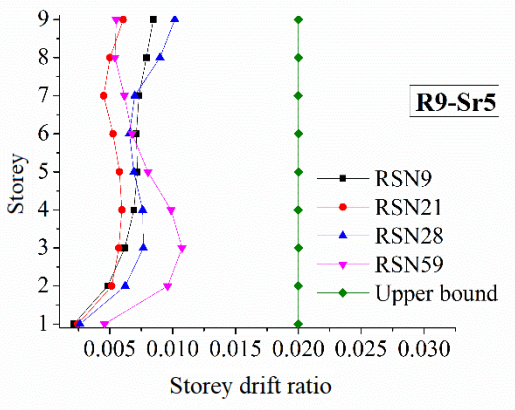
R9-Sr5
RSN9
RSN21
RSN28
RSN59
Upper bound
Storey
Storey drift ratio
0.005 0.010 0.015 0.020 0.025 0.030

(j)

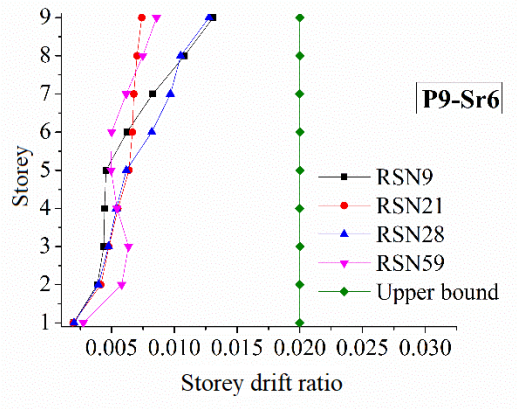
P9-Sr6
RSN9
RSN21
RSN28
RSN59
Upper bound
Storey
Storey drift ratio
0.005 0.010 0.015 0.020 0.025 0.030

(k)

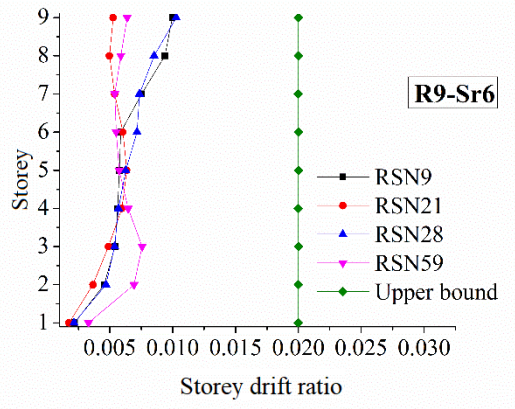
R9-Sr6
RSN9
RSN21
RSN28
RSN59
Upper bound
Storey
Storey drift ratio
0.005 0.010 0.015 0.020 0.025 0.030

(l)

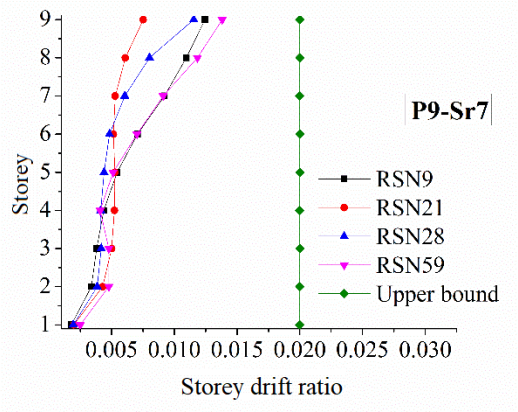

(m)

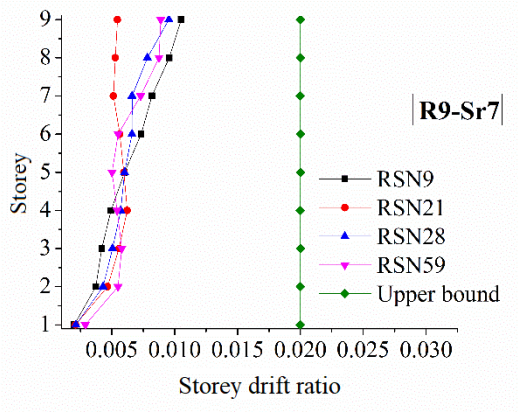

(n)

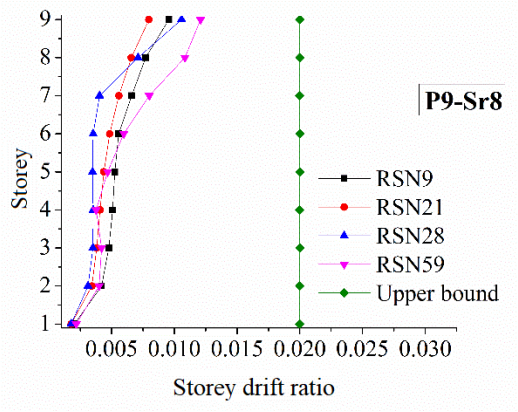

(o)

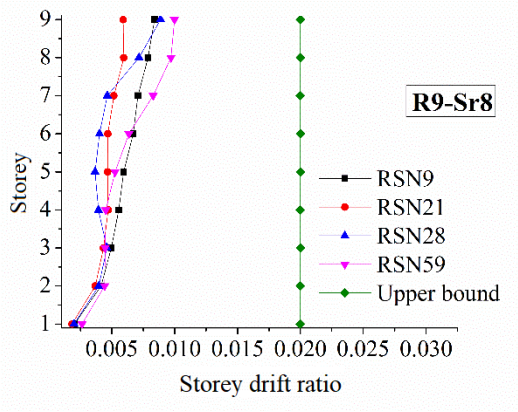

(p)

Figure 6.6 Inter-storey drift ratios of the 9-storey models

The overall patterns showing the storey-drift ratios along the storey height of the 5-storey models (Figure 6.7) are found to be similar to those of the 9-storey models except that such patterns in 5-storey models are more pronounced. The inter-storey drifts are more intense when the S_r values are smaller. For majority of the cases, the inter-storey drift ratios in the P-group increase along the structural height, whereas in the R-group the ratios increase to the mid-height of the structure and converge at the roof level. The differences between the two groups become less obvious when the S_r values increase. Additionally, the inter-storey drift ratios exceed the upper bound value to different extents when S_r is under 6 and 4 for the P-group and R-group, respectively. Similar to the 9-storey models, the R-group of the 5-storey models also demonstrate better seismic performances in terms of the inter-storey drift ratios. Further, in both 9-storey and 5-

storey models, the shapes of the inter-storey drifts in the R-group models bear a certain resemblance to the flexural deformation of the frame structure. This implies a more reasonable force distribution of the R-group models than the P-group equivalents.

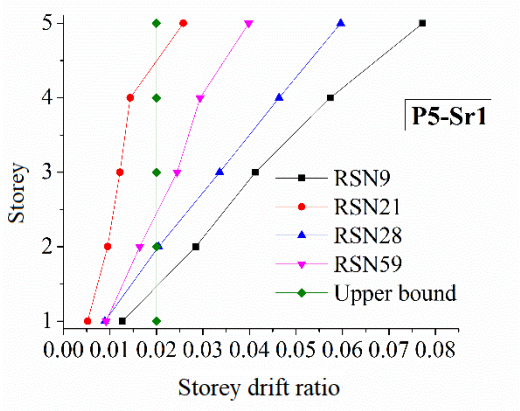

(a)

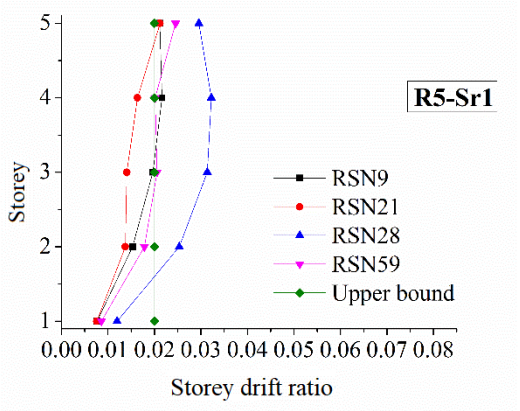

(b)

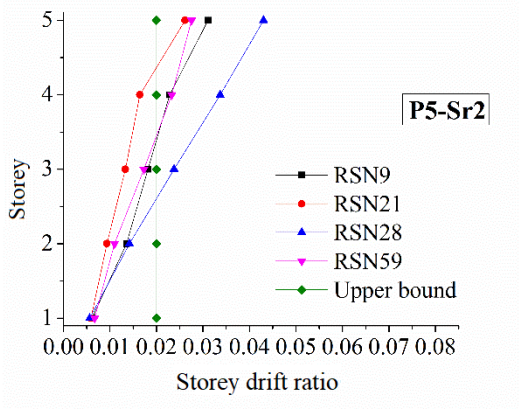

(c)

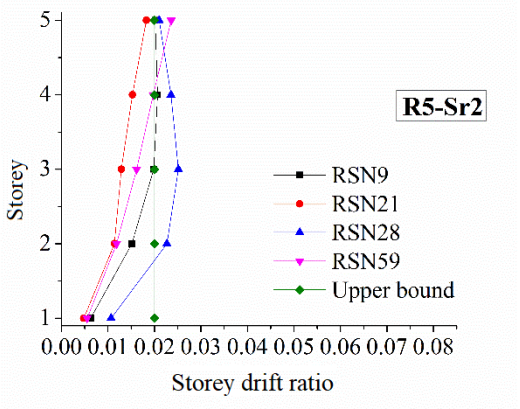

(d)

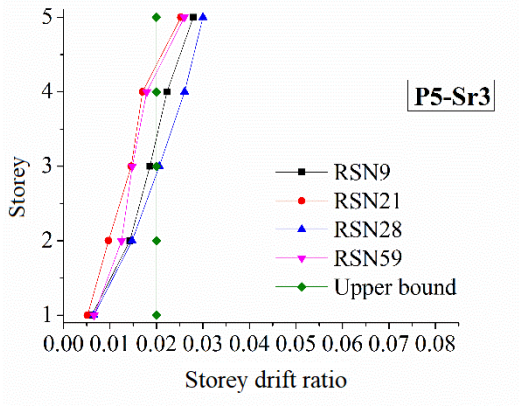

(e)

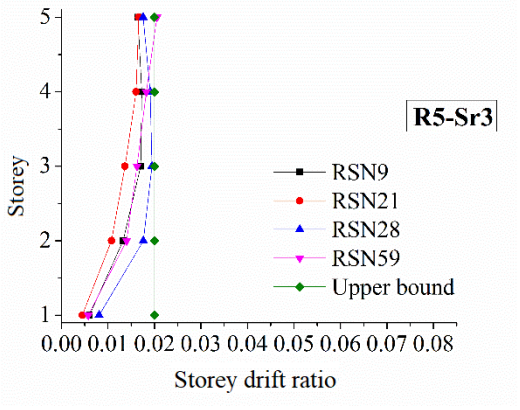

(f)

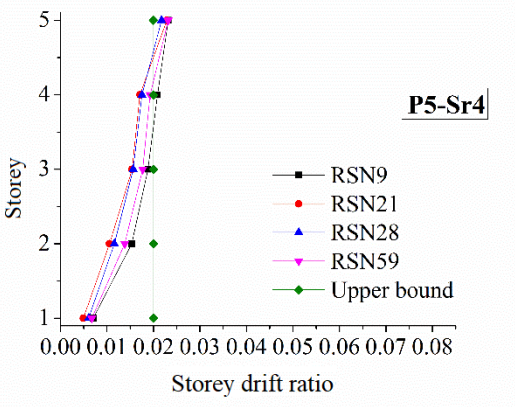
P5-Sr4
RSN9
RSN21
RSN28
RSN59
Upper bound
Storey
Storey drift ratio
1
2
3
4
5
0.00 0.01 0.02 0.03 0.04 0.05 0.06 0.07 0.08

(g)

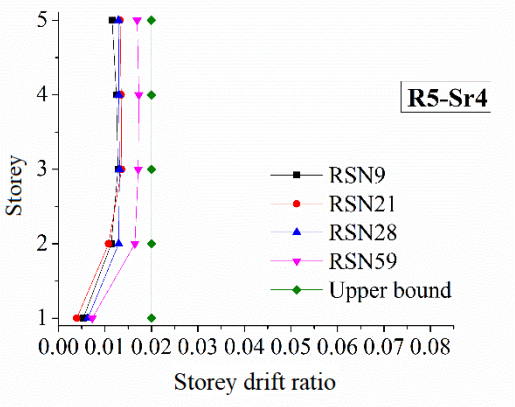
R5-Sr4
RSN9
RSN21
RSN28
RSN59
Upper bound
Storey
Storey drift ratio
1
2
3
4
5
0.00 0.01 0.02 0.03 0.04 0.05 0.06 0.07 0.08

(h)

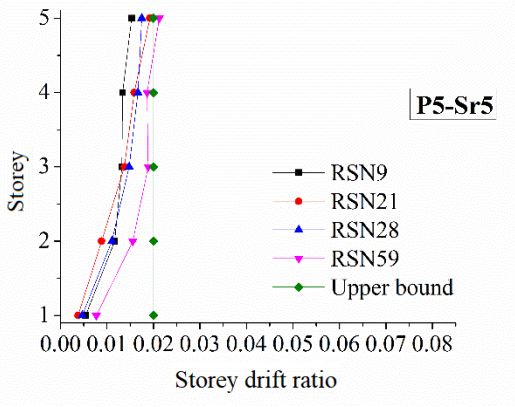
P5-Sr5
RSN9
RSN21
RSN28
RSN59
Upper bound
Storey
Storey drift ratio
1
2
3
4
5
0.00 0.01 0.02 0.03 0.04 0.05 0.06 0.07 0.08

(i)

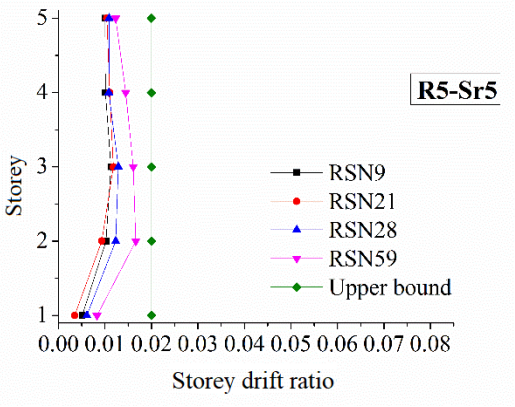
R5-Sr5
RSN9
RSN21
RSN28
RSN59
Upper bound
Storey
Storey drift ratio
1
2
3
4
5
0.00 0.01 0.02 0.03 0.04 0.05 0.06 0.07 0.08

(j)

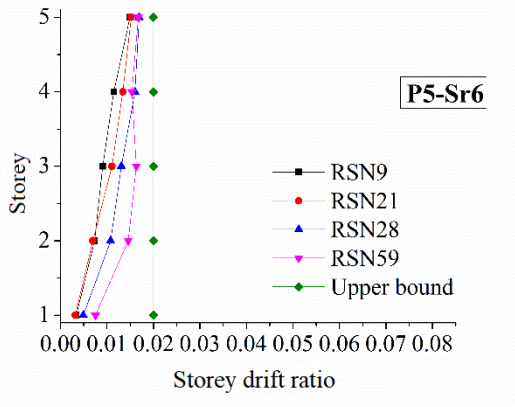
P5-Sr6
RSN9
RSN21
RSN28
RSN59
Upper bound
Storey
Storey drift ratio
1
2
3
4
5
0.00 0.01 0.02 0.03 0.04 0.05 0.06 0.07 0.08

(k)

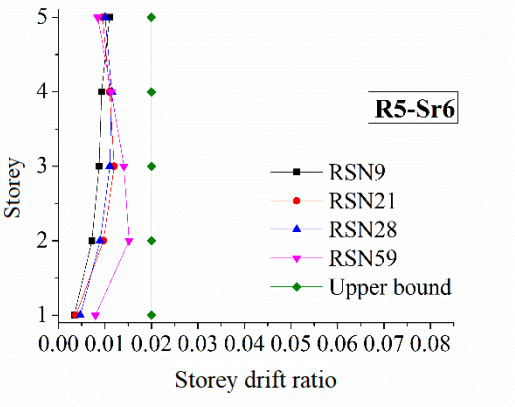
R5-Sr6
RSN9
RSN21
RSN28
RSN59
Upper bound
Storey
Storey drift ratio
1
2
3
4
5
0.00 0.01 0.02 0.03 0.04 0.05 0.06 0.07 0.08

(l)

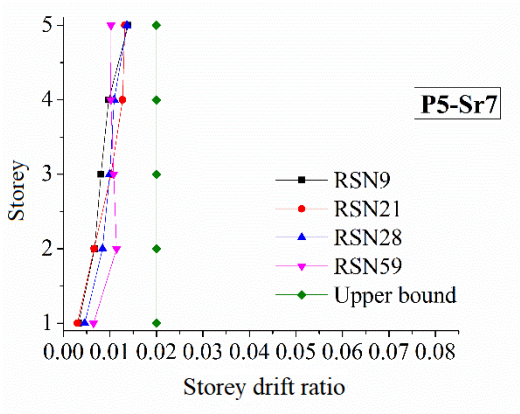

(m)

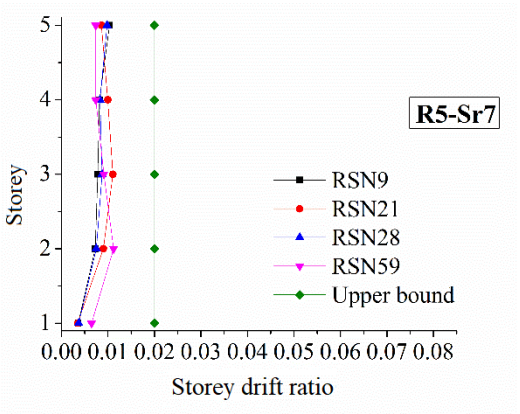

(n)

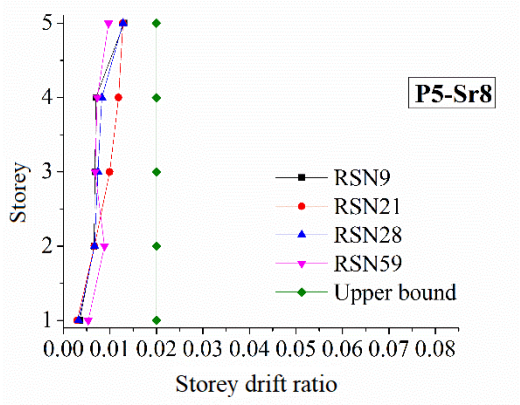

(o)

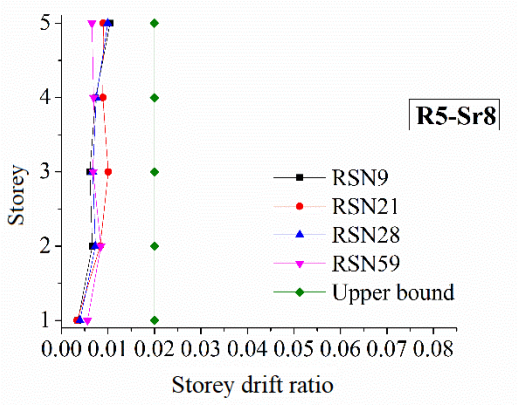

(p)

Figure 6.7 Inter-storey drift ratios of the 5-storey models

To better understand the effect of S_r on the responses of various models, the RSN28 results are reproduced and summarised in Figure 6.8 for both the P- and R-groups of the 5-storey and 9-storey models. It can be seen, for all the models, that the inter-storey drift ratio decreases when the stiffness ratio S_r increases. The inter-storey drift ratios of the 5-storey models are found to be larger than those of the 9-storey models because the designed stiffness of a 9-storey model is relatively larger than a 5-storey one. For the 5-storey models, there is a distinct difference observed in the inter-storey drifts of models with S_r >3 and those with S_r <3. At 4< S_r <8 the storey drift ratios are within the allowable limit but when Sr<3, the drifts in the top stories exceed the 0.02 limit. Unlike the 5-storey models, the overall inter-storey drift ratio in P9 and R9 are more uniform and relatively low. The inter-storey drift ratios of the 9-storey models are within the

limit for most cases except for P9- S_r 1. From the comparisons between the 5 and 9-storey models under RSN28, it can be concluded that there is no significant variation in the magnitude of the inter-storey drift ratios along the structural height for 5< S_r <8. This implies that there is no substantial improvement to the seismic performances by increasing the stiffness of the BRBs to be more than 5 times that of the entire frame. Overall, S_r 3 and S_r 4 in all groups result in more favourable storey drift shapes.

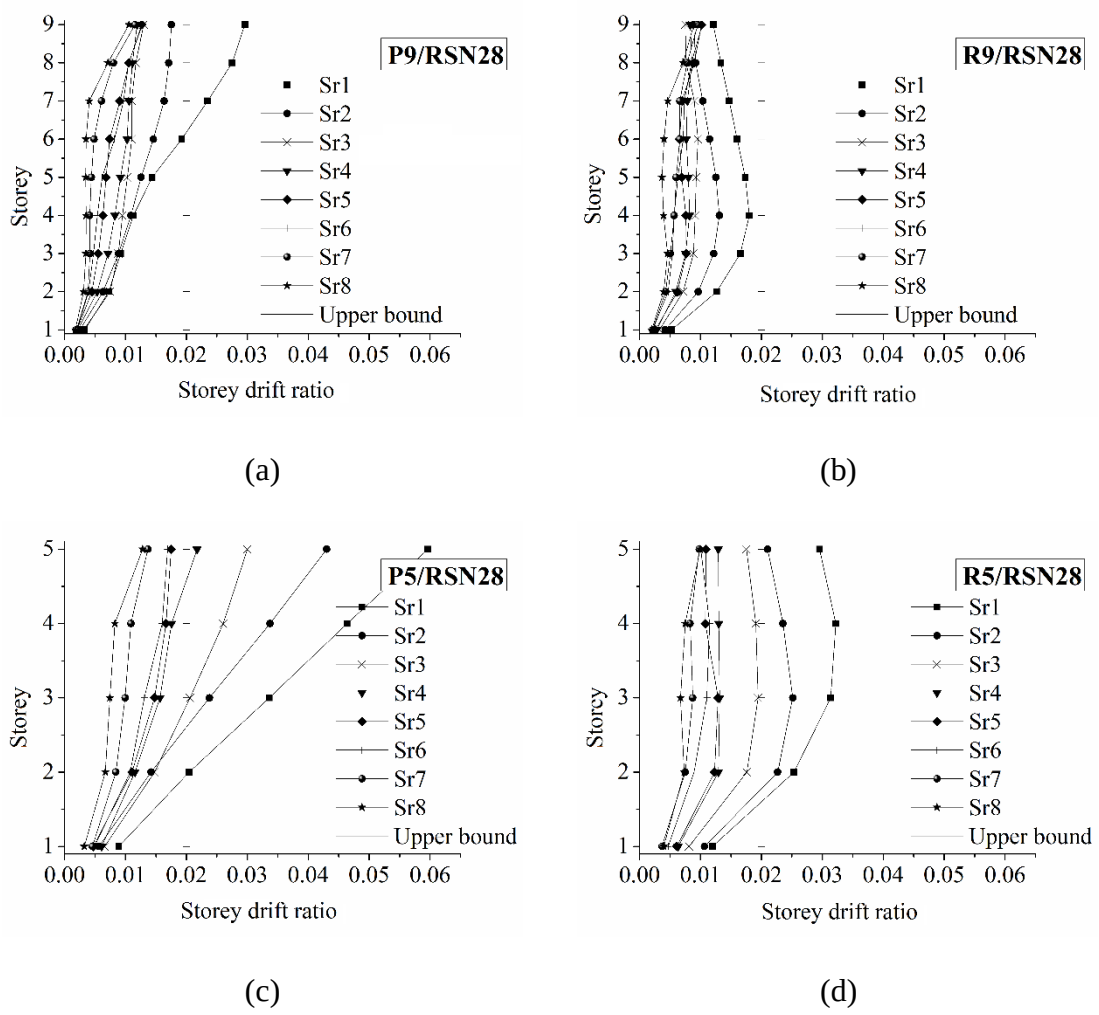

Figure 6.8 Comparison of inter-storey drift ratios for different S_r values under RSN28

Figure 6.9 shows the storey shear versus the inter-storey drift ratio in the 1st storey of all the 9-storey and 5-storey models (S_r= 4) under RSN28. The hysteresis loops for the 9-storey models are not as "fat" as the 5-storey models, implying that the 5-storey models exhibit better energy dissipation capacity for this particular case being studied.

Although the P-group models were expected to be more flexible than their R-group counterparts, the R-group demonstrates more rounded hysteresis behaviour than the P-group for both 9- and 5-storeys. This indicates that the proposed system with rigid beam-column-brace connections exhibits higher earthquake energy dissipation capacity.

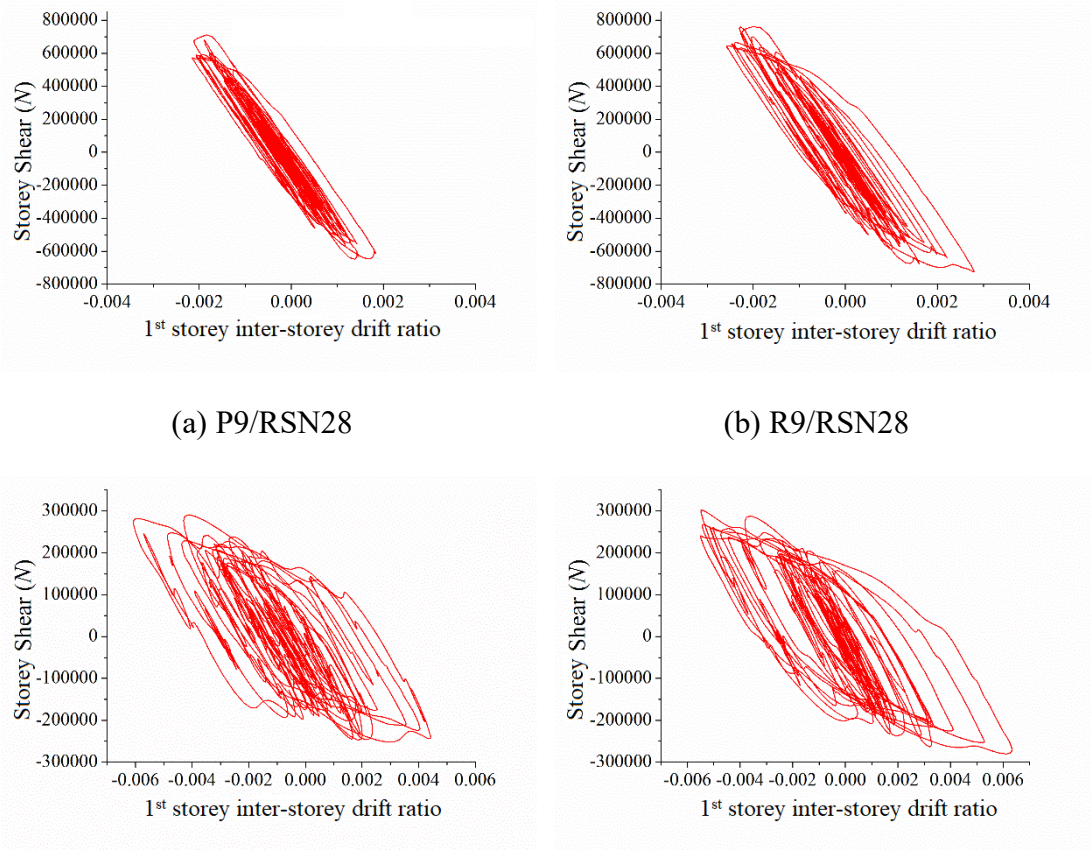

(a) P9/RSN28 (b) R9/RSN28

(c) P5/RSN28 (d) R5/RSN28

Figure 6.9 Storey shear versus inter-storey drift ratio in the 1st storey of four BRBF models (S_r=4)

6.4 Influence of Different BRB Area Distributions

In Section 6.3, the cross-sectional areas of the BRBs along the storey height were calculated based on the distribution of the storey shear forces. As described in a previous study on the conventional BRBFs (Kim and Choi, 2004), four different methods of designing the cross-sectional areas of BRBs can be adopted:

- Method 1: BRB areas are distributed proportionally to storey shear force,

- Method 2: BRB areas are distributed proportionally to storey stiffness,
- Method 3: BRB areas are distributed proportionally to inter-storey drift ratio
- Method 4: BRB areas are of the same size for every storey.

To examine the most effective method for determining the BRB area distributions for the proposed system, the abovementioned four methods are applied to design the BRB areas in this section. As a representative case, only the R-group with S_r 4 under RSN 28 is investigated herein. The storey stiffnesses, the inter-storey drift ratios, and the storey shear forces of both R9 and R5 models are obtained from the nonlinear pushover analyses conducted in SAP 2000. The pushover analysis is based on the displacement-controlled method: a 1 *N* lateral load is applied monotonically at the top right corner of the frame models, until the target displacement (4000 *mm* for the 9-storey models and 2000 *mm* for the 5-storey models) is reached. The pushover results of S_r 4 models are shown in Figure 6.10 for the case when the BRB areas are distributed proportionally to the storey shear force. The normalised pushover analysis results and the correspondingly calculated BRB areas are presented in Tables 6.6 and 6.7, for R9 and R5, respectively.

In Tables 6.6 and 6.7, the normalised storey stiffness is taken as unity in the first storey (i.e. K_1=1) and stiffness of the other stories (K_i/K_1, where i=2, 3, N, and N represents the total number of stories) are calculated accordingly from the SAP2000 analyses. The normalised storey shear forces and inter-storey drift ratios are determined in a similar manner. Note that the inter-storey drift ratios are normalised with respect to the 4th and 3rd storey drift of unity for R9 and R5, respectively. Note also that, for Method 4, the constant BRB area is set to be identical to that of the 1st storey adopted by Methods 1 and 2.

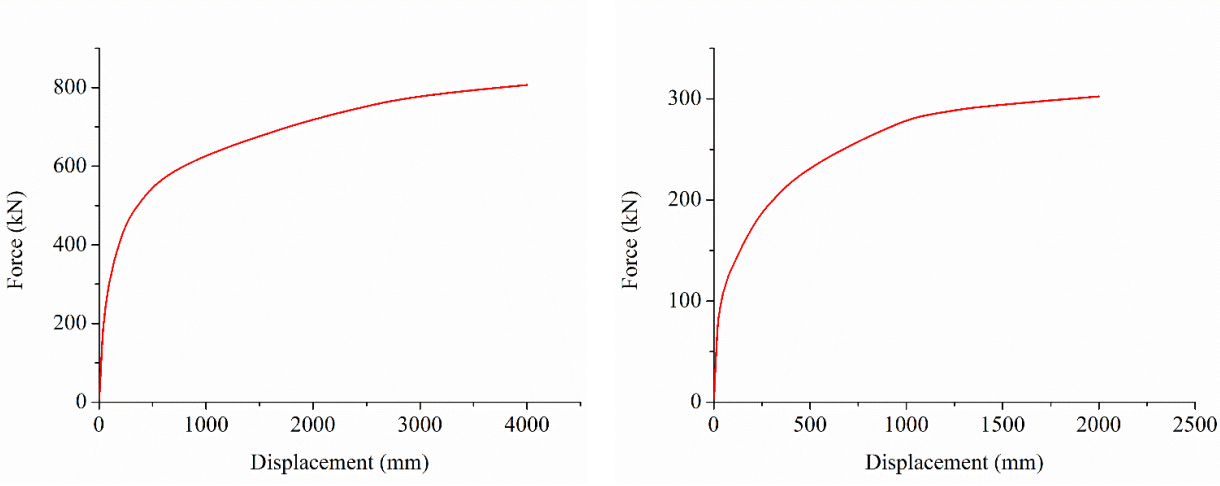

(a) 9-storey (b) 5-storey

Figure 6.10 Pushover results of S_r-4 models when BRB areas distributing proportionally to storey shear force

Table 6.6 Pushover results and corresponding BRB areas for R9

Storey	Storey stiffness (kN/mm)	Method 1		Method 2		Method 3		Method 4
		Normalised Storey shear force	BRB areas (mm^2)	Normalised Storey stiffness	BRB areas (mm^2)	Normalised Inter-storey drift ratio	BRB areas (mm^2)	BRB areas (mm^2)
9	2761.31	0.20	423	0.10	212	0.59	1266	2113
8	4472.38	0.38	798	0.16	343	0.69	1477	2113
7	5393.83	0.53	1127	0.19	414	0.82	1728	2113
6	5977.48	0.67	1409	0.21	459	0.92	1950	2113
5	6488.95	0.78	1644	0.23	498	0.99	2095	2113
4	7168.81	0.87	1832	0.26	550	1	2113	2113
3	8408.82	0.93	1972	0.31	645	0.92	1944	2113
2	11456.3	0.98	2066	0.41	879	0.71	1498	2113
1	27540.4	1	2113	1	2113	0.3	638	2113

Table 6.7 Pushover results and corresponding BRB areas for R5

Storey	Storey stiffness (kN/mm)	Method 1		Method 2		Method 3		Method 4
		Normalised Storey shear force	BRB areas (mm^2)	Normalised Storey stiffness	BRB areas (mm^2)	Normalised Inter-storey drift ratio	BRB areas (mm^2)	BRB areas (mm^2)
5	272.90	0.33	213	0.16	103	0.81	520	638
4	616.21	0.6	383	0.25	160	0.95	605	638
3	1167.16	0.8	511	0.32	202	1	638	638
2	2447.66	0.93	596	0.43	274	0.86	548	638
1	8317.16	1	638	1	638	0.39	252	638

Non-linear time history analyses of R9 and R5 with different BRB area distributions given in Tables 6.6 and 6.7 are carried out under RSN28 ground motion record using OpenSees and the inter-storey drifts are plotted in Figure 6.11. As can be observed, in both 9-storey and 5-storey models, the seismic performances are more satisfactory when the BRB cross-sectional areas are proportional to the storey shear force (Method 1), the storey stiffness (Method 2), and the inter-storey drift ratio (Method 3), as most inter-storey drift values are within the upper bound value. Particularly, Method 1 yields the best seismic performance because it produces the most uniform distribution of the inter-storey drift ratio in both R9 and R5. However, Kim and Choi (2004)'s study indicated that the storey-wise distribution of the BRBs in proportion to the storey drifts (Method 3) and the storey shear forces (Method 1) yield better seismic performance. This could be due to the fact that the structural arrangements are somewhat different between the present study and Kim and Choi's study. Moreover, the ground motion used in Kim and Choi's study was idealised which resulted in a more uniform distribution of the storey drift, whereas the present study adopted recorded ground motions which produces a non-uniform distribution of the storey drift.

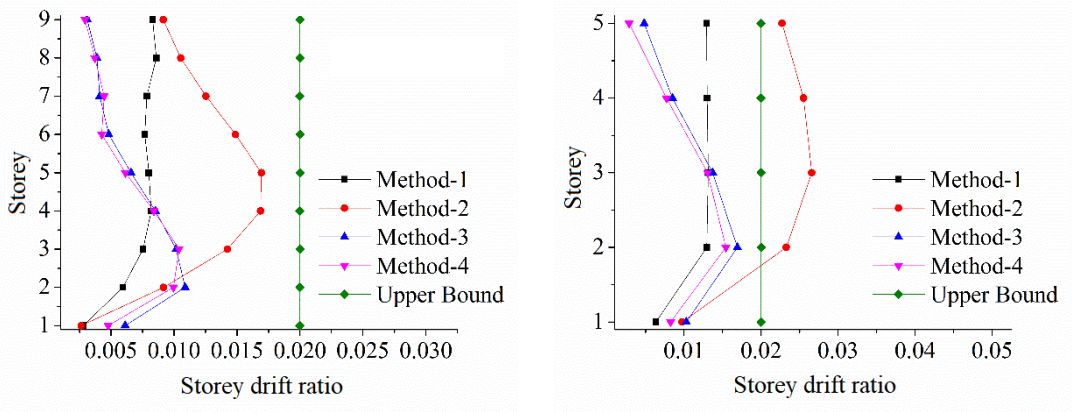

(a) R9 (b) R5

Figure 6.11 Inter-storey drift ratios due to different methods for BRB area design

6.5 Concluding Remarks

In this chapter, seismic performances of an improved BRBF system with bolted beam-column connections under various earthquake inputs were studied through dynamic time-history analyses. Both 9-storey and 5-storey models with moment-resisting (R-group) and non-moment-resisting (P-group) beam-column-brace connections and different BRB area distributions were studied and results were presented in form of the inter-storey drift ratios-and the storey shear-storey drift ratio relationships. Further the BRB areas were designed based on four different methods and the results were compared to examine the most effective design approach for the cross-sectional areas of the braces in the proposed BRBFs. In general, the results showed that the proposed system performs well in energy dissipation under severe earthquakes. The outcome of this study has confirmed that the BRBFs with pin beam-column connections (P-group) could be an appropriate alternative to the conventional rigidly connected frames (R-group) in resisting seismic actions. The main findings obtained from the present study are summarised below:

- In the proposed system, the use of moment-resisting beam-column-brace connections (R-group) is demonstrated to be more beneficial in resisting earthquake actions compared to the non-moment-resisting counterparts (P-group), especially when S_r is between 1 and 4.

- The relatively ideal stiffness ratio (S_r) for the proposed BRBF system is found to be between 3 and 5 for both R-group and P-group regardless of the building height.
- For the proposed system, the storey-wise BRB area distributions proportional to the storey shear force yield a better seismic performance in terms of the inter-storey drift ratio.
- Results of parametric study on various methods for distributing the BRB areas along the height of R9 or R5 show that, in either structure, the most uniform patterns of the inter-storey drift ratios are resulted when the BRB areas are distributed proportionally to the storey shear force.

CHAPTER 7

FRAGILITY ANALYSIS

7.1 General Remarks

In Chapter 6, the parametric study of the proposed system involved dynamic time-history analysis that only required a limited number of ground motion records. However, the calculated structural dynamic responses can be very sensitive to the characteristics of the individual ground motion and the intensity of the seismic shaking (Wilson and Clough, 1999); therefore, substantial nonlinear dynamic analyses for various levels of intensity are required using different ground motion records to achieve a reliable estimation of the probabilistic distribution of the structural dynamic responses. This has necessitated a probabilistic-based method like fragility analysis approach.

Seismic fragility can be defined as the conditional probability of exceeding a prescribed limit state for a given intensity measure (IM) (Lupoi et al., 2006). It gives the probability that a structure or structural component will reach or exceed a specific level of damage during earthquakes of certain intensity.

This chapter first describes the existing common methods of fragility assessment, followed by the comparison of the methods in application. As the most efficient and least time-consuming approach, Cloud analysis is chosen for the seismic evaluation of

the proposed structural system in this study. Subsequently, recent applications of fragility assessment on building structures are reviewed. Moreover, the methodology for generating fragility curves by using Cloud analysis is introduced. Lastly, 12 BRBF models with three different storey heights and four different numbers of non-moment resisting bays are analysed using the Cloud method. For the purpose of design recommendations, the obtained fragility curves of all the models are discussed in some detail in this chapter.

7.2 Overview of Fragility Analyses of Building Structures

7.2.1 Background

A fragility curve (as shown in Figure 7.1) represents the probability that a given structure's response to various loading conditions exceeds a certain performance limit state (LS) (Sfahani et al., 2015). Specifically, a fragility curve is a conditional probability of a structure meeting or exceeding a given level of damage for a given IM. As such, fragility curves are a measure of performance in probabilistic terms. For seismic evaluation of structures, fragility curves may be used to make probabilistic estimation of different damages subject to different ground motions (Ellingwood et al., 2007).

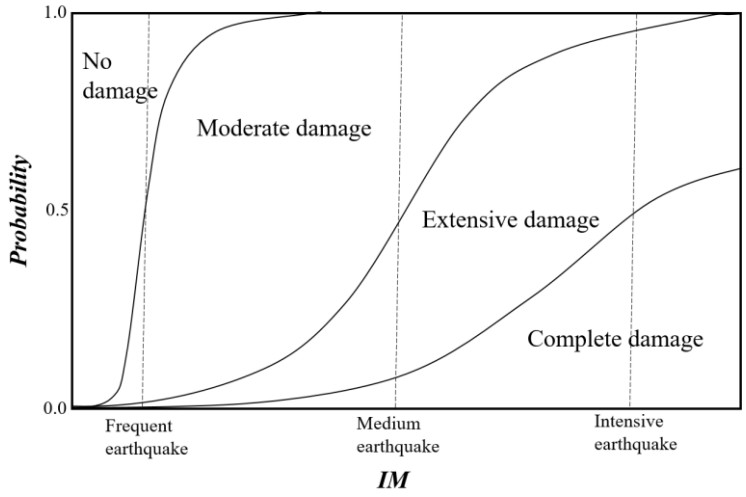

Figure 7.1 Standard fragility curve (Sfahani et al., 2015)

The generation of fragility curves can be distinguished into three generic approaches (Porter, 2015):

1. Empirical method

The fragility curves can be created by fitting a function to observational data from previous earthquakes (Basöz and Kiremidjian, 1997). This method has been used since 1982 (Kustu et al., 1982) and is based on post-earthquake surveys which considered to be the most reliable source for the fragility estimation (Maio and Tsionis, 2015). However, empirical investigations are usually limited to particular sites or geotechnical conditions with abundant seismic hazards therefore lacking generality (Billah and Alam, 2014). Moreover, this method is also based on a subjective evaluation which is not always an accurate instrumental measurement.

2. Analytical method

A fragility function can be derived analytically by creating and analysing a structural model with static or dynamic non-linear approaches (Ebrahimian et al., 2015). The earliest study can be found in Czarnecki's (1973) work. More detailed assessment algorithms with direct physical meaning can be produced by using this method, thus it is considered to be more reliable than the empirical evaluations (Calvi et al., 2006).

3. Judgment-based expert opinion

A fragility function can also be created based on experts' experience, so that the failure probability function can be educatedly guessed or judged (Padgett and DesRoches, 2006). ATC-13 (1985) conducted a large number of judgment-based fragility functions for California buildings. It should be noted however that the fragility curves generated based on one's opinion could be subjective and lacking certainties (Ghalami Sfahani et al., 2015).

In summary, in view of quantifying accurate seismic risk exposures for decision-

making in engineering judgements, the analytical fragility function is the most reliable way for generating fragility curves.

7.2.2 Analytical fragility assessment based on Cloud analysis

In general, the development of analytical fragility curves relies on extensive numerical simulations, based on time history analysis (THA), of structural seismic demand and capacity of structural models subjected to earthquake loads (Cornell and Krawinkler, 2000). Various analysis methods can be adopted for this purpose including the capacity spectrum method (CSM) (Fajfar, 2000), multiple stripe analysis (MSA) (Baker, 2015), incremental dynamic analysis (IDA) (Vamvatsikos & Cornell, 2002) and Cloud analysis (Jalayer, 2003). The distinctions between these methods include the integrity of simulation, efficiency of computation and versatility in application of the earthquake loads.

The non-linear dynamic methods such as IDA and MSA are suitable for evaluating the relationship between the engineering demand parameter (EDP) and the IM for a wide range of IM values. The application of MSA and IDA can sometimes be quite time-consuming as the non-linear dynamic analyses are to be repeatedly performed (usually for scaled ground motion time-histories) for increasing levels of ground motion intensities.

Cloud Analysis is a nonlinear dynamic analysis procedure which fits a linear regression model, in the logarithmic scale, to the EDP (i.e., inter-storey drift) and IM (i.e., first-mode spectral acceleration) for a suite of ground motions (Jalayer et al., 2015). It is particularly efficient since it involves the non-linear analysis of the structure subjected to a set of un-scaled ground motion time-histories. The simplicity of its underlying formulation makes it a quick and efficient analysis procedure for fragility assessment or safety-checking in the context of the SAC-FEMA formulation (Cornell et al., 2002), in a steel frame project named SAC, funded by FEMA. The Cloud Method has been used, not only to model the record-to-record variability in ground motion, but also to

propagate structural modelling uncertainties such as uncertainty in component capacity (Jalayer et al., 2007) and the uncertainties in mechanical material properties and construction details (Jalayer et al., 2011a). Furthermore, a modified version of the Cloud Method has been proposed in (Elefante et al., 2010) that implements a weighting scheme for taking into account magnitude and shape-factor dependence conditioned on the adopted IM. An information-based relative measure for the sufficiency (Luco and Cornell 2007) of the adopted IM has been derived based on Cloud Method's underlying probabilistic model in (Jalayer et al., 2011a). The efficiency and simplicity of the Cloud Method can also be exploited in order to estimate the cumulative damage caused by a sequence of aftershocks through back-to-back or sequential Cloud Analysis (Jalayer et al., 2011b; Ebrahimian et al., 2014). Considering the abovementioned advantages, Cloud Analysis is chosen herein for evaluating the seismic performance of the proposed system.

7.2.3 Existing fragility analyses of building structures

Over the past decades, fragility analyses have played an effective role in post-earthquake evaluation of building structures. Development of fragility curves is an effective tool for risk assessment of structural systems as it can be used for probabilistic estimation of seismic losses and eventually enables decision-making activities for seismic risk reduction (Kinali and Ellingwood, 2007). In this regard, various derivations of the analytical fragility curves can be found in the literatures. Initially, the analytical fragility curves for bridge type structures were developed by Karim and Yamazaki (2001, 2003), Choi et al., (2004), Elnashai et al., (2004), Kim and Shinozuka (2004). However, seismic analytical fragility curves are not only used for bridges, but also for the evaluation of building structures.

Kircil and Polat (2006) developed the fragility curves for mid-rise reinforced concrete (RC) frame buildings in terms of elastic pseudo spectral acceleration, peak ground acceleration (PGA) and elastic spectral displacement for yielding and collapse damage levels with lognormal distribution assumption. The relationship between the number of

building stories and fragility parameters was investigated, the results showed that the fragility parameters in terms of the spectral displacement limits vary significantly for different numbers of building stories.

Kinali and Ellingwood (2007) described the process of fitting building fragility modelling into Consequence-Based Engineering (CBE) decision framework, and assessed the seismic performance of three steel buildings: two moment frames with fully restrained and partially restrained connections, and one braced frame. The fragility analysis results showed that the braced frame experiences nonlinear deformations at a lower level of seismic demand in comparison with those of the moment resisting frames; however, it can sustain higher inter-storey drift angles without significant loss in lateral stiffness due to the axial force contribution of the diagonal braces. Moreover, the braced frame is the least likely to experience a collapse after a severe earthquake compare to the other two frames.

Erberik and Elnashai (2004) derived fragility curves for medium-rise flat-slab buildings with masonry infill walls. Four limit states were estimated in this study with intensity measures in terms of displacement spectral ordinates. The obtained fragility curves were then compared with those for the conventional moment-resisting RC frames. It showed that although differences exist, earthquake losses for flat-slab structures are in the same range as for moment-resisting frames.

Park et al. (2009) performed seismic fragility analysis for an unreinforced masonry (URM) low-rise building. The results showed that the seismic performance of URM buildings is well below the desirable building seismic performance level recommended by current seismic codes, and is sensitive to the stiffness of the out-of-plane wall.

The fragility assessment of typical low-rise and mid-rise RC buildings in Turkey was conducted after the two devastating earthquakes in 1999 (Erberik, 2008). The influence of modelling techniques, model size, type of hysteresis model and limit state definitions

on the fragility curves was then investigated. It is shown that the uncertainty in capacity and degradation characteristics played a more important role on the final fragility functions than the other investigated parameters.

Bai et al. (2011) developed fragility estimates for proposed storey-specific demand models that consider the maximum inter-storey drift of each storey in multi-storey buildings. The proposed models were used to estimate the seismic fragility of two example buildings. Comparison between the conventional fragility estimates and those based on the demand models for overall inter-storey drifts indicated that the fragility due to the former might be underestimated.

Casotto et al. (2015) analysed a large portion of precast RC buildings with weak beam-column connections in Italy and developed fragility curves to be used in seismic risk assessment. This study demonstrated the importance of considering the connection failure when developing collapse fragility curves for such structures.

Fragility assessment method can also be applied to the evaluation of the retrofitted structures. Hueste and Bai (2007) developed fragility assessment for a RC frame structure representative of 1980s construction in the Central United States. For the evaluation purpose, the results were then compared with the fragility relationships developed for the retrofitted structure based on three possible retrofit techniques and several performance levels. Similarly, a study of the effects of eccentric steel bracing systems on mid-rise RC buildings was carried out through fragility analysis (Ozel and Guneyisi, 2011). The effectiveness of using different types of eccentric steel braces in retrofitting the building, as well as the effect of distributing the steel bracing over the height of the buildings were studied. Navya and Agarwal (2016) presented a complete process of retrofitting on a building designed with two different Indian seismic codes (IS 1893 (Part 1): 2002, IS 456-2000) with steel bracings. Further fragility analysis was carried out, and the resulting fragility curves indicated that the probabilities of damage were considerably reduced after retrofitting of the building.

It can be noted that although extensive fragility studies have been undertaken on RC and masonry structures, fragility assessments of steel structures are still limited. As such, there is a necessity to carry out a comprehensive fragility analysis for seismic performance estimation of the proposed prefabricated steel system.

7.3 Methodology for Generating Fragility Curves Using Cloud Analysis

The rationale of using Cloud analysis for generating fragility curves have been presented in Section 7.2.2. The flow chart shown in Figure 7.2 describes the procedure for obtaining the fragility curves of the proposed structural system. First of all, the target models must be designed (it can be existing structures in some cases), and design considerations of the design of the computational structure models in this study will be introduced in Section 7.4.1. To develop the desired fragility curves, the selection of ground motion records and the criteria of LS (also known as damage states) are essential for developing the fragility functions, which will be discussed in Sections 7.4.2 to 7.4.3 in details. Meanwhile, the IM and EDP must be determined for the function generation as well.

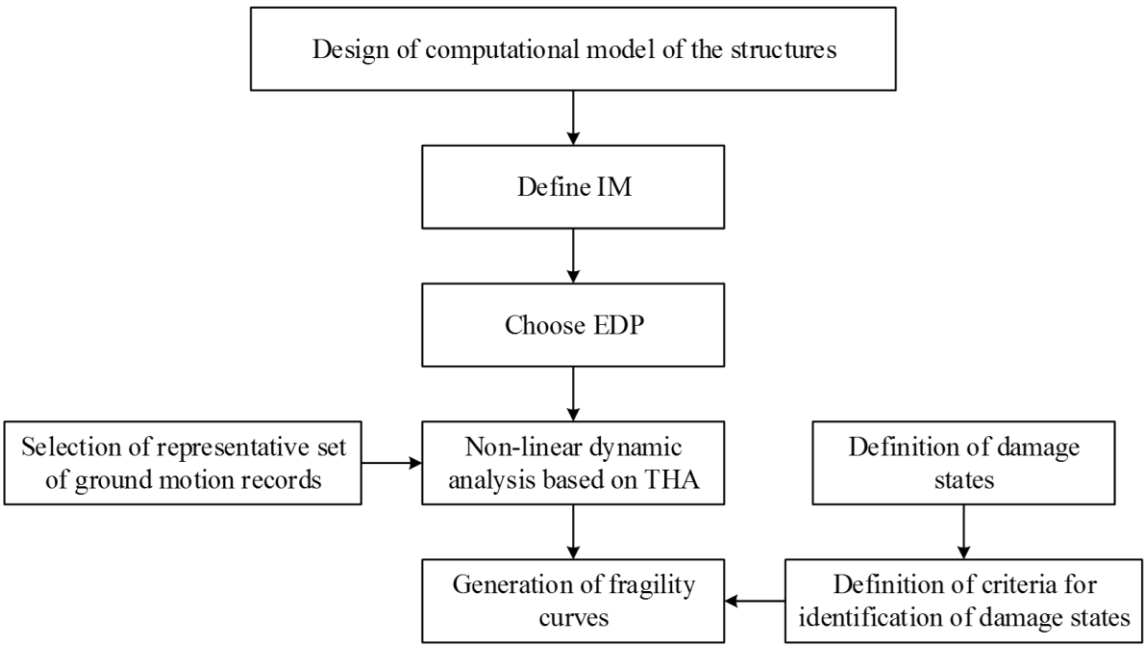

Figure 7.2 Procedure of fragility curve development

The fragility functions used in this Chapter follow Jalayer's previous research (Jalayer et al., 2017). For the purpose of integrity of presentation, relevant formulations are reproduced herein as follows:

The structural performance variable herein is taken to be the critical demand to capacity ratio (*DCR*) for a desired LS, denoted as DCR_{LS}. It is defined as the demand to capacity ratio for the component or mechanism that brings the system closer to the onset of a LS, and it is always equal to unity at the onset of LS.

$$DCR_{LS} = max_{l}^{N_{mech}} min_{j}^{N_l} \frac{D_{jl}}{C_{jl}(LS)} \tag{7-1}$$

where N_{mech} is the number of considered potential failure mechanisms, N_l is the number of components taking part in the l^{th} mechanism, D_{jl} is the demand evaluated for the j^{th} structural component of the l^{th} mechanism, and $C_{jl}(LS)$ is the limit state capacity for the j^{th} component of the l^{th} mechanism.

The small-amplitude first-mode spectral acceleration S_a is adopted as the IM in this

study. Herein, a regression-based probability model is used to describe the DCR_{LS} for a given IM = $S_a(T_1)$ level. Let DCR_{LS} = {DCR_{LS}, i, i = 1:N} be the set of critical demand to capacity ratio for LS, calculated through nonlinear time-history analyses performed for a suite of N recorded ground motions, and S_a = {$S_{a,i}$, i = 1:N} be the set of corresponding spectral acceleration values (where $DCR_{LS,i}$ and $S_{a,i}$ are calculated for the i^{th} ground motion record). The Cloud Analysis data or simply data hereafter refer to the set D = {($S_{a,i}$, $DCR_{LS,i}$), i = 1:N}.

The regression probabilistic model can be described as follows:

$$E[\ln DCR_{LS}|S_a] = \ln \eta_{DCR_{LS}|S_a} = \ln a + b \ln S_a,$$
$$\sigma_{\ln \beta_{DCR_{LS}|S_a}} = \sqrt{\frac{\sum_{i=1}^{n}(\ln DCR_{LS,i} - \ln \eta_{DCR_{LS}|S_{a,i}})^2}{N-2}}, \quad (7\text{-}2)$$

where $E[\ln DCR_{LS}|S_a]$ is the expected value for the natural logarithm of DCR_{LS} given S_a, $\eta_{DCR_{LS}|S_a}$ is the median for DCR_{LS} given S_a, and $\sigma_{\ln \beta_{DCR_{LS}|S_a}}$ is the logarithmic standard deviation for DCR_{LS} given S_a. The structural fragility obtained based on the Cloud Analysis can be expressed as the probability that DCR_{LS} exceeds unity given S_a:

$$P(DCR_{LS} > 1|S_{a,\chi}) = P(lnDCR_{LS} > 0|S_{a,\chi}) = 1 - \emptyset\left(\frac{-\ln \eta_{DCR_{LS}|S_a}}{\sigma_{\ln DCR_{LS}|S_a}}\right)$$
$$= \emptyset\left(\frac{\ln \eta_{DCR_{LS}|S_a}}{\beta_{DCR_{LS}|S_a}}\right) \quad (7\text{-}3)$$

where $\Phi(\cdot)$ is the standardized Gaussian cumulative distribution function (CDF) and χ = [ln$a$, b, $\beta_{\ln DCR_{LS}|S_a}$] denotes the model parameters and $\beta_{DCR_{LS}|S_a} \triangleq \sigma_{\ln DCR_{LS}|S_a}$ ($\triangleq$ denotes equal delta which is defined as a quantity is equal to another by definition). Note that Equation (7-3) is a three-parameter fragility model that can be determined as a function of the known vector χ.

Equation (7-3) denotes that for any specific value of $S_{a,\chi}$, the probability of exceedance P can be obtained, resulting in a fragility curve. Note that in this chapter, LS is specified into three levels (i.e., moderate damage, extensive damage and complete damage) as described in Section 7.4.2, the small-amplitude first-mode spectral acceleration S_a is adopted as the IM, and the number of record ground motions N is chosen as 25.

7.4 Fragility Analysis of the Proposed System

7.4.1 Description of the structural models

The investigated structural models are the expansion of the R-group models discussed in Chapter 6. As recommended in the Chinese Residential Design Specification (GB50096, 2011), three different building heights are considered herein to represent low-rise, medium-rise and high-rise buildings: i.e., 6-storey, 9-storey and 12-storey, with a standard 3m storey height. For each building height, different numbers of non-moment-resisting bays (NMRBs), where the beams are pin-connected to the columns, are considered: from one to four non-moment-resisting bays, representing the normal construction practice. This makes a total of 12 models. For each model, one buckling restrained braced frame (BRBF) is assembled with the non-moment-resisting bay/bays, as shown in Figure 7.3 (a), and Figure 7.3 (b) shows the standard beam/column cross sections. Both BRBF and NMRBs have a standard width of 7.2m. The models are designated as Sx-Ny, where S donates “storey”, N denotes “non-moment-resisting”, x denotes the number of stories and y denotes the number of non-moment-resisting-bay (s).

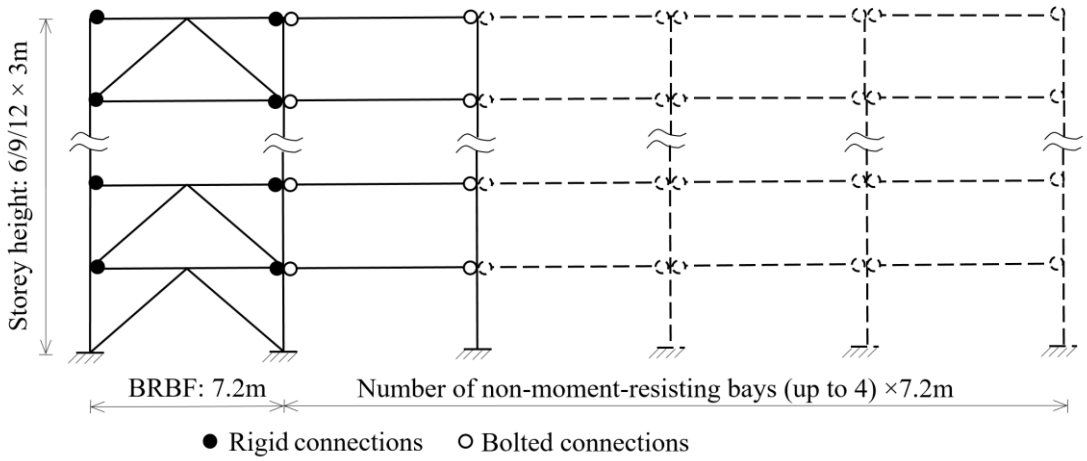

(a) Elevation view of the designed structural models

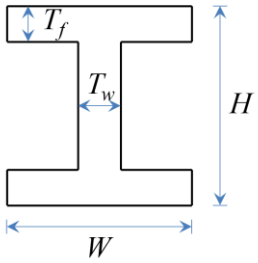

(b) Beam/column cross sections

Figure 7.3 Designed structural models

(Note: H represents the total height of the cross section of beam and column, W represents the flange width, T_w is the web thickness and T_f is the flange thickness)

The design of the models was performed in accordance with the current Chinese seismic design provision (GB50011, 2010). The seismic requirements including the seismic fortification intensity, the design basis earthquake acceleration value, design earthquake group, site classification and design working life, are identical with those used in the parametric study presented in Chapter 6, Section 6.2.1. Besides, all columns are assumed to be fixed to the ground. Beams and columns adopt I-shaped steel sections with the yield stress of 235*MPa*. The design dead and live loads of the floor are 10.8*N*/*mm* and 9*N*/*mm* respectively, and the loading combination is 1.2Dead load+1.2Live load +1.3Earthquake. Detailed parameters of the models are listed in Table 7.1. Table 7.2 shows the BRB areas of the models, which are designed following the approach presented in Chapter 6. Note that for the same building height, the BRB

areas remain unchanged for the frames with different numbers of non-moment-resisting bays.

The finite element models of the frames are constructed, using the OpenSees software (McKenna et al., 2006). The modelling techniques including the element types, the material behaviour and geometric nonlinearity follow the methodology introduced in Chapter 3, Section 3.3.

Table 7.1 Beam and column properties

Number of stories	Model height (m)	Yield stress of beams and columns (MPa)	Size of beam (mm) ($H \times W \times T_w \times T_f$)	Size of column (mm) ($H \times W \times T_w \times T_f$)	Yield stress of BRB (MPa)
6	18	235	300×200×10×14	300×300×10×15	160
9	27	235	300×200×10×14	350×350×14×16	160
12	36	235	300×200×10×14	400×400×14×16	160

(Note: Refer to Figure 7.3 (b) for beam and column sizes.)

Table 7.2 BRB areas

Storey number	BRB areas (mm^2)		
	6-storey	9-storey	12-storey
12			185.72
11			355.97
10			510.74
9		200.58	650.03
8		378.87	773.85
7		534.88	882.18
6	223.2	668.6	975.05
5	409.2	780.03	1052.43
4	558	869.18	1114.34
3	669.6	936.04	1160.77
2	744	980.61	1191.72
1	781.18	1002.9	1207.2

The fundamental period of vibration (known as the first mode of vibration) for the models can be found in Tables 7.3 to 7.5, obtained from the model analysis using

OpenSees.

Table 7.3 Fundamental period of vibration for 6-storey models

Models	S6-N1	S6-N2	S6-N3	S6-N4
Period (*s*)	0.93	1.17	1.53	2.12

Table 7.4 Fundamental period of vibration for 9-storey models

Models	S9-N1	S9-N2	S9-N3	S9-N4
Period (*s*)	1.46	1.88	2.39	3.12

Table 7.5 Fundamental period of vibration for 12-storey models

Models	S12-N1	S12-N2	S12-N3	S12-N4
Period (*s*)	2.05	2.52	3.13	4.09

7.4.2 Definition of Limit States

To obtain accurate fragility curves, an appropriate definition of the performance states is essential. In the existing studies, the inter-storey drift ratio was chosen as the main EDP for fragility evaluation, which is specified in FEMA 356 (2000) to distinguish the three performance state levels: Immediate Occupancy, Life Safety, and Collapse Prevention, with the corresponding inter-storey drift ratios of 0.7, 2.5, and 5%, respectively. The Immediate Occupancy state corresponds to a damage state where the building is safe to occupy after an earthquake, while the Life Safety state refers to a state at which significant damage was experienced by the structure but the risk for life-threatening injuries to the occupants remains low. Finally, the Collapse Prevention state describes the situation where the structure is on the verge of partial or total collapse under lateral loads, albeit still maintaining its ability to support gravity loads. In the current study, similar limit states (LS) regulated by the Chinese seismic design provision (GB50011, 2010) are applied for the development of fragility curves. Three specific LSs and the corresponding definitions are summarised in Table 7.6. The relationship between the LS and the corresponding descriptions can be more directly

demonstrated in Figure 7.4.

Table 7.6 Definition of limit states

Limit states	Description	Inter-storey drift ratio
LS1- Moderate damage	Non-structural damage, no need to repair or after slightly repairing, can be used directly.	0.5%
LS2- Extensive damage	Structural damage, building still remain serviceability. Certain repair work should be done before continued use.	2%
LS3- Complete damage	Majority components have serious damage, building structure is close to collapse or already collapsed.	4%

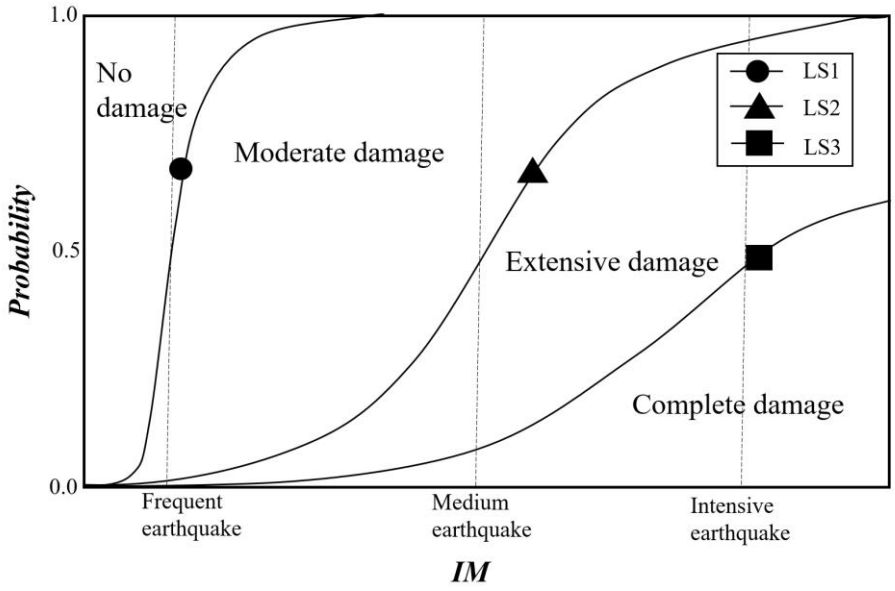

Figure 7.4 LS and the corresponding definitions

7.4.3 Selected suite of ground-motion records

The selection of ground-motion records also plays an important role in establishing fragility curves. A few parameters must be considered in selecting the ground motions, such as event magnitude, PGA, distance between epicentre source and affected area, soil type (Nazri and Alexander 2012), as well as ground motion characteristics including ground motion intensity, spectral shape, duration, frequency content, near-fault, amplitude, and number of cycles (Ibrahim and El-Shami 2011; Ruiz-García and Negrete-Manriquez 2011; Song et al., 2014).

A set of 25 ground motion records are used for performing the Cloud analysis in this study. The records are selected from the NGA-West2 database (Ancheta et al., 2014), and listed in Table 7.7. Note that each record is given a unique record sequence number (RSN). This suite of records was used in Ebrahimian et al., (2015)'s previous cloud analysis study, it covers a wide range of earthquake magnitudes from 5.50 up to 7.51, and closest distance to ruptured area of up to about 16 km. The spectral accelerations of the 25 records are shown in Figure 7.5. It should be noted that the main target of the cloud analysis is to assess the seismic performance of the proposed system, therefore the adoption of the widely used earthquake records is considered as an efficient way to obtain more precise fragility curves.

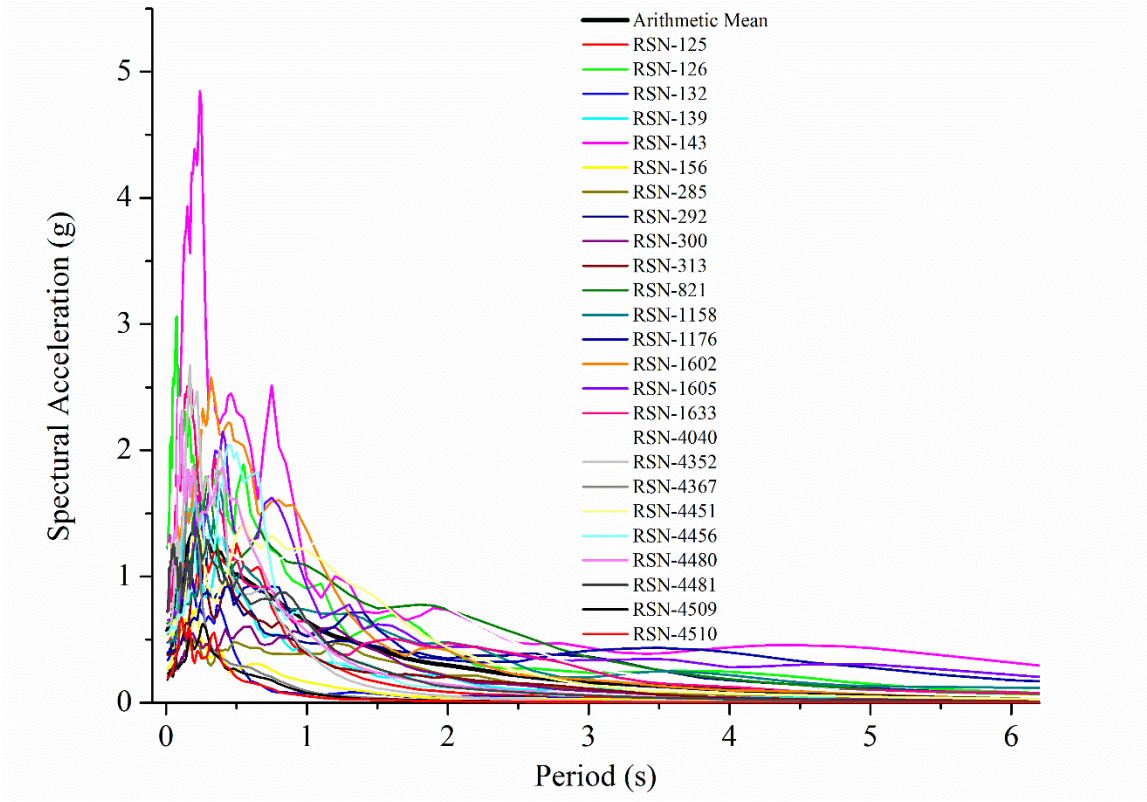

Figure 7.5 Spectral shape for the suite of ground motion records

Table 7.7 The suite of ground motion records for Cloud Analysis (Ebrahimian et al., 2015)

Record no.	RSN record no.	Earthquake name	Station name	Mw	Closest distance to the ruptured area (*km*)	Fault mechanism	Lowest usable frequency (*Hz*)
1	125	Friuli, Italy-01	Tolmezzo	6.5	15.82	Reverse	0.1625
2	126	Gazli, USSR	Karakyr	6.8	5.46	Reverse	0.1625
3	132	Friuli, Italy-02	Forgaria Cornino	5.91	14.75	Reverse	0.1875
4	139	Tabas, Iran	Dayhook	7.35	13.94	Reverse	0.25
5	143	Tabas, Iran	Tabas	7.35	2.05	Reverse	0.1
6	156	Norcia, Italy	Cascia	5.9	4.64	Normal	0.25
7	285	Irpinia, Italy-01	Bagnoli Irpinio	6.9	8.18	Normal	0.1125
8	292	Irpinia, Italy-01	Sturno (STN)	6.9	10.84	Normal	0.1125
9	300	Irpinia, Italy-02	Calitri	6.2	8.83	Normal	0.1625
10	313	Corinth, Greece	Corinth	6.6	10.27	Normal-Oblique	0.25
11	821	Erzican, Turkey	Erzincan	6.69	4.38	Strike-Slip	0.1125
12	1158	Kocaeli, Turkey	Duzce	7.51	15.37	Strike-Slip	0.1
13	1176	Kocaeli, Turkey	Yarimca	7.51	4.83	Strike-Slip	0.0875
14	1602	Duzce, Turkey	Bolu	7.14	12.04	Strike-Slip	0.0625
15	1605	Duzce, Turkey	Duzce	7.14	6.58	Strike-Slip	0.1
16	1633	Manjil, Iran	Abbar	7.37	12.55	Strike-Slip	0.13
17	4040	Bam, Iran	Bam	6.6	1.7	Strike-Slip	0.0625
18	4352	Umbria Marche, Italy	Nocera Umbra	6	8.92	Normal	0.875
19	4367	Umbria Marche (aftershock 1), Italy	Nocera Umbra	5.5	9.33	Normal	0.75
20	4451	Montenegro, Yugo	Bar-Skupstina Opstine	7.1	6.98	Reverse	0.1625
21	4456	Montenegro, Yugo	Petrovac - Hotel Olivia	7.1	8.01	Reverse	0.375
22	4480	L'Aquila, Italy	L'Aquila-V. Aterno-C1entro Valle	6.3	6.27	Normal	0.0375
23	4481	L'Aquila, Italy	L'Aquila-V. Aterno-Colle Grilli	6.3	6.81	Normal	0.05
24	4509	L'Aquila (aftershock 1), Italy	L'Aquila-V. Aterno-Colle Grilli	5.6	14.95	Normal-Oblique	0.125
25	4510	L'Aquila (aftershock 1), Italy	L'Aquila-V. Aterno-Centro Valle	5.6	14.81	Normal-Oblique	0.1125

7.4.4 Cloud analysis results

Figure 7.6 illustrates the fragility curves based on the Cloud analysis for all 12 models. Obviously, when the storey height is constant, the probability of exceeding a LS criterion always increases at a given S_a when the number of bays increases. Overall, for models with a constant storey height, it can be inferred by contrasting the shape of the fragility curves that the deviation between different LS reduces for more numbers of bays. Furthermore, let the number of stories be n (n= 6, 9, 12), it can be observed that $P_{Sn\text{-}N1}[LSi|S_a]$ (i.e., the probability of exceeding LSi (i= 1, 2, 3) of model Sn-N1 at a given S_a) < $P_{Sn\text{-}N2}[LSi|S_a]$ < $P_{Sn\text{-}N3}[LSi|S_a]$ < $P_{Sn\text{-}N4}[LSi|S_a]$ for most of the cases. Typically, for model S6-N1, Figure 7.6 (a) demonstrates the specific probabilities on the fragility curves at a given earthquake intensity. Under a spectral acceleration of 0.5g, it can be extracted from the fragility curve that, the LS1, LS2 and LS3 are reached with a probability of 98%, 19% and 0% (see Figure 7.6 (a)), respectively.

It can be seen that under a S_a of 0.3g, the likelihood of most of the models reaching LS1 is high. For models S6-N1, S6-N2, S6-N3, S9-N1, S9-N2, S9-N3, S12-N1, S12-N2, S12-N3, the probabilities of exceeding LS2 are fairly low when S_a is less than 0.15g, and increased significantly beyond 0.15g for most cases. On the other hand, LS3 is rarely reached at a S_a of 0.2g for all models, the models with 4 NMRBs (Sn-N4, n= 6, 9, 12). Under a S_a of 0.5g, the PE percentages in LS3 are still found to be minor, especially for models with less than 4 bays. Note that when comparing the probabilities of exceeding LS3 among models S6-N4, S9-N4, S12-N4, it is found that $P_{S9\text{-}N4}[LS3|S_a]$ (37%) < $P_{S12\text{-}N4}[LS3|S_a]$ (38%) < $P_{S6\text{-}N4}[LS3|S_a]$ (62%). Although these PE percentages are reasonably high for the serviceability requirement of the buildings, it can still be revealed that the buildings with a slenderness of 0.75 (S9-N4) to 1 (S12-N4) have much lower chance of collapse than the building with a slenderness of 0.5 (S6-N4) in this circumstance.

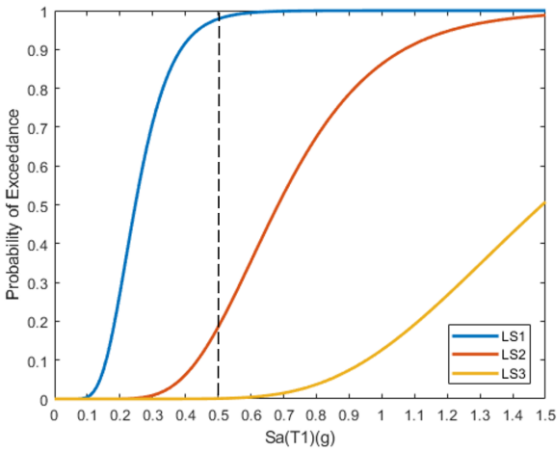

(a) S6-N1

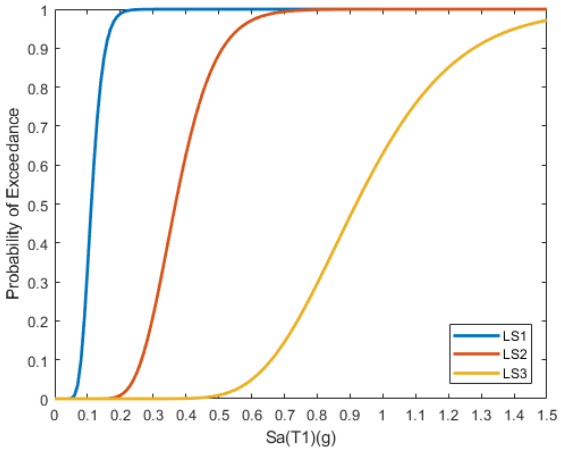

(b) S6-N2

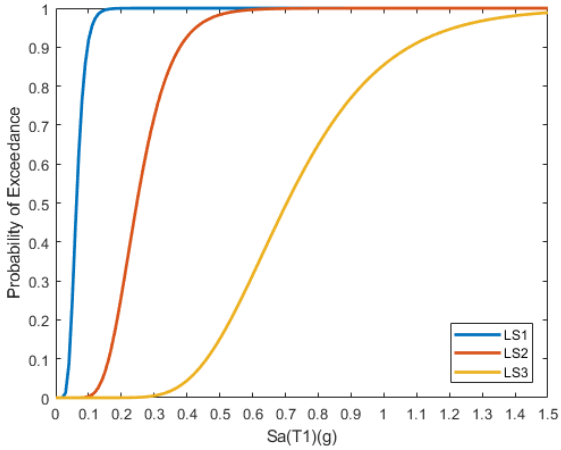

(c) S6-N3

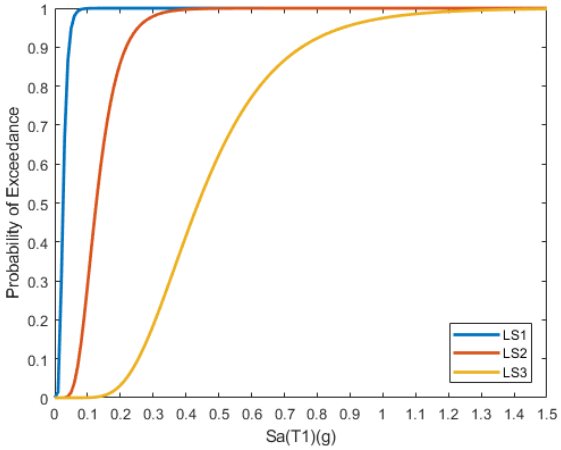

(d) S6-N4

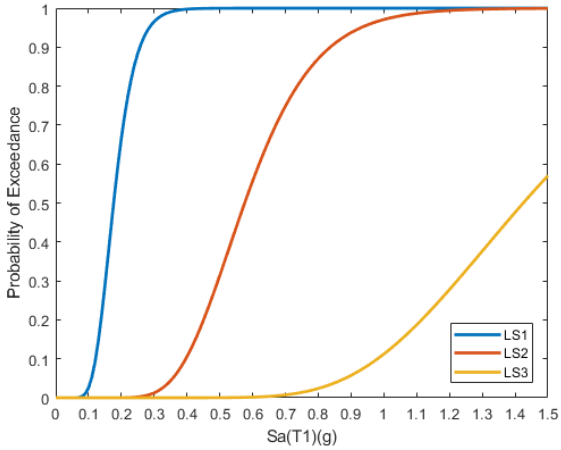

(e) S9-N1

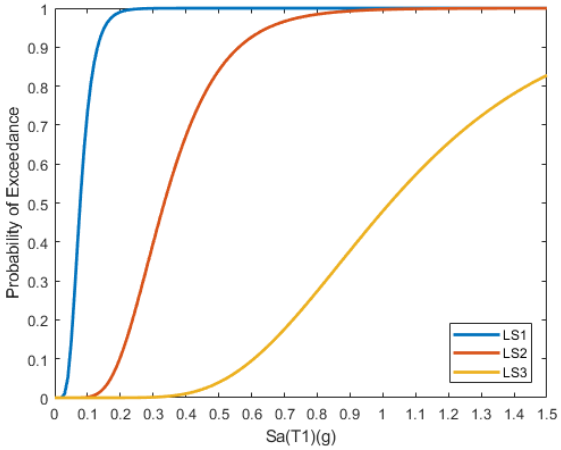

(f) S9-N2

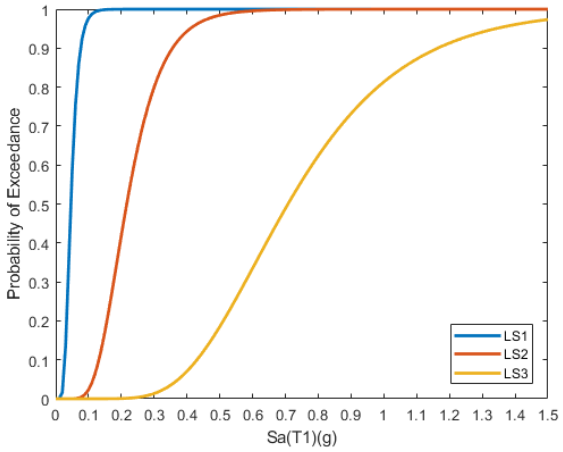

(g) S9-N3

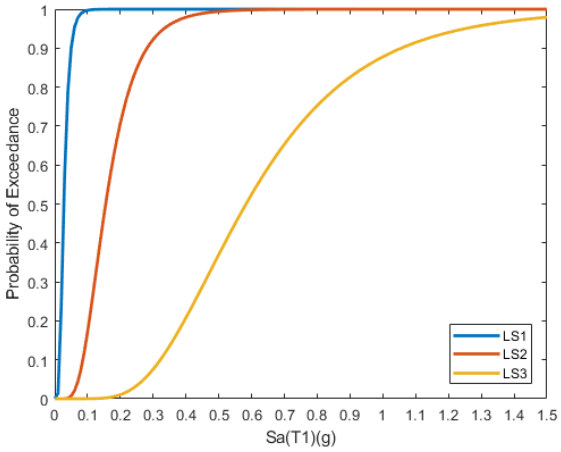

(h) S9-N4

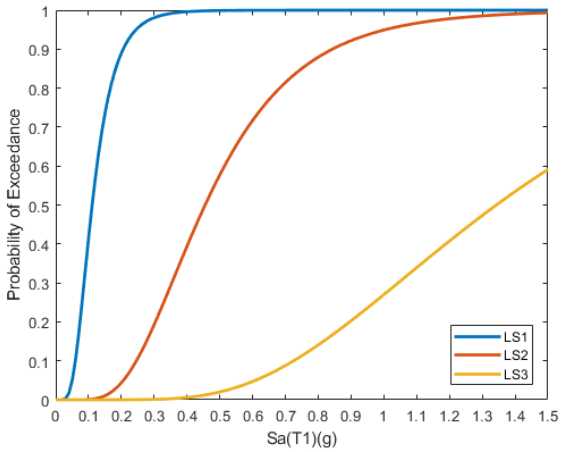

(i) S12-N1

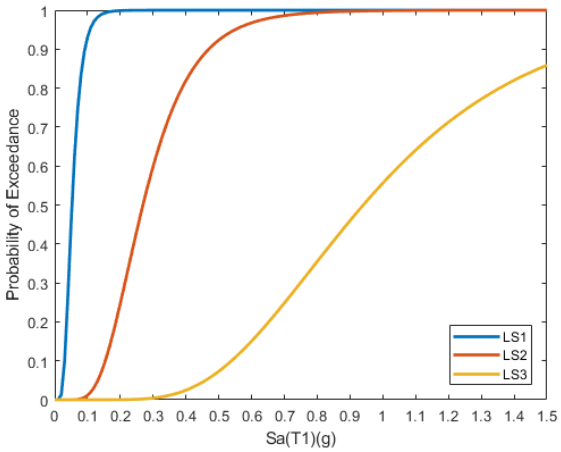

(j) S12-N2

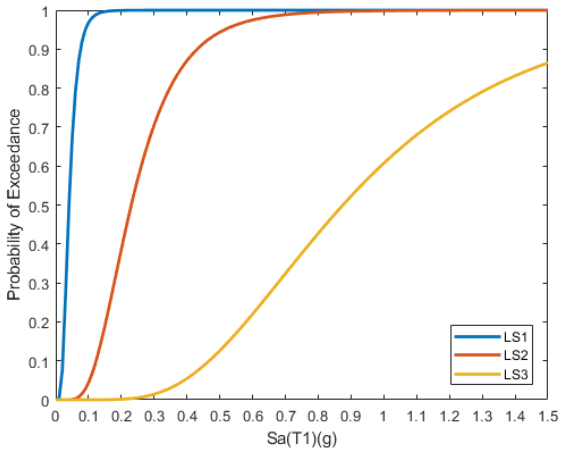

(k) S12-N3

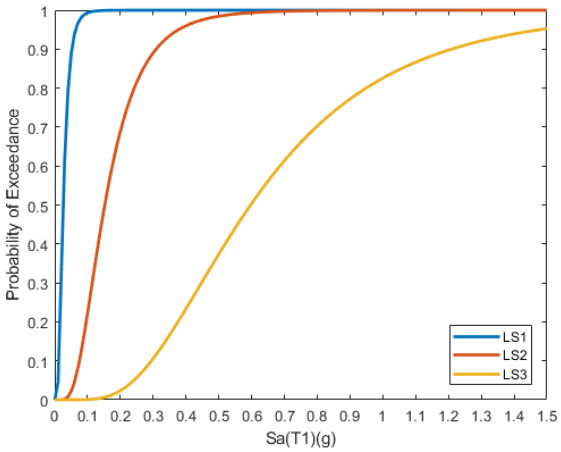

(l) S12-N4

Figure 7.6 Fragility curves for 12 models

Figure 7.7 compares the PE percentages at a given performance level (LS) for models with same number of NMRBs but vary in structural height. Note that the sub-figures are named as 'number of NMRB-LS level', e.g. Figure 7.7 (a) 1NMRB-LS1 denotes the comparison of the probabilities of exceeding LS1 in 6-storey, 9-storey and 12-storey models, all with one non-moment-resisting bay. At LS1, it can be clearly seen that $P_{S6\text{-}N1}[LS1|S_a] < P_{S9\text{-}N1}[LS1|S_a] < P_{S12\text{-}N1}[LS1|S_a]$ at a given S_a prior to 0.5g. However, the difference in PE percentages narrows down with increased number of NMRB. Moreover, for all storey heights, at a given S_a, the overall PE percentage of $P[LS1|S_a]$ is always higher with more NMRBs. The models with 4 NMRBs show almost no difference at very high PE percentages when S_a is less than 0.1g.

As can be inferred by contrasting the shape of the fragility curves, the deviation of the fragility is larger at LS2 than that at LS1. While LS1 is reached in nearly all the fragility curves at relatively lower seismic demand areas (for buildings in the S_a (T1) regions of approximately 0-0.3g), LS2 is reached in the regions of approximately 0.2-0.7g. Moreover, the 6-storey models with any number of NMRBs are found to be advantageous over other models as their PE percentages are the lowest at LS1, i.e. $P_{S6}[LS1|S_a] < P_{S9}[LS1|S_a] < P_{S12}[LS1|S_a]$. However, at LS2 and LS3, especially with more NMRBs, the PE percentages for the 9-storey and 12-storey models begin to drop and sometimes are lower than the PE percentages for the 6-storey models after certain S_a (T1), i.e. $P_{6\text{-}2}[LS2|S_a>0.42g] > P_{9\text{-}2}[LS2|S_a>0.42g]$ (Figure 7.7 (f)), $P_{6\text{-}3}[LS2|S_a>0.24g] > P_{12\text{-}3}[LS2|S_a>0.24g]$ (Figure 7.7 (g)), $P_{6\text{-}2}[LS3|S_a>0.76g] > P_{9\text{-}2}[LS3|S_a>0.76g]$ (Figure 7.7 (j)).

At LS3, the PE percentages for all the models are much lower than those at LS2 within an even further S_a (T1) region (0.5-1g). It can be observed that the more NMRBs in a structure, the lower the probabilities of collapse are found in taller buildings, i.e. in Figures 7.7 (j) to 7.7 (l), $P_{6\text{-}2}[LS3|S_a>0.9g] > P_{12\text{-}2}[LS3|S_a>0.9g] > P_{9\text{-}2}[LS3|S_a>0.9g]$, $P_{6\text{-}3}[LS3|S_a>0.7g] > P_{9\text{-}3}[LS3|S_a>0.7g] > P_{12\text{-}3}[LS3|S_a>0.7g]$, and $P_{6\text{-}4}[LS3|S_a>0.5g] > P_{9\text{-}3}[LS3|S_a>0.5g] > P_{12\text{-}4}[LS3|S_a>0.5g]$. The above observations highlight that when S_a

is greater than 0.5g, the collapse fragility of the structures is more sensitive to the slenderness of the structures. Although for all building heights, the probabilities of exceeding LS3 increase with more numbers of NMRBs, for buildings with the same number of NMRBs, the taller buildings have lower PE percentages at LS3. In other words, with the same numbers of NMRBs, the taller buildings have a less likelihood to collapse. This could be related to the fact that the flexibility of buildings with a larger slenderness is always higher, which therefore results in a better energy dissipation capability under severe earthquakes. Further, for all building heights, when with 1 to 3 NMRBs, the PE percentages of the builds at LS3 are lower than 20% when S_a<0.5g. This implies that for the purpose of collapse prevention, the proposed system is only recommended to be built with no more than 3 NMRBs, specifically for 6-, 9- and 12-stories.

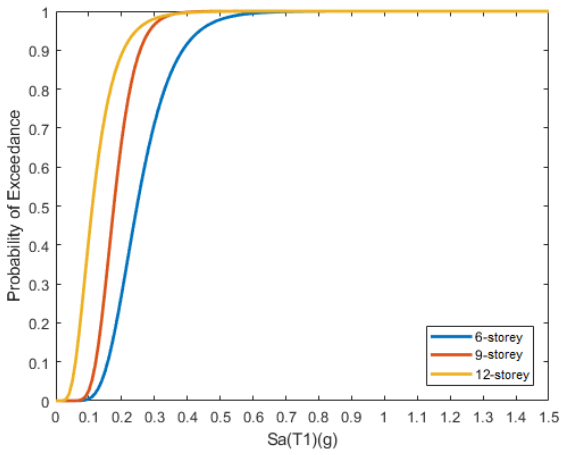

(a) 1NMRB-LS1

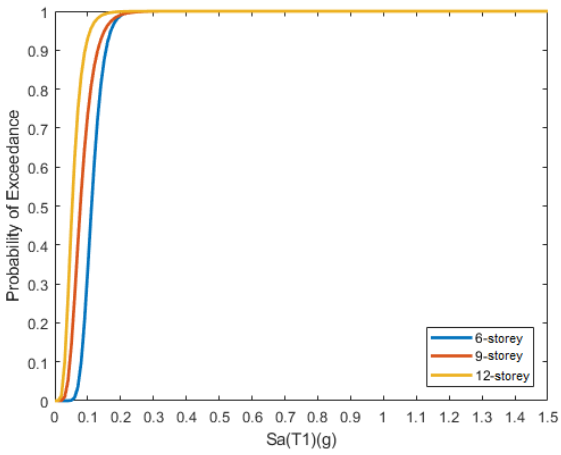

(b) 2NMRB-LS1

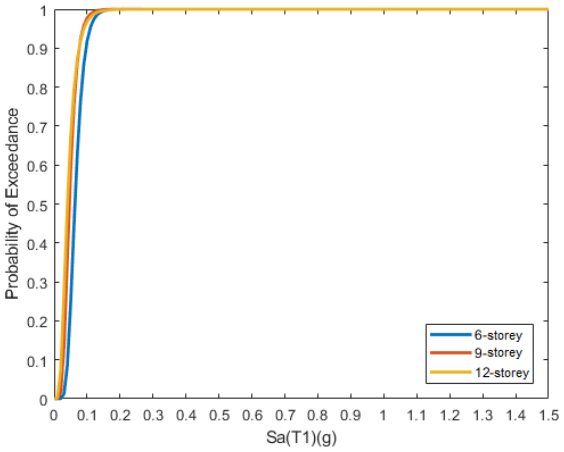

(c) 3NMRB-LS1

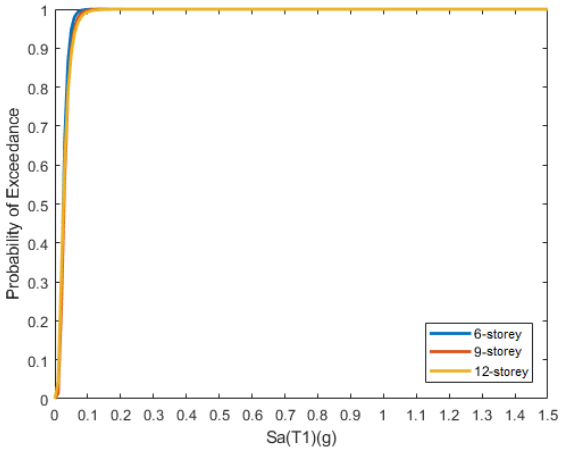

(d) 4NMRB-LS1

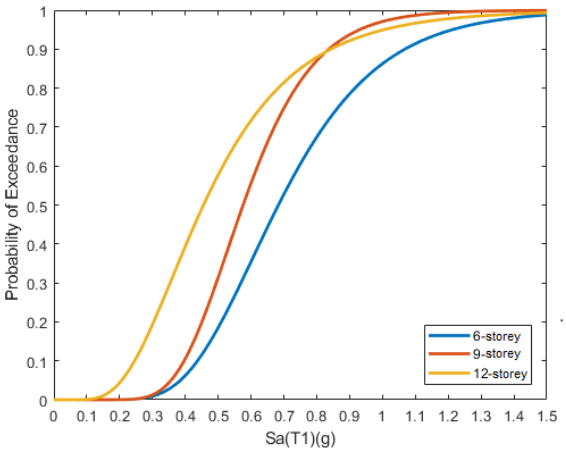

(e) 1NMRB-LS2

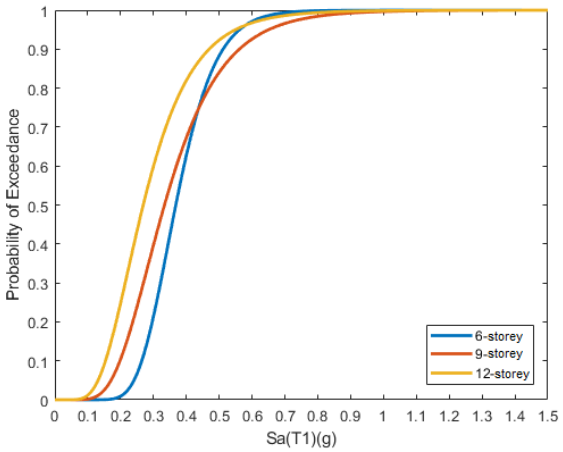

(f) 2NMRB-LS2

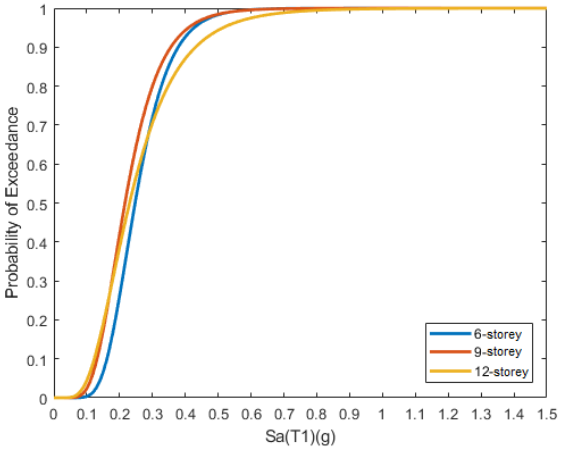

(g) 3NMRB-LS2

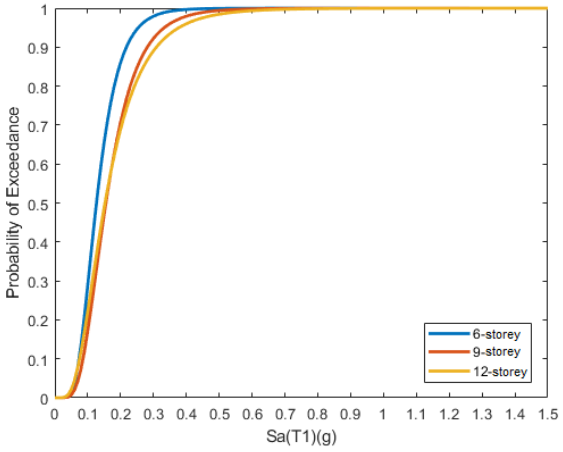

(h) 4NMRB-LS2

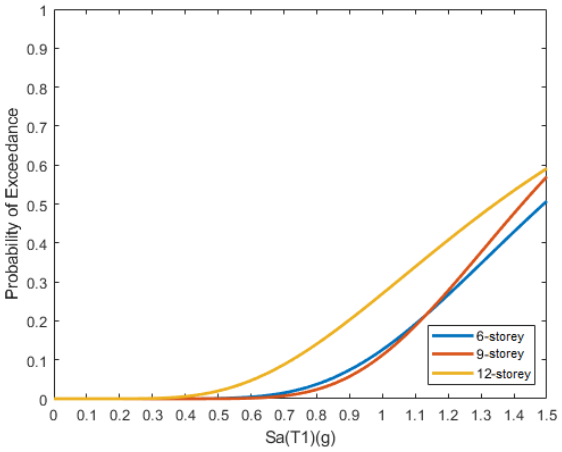

(i) 1NMRB-LS3

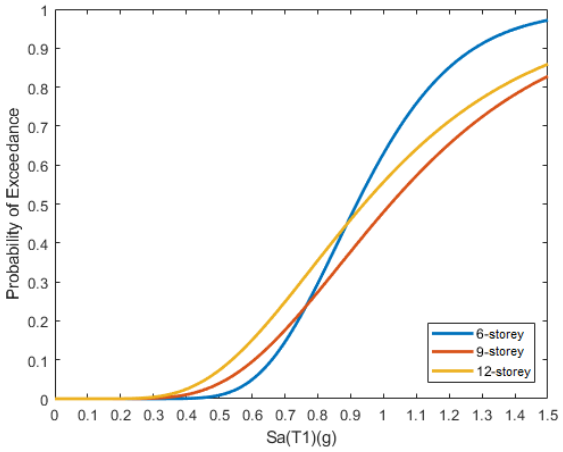

(j) 2NMRB-LS3

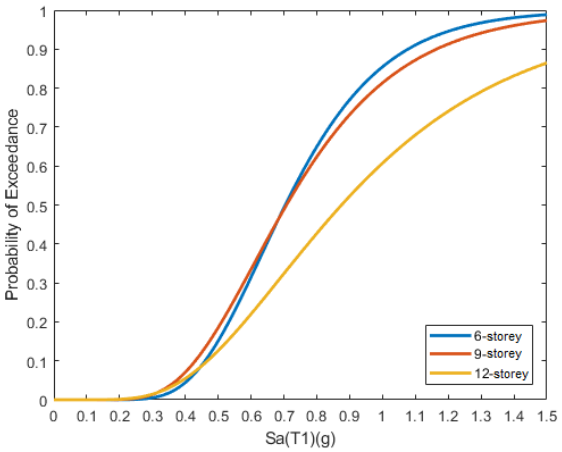

(k) 3NMRB-LS3

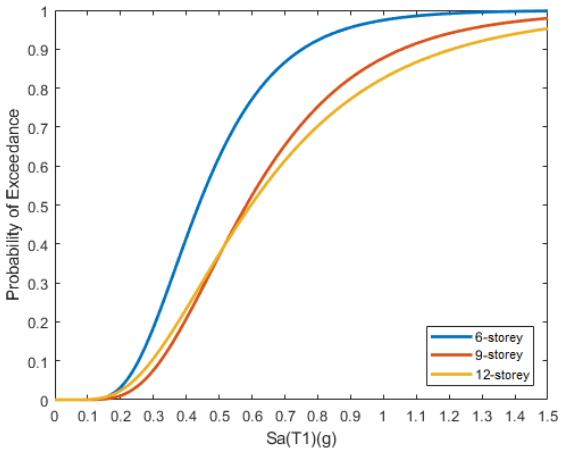

(l) 4NMRB-LS3

Figure 7.7 Comparison of probabilities of exceedance between models of different storey numbers

7.5 Concluding Remarks

Analytical fragility analysis is an efficient tool and a major step for seismic assessment of structural systems. In this chapter, Cloud analysis was used as the conventional NTHA-based method for this purpose. As was described, compared to other nonlinear dynamic methods such as IDA and MSA, Cloud analysis is a more straightforward and less time-consuming approach to assess the proposed system. With this method, 12 designed models in three different storey heights and four different numbers of non-moment resisting bays were analysed. Subsequently, the obtained fragility curves of all

the models were then discussed in details. The main findings obtained from the present study in this chapter are summarised below:

- Most buildings can still remain serviceable under a S_a of 0.5g.
- The fragility of the structures are more sensitive to the slenderness of the structures at higher performance levels.
- With the same building height, the probabilities of exceeding a given performance level (especially for LS1 and LS2) are always higher with more numbers of NMRBs for most of the cases.
- With the same numbers of NMRBs, the taller buildings have less likelihood to collapse.
- For the purpose of collapse prevention, the proposed system is only recommended to be built with no more than 3 NMRBs, specifically for 6-, 9- and 12-stories.

CHAPTER 8

CONCLUSIONS

8.1 Research Findings and Achievements

In recent years, building and construction industry worldwide has been facing ever-increasing challenges and sophisticated demands in safeguarding civil infrastructure against natural hazards such as earthquakes. Conventional structural design approaches can no longer satisfy the needs for the rapid development of advanced modular constructions. Similarly, conventional prefabrication is not necessary an appropriate choice for countries in earthquake-disaster prone areas due to the possible connection failure, insufficient stiffness and strength of columns under lateral loads. On the other hand, the steel frame system has always been one of the most popular structural options in seismic design. Conventionally designed rigid beam-column connections of the steel frame usually require on-field welding. Although this type of connections can provide higher ductility to the structural system, there are recognised drawbacks in terms of high-volume workload, lacking in construction quality assurance and high likelihood of industrial accidents. Moreover, once extensive plastic deformations occurred in individual structural members under a severe earthquake, the cost of replacing or repairing the damaged components is comparatively very high.

To overcome the prevailing problems, a new prefabricated structural system of bolt-

connected beams and columns with buckling restrained braces (BRBs) is proposed in this thesis. In this system, the potential damage to the main structural members caused by earthquake ground motions can be effectively reduced. This is achieved by utilising the BRBs to resist all the lateral seismic loads, whereas the bolt-connected beams and columns are designed to carry gravity loads only. As such, the bolt-connected beams and columns would remain elastic where the compressive buckling of the conventional braces can also be avoided.

This thesis research aims to evaluate the seismic performance of the proposed structural system. In this regard, the completed tasks may be summarised as follows.

A comprehensive literature review has led to a thorough understanding of the background of prefabrication, as well as the performance characteristics of bolted connections, the BRBs, and the buckling retrained braced frame (BRBFs). The research gaps are thereby clearly identified.

Numerical analyses are then carried out to realise the research objectives. Specifically, three-dimensional beam-column connections (including end plate connection, fin plate connection and top- and seat-angle connection) are modelled using ABAQUS to investigate the rotational capacities. The numerical results show that the three types of connections should be classified as pinned connections. To simulate the structural behaviour of the proposed system, finite element models are developed via OpenSees and validated using available published experimental results. Predictions based on the finite element simulation are presented in terms of inter-storey drift ratio, axial force time-history of BRBs, hysteretic loops of the BRBs, and storey displacement time history. The simulation results agree reasonably well with the experimental records.

Cyclic loading tests have been conducted on three half-scaled 2-storey models: two BRBFs with non-moment-resisting frames which are assembled with two different bolted only beam-column connections; and, one single 2-storey BRBF (without a non-

moment-resisting frame). In addition, a pushover test has been performed on one BRBF with a non-moment-resisting frame. The experimental studies are discussed in regard to the hysteretic behaviour, energy-dissipating capacity, and stiffness degradation of the test specimens. Moreover, the laboratory-based results are compared with the finite-element simulations, which utilised rigid boundary conditions with pinned beam-column connections in the non-moment-resisting bays. This leads to the conclusion that the rotational stiffness of the beam-column connections has a negligible effect on the global behaviour of the BRBFs.

To provide useful guidelines for design, a parametric study of the proposed BRBF system is carried out through dynamic time-history analyses. Specifically, the impact of the beam-column-brace connection rigidity and the BRB area distributions on the seismic resistance capacity of the system is studied. Two groups of models, namely the R-and P-Groups each of which comprises 9-storey and 5-storey frames, are investigated. The frames in the R-Group are with moment-resisting beam-column-brace connections; those in the P-Group are with non-moment-resisting ones. Further, the design approach for BRB areas is evaluated in terms of structural seismic performance. The results of the parametric study show that the proposed system performs well in seismic resistance under severe earthquakes. The use of moment-resisting beam-column-brace connections is shown to be more beneficial in resisting earthquake actions compared to their non-moment-resisting counterparts, especially when the stiffness ratio (Sr) is between 1 and 4. Moreover, the ideal value of Sr for the system is found to be between 3 and 5 regardless of the building height. For the design distribution of BRB areas along the storey height, the most uniform pattern of the inter-storey drift ratios is produced when the said areas are distributed proportionally to the storey shear force.

Last but not least, a fragility analysis is conducted to fully understand the structural demand caused by various levels of ground shaking. For a more straightforward and less time-consuming analytical method of fragility study, the conventional nonlinear time history analysis-based Cloud method is adopted. A set of earthquake records are

employed to represent the variability of ground motion. Twelve prototype frames with three different storey heights and various numbers of non-moment resisting bays have been designed and analysed. In the fragility study, damage states are defined and the engineering demand parameters of structural capacity corresponding to each damage state are established. Then, the conditional probabilities of structural demand are computed where the results are displayed as fragility curves. These curves demonstrate that, the fragility of the structures are more sensitive to the slenderness of the structures at higher performance levels; with the same numbers of NMRBs, the taller buildings have less likelihood to collapse. In addition, in regard to collapse prevention, the proposed system is only recommended to use with no more than 3 NMRBs.

8.2 Recommendations for Future Study

To complement the findings in this thesis, recommendations may be made for future study as follows:

- In the present research, floor slabs have been ignored as a strength-contributing factor for seismic performance of the proposed BRBF system. In general, the contribution of a slab is not explicitly considered in structural design (Ahmed et al., 2013). However, existing experimental tests have indicated that the impact of floor slabs in imparting strength and stiffness to a frame may have been underestimated (Yalcin and Durrani, 1993; Fenwick et al., 2005). Therefore, the mechanisms of slab action and its influence on the behaviour of the proposed system subjected to lateral loads should be further investigated.
- In the present experimental investigation, each of the BRBFs used in the tests was produced as a whole component in the factory. This is to ensure the rigidity of the beam-column-brace connections is maintained to provide adequate stiffness for the structural system. Unfortunately, such components in whole would present transportation difficulties in practice. Thus, it is preferable to split the said rigid connections from the BRBF at, say, the contraflexural points of the column and the beam of the frame. Then on the designated site, the

components can be reassembled to form the whole BRBFs. The feasibility of this two-stage construction approach should be examined in a future study.

REFERENCES

Abdalla, K. M., & Chen, W.-F. (1995). Expanded database of semi-rigid steel connections. *Computers & Structures, 56*(4), 553-564.

Abolmaali, A., Matthys, J. H., Farooqi, M., & Choi, Y. (2005). Development of moment–rotation model equations for flush end-plate connections. *Journal of Constructional Steel Research, 61*(12), 1595-1612.

AISC. (1978). Specification for the Design In *Fabrication and Erection of Structural Steel for Buildings*. Chicago: American Institute of Steel Construction.

AISC. (1989). *Manual of steel construction–allowable stress design*. Chicago: American Institute of Steel Construction.

AISC. (2002). *Seismic provisions for structural steel buildings*. Chicago: American Institute of Steel Construction.

AISC. (2005a). *Seismic provisions for structural steel buildings*. Chicago: American Institute of Steel Construction.

AISC. (2005b). *Specification for Structural Steel Buildings* Chicago: American Institute of Steel Construction.

AISC. (2010). *Seismic provisions for structural steel buildings*. Chicago: American Institute of Steel Construction.

Ancheta, T. D., Darragh, R. B., Stewart, J. P., Seyhan, E., Silva, W. J., Chiou, B. S.-J., . . . Boore, D. M. (2014). NGA-West2 database. *Earthquake Spectra, 30*(3), 989-1005.

Antonucci, R., Balducci, F., Castellano, M., & Donà, F. (2006). *Pre-casted RC buildings with buckling restrained braces: the example of the new building of the faculty of engineering in Ancona.* Paper presented at the the Second International fib Congress, Napoli, Italy.

Ariyaratana, C., & Fahnestock, L. A. (2011). Evaluation of buckling-restrained braced frame seismic performance considering reserve strength. *Engineering Structures, 33*(1), 77-89.

Astaneh-Asl, A. (1998). *Seismic behavior and design of gusset plates*: Structural Steel Educational Council.

ATC-13. (1985). *Earthquake Damage Evaluation Data for California, Report ATC-13*. Redwood City, California: Applied Technology Council

Attiogbe, E., & Morris, G. (1991). Moment-rotation functions for steel connections. *Journal of Structural Engineering, 117*(6), 1703-1718.

Azizinamini, A., Bradburn, J., & Radziminski, J. (1985). *Static and cyclic behavior of semi-rigid steel beam-column connections*. Structual Research Studies, Department of Civil Engineering, University of South Carolina, Columbia, S.C. 219.

Badir, Y. F., Kadir, M. A., & Hashim, A. H. (2002). Industrialized building systems construction in Malaysia. *Journal of architectural engineering, 8*(1), 19-23.

Baghchesaraei, O. R., Lavasani, H. H., & Baghchesaraei, A. (2016). Behavior of prefabricated structures in developed and developing countries. *Bulletin de la Société des Sciences de Liège, 85*, 1229-1234.

Bahaari, M. R., & Sherbourne, A. N. (2000). Behavior of eight-bolt large capacity endplate connections. *Computers & Structures, 77*(3), 315-325.

Bai, J.-W., Gardoni, P., & Hueste, M. B. D. (2011). Story-specific demand models and seismic fragility estimates for multi-story buildings. *Structural Safety, 33*(1), 96-107.

Baker, J. W. (2015). Efficient analytical fragility function fitting using dynamic structural analysis. *Earthquake Spectra, 31*(1), 579-599.

Barlow, J., Childerhouse, P., Gann, D., Hong-Minh, S., Naim, M., & Ozaki, R. (2003).

Choice and delivery in housebuilding: lessons from Japan for UK housebuilders. *Building research & information, 31*(2), 134-145.

Basoz, N. (1997). *Risk assessment for highway transportation systems.* (Ph.D.), Stanford University, Boston.

Bayo, E., Cabrero, J., & Gil, B. (2006). An effective component-based method to model semi-rigid connections for the global analysis of steel and composite structures. *Engineering Structures, 28*(1), 97-108.

Bell, W. G., Chesson Jr, E., & Munse, W. (1958). *Static tests of standard riveted and bolted beam-to-column connections*: Engineering Experiment Station, University of Illinois.

Berman, J. W., & Bruneau, M. (2009). Cyclic testing of a buckling restrained braced frame with unconstrained gusset connections. *Journal of Structural Engineering, 135*(12), 1499-1510.

Billah, A. M., & Alam, M. S. (2014). Seismic performance evaluation of multi-column bridge bents retrofitted with different alternatives using incremental dynamic analysis. *Engineering Structures, 62*, 105-117.

Black, C., Aiken, I. D., & Makris, N. (2002). *Component testing, stability analysis, and characterization of buckling-restrained unbonded braces*: Pacific Earthquake Engineering Research Center, University of California, Berkeley.

Black, C. J., Makris, N., & Aiken, I. D. (2004). Component testing, seismic evaluation and characterization of buckling-restrained braces. *Journal of Structural Engineering, 130*(6), 880-894.

Blismas, N., Pasquire, C., & Gibb, A. (2006). Benefit evaluation for off‐site production in construction. *Construction Management Economics, 24*(2), 121-130.

Boafo, F., Kim, J.-H., & Kim, J.-T. (2016). Performance of modular prefabricated architecture: case study-based review and future pathways. *Sustainability, 8*(6), 558.

Bosco, M., Marino, E., & Rossi, P. (2015). Design of steel frames equipped with BRBs in the framework of Eurocode 8. *Journal of Constructional Steel Research, 113*, 43-57.

Bosco, M., & Marino, E. M. (2013). Design method and behavior factor for steel frames with buckling restrained braces. *Earthquake Engineering & Structural Dynamics, 42*(8), 1243-1263.

Bose, S., McNeice, G., & Sherbourne, A. (1972). Column webs in steel beam-to-column connexions part II—Design recommendations. *Computers & Structures, 2*(1-2), 281-301.

British Standard. (2005). Eurocode 8: Design of structures for earthquake resistance. In. Brussels: European Committee for Standardization.

Bursi, O., & Jaspart, J.-P. (1997a). Benchmarks for finite element modelling of bolted steel connections. *Journal of Constructional Steel Research, 43*(1), 17-42.

Bursi, O., & Jaspart, J.-P. (1997b). Calibration of a finite element model for isolated bolted end-plate steel connections. *Journal of Constructional Steel Research, 44*(3), 225-262.

Bursi, O., & Jaspart, J.-P. (1998). Basic issues in the finite element simulation of extended end plate connections. *Computers & Structures, 69*(3), 361-382.

Calvi, G. M., Pinho, R., Magenes, G., Bommer, J. J., Restrepo-Vélez, L. F., & Crowley, H. (2006). Development of seismic vulnerability assessment methodologies over the past 30 years. *ISET Journal of Earthquake Technology, 43*(3), 75-104.

Casotto, C., Silva, V., Crowley, H., Nascimbene, R., & Pinho, R. (2015). Seismic fragility of Italian RC precast industrial structures. *Engineering Structures, 94*, 122-136.

Chan, W., & Hu, H. (2002). Production scheduling for precast plants using a flow shop sequencing model. *Journal of Computing in Civil Engineering, 16*(3), 165-174.

Chasten, C. P., Lu, L.-W., & Driscoll, G. C. (1992). Prying and shear in end-plate connection design. *Journal of Structural Engineering, 118*(5), 1295-1311.

Chen, S.-J., Yeh, C., & Chu, J. (1996). Ductile steel beam-to-column connections for seismic resistance. *Journal of Structural Engineering, 122*(11), 1292-1299.

Chen, W.-F., & Kishi, N. (1989). Semirigid steel beam-to-column connections: Data base and modeling. *Journal of Structural Engineering, 115*(1), 105-119.

Chiang, Y.-H., Chan, E. H.-W., & Lok, L. K.-L. (2006). Prefabrication and barriers to entry—a case study of public housing and institutional buildings in Hong Kong. *Habitat International, 30*(3), 482-499.

Choi, E., DesRoches, R., & Nielson, B. (2004). Seismic fragility of typical bridges in moderate seismic zones. *Engineering Structures, 26*(2), 187-199.

Choi, H., & Kim, J. (2006). Energy-based seismic design of buckling-restrained braced frames using hysteretic energy spectrum. *Engineering Structures, 28*(2), 304-311.

Chou, C.-C., & Chen, S.-Y. (2010). Subassemblage tests and finite element analyses of sandwiched buckling-restrained braces. *Engineering Structures, 32*(8), 2108-2121.

Chou, C.-C., Liou, G.-S., & Yu, J.-C. (2012). Compressive behavior of dual-gusset-plate connections for buckling-restrained braced frames. *Journal of Constructional Steel Research, 76*, 54-67.

Christopulos, A. S. (2005). *Improved seismic performance of buckling restrained braced frames.* (Ph.D.), University of Washington, Seattle.

Chu, X. F. (2009). Industrialised housing industry development process in China. *Housing Industry, 5*, 12-14.

Citipitioglu, A., Haj-Ali, R., & White, D. (2002). Refined 3D finite element modeling of partially-restrained connections including slip. *Journal of Constructional Steel research, 58*(5), 995-1013.

Clark, P. (1999). *Design procedures for buildings incorporating hysteretic damping*

devices. Paper presented at the International Post-SMiRT Conference Seminar on Seismic Isolation, Korea.

Clark, P., Kasai, K., Aiken, I., & Kimura, I. (2000). *Evaluation of design methodologies for structures incorporating steel unbonded braces for energy dissipation.* Paper presented at the Proceedings 12th WCEE, Auckland, New Zealand.

Clough, R. W., & Wilson, E. L. (1999). *Early finite element research at Berkeley.* Paper presented at the Fifth US National Conference on Computational Mechanics.

Cornell, C., & Krawinkler, H. (2000). *Progress and challenges in seismic performance assessment*: PEER Center News.

Cornell, C. A., Jalayer, F., Hamburger, R. O., & Foutch, D. A. (2002). Probabilistic basis for 2000 SAC federal emergency management agency steel moment frame guidelines. *Journal of Structural Engineering, 128*(4), 526-533.

Czarnecki, R. M. (1973). *Earthquake damage to tall buildings*. Cambridge, MA: Massachusetts Institute of Technology.

Dai, X., Wang, Y., & Bailey, C. (2010). Numerical modelling of structural fire behaviour of restrained steel beam–column assemblies using typical joint types. *Engineering Structures, 32*(8), 2337-2351.

Davison, J., Kirby, P., & Nethercot, D. (1987). Rotational stiffness characteristics of steel beam-to-column connections. *Journal of Constructional Steel Research, 8*, 17-54.

Della Corte, G., D'Aniello, M., Landolfo, R., & Mazzolani, F. M. (2011). Review of steel buckling‐restrained braces. *Steel Construction, 4*(2), 85-93.

Della Corte, G., Landolfo, R., & Mazzolani, F. M. (2010). Displacement‐based seismic design of braced steel structures. *Steel Construction, 3*(3), 134-139.

Diaz, C., Marti, P., Victoria, M., & Querin, O. M. (2011). Review on the modelling of joint behaviour in steel frames. *Journal of Constructional Steel Research, 67*(5),

741-758.

Díaz Gómez, C. (2010). *Optimum design of semi-rigid joint by numeric simulation and kriging models.* (Ph. D.), Technical University of Cartagena, Cartagena (Murcia), Spain.

Dlubal. (2018). Fin Plate Connections: Theory and Application. Retrieved from https://www.dlubal.com/en-US/support-and-learning/support/knowledge-base/001532

Eastman, C., Sacks, R., & Lee, G. (2003). Development and implementation of advanced IT in the North American precast concrete industry. *Journal of Information Technology in Construction, 8*(18), 247-262.

Eatherton, M. R., Ma, X., Krawinkler, H., Mar, D., Billington, S., Hajjar, J. F., & Deierlein, G. G. (2014). Design concepts for controlled rocking of self-centering steel-braced frames. *Journal of Structural Engineering, 140*(11), 04014082.

Ebrahimian, H., Astroza, R., & Conte, J. P. (2015). Extended Kalman filter for material parameter estimation in nonlinear structural finite element models using direct differentiation method. *Earthquake Engineering & Structural Dynamics, 44*(10), 1495-1522.

Ebrahimian, H., Jalayer, F., Asprone, D., Lombardi, A. M., Marzocchi, W., Prota, A., & Manfredi, G. (2014). A performance ‐ based framework for adaptive seismic aftershock risk assessment. *Earthquake Engineering & Structural Dynamics, 43*(14), 2179-2197.

Ebrahimian, H., Jalayer, F., & Manfredi, G. (2015). *Seismic retrofit decision-making of bridges based on life-cycle cost criteria.* Paper presented at the 5th ECCOMAS Thematic Conference on Computational Methods in Structural Dynamics and Earthquake Engineering (COMPDYN 2015).

Elefante, L., Jalayer, F., Iervolino, I., & Manfredi, G. (2010). Disaggregation-based response weighting scheme for seismic risk assessment of structures. *Soil*

Dynamics and Earthquake Engineering 30(12), 1513-1527.

Ellingwood, B. R., Celik, O. C., & Kinali, K. (2007). Fragility assessment of building structural systems in Mid‐America. *Earthquake Engineering & Structural Dynamics, 36*(13), 1935-1952.

Elnashai, A., Borzi, B., & Vlachos, S. (2004). Deformation-based vulnerability functions for RC bridges. *Structural Engineering and Mechanics, 17*(2), 215-244.

Erberik, M. A. (2008). Fragility-based assessment of typical mid-rise and low-rise RC buildings in Turkey. *Engineering Structures, 30*(5), 1360-1374.

Erberik, M. A., & Elnashai, A. S. (2004). Fragility analysis of flat-slab structures. *Engineering Structures, 26*(7), 937-948.

Faella, C., Piluso, V., & Rizzano, G. (1994). *Connection influence on the elastic and inelastic behavior of steel frames.* Paper presented at the International workshop and seminar on behaviour of steel structures in seismic areas, STESSA.

Faella, C., Piluso, V., & Rizzano, G. (1999). *Structural steel semirigid connections: theory, design, and software* (Vol. 21): CRC press.

Faella, C., Piluso, V., & Rizzano, G. (2000). Cyclic behaviour of bolted t-stubs: experimental analysis and modelling. In M. Tremblay (Ed.), *Behaviour of Steel Structures in Seismic Areas* (pp. 183-190). Balkema, Rotterdam.

Fahnestock, L. A., Ricles, J. M., & Sause, R. (2007). Experimental evaluation of a large-scale buckling-restrained braced frame. *Journal of Structural Engineering, 133*(9), 1205-1214.

Fahnestock, L. A., Sause, R., & Ricles, J. M. (2006). *Analytical and large-scale experimental studies of earthquake-resistant buckling-restrained braced frame systems*: ATLSS report number 06-01, Lehigh University.

Fahnestock, L. A., Sause, R., Ricles, J. M., & Lu, L.-W. (2003). Ductility demands on buckling-restrained braced frames under earthquake loading. *Earthquake*

Engineering & Structural Dynamics, 2(2), 255-268.

Fajfar, P. (2000). A nonlinear analysis method for performance-based seismic design. *Earthquake Spectra, 16*(3), 573-592.

Fan, Y. (2010). Industrialization residential housing development in China: roadmap in the new age. *Shanghai Real Estate, 10*(2), 16-18.

Federal Emergency Management Agency. (2000). *Prestandard and commentary for the seismic rehabilitation of buildings*: American Society of Civil Engineers.

Fenwick, R., Davidson, B., & Lau, D. (2005). *Interaction between ductile RC perimeter frames and floor slabs containing precast units.* Paper presented at the New Zealand Society for Earthquake Engineering Conference.

Frye, M. J., & Morris, G. A. (1975). Analysis of flexibly connected steel frames. *Canadian Journal of Civil Engineering, 2*(3), 280-291.

Gaull, B., Michael‐Leiba, M., & Rynn, J. (1990). Probabilistic earthquake risk maps of Australia. *Australian Journal of Earth Sciences, 37*(2), 169-187.

GB50011. (2010). Code for seismic design of buildings. In. Beijing: China Building Industry Press.

GB50017. (2003). Chinese Steel Structure Code In. Beijing: China Planning Press.

GB50096. (2011). Chinese Residential Design Specification. In. Beijing: China Planning Press.

GB/T2975. (1998). Steel and Steel Products-Location and Preparation of Test Pieces for Mechanical Testing. In. Beijing: Standards Press of China.

Gebbeken, N., Rothert, H., & Binder, B. (1994). On the numerical analysis of endplate connections. *Journal of Constructional Steel Research, 30*(2), 177-196.

Genna, F., & Gelfi, P. (2011). Analysis of the lateral thrust in bolted steel buckling-restrained braces. I: Experimental and numerical results. *Journal of Structural Engineering, 138*(10), 1231-1243.

Goverdhan, A. V. (1983). *A collection of experimental moment-rotation curves and evaluation of prediction equations for semi-rigid connections*: Vanderbilt University.

Guo, Y.-L., Tong, J.-Z., Zhang, B.-H., Zhu, B.-L., & Pi, Y.-L. (2017). Theoretical and experimental investigation of core-separated buckling-restrained braces. *Journal of Constructional Steel Research, 135*, 137-149.

Guo, Y.-l., Zhang, B.-h., Jiang, Z.-q., & Chen, H. (2015). Critical load and application of core-separated buckling-restrained braces. *Journal of Constructional Steel Research, 106*, 1-10.

Habibullah, A. (1989). *ETABS users manual*. Berkeley, California: Computers Structures.

Hancock, J., Watson-Lamprey, J., Abrahamson, N. A., Bommer, J. J., Markatis, A., McCOY, E., & Mendis, R. (2006). An improved method of matching response spectra of recorded earthquake ground motion using wavelets. *Journal of Earthquake Engineering, 10*(spec01), 67-89.

Heo, Y., & Kunnath, S. K. (2009). Sensitivity to constitutive modeling in fiber-based discretization of reinforced concrete members for performance-based seismic evaluation. *Advances in Structural Engineering, 12*(1), 37-51.

Hibbett, Karlsson, & Sorensen. (1998). *ABAQUS/standard: User's Manual* (Vol. 1): Hibbitt, Karlsson & Sorensen.

Hibbitt, H., Karlsson, B., & Sorensen, E. (1993). ABAQUS, Structural and Heat Transfer Analysis Program, Version 5.3-1: HKS, Inc., Providence RI.

Holguin, R. E. (1998). Building department's response to EQ damage to steel frame buildings. *Journal of Performance of Constructed Facilities, 12*(4), 199-201.

Hoveidae, N., Tremblay, R., Rafezy, B., & Davaran, A. (2015). Numerical investigation of seismic behavior of short-core all-steel buckling restrained braces. *Journal of Constructional Steel Research, 114*, 89-99.

Hueste, M. B. D., & Bai, J.-W. (2007). Seismic retrofit of a reinforced concrete flat-slab structure: Part II—Seismic fragility analysis. *Engineering Structures, 29*(6), 1178-1188.

Hussain, S., Benschoten, P., Satari, M., & Lin, S. (2006). *Buckling restrained braced frame (BRBF) structures: analysis, design and approvals issues.* Paper presented at the 75th SEAOC Annual Convention.

Ibrahim, Y. E., & El-Shami, M. M. (2011). Seismic fragility curves for mid-rise reinforced concrete frames in Kingdom of Saudi Arabia. *The IES Journal Part A: Civil Structural Engineering and Mechanics, 4*(4), 213-223.

Indian Standard. (2002). Criteria for earthquake resistant design of structures. In. India: Bureau of Indian Standards.

International Code Council. (2000). *International building code 2000* (Vol. 1): Dearborn Trade Publishing.

Iwata, M., Kato, T., & Wada, A. (2000). Buckling-restrained braces as hysteretic dampers. In *Behavior of Steel Structures in Seismic Areas* (pp. 33-38).

Jaillon, L., & Poon, C.-S. (2008). Sustainable construction aspects of using prefabrication in dense urban environment: a Hong Kong case study. *Construction Management Economics, 26*(9), 953-966.

Jaillon, L., & Poon, C. S. (2009). The evolution of prefabricated residential building systems in Hong Kong: A review of the public and the private sector. *Automation in construction, 18*(3), 239-248.

Jalayer, F. (2003). *Direct probabilistic seismic anaysis: implementing non-linear dynamic assessments*: Stanford University Stanford.

Jalayer, F., Asprone, D., Prota, A., & Manfredi, G. (2011b). A decision support system for post-earthquake reliability assessment of structures subjected to aftershocks: an application to L'Aquila earthquake, 2009. *Bulletin of Earthquake Engineering, 9*(4), 997-1014.

Jalayer, F., De Risi, R., & Manfredi, G. (2015). Bayesian Cloud Analysis: efficient structural fragility assessment using linear regression. *Bulletin of Earthquake Engineering, 13*(4), 1183-1203.

Jalayer, F., Ebrahimian, H., Miano, A., Manfredi, G., & Sezen, H. (2017). Analytical fragility assessment using unscaled ground motion records. *Earthquake Engineering & Structural Dynamics, 46*(15), 2639-2663.

Jalayer, F., Elefante, L., Iervolino, I., & Manfredi, G. (2011a). Knowledge-based performance assessment of existing RC buildings. *Journal of Earthquake Engineering, 15*(3), 362-389.

Jalayer, F., Franchin, P., & Pinto, P. (2007). A scalar damage measure for seismic reliability analysis of RC frames. *Earthquake Engineering & Structural Dynamics, 36*(13), 2059-2079.

Jaspart, J.-P., & Maquoi, R. (1990). *Guidelines for the design of braced frames with semi-rigid connections.* Paper presented at the the International colloquium on stability of steel structures.

Jaspart, J. (1991). *Study of the semi-rigidity of beam-to-column joints and its influence on the resistance and stability of steel buildings.* (Ph.D.), Liège University, Wallonia, Belgium.

JGJ/T 101. (2015). Specification for seismic test of buildings. In. Beijing: Ministry of Housing and Urban-Rural Development of the People's Republic of China.

Jia, M., Lu, D., Guo, L., & Sun, L. (2014). Experimental research and cyclic behavior of buckling-restrained braced composite frame. *Journal of Constructional Steel Research, 95*, 90-105.

Karim, K. R., & Yamazaki, F. (2001). Effect of earthquake ground motions on fragility curves of highway bridge piers based on numerical simulation. *Earthquake Engineering & Structural Dynamics, 30*(12), 1839-1856.

Karim, K. R., & Yamazaki, F. (2003). A simplified method of constructing fragility

curves for highway bridges. *Earthquake Engineering & Structural Dynamics, 32*(10), 1603-1626.

Katsanos, E. I., Sextos, A. G., & Manolis, G. D. (2010). Selection of earthquake ground motion records: A state-of-the-art review from a structural engineering perspective. *Soil Dynamics and Earthquake Engineering, 30*(4), 157-169.

Kaushik, K., Sharma, A. K., & Kumar, R. (2013). A Review on Finite Element Analysis of Beam to Column Endplate Bolted Connection. *IOSR Journal of Mechanical and Civil Engineering, 8*(1), 97-103.

Kelly, J. M., Skinner, R., & Heine, A. (1972). Mechanisms of energy absorption in special devices for use in earthquake resistant structures. *Bulletin of NZ Society for Earthquake Engineering, 5*(3), 63-88.

Kiggins, S., & Uang, C.-M. (2006). Reducing residual drift of buckling-restrained braced frames as a dual system. *Engineering Structures, 28*(11), 1525-1532.

Kim, J., & Choi, H. (2004). Behavior and design of structures with buckling-restrained braces. *Engineering Structures, 26*(6), 693-706.

Kim, J., Ghaboussi, J., & Elnashai, A. S. (2010). Mechanical and informational modeling of steel beam-to-column connections. *Engineering Structures, 32*(2), 449-458.

Kim, S.-H., & Shinozuka, M. (2004). Development of fragility curves of bridges retrofitted by column jacketing. *Probabilistic Engineering Mechanics, 19*(1-2), 105-112.

Kim, T. (2009). *Comparison of prefab homes and a site-built home: Quantitative evaluation of four different types of prefab homes and a site-built home*: University of Southern California.

Kinali, K., & Ellingwood, B. R. (2007). Seismic fragility assessment of steel frames for consequence-based engineering: A case study for Memphis, TN. *Engineering structures, 29*(6), 1115-1127.

Kirçil, M. S., & Polat, Z. (2006). Fragility analysis of mid-rise R/C frame buildings. *Engineering Structures, 28*(9), 1335-1345.

Kishi, N., & Chen, W.-F. (1990). Moment-rotation relations of semirigid connections with angles. *Journal of Structural Engineering, 116*(7), 1813-1834.

Kishi, N., Chen, W., Goto, Y., & Matsuoka, K. (1993). Design aid of semi-rigid connections for frame analysis. *Engineering Journal, 30*(3), 90-107.

Kishi, N., Chen, W., Matsuoka, K., & Nomachi, S. (1987). *Moment-rotation relation of single/double web-angle connections*: School of Civil Engineering, Purdue University.

Kishi, N., & Daigaku, M. K. (1987). *Moment-rotation relation of top-and seat-angle with double web-angle connections*: School of Civil Engineering, Purdue University.

Kishi, N., Hasan, R., Chen, W., & Goto, Y. (1994). Power model for semi-rigid connections. *Journal of Singapore Structural Steel Society, 5*(1), 37-48.

Korzekwa, A., & Tremblay, R. (2009). Numerical simulation of the cyclic inelastic behaviour of buckling restrained braces. In *Behaviour of Steel Structures in Seismic Areas* (pp. 671-676): CRC Press.

Krauss, G. (1999). Martensite in steel: strength and structure. *Materials Science and Engineering: A, 273*, 40-57.

Krishnamurthy, N. (1978). A fresh look at bolted end-plate behavior and design. *Engineering Journal, 15*(2), 39-49.

Krishnamurthy, N., & Graddy, D. E. (1976). Correlation between 2-and 3-dimensional finite element analysis of steel bolted end-plate connections. *Computers & Structures, 6*(4), 381-389.

Kukreti, A., Murray, T., & Abolmaali, A. (1987). End-plate connection moment-rotation relationship. *Journal of Constructional Steel Research, 8*, 137-157.

Kustu, O., Miller, D. D., & Brokken, S. T. (1982). *Development of damage functions for high-rise building components*: URS/John A. Blume and Associates.

Lemonis, M. E., & Gantes, C. J. (2009). Mechanical modeling of the nonlinear response of beam-to-column joints. *Journal of Constructional Steel Research, 65*(4), 879-890.

Lewitt, C. W., Chesson Jr, E., & Munse, W. H. (1966). *Restraint characteristics of flexible riveted and bolted beam-to-column connections*. Engineering Experiment Station, University of Illinois.

Liew, J. R., White, D., & Chen, W.-F. (1993). Second-order refined plastic-hinge analysis for frame design. Part I. *Journal of Structural Engineering, 119*(11), 3196-3216.

Lin, P. C., Tsai, K. C., Wang, K. J., Yu, Y. J., Wei, C. Y., Wu, A. C., . . . Schellenberg, A. H. (2012). Seismic design and hybrid tests of a full‐scale three‐story buckling‐restrained braced frame using welded end connections and thin profile. *Earthquake Engineering & Structural Dynamics, 41*(5), 1001-1020.

Loeding, S., Kowalsky, M. J., & Priestley, M. N. (1998). *Direct displacement-based design of reinforced concrete building frames* (Vol. 98): Division of Structural Engineering, University of California, San Diego.

López-Almansa, F., Castro-Medina, J. C., & Oller, S. (2012). A numerical model of the structural behavior of buckling-restrained braces. *Engineering Structures, 41*, 108-117.

Lu, X., Xie, L., Guan, H., Huang, Y., & Lu, X. (2015). A shear wall element for nonlinear seismic analysis of super-tall buildings using OpenSees. *Finite Elements in Analysis and Design, 98*, 14-25.

Luco, N., & Cornell, C. A. (2007). Structure-specific scalar intensity measures for near-source and ordinary earthquake ground motions. *Earthquake Spectra, 23*(2), 357-392.

Lupoi, G., Franchin, P., Lupoi, A., & Pinto, P. E. (2006). Seismic fragility analysis of structural systems. *Journal of Engineering Mechanics, 132*(4), 385-395.

Maggi, Y., Gonçalves, R., Leon, R., & Ribeiro, L. (2005). Parametric analysis of steel bolted end plate connections using finite element modeling. *Journal of Constructional Steel Research, 61*(5), 689-708.

Mahin, S. A. (1998). Lessons from damage to steel buildings during the Northridge earthquake. *Engineering Structures, 20*(4-6), 261-270.

Maio, R., & Tsionis, G. (2015). *Seismic fragility curves for the European building stock*. Brussels: JRC Technical Report, European Commission.

Maley, T. J., Sullivan, T. J., & Corte, G. D. (2010). Development of a displacement-based design method for steel dual systems with buckling-restrained braces and moment-resisting frames. *Journal of Earthquake Engineering, 14*(S1), 106-140.

Mazzolani, F. M., Corte, G. D., & D'Aniello, M. (2009). Experimental analysis of steel dissipative bracing systems for seismic upgrading. *Journal of Civil Engineering and Management, 15*(1), 7-19.

Mazzoni, S., McKenna, F., Scott, M. H., & Fenves, G. L. (2006). *OpenSees command language manual* (Vol. 264): Pacific Earthquake Engineering Research Center, University of California, Berkeley.

McCue, K. (2015). *Historical earthquakes in Tasmania*: Central Queensland University, Rockhampton, Queensland.

Mckenna, F. T. (1999). *Object-oriented finite element programming: Frameworks for analysis, algorithms and parallel computing.* (Ph.D.), University of California, Berkeley,

Medhekar, M., & Kennedy, D. (2000). Displacement-based seismic design of buildings—theory. *Engineering Structures, 22*(3), 201-209.

Menegotto, M., & Pinto, P. E. (1973). *Method of analysis for cyclically loaded RC plane*

frames including changes in geometry and non-elastic behavior of elements under combined normal force and bending. Paper presented at the IABSE symposium on resistance and ultimate deformability of structures.

Merritt, S., Uang, C.-M., & Benzoni, G. (2003). *Subassemblage testing of corebrace buckling-restrained braces*. San Diego: Department of Structural Engineering, University of California.

Mohamadi-Shooreh, M., & Mofid, M. (2008). Parametric analyses on the initial stiffness of flush end-plate splice connections using FEM. *Journal of Constructional Steel Research, 64*(10), 1129-1141.

Mokhtar, S. N., & Mahmood, N. Z. (2008). *Approach in construction industry: A study on prefabrication method as a tool for waste minimization.* Paper presented at the International Conference on Environmental Research and Technology (ICERT. 2008). .

Moncarz, P. D., & Gerstl, K. H. (1981). Steel frames with nonlinear connections. *Journal of the Structural Division, 107*(8), 1427-1441.

Moreno, A. (2005). *Un modelo de elementos finitos para el análisis de uniones atornilladas viga-pilar con comportamiento semirrígido.* (Ph. D.), Universidad de La Coruña, Spain.

Naeim, F., Alimoradi, A., & Pezeshk, S. (2004). Selection and scaling of ground motion time histories for structural design using genetic algorithms. *Earthquake Spectra, 20*(2), 413-426.

Naeim, F., & Kelly, J. M. (1999). *Design of seismic isolated structures: from theory to practice*: John Wiley & Sons.

Nazri, F. M., & Alexander, N. A. (2012). Determining yield and ultimate loads for moment-resisting frame buildings. *Proceedings of the Institution of Civil Engineers Structures and Buildings, 165*(2), 57-67.

Nethercot, D. A. (1985a). Steel Beam to Column Connections—A Review of Test Data

and Their Applicability to the Evaluation of the Joint Behaviour of the Performance of Steel Frames. In. London, England: CIRIA.

Nethercot, D. A. (1985b). *Utilization of experimentally obtained connection data in assessing the performance of steel frames.* Paper presented at the Connection flexibility and steel frames.

Ozcelik, R., Dikiciasik, Y., & Erdil, E. F. (2017). The development of the buckling restrained braces with new end restrains. *Journal of Constructional Steel Research, 138*, 208-220.

Özel, A. E., & Güneyisi, E. M. (2011). Effects of eccentric steel bracing systems on seismic fragility curves of mid-rise R/C buildings: A case study. *Structural Safety, 33*(1), 82-95.

Padgett, J., & DesRoches, R. (2006). *Bridge damage-functionality using expert opinion survey.* Paper presented at the 8th National Conference on Earthquake Engineering.

Palmer, K. D., Christopulos, A. S., Lehman, D. E., & Roeder, C. W. (2014). Experimental evaluation of cyclically loaded, large-scale, planar and 3-d buckling-restrained braced frames. *Journal of Constructional Steel Research, 101*, 415-425.

Palmer, K. D., Roeder, C. W., Lehman, D. E., Okazaki, T., & Shield, C. (2012). Experimental performance of steel braced frames subjected to bidirectional loading. *Journal of Structural Engineering, 139*(8), 1274-1284.

Pan, W., Gibb, A. G., & Dainty, A. R. (2007). Perspectives of UK housebuilders on the use of offsite modern methods of construction. *Construction management and Economics, 25*(2), 183-194.

Park, J., Towashiraporn, P., Craig, J. I., & Goodno, B. J. (2009). Seismic fragility analysis of low-rise unreinforced masonry structures. *Engineering Structures, 31*(1), 125-137.

Pasquire, C., Gibb, A., & Blismas, N. (2005). *What Should You Really Measure If You Want to Compare Pre-fabrication with Traditional Construction?* Paper presented

at the 13th International Group for Lean Construction Conference.

Pheng, L. S., & Chuan, C. J. (2001). Just-in-time management of precast concrete components. *Journal of Construction Engineering and Management, 127*(6), 494-501.

Piedrafita, D., Cahis, X., Simon, E., & Comas, J. (2015). A new perforated core buckling restrained brace. *Engineering Structures, 85*, 118-126.

Pirmoz, A., Daryan, A. S., Mazaheri, A., & Darbandi, H. E. (2008). Behavior of bolted angle connections subjected to combined shear force and moment. *Journal of Constructional Steel Research, 64*(4), 436-446.

Porter, K. (2015). Beginner's guide to fragility, vulnerability, and risk. *Encyclopedia of Earthquake Engineering*, 235-260.

Powell, G. H. (2008). Displacement-based seismic design of structures. *Earthquake Spectra, 24*(2), 555-557.

Prakash, V., Powell, G., & Campbell, S. (1993). *DRAIN-2DX, element description and user guide*. Berkeley, CA: Univ. of California.

Rathbun, J. C. (1936). Elastic properties of riveted connections. *Transactions of the American Society of Civil Engineers, 101*, 524-563.

Ricles, J., Sause, R., Peng, S., & Lu, L. (2002). Experimental evaluation of earthquake resistant posttensioned steel connections. *Journal of Structural Engineering, 128*(7), 850-859.

Ricles, J. M., Sause, R., Garlock, M. M., & Zhao, C. (2001). Posttensioned seismic-resistant connections for steel frames. *Journal of Structural Engineering, 127*(2), 113-121.

Rojahn, C., & Sharpe, R. L. (1985). *Earthquake damage evaluation data for California*: Applied technology council.

Ruiz-García, J., & Negrete-Manriquez, J. C. (2011). Evaluation of drift demands in

existing steel frames under as-recorded far-field and near-fault mainshock–aftershock seismic sequences. *Engineering Structures, 33*(2), 621-634.

Sabelli, R. (2001). *Research on improving the design and analysis of earthquake-resistant steel-braced frames*: EERI.

Sabelli, R., Mahin, S., & Chang, C. (2003). Seismic demands on steel braced frame buildings with buckling-restrained braces. *Engineering Structures, 25*(5), 655-666.

Sambridge, M., Sinadinovski, C., & McCue, K. (2016). *Earthquake Source Zones in Intraplate Australia without Binning.* Paper presented at the Australian Earthquake Engineering Society Annual Conference, Melbourne, Australia.

SAP2000. (2006). *Integrated finite element analysis and design of structures basic analysis reference manual, Ver. 10.07*. Berkeley, CA: Computers and Structures INC.

Sarraj, M., Burgess, I., Davison, J., & Plank, R. (2007). Finite element modelling of steel fin plate connections in fire. *Fire Safety Journal, 42*(6-7), 408-415.

Scawthorn, C., & Yanev, P. I. (1995). 17 January 1995, Hyogo-ken Nambu, Japanese earthquake. *Engineering Structures, 17*(3), 146-157.

Sfahani, M., Guan, H., & Loo, Y.-C. (2015). Seismic reliability and risk assessment of structures based on fragility analysis–a review. *Advances in Structural Engineering, 18*(10), 1653-1669.

Sherbourne, A. N., & Bahaari, M. R. (1994). 3D simulation of end-plate bolted connections. *Journal of Structural Engineering, 120*(11), 3122-3136.

Song, R., Li, Y., & van de Lindt, J. W. (2014). Impact of earthquake ground motion characteristics on collapse risk of post-mainshock buildings considering aftershocks. *Engineering Structures, 81*, 349-361.

Steel Construction.info. (2018). Structural steel design awards. Retrieved from https://www.steelconstruction.info/Structural_steel_design_awards

Structural Engineering Institute. (2006). *Minimum design loads for buildings and other structures* (Vol. 7): American Society of Civil Engineers.

Sumner, E. A., Mays, T. W., & Murray, T. M. (2000). *End-plate moment connections: test results and finite element method validation.* Paper presented at the Connections in Steel Structures IV: Steel Connections in the New Millennium: Proceedings of the Fourth International Workshop.

Tagawa, H., & Gurel, S. (2005). Application of steel channels as stiffeners in bolted moment connections. *Journal of Constructional Steel Research, 61*(12), 1650-1671.

Tam, C., Tam, V. W., Chan, J. K., & Ng, W. C. (2005). Use of prefabrication to minimize construction waste-a case study approach. *International Journal of Construction Management, 5*(1), 91-101.

Tam, V. W., Shen, L., & Tam, C. M. (2007). Assessing the levels of material wastage affected by sub-contracting relationships and projects types with their correlations. *Building and environment, 42*(3), 1471-1477.

Taranath, B. S. (2011). *Structural analysis and design of tall buildings: Steel and composite construction*: CRC press.

Troup, S., Xiao, R., & Moy, S. (1998). Numerical modelling of bolted steel connections. *Journal of Constructional Steel Research, 1*(46), 269.

Tsai, K.-C., Chen, H.-W., Hong, C.-P., & Su, Y.-F. (1993). Design of steel triangular plate energy absorbers for seismic-resistant construction. *Earthquake Spectra, 9*(3), 505-528.

Tsai, K.-C., Lai, J.-W., Hwang, Y.-C., Lin, S.-L., & Weng, C.-H. (2004). *Research and application of double-core buckling restrained braces in Taiwan.* Paper presented at the 13th World Conference on Earthquake Engineering.

Tsai, K. C., Hsiao, P. C., Wang, K. J., Weng, Y. T., Lin, M. L., Lin, K. C., . . . Lin, S. L.

(2008). Pseudo‐dynamic tests of a full‐scale CFT/BRB frame—Part I: Specimen design, experiment and analysis. *Earthquake Engineering & Structural Dynamics, 37*(7), 1081-1098.

Uriz, P., Filippou, F. C., & Mahin, S. A. (2008). Model for cyclic inelastic buckling of steel braces. *Journal of Structural Engineering, 134*(4), 619-628.

Uriz, P., & Mahin, S. (2008). *Toward earthquake-resistant design of concentrically braced steel-frame structures*. PEER rep no. 2008/08, Pacific Earthquake Engineering Research Center, College of Engineering, University of California, Berkeley.

Vamvatsikos, D., & Cornell, C. A. (2002). Incremental dynamic analysis. *Earthquake Engineering & Structural Dynamics, 31*(3), 491-514.

Vargas, R., & Bruneau, M. (2009). Analytical response and design of buildings with metallic structural fuses. *Journal of Structural Engineering, 135*(4), 386-393.

Vargas, R., & Bruneau, M. (2009). Experimental response of buildings designed with metallic structural fuses. II. *Journal of Structural Engineering, 135*(4), 394-403.

Vigh, L. G., Zsarnóczay, Á., & Balogh, T. (2017). Eurocode conforming design of BRBF–Part I: Proposal for codification. *Journal of Constructional Steel Research, 135*, 265-276.

Wald, F., da Silva, L. S., Moore, D., Lennon, T., Chladna, M., Santiago, A., . . . Borges, L. (2006). Experimental behaviour of a steel structure under natural fire. *Fire Safety Journal, 41*(7), 509-522.

Wang, C.-L., Usami, T., Funayama, J., & Imase, F. (2013). Low-cycle fatigue testing of extruded aluminium alloy buckling-restrained braces. *Engineering Structures, 46*, 294-301.

Wang, Y. (2006). *Housing industrialised buildings in China: status quo and future development.* (Master), South China University of Technology, Guangzhou, China.

Watanabe, A., Hitomi, Y., Saeki, E., Wada, A., & Fujimoto, M. (1988). *Properties of brace encased in buckling-restraining concrete and steel tube.* Paper presented at the Ninth World Conference on Earthquake Engineering.

Weynand, K., Jaspart, J.-P., & Steenhuis, M. (1998). *Economy studies of steel building frames with semi-rigid joints.* Paper presented at the Second World Conference on Constructional Steel Design.

Whittaker, A. S., Bertero, V. V., Thompson, C. L., & Alonso, L. J. (1991). Seismic testing of steel plate energy dissipation devices. *Earthquake Spectra, 7*(4), 563-604.

Wijanto, S. (2012). *Behaviour and Design of Generic Buckling Restrained Brace Systems.* (Master of Engineering), The University of Auckland, New Zealand.

Wilson, W. M., & Moore, H. F. (1917). *Tests to determine the rigidity of riveted joints of steel structures*. Engineering Experiment Station: University of Illinois.

Wong, A. K., & Yeh, S. H. K. (1985). *Housing a nation: 25 years of public housing in Singapore*: Brook House Pub.

Xiao, R., & Pernetti, F. (2005). Numerical analysis of steel and composite steel and concrete connections. *Eurosteel*.

Xie, Q. (2005). State of the art of buckling-restrained braces in Asia. *Journal of constructional steel research, 61*(6), 727-748.

Xu, Y., Guan, H., Zhou, X., & Loo, Y. (2015). *Preliminary seismic analysis of fabricated steel frame systems with pin beam-column connections and buckling restrained braces.* Paper presented at the Second International Conference on Performance-based and Life-cycle Structural Engineering.

Yalçin, Ü., & Durrani, A. J. (1993). Effect of Slab on Inelastic Response of R/C Building. *Journal of Structural Engineering, 119*(5), 1374-1387.

Yang, J., Zhu, X., & Zhang, H. (2012). Group model exploration of housing

industrialization. *Shigong Jishu/Construction Technology, 41*(364), 95-98.

Yee, A. A. (2001). Social and environmental benefits of precast concrete technology. *PCI journal, 46*(3).

Yee, Y. L., & Melchers, R. E. (1986). Moment-rotation curves for bolted connections. *Journal of Structural Engineering, 112*(3), 615-635.

Yu, H., Burgess, I., Davison, J., & Plank, R. (2009). Experimental investigation of the behaviour of fin plate connections in fire. *Journal of Constructional Steel Research, 65*(3), 723-736.

Zhang, X., & Skitmore, M. (2012). Industrialized housing in China: a coin with two sides. *International Journal of Strategic Property Management, 16*(2), 143-157.

Zsarnóczay, Á., & Vigh, L. G. (2017). Eurocode conforming design of BRBF–Part II: Design procedure evaluation. *Journal of Constructional Steel Research, 135*, 253-264.